THE JOURNAL
OF
CHEMICAL PHYSICS

VOLUME 21, NUMBER 8 AUGUST, 1953

The Determination of the Fluorescence Lifetimes of Dissolved Substances by a Phase Shift Method

E. A. BAILEY, JR., AND G. K. ROLLEFSON
Department of Chemistry and Chemical Engineering, University of California, Berkeley, California
(Received December 23, 1952)

The lifetimes of fluorescent substances are determined by exciting the fluorescence with light modulated at a high frequency and measuring the difference in phase between the exciting light and the resulting fluorescence. The exciting light is modulated by an ultrasonic standing wave in a liquid which causes the latter to act as an intermittent diffraction grating. Photomultiplier tubes are used to pick up the exciting and fluorescent light. Tuned circuits are used to isolate a single harmonic of the signal from the phototubes and the phase shift determined by comparison with a calibrated phase shifting circuit. The phase angle ϕ is related to the lifetime by $\tan\phi=\omega\tau$. In which ω is 2π times the frequency of modulation and τ is the lifetime of the excited state. The data show that lifetimes can be determined with a precision of 1 to 2×10^{-10} second.

The lifetimes of acridone in neutral solution (saturated to 10 percent saturated) and quinine sulfate (4×10^{-6} to $4\times10^{-5}M$) in 0.01 M nitric acid are independent of the concentration. The values found are acridone $1.59\pm0.01\times10^{-8}$ second, and quinine sulfate $2.28\times0.02\times10^{-8}$ second. The lifetime of fluorescein in $0.005M$ potassium hydroxide increases with concentration over the range 10^{-6} to $5\times10^{-4}M$. This fact can be explained by assuming that some of the fluorescent light is absorbed and re-emitted. The lifetime of fluorescein extrapolated to zero concentration is $4.5\pm0.1\times10^{-9}$ second.

INTRODUCTION

THE rate of disappearance of photoactivated molecules by emission of fluorescent light, and consequently the decay in intensity of fluorescence by this process, is generally considered to be first order. Deactivation may also take place through other processes which are first order with respect to the activated species, such as interaction with solvent molecules or quenching by specific ions in solution. The differential equation for decay in intensity of fluorescence is

$$dI/dt=-k_1I, \tag{1}$$

in which k_1 is considered to be the sum of all first-order rate constants. Photoactivation occurs at a rate proportional to the intensity of exciting light. When excitation is by light varying in intensity in a periodic manner, the equation becomes

$$dI/dt=-k_1I+k_2J(t), \tag{2}$$

where the intensity of exciting light $J(t)$ may be represented as a Fourier series,

$$J(t)=a_0/2+\sum(a_n\cos n\omega t+b_n\sin n\omega t). \tag{3}$$

The value of k_2 is determined by the absorption coefficient and concentration of the fluorescer and by the thickness of the layer of solution used, but in any given experiment it is a constant. Substitution of (3) into (2) gives a linear first-order equation which may be solved by standard methods. With the additional substitutions,

$$\sin\phi_n=n\omega/(k_1^2+n^2\omega^2)^{\frac{1}{2}},$$
$$\cos\phi_n=k_1/(k_1^2+n^2\omega^2)^{\frac{1}{2}},$$

one obtains

$$I=\frac{a_0k_2}{2k_1}+k_2\sum\frac{a_n\cos(n\omega t-\phi_n)}{(k_1^2+n^2\omega^2)^{\frac{1}{2}}}+k_2\sum\frac{b_n\sin(n\omega t-\phi_n)}{(k_1^2+n^2\omega^2)^{\frac{1}{2}}}+Ce^{-k_1t}. \tag{4}$$

In Eq. (3) the constant term $(a_0/2)$ indicates the average intensity of the exciting light and the term under the summation the periodic variation about this average. Since the intensity of exciting light can never have a negative value, the constant term is equal to or greater than the maximum absolute value of the periodic term. In Eq. (4) it is seen that the intensity

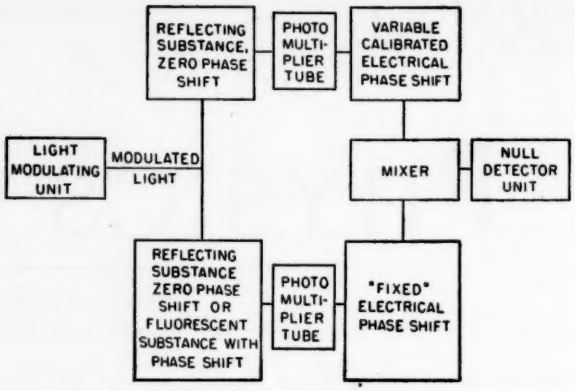
REFLECTING SUBSTANCE, ZERO PHASE SHIFT
PHOTO MULTI-PLIER TUBE
VARIABLE CALIBRATED ELECTRICAL PHASE SHIFT
LIGHT MODULATING UNIT
MODULATED LIGHT
MIXER
NULL DETECTOR UNIT
REFLECTING SUBSTANCE ZERO PHASE SHIFT OR FLUORESCENT SUBSTANCE WITH PHASE SHIFT
PHOTO MULTI-PLIER TUBE
"FIXED" ELECTRICAL PHASE SHIFT

FIG. 1. Fluorescence lifetime apparatus.

of fluorescence is given by an expression containing terms similar to those in Eq. (3) plus an additional exponential term in t. This final term, however, becomes negligibly small as t becomes large relative to $1/k_1(=\tau)$ which is of the order of 10^{-7} to 10^{-9} second in the present instance. Thus within a small fraction of a second after the exciting light is applied to the fluorescent material this transient term may be neglected and the fluorescence represented by a Fourier series. For a given component of exciting light a component of the same frequency is obtained in the fluorescent light, but retarded in phase by the angle ϕ_n. This angle is related to the rate constant k_1 and to the mean lifetime τ by

$$\tan\phi_n = n\omega/k_1 = n\omega\tau. \tag{5}$$

The behavior of the fluorescence intensity as a function of frequency of exciting light can be conveniently illustrated for the case in which excitation is by sinusoidally varying light, i.e., all of the coefficients a_n and b_n for n greater than 1 are zero so that only the first component of the Fourier series remains. By a proper choice of the time base either a_1 or b_1 can be made equal to zero so that the exciting light for this case may be represented by

$$J(t) = a_0/2 + a_1 \sin\omega t.$$

The fraction modulation of the exciting light is given by $2a_1/a_0$. The intensity of fluorescence in this case is

$$I = \frac{k_2}{k_1}\cdot\frac{a_0}{2} + \frac{k_2}{(k_1^2+\omega^2)^{\frac{1}{2}}}\cdot a_1 \sin(\omega t - \phi).$$

The fraction modulation of fluorescent light is given by

$$\frac{2a_1}{a_0}\cdot\frac{k_1}{(k_1^2+\omega^2)^{\frac{1}{2}}},$$

and the phase relationship by $\tan\phi = \omega/k_1$. It is seen that for low frequencies in which ω is very small with respect to k_1 the fraction modulation of fluorescent light will be essentially the same as that of the exciting light and the phase angle ϕ will be very small. If, on the other hand, excitation is by light modulated at very high frequencies such that ω is large with respect to k_1, the fraction modulation of fluorescent light will be very small and the phase angle will approach ninety degrees. If the frequency is chosen so that ω is approximately $1/\sqrt{2}$ times that of the exciting light, the phase angle will be approximately 45° and the value of this angle for a given frequency of excitation will be a fairly sensitive function of the value of k_1.

The apparatus described below provides for measurement of the phase shift of a single component when fluorescence is excited by modulated light. Experimental data are given which indicate the precision with which lifetimes may be obtained.

DESCRIPTION OF APPARATUS

The two principal components of the apparatus for measuring fluorescence lifetimes are the light modulating unit and the device for measuring the phase shift. The block diagram given in Fig. 1 indicates the general features of the present apparatus.

Light is modulated by a method described by Maercks,[1] using ultrasonic standing waves in a liquid medium as an intermittent diffraction grating. The method of detection and measurement is similar to one suggested by Tumerman.[2] Modulated light is allowed to fall on two sample cells, one containing a suspension of some reflecting material and the other containing either reflecting material or a solution of a fluorescent substance. Two photomultiplier tubes are used to detect the light from these two cells.

The signals from the two phototubes are fed into similar electrical circuits, the first containing a calibrated phase shifting network and the second a variable but uncalibrated network. With a reflecting medium exposed to the phototube in the uncalibrated circuit, the calibrated circuit can be adjusted to bring the two output signals into phase. This initial or zero setting of the calibrated phase shift circuit depends upon the setting of the variable phase shifter of the other circuit.

The phase shift resulting from substitution of a fluorescent material for the reflecting material in the second circuit is measured

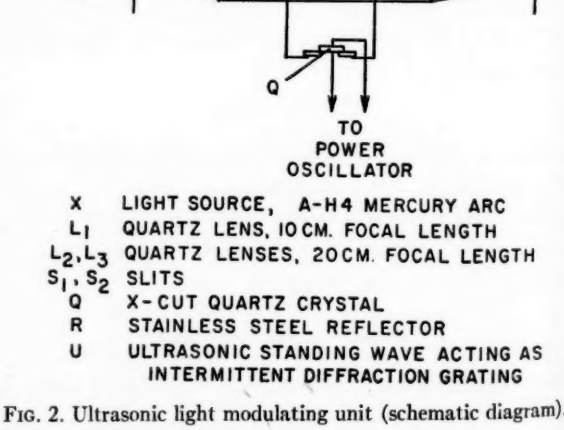

X LIGHT SOURCE, A-H4 MERCURY ARC
L_1 QUARTZ LENS, 10 CM. FOCAL LENGTH
L_2, L_3 QUARTZ LENSES, 20 CM. FOCAL LENGTH
S_1, S_2 SLITS
Q X-CUT QUARTZ CRYSTAL
R STAINLESS STEEL REFLECTOR
U ULTRASONIC STANDING WAVE ACTING AS INTERMITTENT DIFFRACTION GRATING

FIG. 2. Ultrasonic light modulating unit (schematic diagram).

[1] O. Maercks, Z. Physik **109**, 598–605 (1938).
[2] L. A. Tumerman, J. Phys. (Moscow) **4**, 151–166 (1941).

by determining the phase shift which must be introduced by the calibrated phase shifter in the first circuit to bring the two output signals again into phase.

Light Modulating Unit

A schematic diagram of the experimental arrangement of the light modulating unit is indicated in Fig. 2. Light from an A-H4 mercury arc lamp is focused on slit *S*1. Light from this slit is rendered essentially parallel and allowed to pass through the cell in which an ultrasonic standing wave has been produced by the quartz crystal *Q*. The image of slit *S*1 is then focused on slit *S*2. The standing wave in the ultrasonic cell acts as a diffraction grating as a result of the alternate regions of compression and rarefaction in the standing wave. These regions of compression and rarefaction alternate in their positions according to the frequency of the wave, a region of compression becoming a region of rarefaction one-half cycle later. Thus twice during each cycle the liquid passes through an intermediate condition in which the pressure, and therefore the index of refaction, is uniform throughout. During these periods in which the liquid is essentially isotropic, most of the light in the image focused at *S*2 passes through the slit. During the periods in which an effective optical grating is present, however, a large fraction of the light is found in higher orders of the diffraction pattern, which are focused to either side of *S*2. Light passing through *S*2 is therefore modulated at twice the frequency of the standing wave.

The ultrasonic standing wave is set up by means of an X-cut quartz crystal driven at its resonant frequency by a crystal controlled oscillator and amplifier. The X-cut crystal is in the form of a disk about one inch in diameter. It is mounted over a hole in a polystyrene disk by moistening the polystyrene with benzene or other solvent and pressing the quartz crystal into place. The diameter of the quartz disk is about $\frac{1}{16}$ inch greater than that of the hole. This procedure was found to provide a satisfactory and permanent mounting.

The side of the crystal facing into the ultrasonic cell is provided with an electrode of sputtered gold and electroplated silver. Contact to this electrode is made by means of a small drop of solder in a loop on the end of a piece of thin copper wire. This drop of solder was flattened to give a larger area of contact and is held in place by a drop of cement prepared by dissolving polystyrene in benzene.

The electrode on the other side of the crystal is a disk of thin copper foil cemented onto the crystal. A spring contact makes connection with this electrode. When a plated electrode was used here, rather than the copper foil disk, the electrode was found to deteriorate in the immediate vicinity of the contact.

The polystyrene disk is mounted on the side of a well protruding into the ultrasonic cell from the cover. It is secured in place by means of a brass collar and rubber gasket which can be screwed into place. This provides a convenient arrangement for changing from one crystal to another.

A stainless steel plate is provided at the other end of the cell as a reflector for the ultrasonic waves. This plate is provided with screw adjustments so that it can be precisely aligned to give the optimum standing wave pattern. In making these adjustments, observation of the diffraction pattern focused on a screen placed in front of slit *S*2 may be used to determine when a good standing wave is obtained. By replacing the last lens in the optical system by a short focal length lens one may focus the image of the standing wave pattern itself on the screen. When the reflector is correctly adjusted, this image should show a distinct pattern of light and dark vertical lines of uniform intensity throughout the field.

The cell itself is a rectangular brass tank provided with windows of high silica glass (Corning filter No. 7910) on each side so that light may be passed through the cell perpendicular to the line between the crystal and reflector. In the present instance water was used as the liquid in the tank.

Ultraviolet light is used for exciting fluorescence, the visible light being cut out by means of a filter (Corning filter No. 5840) placed beyond slit *S*2. Since the point of focus of the ultraviolet light is not the same as that of the visible, the final adjustment of focusing the image on slit *S*2 is most conveniently made by adjusting to give maximum amplitude of the signal obtained from the detecting system (to be described) rather than visual observation of the image on the slit.

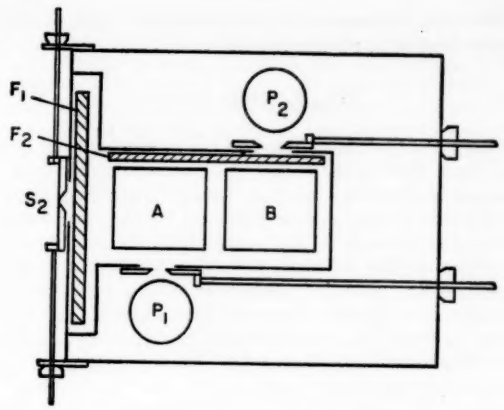

S_2 SLIT S_2 OF FIGURE 2
F_1 FILTER, CORNING NO. 5840
F_2 FILTER, CORNING NO. 3389 REMOVED FOR ZERO SETTING WITH $BaSO_4$ SOL
P_1, P_2 PHOTOMULTIPLIER TUBES
A SAMPLE CELL, $BaSO_4$ SOL
B SAMPLE CELL, $BaSO_4$ SOL OR FLUORESCENT SOLUTION

FIG. 3. Light detecting unit.

Light Detecting Unit

The arrangement of the sample cells and photomultiplier tubes is shown in Fig. 3. Cylindrical sample cells about 2 cm in diameter and 2 cm long with quartz windows on the ends were used. Initially it was planned to use a small reflector placed in the exciting beam to obtain the signal for the first phototube. It was discovered, however, that slight changes in the nature of the standing wave or in the position of the reflector frequently resulted in variation in the phase relationship between the signals from the two phototubes.

The difficulty was overcome by using a sample cell containing a barium sulfate sol as reflecting medium to provide light for the first phototube. This effectively integrates over the entire light beam in the same way as does fluorescent material in the second cell. Even with this arrangement difficulties may arise if the area of the beam is not made small enough so that the entire beam passing through the first cell also passes through the second. The effectiveness of the arrangement can be tested by observing whether or not a phase shift results when a portion of slit *S*2 is covered. The area of the beam is determined by a suitable mask (not indicated in the figure) placed between filter F_1 and cell *A*.

A barium sulfate sol is also used in the second cell when obtaining the zero setting. The sol was prepared by mixing 0.005 molar solutions of $BaCl_2$ and $NaSO_4$ in fifty percent ethyl alcohol-water mixtures. The sol was further diluted by a factor of two or three with alcohol-water solution before placing in the cells. The resulting sol showed little or no tendency to settle out.

When a fluorescent solution is exposed to the second phototube a filter (Corning filter No. 3389) is placed between the sample cell and the phototube. This eliminates the small amount of exciting light which otherwise finds its way to the phototube even though the tube views the sample cell at right angles to the exciting beam.

This filter must be removed in order to obtain a zero setting with reflecting material in the sample cell.

Phase Shift Unit

The output signals from the two phototubes are fed into two similar phase shifting networks. The photomultiplier tube has a high output impedance and must operate into a high-impedance circuit if a strong signal is to be obtained. On the other hand, with capacitance of from 40 to 400 $\mu\mu$f as used, the resistance-capacitance phase shifting network offers a rather low impedance for frequencies of the order of 5 megacyles. With a smaller condenser the problem of calibration becomes more difficult. It is therefore desirable to introduce an impedance matching device between the phototube and the RC network. For this purpose a cathode follower amplifying stage is used.

Although the voltage amplification of a cathode follower circuit is less than one, this circuit is well adapted for use in coupling between the photomultiplier tube and the phase shifting network. It has a very high-input impedance and a low-output impedance. Tuned circuits in the coupling stages were avoided since such circuits introduce phase shifts which are very strongly dependent upon frequency and variation in circuit components, especially in the immediate vicinity of the resonant frequency. The wiring diagram for one of the phase shifting circuits is shown in Fig. 4 together with the equivalent circuit and approximate equivalent circuit.

The output signal from the first cathode follower is connected to the RC circuit as indicated. In the calibrated circuit C is a precision variable air condenser of 40 to 150 $\mu\mu$f together with three fixed air condensers which can be added by means of switches. The capacitance is continuously variable from about 40 to 400 $\mu\mu$f. In the other circuit C is a small padding condenser variable from about 40 to 80 $\mu\mu$f. The output from the RC circuit goes to the grid of the second cathode follower. The phase shift which can be varied in one circuit relative to the other is that which takes place in the part of the circuit between the broken lines in Fig. 4. The phase shift is influenced by the cathode resistor R_K,

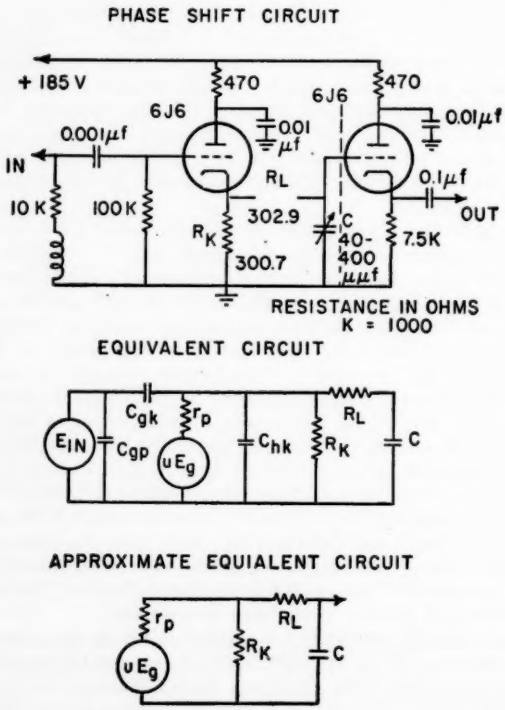

FIG. 4. Phase shift circuit.

the amplification factor μ, and the plate resistance r_p of the first tube as well as by the values of R_L and C. In order to reduce the effect of tube characteristics to a minimum the value of R_K was made as small as possible without exceeding the rated plate dissipation of the tube. The values of R_K and R_L used are both about 300 ohms. In both of the phase shifting circuits precision resistors having good high-frequency characteristics were used for R_K and R_L. A regulated power supply was used to provide the plate voltage for the tubes in the phase shifting circuits.

Phase Detecting Unit

The output signals from the final cathode followers of the two phase shifting circuits are connected, by means of a shielded twin-lead cable, to the antenna terminals of a radio receiver provided with a balanced antenna circuit. With this arrangement, when in phase and of the same amplitude, the two signals cancel one another. By adjusting phase and amplitude to give a null in the output from the radio receiver, the condenser setting corresponding to equal phase shift of the two signals can be determined. Adjustment of the amplitude without introducing phase shift is accomplished through use of adjustable slits between the sample cells and the photomultiplier tubes. In addition to amplification, the radio receiver serves to pick out a single component of the signal. In the present instance the fundamental frequency, 5.208 megacycles, was used.

In the determination of the null point a serious problem is encountered due to the high noise level which is characteristic of photomultiplier tubes. This difficulty is overcome here through use of a very narrow band pass detecting system. For this purpose a second crystal controlled oscillator is used which can be adjusted over a narrow range to a frequency differing from that of the light modulation by about 1000 cps. This signal is loosely coupled to the antenna of the receiver. The difference frequency is then obtained from the audio output of the receiver. This signal is amplified by means of a narrow band pass twin-T audioamplifier.[3] The output from the amplifier is connected to the vertical plates of an oscilloscope. For ease in viewing the signal at low signal strengths, the sweep of the scope is synchronized with the 60-cycle line frequency and the audiofrequency adjusted to be an exact multiple of 60 cycles. With this arrangement the band pass of the detecting system is reduced to about five to ten cycles per second, and a satisfactory signal to noise ratio is obtained.

CIRCUIT ANALYSIS AND CALCULATIONS

In the circuit employed in the calibrated phase shift network the measurable phase shift occurs between the grids of the two tubes and depends upon the values of frequency, R_K, R_L, C, and r_p of the first tube. The approximate equivalent circuit shown in Fig. 4 was used for all calculations which follow. In this approximate circuit interelectrode capacitances, which are small, have been neglected. Analysis of this circuit yields the following relationship.

$$\tan\phi = R/X_c, \tag{6}$$

where

$$R = R_L + \frac{R_K}{1+R_K(1+\mu)/r_p}$$

$$X_c = 1/(2\pi fC)$$

f = frequency (5.208×10^6 cps).

Experimental measurements yield values of C corresponding to two values of phase angle, ϕ_1 using reflecting material and ϕ_2 using fluorescent material. The phase shift resulting from fluorescence is the difference between these two values.

$$\phi_f = \phi_2 - \phi_1. \tag{7}$$

From Eq. (5) $\tan\phi_f = 2\pi f\tau$. Making use of the proper trigonometric

[3] G. E. Valley, Jr., and H. Wallman, *Vacuum Tube Amplifiers* (McGraw-Hill Book Company, Inc., New York, 1948).

relationships one obtains

$$\tau=\frac{R(C_2-C_1)}{1+4\pi^2f^2R^2C_2C_1}. \tag{8}$$

The precision condenser used in the phase shift circuit together with the three fixed condensers and their associated switches and wiring were calibrated by means of a precision capacitance bridge. The calibration is considered to be accurate to better than $\pm 0.2\,\mu\mu f$. For purposes of calculating phase shift an additional $3.5\,\mu\mu f$ was added to the calibration value to include the grid-to-plate capacitance of the final cathode follower stage.

Tube characteristics must be considered in order to evaluate R. The tube used is a 6J6 miniature twin triode connected with the two sides in parallel. Average values for the amplification factor and plate resistance as functions of plate and grid voltages for this type of tube can be obtained from the data sheets in the RCA Tube Manual. As an additional check on the values for these tube characteristics for the specific tube being used the amplification, A, of the cathode follower in the phase shifting network was measured, using a sensitive vacuum tube voltmeter, and found to be 0.64. The amplification of a cathode follower is given by the expression

$$A=\left[\frac{\mu}{1+\mu}Z_b\right]\Big/\left[\frac{r_p}{1+\mu}+Z_b\right]. \tag{9}$$

In this equation Z_b is the impedance of the load. In the present circuit the load consists of R_K in one branch of a parallel circuit with R_L and C in series in the other branch. Measurements of the amplification were made at a frequency of 100 cps. At this frequency the impedance of the condenser $C(=40\,\mu\mu f)$ is so large that this branch of the circuit may be neglected and the load impedance becomes simply R_K.

The value of μ is not a very sensitive function of the plate and grid voltages, and a reasonably accurate estimate of the value of the ratio $\mu(1+\mu)$ can be made from the tube manual data sheet. In the present apparatus the tube is operated with the plate at 185 volts and the grid at -3.4 volts. For these conditions the tube manual data sheet gives 36 for the value of μ. Using this value and the measured values of $R_K(=300.7$ ohms) and A $(=0.64)$ in Eq. (9) gives 157 as the value of the ratio $r_p/(1+\mu)$. The tube manual data sheet gives 11 500 ohms as the value for r_p for one section of the tube under the present operating conditions, or half this value for both sections in parallel. Making use of this value to evaluate the ratio directly gives 156. The close agreement between the first value obtained and that determined using average tube characteristics is probably fortuitous but gives one added confidence in using the value 157 in calculating the value of R. Making use of the above values and the measured value of $R_L(=302.9$ ohms), R is found to be 406 ohms.

From Eq. (8) one can obtain the expression for the error in lifetime resulting from error in the value of R. This is given in Eq. (10):

$$\frac{d\tau}{\tau}=\frac{(1-R^2\omega^2C_2C_1)}{(1+R^2\omega^2C_2C_1)}\frac{dR}{R}. \tag{10}$$

It can be seen that the numerator in Eq. (10) vanishes when $R^2\omega^2C_2C_1$ is equal to one. The geometric mean of the capacitance values then correspond to an average phase angle of 45° (Eq. 6). For the approximate values of 400 ohms for R and 1.07×10^{15} for ω^2 the numerator in (10) vanishes when the product C_2C_1 is equal to 5.82×10^{-21}. With the apparatus in its present form the values of this product generally range from 2 to 18×10^{-21} farad². For these extreme values the percent error in lifetime becomes approximately 0.5 times the percent error in R. Most of the measurements reported here were made in the intermediate region in which error in evaluation of R has small effect upon the value of the lifetime. Error from this source is believed to be much less than one percent.

The principal limitation on the accuracy of lifetime measurements is the precision with which the null point in the phase detecting system can be determined. The error in the value of the capacitance for a given null setting depends upon the uncertainty in observing the minimum point of the amplitude A of the signal observed on the oscilloscope. The relationship is indicated in the following equation:

$$\frac{dC}{C}=K\frac{dA}{\sin\phi\cos\phi}. \tag{11}$$

In this equation K is a proportionality constant which cannot be evaluated readily, and ϕ is the phase shift introduced by the calibrated phase shift circuit at the null point. It is obvious from this equation that the percentage error approaches infinity as ϕ approaches either zero or ninety degrees. The error is at a minimum when ϕ equals forty-five degrees. With the present apparatus the value of the angle varies from about twenty-six to about seventy-two degrees. Somewhat higher values can be obtained using the maximum capacity available, but considerable difficulty is encountered in determining the null point when the capacity is much greater than about $300\mu\mu f$. A quantitative estimate of the reproducibility is best obtained from analysis of the experimental

TABLE I. Fluorescent lifetime measurements. The first four sets of data are for solutions of acridone recrystallized from glacial acetic acid. Eighty percent saturated neutral solutions in equilibrium with air. Potassium iodide quencher as indicated. The last set is for a solution of quinine sulfate dihydrate, Merck U.S.P., $4\times10^{-5}M$ in $0.01M$ HNO_3 in equilibrium with air.

	$C_1(\mu\mu f)$	$C_2(\mu\mu f)$	τ(sec)
1-a	0.0M KI		
	48.4	132.4	1.600×10^{-8}
	50.8	138.4	1.587
	52.8	144.4	1.585
	55.3	152.5	1.586
	57.2	159.8	1.594
		Average	$1.59\pm0.01\times10^{-8}$
1-b	0.004M KI		
	60.8	128.0	1.149
	57.9	121.0	1.145
	55.1	114.0	1.134
	49.3	102.2	1.137
	47.2	98.3	1.141
		Average	$1.14\pm0.01\times10^{-8}$
1-c	0.01M KI		
	47.3	79.6	0.789
	56.4	94.0	0.789
	60.9	102.3	0.801
	67.0	112.6	0.794
	51.2	85.4	0.784
		Average	$0.79\pm0.01\times10^{-8}$
1-d	0.02M KI		
	51.1	72.0	0.514
	58.3	81.0	0.503
	61.8	85.8	0.503
	65.8	91.9	0.513
	53.2	75.2	0.524
	54.0	75.4	0.506
	49.5	69.8	0.512
	59.2	82.4	0.506
	63.2	87.8	0.505
	69.6	97.8	0.520
		Average	$0.51\pm0.01\times10^{-8}$
1-e	0.0M KBr		
	48.6	200.2	2.265×10^{-8}
	50.4	209.6	2.256
	53.0	226.8	2.260
	55.2	240.4	2.250
	56.0	251.4	2.277
		Average	$2.26\pm0.01\times10^{-8}$

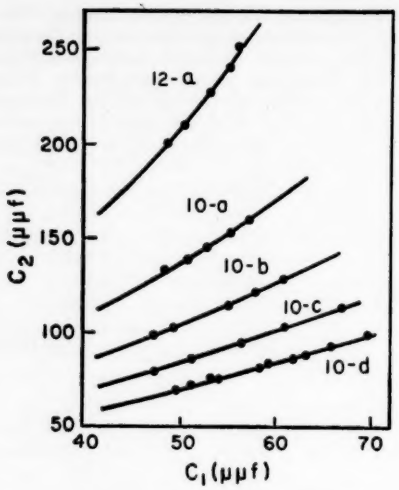

C_1 - INITIAL CAPACITANCE
C_2 - FINAL CAPACITANCE

CURVE	LIFETIME x 10^8
12-a	2.26
10-a	1.59
10-b	1.14
10-c	0.79
10-d	0.51

FIG. 5.

results. Values of lifetimes are in general reproducible to within about 10^{-10} second.

The range of values of ϕ given above corresponds to a maximum lifetime of about 3×10^{-8} second, which can be measured accurately with the apparatus as described. The range can be extended to about 9×10^{-8} second by means of a switch which has been provided to remove the "fixed" capacitance in the uncalibrated phase shift network. With this capacitance removed a zero setting cannot be obtained in the manner previously described since a corresponding decrease in the capacity of the calibrated condenser is not possible. The appropriate value of C_1 for use under these conditions can be determined, however, from values of C_2 obtained for solutions of known lifetimes. This value was not required for the measurements to be reported here.

The range within which accurate lifetimes can be measured is determined by the frequency of modulation of the light. The units which must be changed in order to make use of different frequencies are the power oscillator which drives the ultrasonic crystal, the ultrasonic crystal itself if lower frequencies are desired, though for higher frequencies the crystal can be driven at odd harmonics, and the phase shifting network.

EXPERIMENTAL RESULTS

For each lifetime measurement the zero setting and final setting of the calibrated condenser were obtained for a number of different settings of the phase shift in the uncalibrated circuit. This procedure provides a means for testing the equations obtained from the circuit analysis as well as providing a number of essentially independent measurements.

Values of τ can be calculated according to Eq. (8) for each set of values of C_1 and C_2. The value obtained should be independent of the setting of the uncalibrated circuit if the approximate equivalent circuit is adequate and if proper values for tube characteristics have been used. Values of C_1, C_2, and the calculated values of τ for a number of fluorescent solutions are given in Table I. It can be seen that the lifetimes calculated in this manner for a given sample are constant within experimental error as previously discussed.

TABLE II.

	R Least square	Least square	Eq. (18) $R=406$
1-e	413	2.25×10^{-8}	2.26×10^{-8}
1-a	406	1.58	1.59
1-b	422	1.14	1.14
1-c	418	0.794	0.791
1-d	416	0.510	0.511

TABLE III. Acridone solutions with KI as quencher.

		τ_0/τ	I_0/I
1-a	1.59×10^{-8}		
1-b	1.14	1.39	1.39
1-c	0.79	2.01	2.01
1-d	0.51	3.12	3.10

Alternatively the data may be presented as a plot of C_2 against C_1. Equation (8) may be rearranged to give the relation between the two values indicated in Eq. (12):

$$C_2=\frac{A+C_1}{1-BC_1}. \tag{12}$$

In this equation $A=\tau/R$ and $B=R\omega^2\tau$. Curves of this type are shown in Fig. 5. Experimental points indicated are from Table I. The curves were calculated according to Eq. 12 using 406 as the value for R and the average value of τ calculated from the experimental points using Eq. (8).

TABLE IV. Concentration effect on lifetime of aqueous acridone in neutral solution (20°C).

Conc.	τ
Saturated solution	$1.60\pm0.01\times10^{-8}$
80 percent sat.	1.59 ± 0.01
40 percent sat.	1.59 ± 0.01
20 percent sat.	1.58 ± 0.01
10 percent sat.	1.56 ± 0.02

One may also obtain not only the value of τ but also the value of R from the measured values of C_1 and C_2 through use of the method of least squares to determine the parameters in Eq. (12). This has been done for the data indicated in Fig. 5. The results are given in Table II.

The lifetimes obtained by the method of least squares are in good agreement with those obtained by direct calculation. There appears to be an appreciable deviation, however, in the value of R from the value 406 previously determined. The average value obtained

by the method of least squares is 415 with a root-mean-square deviation of 6. It should be recalled that in the region in which the measurements were made the value of the lifetime is not very sensitive to variation in the value of R. Similarly the curves given in Fig. 5 are insensitive to small changes in R, or conversely, the value of R is quite sensitive to small variations in the curve. For this reason the value 406 has been retained for all further calculations as being probably more reliable, although the change would make no significant difference in the results given.

TABLE V. Concentration effect on lifetime of quinine sulfate in 0.01M HNO_3.

Conc.	τ
$4\times10^{-5}M$	$2.26\pm0.02\times10^{-8}$
$1\times10^{-5}M$	2.29
$4\times10^{-6}M$	2.30

As a further test of the apparatus one may compare the results of lifetime measurements with fluorescence intensity measurements on solutions to which quencher has been added. Considering k_1 to be the sum of all first-order decay constants in the absence of quencher and k_3 to be the constant for the second-order process of deactivation by quencher of concentration Q, Eq. 2 becomes

$$dI/dt=-(k_1+k_3Q)I+k_2J(t). \tag{13}$$

TABLE VI. Concentration effect on lifetime of fluorescein in 0.005M KOH.

Conc.	τ
$1.6\times10^{-6}M$	$4.6\pm0.1\times10^{-9}$
$8.0\times10^{-6}M$	4.6
$1.0\times10^{-5}M$	5.0
$8.0\times10^{-5}M$	6.1
$8.0\times10^{-5}M$	6.5
$1.0\times10^{-4}M$	6.6
$2.0\times10^{-4}M$	7.0
$2.0\times10^{-4}M$	7.0
$3.0\times10^{-4}M$	7.4
$4.0\times10^{-4}M$	7.5
$4.0\times10^{-4}M$	7.7
$5.0\times10^{-4}M$	7.9

The measured rate constant in this case is (k_1+k_3Q), the measured lifetime being the reciprocal of this expression.

The steady-state solution for (13), setting dI/dt equal to zero, gives

$$I=\frac{k_2J}{k_1+k_3Q}. \tag{14}$$

For constant concentration of fluorescer, constant geometry, and for quenchers which do not change the absorption spectrum of the fluorescent species, this expression yields the Stern-Volmer law for fluorescence quenching given in Eq. (15), where I_0 is the intensity of fluorescence in the absence of quencher and I is the intensity with quencher added:

$$\frac{I_0}{I}=\frac{k_1+k_3Q}{k_1}. \tag{15}$$

Since the right-hand side of this expression is simply τ_0/τ, intensity measurements and lifetime measurements on solutions without and with quencher should be related by

$$\frac{\tau_0}{\tau}=\frac{I_0}{I}. \tag{16}$$

The ratios of lifetimes and of intensities for the acridone solutions with KI as quencher indicated in Fig. 5 and Table I are given in Table III. The ratios of lifetime measurements are in good agreement with the ratios of intensity measurements. It is felt that these results, together with the considerations previously discussed, indicate that reliable values of fluorescence lifetimes may be obtained with the apparatus.

Concentration effects on observed lifetimes of acridone, quinine sulfate, and fluorescein in aqueous solutions were studied. Average values are shown in Tables IV, V, and VI.

TABLE VII. Fluorescence lifetime of quinine sulfate.

Author	$\tau(\times10^8)$
Perrin[a]	4
Bruninghaus[b]	4.6
Bruninghaus[c]	4.8
Present work (Acid solution)	2.28 ± 0.02
(Neutral solution)	1.89 ± 0.04

[a] F. Perrin, Ann. phys. (10S) **12**, 169–275 (1929).
[b] Louis Bruninghaus, Compt. rend. **211**, 253–256 (1940).
[c] Louis Bruninghaus, Ann. Physic (12) **3**, 199–274 (1948).

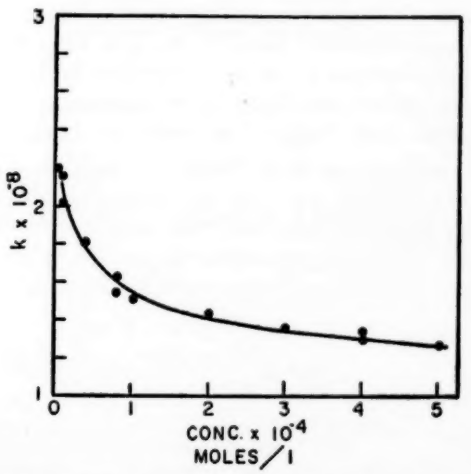

FIG. 6. Variation in rate of fluorescence decay with concentration of fluorescein.

TABLE VIII. Lifetime of fluorescence of fluorescein.

Author	Lifetime
Gaviola[a] (MeOH)	5.0×10^{-9}
Perrin[b]	4.3×10^{-9}
Syzmanowski[c]	5.1×10^{-9}
Bruninghaus[d]	$0\text{–}2\times10^{-8}$
Kirchhoff[e]	4.90×10^{-9}
Galanin[f]	$\sim5.5\times10^{-9}$
Present work (Inf. dil.)	$4.5\pm0.1\times10^{-9}$

[a] E. Gaviola, Z. Physik **42**, 853–861 (1927).
[b] F. Perrin, Ann phys. (10S) **12**, 169–275 (1929).
[c] W. Syzmanowski, Z. Physik **95**, 440–449 (1936).
[d] Louis Bruninghaus, Compt. rend. **211**, 253–256 (1940).
[e] W. Kirchhoff, Z. Physik **116**, 115–121 (1940).
[f] M. C. Galanin, Doklady Akad. Nauk. S. S. R. **70**, 989–990 (1950).

Acridone and quinine sulfate show no significant change in observed lifetime with change in concentration. This result is to be expected in the absence of self-quenching or other complicating phenomena. No value for the lifetime of acridone has been found in the literature. Several published values for quinine sulfate are listed in Table VII. The values obtained in the present work are not in agreement with the published values.

The observed lifetime of fluorescein shows a marked increase with the concentration of the dissolved dye in striking contrast to the absence of such an effect with the other substances studied. There are two ways by which the fluorescent substance may affect the apparent lifetime: (1) a quenching by the unactivated molecules may decrease the lifetime just as any other quencher does; (2) the fluorescent light may be partially absorbed and re-emitted before it gets out of the solution because of a significant overlap of the fluorescence emission band by a strong absorption band and thus increase the apparent duration of the excited state. In the case of fluorescein the magnitude of the first effect may be estimated from the work of Rollefson and Dodgen[4] who found a value of 310 for the quenching constant of fluorescein acting on itself. This value leads to the conclusion that the lifetime could be decreased a maximum of fifteen percent by self-quenching at the highest concentrations used by us. The large increase in lifetime observed by us must therefore be accounted for by the second possibility listed above.

Umberger and LaMer,[5] in order to explain their fluorescence quenching experiments on fluorescein, have treated fluorescence absorption by considering the probability that a given photon will reach the photocell under conditions which allow absorption and re-emission. A different treatment of the problem will be given here by which the desired relationships are more readily obtained.

The absorption of a fraction of the fluorescent light by the solution, with the production of excited molecules, may be taken into account by introducing another term into Eq. (2):

$$dI/dt=-k_1I+k_2J+k_4(1-e^{-k_5C})I. \tag{17}$$

The measured rate constant k_m is then given by

$$k_m=k_1-k_4(1-e^{-k_5C}). \tag{18}$$

C is the concentration of the fluorescein in the solution, and k_5 is the product of the two terms, the average path length of fluorescent light through absorbing solution and an absorption coefficient averaged over the emission band. At low concentrations expansion of the exponential and neglecting second and higher order terms reduces Eq. (18) to

$$k_m=k_1-k_4k_5C. \tag{19}$$

Equation (18) shows that a plot of k_m against C should approach a constant value (k_1-k_4) at high concentrations and (19) shows that a linear extrapolation to zero concentration may be used to obtain k_1. The curve shown in Fig. 6 is in qualitative agreement with these equations. The limiting value at high concentrations is about 1.2×10^8. A precise value cannot be calculated from the data because k_5 deviates considerably from constancy as the concentration is varied over a wide range. Extrapolation to zero concentration gives k_1 as 2.23×10^8. This corresponds to a lifetime of 4.5×10^{-9} second for fluorescein at infinite dilution. Some values for the lifetime of fluorescein which have been reported in the literature are listed in Table VIII. Although these apparently claim the same accuracy that we have obtained it is worth noting that the dependence on concentration has not been detected in these earlier measurements.

The authors wish to express their thanks to Professor W. D. Gwinn and Dr. R. J. Myers whose many helpful suggestions were invaluable to the success of the work.

[4] G. K. Rollefson and H. W. Dodgen, J. Chem. Phys. **12**, 107 (1944).

[5] J. Q. Umberger and V. K. LaMer, J. Am. Chem. Soc. **67**, 1099–1109 (1945).

Solution of the Debye-Hückel Equations for a Polarized Electrode

B. BREYER
Physico-Chemical Laboratory, Faculty of Agriculture, University of Sydney, Sydney, Australia

AND

F. GUTMANN
New South Wales University of Technology, Department of Applied Chemistry, Broadway, Sydney, Australia

(Received September 17, 1952)

The Debye-Hückel equations are solved for the case of a polarized electrode, yielding, for the mean ionic concentration at a distance x from a plane cathode immersed into an aqueous solution of a uni-univalent electrolyte of concentration aN_0 molecules/cm³,

$$n_1 = aN_0 \operatorname{cotanh}^2 Kx/2,$$

$1/K$ being the Debye length. The mean local charge density and the mean local potential are calculated, and it is shown that the latter quantity is merely the thermodynamical potential resulting from the increased activity of the cations near the electrode, the system behaving as a concentration cell.

NOTATION

Mean local concentration of cations	n_1 ions/cc
Mean local concentration of anions	n_2 ions/cc
Bulk concentration of ionized solute	aN_0 ions/cc
Avogadro's number	N_0
Mean local potential at a distance x from the electrode	ψ_1, φ esu
The impressed electric field, assumed to be Laplacian	E esu/cm
The charge on the i'th particle species	e_i esu
Absolute value of charge on each ion	e esu
Boltzmann's constant	k
Dielectric constant of the medium	D
Debye length given by $(8\pi e^2 aN_0)/kTD = K^2$	$1/K$ cm
The mean distance of closest approach of an ion to the electrode	x_1 cm
An external force acting on the i'th particles	$\bar{K}_i$ dynes
Mean local charge density	ρ esu/cm³
Total electric charge contained in the double layer per cm² electrode area	Q esu/cm²
Friction constant	r
Time	t
Absolute temperature	T
$\sqrt{-1}$	j

Boundary conditions: in the bulk of the solution

$$n_1 = n_2 = aN_0, \quad \frac{dn_1}{dx} = \frac{dn_2}{dx} = 0, \quad \frac{d\psi}{dx} = 0 \quad \text{for} \quad x \to \infty.$$

INTRODUCTION

THE system considered consists of a plane inert electrode of semi-infinite extent, immersed into an aqueous solution of a simple uni-univalent salt, say KCl. A potential difference is applied between the bulk of the solution, which is considered to be of infinite extent, and the electrode, which is assumed to be a perfect conductor. In the bulk of the solution the mean concentrations of cations and of anions are equal. The following boundary conditions will be applied.

At an infinite distance from the electrode, the mean local potential, the mean local field, the mean local charge density all vanish; the mean local anion concentration at this point being equal to the mean local cation concentration and equal to the bulk concentration of the ionized solute. Physically, the present paper discusses a diffuse double layer: the most appropriate model seems to be Mackor's[1] modification of the Stern[2] composite layer. Mackor assumes the absence of chemisorption and a "variable χ potential" (in the notation of this paper χ is identical with ψ). The diffuse layer is of the Gouy-Chapman type, terminated at a finite distance x_1 from the electrode, (δ in Mackor's notation) which represents the "distance of closest approach" of ions to the electrode" [see also discussion prior to Eq. (29)].

The basis of the present treatment[3] is the Debye-Hückel[4] "Grundgleichung,"

$$r\frac{\partial n_i}{\partial t} = \operatorname{div}[kT\nabla n_i - n_i \bar{K}]. \tag{1}$$

In the present case

$$\bar{K} = e_i(E + \nabla\psi). \tag{2}$$

The first term arises from the externally impressed field and the second term from interionic forces.

In the vicinity of the electrode, in a space where free charges exist within the double layer, Poisson's equation holds,

$$\nabla^2\psi = -\frac{4\pi}{D}\sum n_i e_i. \tag{3}$$

[1] E. L. Mackor, Rec. trav. chim. **70**, 764 (1951).
[2] O. Stern, Z. Elektrochem. **30**, 508 (1924).
[3] B. Breyer and F. Gutmann, Australian J. Sci. **11**, 96 (1948).
[4] P. Debye and E. Hückel, Physik. Z. **24**, 307 (1923).

ANALYSIS

In the case of a polarized electrode $\partial n_i/\partial t=0$, since no current flows. The cationic charge in a uni-univalent electrolyte is equal and opposite in sign to the anionic charge. Considering a cathode, Eq. (1) becomes

$$\frac{d}{dx}[kT(dn_1/dx)+en_1(E-d\psi/dx)]=0, \tag{4a}$$

$$\frac{d}{dx}[kT(dn_2/dx)-n_2e(E-d\psi/dx)]=0. \tag{4b}$$

The Poisson equation assumes the form

$$\frac{d^2\psi}{dx^2}=\frac{-4\pi e}{D}(n_1-n_2). \tag{5}$$

Integration of this set of second-order differential equations is shown in the appendix to yield

$$\frac{1}{n_1^2}\left(\frac{dn_1}{dx}\right)^2=\frac{2}{kT}\left[\frac{4\pi e^2n_1}{D}-\frac{1}{n_1}\left(\frac{aN_0e^2E^2}{kT}-\frac{4\pi e^2a^2N_0^2}{D}\right)+\frac{2e^2E^2a^2N_0^2}{kTn_1^2}\right]-\frac{2e^2}{kT}\left(\frac{E^2}{kT}+\frac{8\pi aN_0}{D}\right) \tag{6}$$

which can be written in the Weierstrassian normal form[5]

$$M(dn_1/dx)^2=4n_1^3-g_2n_1-g_3, \tag{7}$$

where the g's and M are constants. Equation (7) can be solved in terms of the Weierstrassian function $p(n_1)$: from the equation

$$4n_1^3-\left(\frac{DE^2}{\pi kT}+8aN_0\right)\cdot n_1^2-\left(\frac{DE^2aN_0}{\pi kT}-4a^2N_0^2\right)\cdot n_1+\frac{2E^2Da^2No^2}{\pi kT}=0 \tag{8}$$

the invariants g_2 and g_3 are given by

$$g_2=-\frac{7}{3}\frac{DE^2aN_0}{\pi kT}+\frac{4}{3}(aN_0)^2+\frac{1}{12}\left(\frac{DE^2}{\pi kT}\right)^2, \tag{9}$$

$$g_3=\frac{1}{12}\left(\frac{DE^2}{\pi kT}+8aN_0\right)\left[\frac{DE^2aN_0}{\pi kT}-(2aN_0)^2+\frac{1}{18}\left(\frac{DE^2}{\pi kT}+8aN_0\right)^2\right]-\frac{2D}{\pi kT}(EaN_0)^2. \tag{10}$$

Assuming reasonable values for the constants involved, e.g., an externally applied field of 1 v/cm and a bulk concentration of $m/10$ at 300°K, inserting numerical values into Eqs. (9) and (10) shows that the second term in g_2 is several orders of magnitude larger than the sum of the other two terms,

$$g_2\simeq 4a^2N_0^2/3. \tag{11}$$

Likewise, considering g_3, the term involving $(aN_0)^3$ is many orders of magnitude larger than the other terms, so that

$$g_3\simeq -8a^3N_0^3/27. \tag{12}$$

Equation (7) can now be written as follows:

$$x+\text{const}=\left(\frac{kTD}{2\pi e^2}\right)^{\frac{1}{2}}\int\frac{dz}{(4z^3-g_2z-g_3)^{\frac{1}{2}}}, \tag{13}$$

where

$$z=n_1-1/12(DE^2/\pi kT+8aN_0). \tag{14}$$

The first term in the bracket may again be neglected, being many orders of magnitude smaller than the term involving aN_0.

Substituting now for the invariants the values given in Eqs. (11) and (12) and introducing the new variable ζ defined by

$$\zeta=aN_0z \tag{15}$$

yields on integration

$$\zeta+\text{const}=p\left(\frac{2\pi e^2aN_0}{kTD}\right)^{\frac{1}{2}}=p(\xi). \tag{16}$$

Solving the cubic polynomial in Eq. (13) yields one root at $-2/3$ and a double root at $+1/3$. $p(\xi)$ therefore degenerates, and two cases can be distinguished: One yields two imaginary periods $w_1=-j\pi/2$ and $w_2=j\infty$; this cannot apply because the argument is real. The other solution, however, produces one real period $w_1=\infty$ and the required solution is given by

$$p(\xi)=-(2/3)+\text{cotanh}^2(\xi). \tag{17}$$

This treatment, of course, assumes that the dielectric constant is real, i.e., that the dielectric behaves as a perfect insulator. If this is not the case, i.e., if the dielectric exhibits conductivity becoming permeable to, say, electrons, the present treatment would have to be revised. However once current flows, the electrode then would no longer be polarized.

Introducing the Debye length $1/K$ and resubstituting yields for the mean local cation concentration near a cathode

$$n_1=aN_0\,\text{cotanh}^2(Kx/2). \tag{18}$$

From Eq. (39) in the appendix, using the identity

$$\tanh^2u/2=\frac{\cosh u-1}{\cosh u+1}, \tag{19}$$

the mean local anion concentration follows as

$$n_2=n_1+\frac{D}{4\pi e^2}\left(-\frac{eE\alpha N_0}{n_1}\frac{2K}{\sinh Kx}-\frac{2kTK^2}{\sinh^2Kx}\cosh Kx\right). \tag{20}$$

[5] E. T. Whittaker and G. N. Watson *A Course of Modern Analysis* (Cambridge University Press, Cambridge, 1935), pp. 429 ff.

It is readily seen that for all practicable values of E the first term in the bracket of Eq. (20) is at least 5 orders of magnitude smaller than the second term so that, very nearly,

$$n_2 = n_1 - 4\frac{\cosh xK}{\sinh^2 Kx}. \tag{21}$$

The ratios of the mean local concentrations n_1 and n_2, respectively, to the bulk concentration aN_0, calculated from Eqs. (18) and (21) are plotted in Fig. 1 against Kx.

The mean local charge density ρ is given by

$$\rho = e(n_1 - n_2). \tag{22}$$

and follows on substitution for n_1 and n_2 as

$$\rho = \frac{4aN_0 e \cosh Kx}{\sinh^2 Kx}. \tag{23}$$

The mean local potential ψ in the electric double layer is obtained from Eqs. (5) and (23),

$$\frac{d^2\psi}{dx^2} = -\frac{16aN_0}{D}\frac{\cosh Kx}{\sinh^2 Kx} \tag{24}$$

which integrates to

$$\frac{d\psi}{dx} = \frac{16\pi eaN_0}{DK \sinh Kx} + \text{const.} \tag{25}$$

Since in the bulk of the solution $(d\psi/dx)=0$, $x\to\infty$, the constant vanishes. Equation (25) integrates under the stated boundary conditions to

$$\psi = (2kT/e) \log_e \tanh(Kx/2). \tag{26}$$

The total potential at any point in the double layer then follows as

$$\varphi = \psi + Ex. \tag{27}$$

Figure 1 shows calculated values of φ as $f(Kx)$ for $E=0.1$ V/cm. The total charge Q contained in the electric double layer can be expressed as

$$Q = \int_v \rho dx, \tag{28}$$

where the integration has to be extended over all space containing free charges. If the ions are allowed to approach the electrode infinitely closely, i.e., if x is permitted to approach 0 as a limit, the integral in Eq. (28) also approaches infinity. ψ would also become infinite. A vanishing value of x would further imply ions actually reaching the cathode, causing a flow of current. The electrode then would no longer be polarized.

It therefore appears that the integration must not be carried through right to the surface of the electrode, but only up to a "distance of closest approach," x_1. Physically, the introduction of this quantity implies that the present analysis is concerned with the problem of the diffuse layer; the potential ψ at x_1 is identical with the "zeta potential." x_1 may then be identified with the "rigid boundary" discussed by William, Alberty, and Kraemer:[6] a thin layer of liquid phase is held so tightly on the surface of the electrode that thermal motion within this layer becomes negligible. Its outer edge is called the "rigid boundary" and the potential differences between this boundary and the interior of the solution is the "zeta potential."

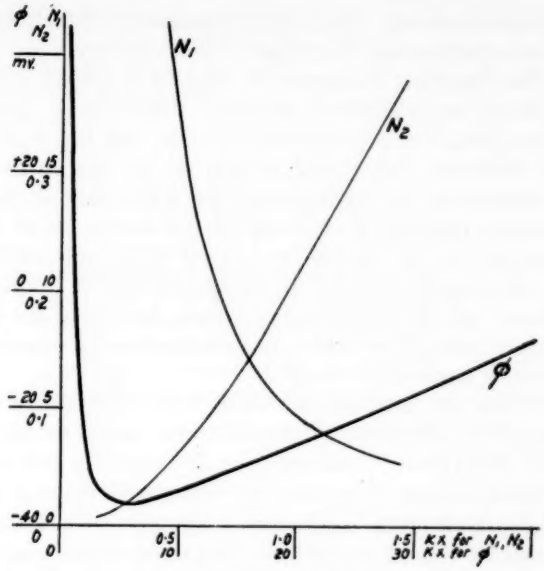

FIG. 1. Plot of calculated values of the mean local potential φ, the mean local cation concentration N_1 and the mean local anion concentration N_2 in the diffuse double layer *versus* the relative distance from the electrode Kx, $1/K$ being the Debye length.

Q thus follows as

$$Q = (-4eaN_0)/(K \sinh Kx). \tag{29}$$

DISCUSSION

It is of interest to combine Eqs. (26) and (18),

$$\psi = (kT/e) \log_e n_1. \tag{30}$$

This shows that the mean local ionic potential in the double layer is merely the thermodynamic potential due to the increased activity of the cations near the electrode, the system behaving as a concentration cell. However, this is not surprising, since the original Debye-Hückel Eq. (1) presupposes a reversible system.

Equation (26) permits experimental verification in the case of certain electrically charged surface layers. Alexander and Powell[7] have found good agreement of this expression with their experimental results.

Equation (30) indicates that a polarized electrode is a

[6] Williams, Alberty, and Kraemer in *A Treatise on Physical Chemistry* edited by H. S. Taylor and S. Glasstone, (D. Van Nostrand Company, Inc., New York, 1951), third edition, p. 633.

[7] A. E. Alexander and B. Powell, J. Phys. Coll. Chem. (to be published), and private communication.

reversible system. That this is the case has been shown in an experimental investigation by Newbery.[8]

The foregoing treatment is valid for a system where a finite, nonvanishing potential difference is maintained between a polarized electrode and the bulk of the solution. The actual magnitude of this potential is immaterial, as follows from the degeneracy of $p(\xi)$. Its only function is to build up the double layer, the structure of the double layer itself being independent of the magnitude of the applied potential. This, of course, will be only approximately true, because the permittivity of the dielectric, assumed to be constant, actually varies with x and E.

While the integrals describing this variation in the immediate proximity of the electrode cannot be solved in a closed form,[9] Grahame[10] has discussed the influence of the lowering of the dielectric constant of water in the double layer. The conclusion is that in a Stern-Gouy model of double layer the deviations introduced by neglecting the effect are not serious.

Once the applied potential vanishes, the present analysis strictly no longer applies. Under these circumstances, the equation given by Grahame[11] is valid,

$$\psi=\pm\frac{4kT}{ze}\tanh^{-1}e^{-Kx}. \tag{31}$$

However, expanding both functions shows that for small values of Kx Eqs. (31) and (26) may be expressed in a similar form differing only by a constant. Equation (26) is to be preferred, since it is of general applicability and not limited to $E=0$.

APPENDIX

Integration of Eqs. (4a), (4b), (5)

Writing

$$E=-dV/dx, \tag{32}$$

Eqs. (4a) and (4b) integrate to

$$kTdn_1/dx+en_1(dV/dx+d\psi/dx)=A, \tag{33a}$$

and

$$kTdn_2/dx-en_2(dV/dx+d\psi/dx)=B. \tag{33b}$$

Dividing (33a) by n_1 and (33b) by n_2, adding and multiplying by n_1n_2 yields, after differentiation with respect to x,

$$\frac{d}{dx}\left[\frac{kT}{n_1}\frac{dn_1}{dx}\right]+e\frac{d^2\psi}{dx^2}=\frac{d}{dx}\left(\frac{A}{n_1}\right), \tag{34a}$$

$$\frac{d}{dx}\left[\frac{kT}{n_2}\frac{dn_2}{dx}\right]-e\frac{d^2\psi}{dx^2}=\frac{d}{dx}\left(\frac{B}{n_2}\right), \tag{34b}$$

noting that $d^2V/dx^2=0$. From the boundary conditions it follows that

$$A=-aN_0eE, \tag{35}$$
$$B=-A.$$

Substituting Eq. (5) into Eq. (34) and solving for n_2,

$$n_2=n_1+\frac{D}{4\pi e^2}\cdot\frac{d}{dx}\left(\frac{A}{n_1}-\frac{kT}{n_1}\frac{dn_1}{dx}\right). \tag{36}$$

On differentiation of Eq. (36) and substitution we obtain, after suitable rearrangement,

$$\frac{2}{\mu}n_1dn_1+d\left[n_1\frac{d}{dx}f(n_1)\right]=\frac{A}{kT}d[f(n_1)], \tag{37}$$

where $\mu=D/4\pi e^2$ and

$$f(n_1)=[A/n_1-(kT/n_1)\cdot(dn_1/dx)]. \tag{38}$$

Integrating Eq. (37),

$$\frac{n_1^2}{\mu}-kT\frac{d^2n_1}{dx^2}+\frac{kT}{n_1}\left(\frac{dn_1}{dx}\right)^2-\frac{A}{kTn_1}+C=0, \tag{39}$$

where, from the boundary conditions,

$$C=aN_0e^2E^2/kT-4\pi e^2a^2N_0^2/D. \tag{40}$$

Equation (39) can readily be written in Bernouilli's form,

$$dp/dn_1-p/n_1=\frac{1}{kT}\cdot\left(n_1^2/\mu+C-\frac{A^2}{kTn_1}\right)\cdot p^{-1}, \tag{41}$$

where $p=dn_1/dx$. This integrates to

$$\frac{p^2}{n_1^2}=\frac{2}{kT}\left(\frac{n_1}{\mu}-\frac{C}{n_1}+\frac{A^2}{2kTn_1^2}\right)+K. \tag{42}$$

From the boundary conditions it follows that

$$K=-\frac{2e^2}{kT}\left(\frac{E^2}{kT}+\frac{8\pi aN_0}{D}\right). \tag{43}$$

Equation (6) is then obtained from Eq. (42) after suitable rearrangement.

[8] E. Newbery, Trans. Faraday Soc. **43**, 127 (1947).
[9] Conway, Bockris, and Amar, Trans. Faraday Soc. **47**, 766 (1951).
[10] D. C. Grahame, J. Chem. Phys. **18**, 903 (1950).
[11] D. C. Grahame, Chem. Revs. **41**, 441 (1947).

Dielectric Constant Theory for Polar Liquids

WILLIAM FULLER BROWN, JR.
Sun Physical Laboratory, Newtown Square, Pennsylvania
(Received February 19, 1953)

In Debye's theory of polar fluids, the electrostatic interaction of the molecules was taken into account by introducing the Lorentz local field formula. This formula is inaccurate, especially for liquids. More recent treatments are of two types. One, developed by Onsager, treats one molecule explicitly and replaces the others with a continuum. The other, developed by Kirkwood, uses the statistical mechanical theory of strongly interacting molecules. The second method is rigorous and can be used to derive the approximate results of the first; nevertheless, the first has remained popular because of its simplicity. The treatment presented here attempts to combine the rigor of Kirkwood's method with the simplicity of Onsager's. This is done by use of several useful theorems of classical electrostatics, which are overlooked when dielectrics are treated in the traditional textbook manner. The result is shown to be equivalent to Kirkwood's; but it is in a more flexible form, and it can, therefore, be used to derive approximations of a more general class.

THE molecular systems treated in the theory of the dielectric constant have three characteristics that complicate the theory: (1) they obey quantum laws; (2) they interact electrostatically; and (3) they are subject to thermal agitation. If all three of these complicating characteristics are neglected, we need only the theory of an assembly of classical noninteracting polarizable particles, each in static equilibrium in the field; the resulting formula is $\epsilon-1=\text{const}\times n\alpha$, where ϵ is the dielectric constant, n is the number of particles per cm^3, and α is the polarizability of a particle. If only one complicating characteristic is introduced, we get: (1) a quantum formula for α; (2) a local field correction such as that of Lorentz [$\epsilon-1$ to be replaced by $3(\epsilon-1)/(\epsilon+2)$]; or (3) a Debye theory of polar molecules (α to be supplemented by a term $\mu_0^2/3kT$, resulting from orientation of the permanent dipole moments μ_0). If two complicating characteristics are introduced simultaneously, any one of the resulting three problems easily fills a book. The book on quantum systems in thermal agitation (1 and 3) is Van Vleck's well-known treatise.[1] The book on quantum systems interacting electrostatically at $T=0$ (1 and 2) apparently has not yet been written. On classical interacting systems in thermal agitation (2 and 3) two books have been written: one by Fröhlich[2] and one by Böttcher.[3] The discussion to be given here relates to this last field of study: in particular, to the dielectric constants of polar liquids.

In this application, the Lorentz local field formula is notoriously unsuccessful. There have been two more recent theoretical approaches to the problem: Onsager's,[4] based on a continuum approximation, and Kirkwood's,[5] based on rigorous methods of statistical mechanics. Kirkwood showed that his general formula reduced to Onsager's when the appropriate approximation was introduced; logically, therefore, Onsager's theory should be regarded as superseded by Kirkwood's. Actually, Onsager's treatment is still widely quoted; for instance, Böttcher's book discusses it in detail but devotes only two sentences to Kirkwood's treatment. The reason is clear. Onsager's calculation requires only elementary statistical mechanics and standard electrostatic theory; it can, therefore, be understood without previous study of highly specialized topics. Kirkwood's, on the contrary, requires considerable familiarity with the statistical mechanical theory of liquids.

The calculation to be presented here combines the simplicity of Onsager's theory with the generality of Kirkwood's. In common with Onsager's calculation, it relies mainly on electrostatic principles and uses only the more elementary formulas of statistical mechanics; but it applies the electrostatic principles in such a way that Onsager's approximation is unnecessary. The result is equivalent to Kirkwood's result but is in a different and slightly more general form. It can be used directly as a basis for approximations of a more general class than Onsager's.

The electrostatic principles required are summarized in Sec. 1. This section deals entirely with macroscopic electrostatics and has no immediate relation to molecular theory. The equations developed relate to the behavior of polarized bodies immersed in a fluid dielectric. Most of the equations are stated without proof, but with page references to publications where proofs can be found. These references will also be useful to readers who desire more complete discussions of the topics covered.

The molecular problem is attacked in Sec. 2. It is partly transformed into a macroscopic problem, to which the formulas of Sec. 1 are applicable. By this device, it is reduced to a simpler molecular problem, which is then solved by elementary methods.

The critical reader will not find the argument in Sec. 2 entirely convincing, and it is not offered as a rigorous one. A rigorous method of deriving the same

[1] J. H. Van Vleck, *The Theory of Electric and Magnetic Susceptibilities* (Oxford University Press, London, 1932).
[2] H. Fröhlich, *Theory of Dielectrics: Dielectric Constant and Dielectric Loss* (Oxford University Press, London, 1949).
[3] C. J. F. Böttcher, *Theory of Electric Polarisation* (Elsevier Publishing Company, Houston, 1952).
[4] Lars Onsager, J. Am. Chem. Soc. **58**, 1486–1493 (1936).
[5] John G. Kirkwood, J. Chem. Phys. **7**, 911–919 (1939).

result is outlined briefly in Sec. 3. This is done by demonstrating the equivalence of the result to Kirkwood's result and by indicating the essential steps in a direct derivation.

Section 4 relates the present formulas to Onsager's; Sec. 5 summarizes the conclusions.

The notation in Sec. 1 has been based on that of the publications from which the main formulas [Eqs. (1.4)–(1.9)] are taken. In the extension of the notation to molecular theory, the following rules have been adopted. The electric moment of a *molecule* is represented by $\boldsymbol{\mu}$, of a *macroscopic region* or body by $\mathbf{m}$, and of a *whole system* (fluid in a container) by $\mathbf{M}$. Various special kinds of moment, within these general classes, are distinguished by subscripts: $\mathbf{m}_q$, $\mathbf{m}_s$. An additional subscript 0 is used to indicate that a *molecular* moment is to be evaluated when the *local field* acting on the molecule is zero ($\boldsymbol{\mu}_0$), or that a *macroscopic* moment is to be evaluated when the *macroscopic field intensity* is zero ($\mathbf{m}_{q0}$). If a *molecular* moment is to be evaluated when the *macroscopic* field intensity is zero, a prime and a subscript zero are used: $\boldsymbol{\mu}_0'$. Finally, all these moments have Cartesian components in various sets of axes. The components along axes fixed *in space* are identified by subscripts x, y, z: μ_{0x}', m_{q0z}. The components along axes fixed *in the molecule* are identified by subscripts 1, 2, 3: μ_{0i}', $m_{q0i}(i=1, 2, 3)$.

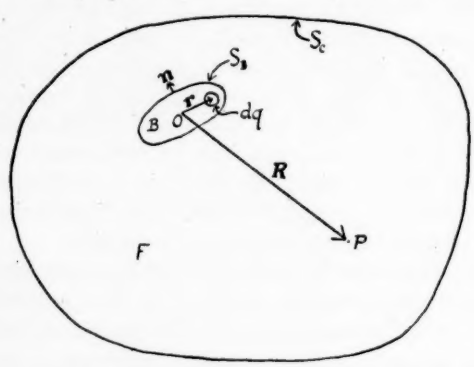

FIG. 1. A polarized body B is immersed in a fluid F, whose dielectric constant is ϵ. The fluid is bounded externally by a container of very large dimensions. Under conditions specified in the text, the behavior of the body can be conveniently described by introduction of an electric moment $\mathbf{m}_q$, different from the moment $\mathbf{m}$ of the body itself, and defined by Eq. (1.7).

1. ELECTROSTATIC PRINCIPLES

The macroscopic field intensity $\mathbf{E}$ is by definition the negative gradient of a scalar potential Φ:

$$\mathbf{E}=-\nabla\Phi. \tag{1.1}$$

The potential Φ can be defined, under all conditions, as[6]

$$\Phi=\frac{\gamma}{4\pi}\int\frac{dq}{R}. \tag{1.2}$$

Here dq is an element of charge, R is distance from the charge element dq to the field point, and γ is a constant (4π in Gaussian units, 1 in Lorentz-Heaviside). The elements dq include: (1) conduction charges dq_c, free to move over macroscopic distances; (2) polarization charges dq_p, able to undergo only small displacements with respect to electrically opposite charges (to which they are bound by intramolecular forces). The elements of polarization charge dq_p are related to the polarization vector $\mathbf{P}$, the electric moment per unit volume. Associated with a volume element $d\tau$ inside a polarized body, there is a charge element $dq_p=-\nabla\cdot\mathbf{P}d\tau$. Associated with a surface element dS on the bounding surface of a polarized body, there is a charge element $dq_p=\mathbf{n}\cdot\mathbf{P}dS$; $\mathbf{n}$ is the unit outward normal.

In Eq. (1.2) the contribution of polarization charges to the potential has been taken into account by writing $dq(=dq_c+dq_p)$ in the formula rather than merely dq_c. An alternative formula is often encountered, in which only the conduction charge elements dq_c appear in the integral; the effect of the polarization charges is then taken into account by inserting a dielectric constant in the denominator. This alternative formula is valid only under special conditions;[7] it will not be used here.

For a fluid dielectric at constant and uniform temperature and at field intensities of ordinary magnitude,

$$\mathbf{P}=[(\epsilon-1)/\gamma]\mathbf{E}, \tag{1.3}$$

where ϵ is the dielectric constant. For given density, ϵ is independent of $\mathbf{E}$; but, in general, ϵ varies with the density. A thermodynamic argument[8,9] then shows that in a body of fluid in equilibrium, within a container at uniform temperature, but in a nonuniform electric field, the density varies with the field intensity $\mathbf{E}$. Consequently, ϵ varies with position, in accordance with the variations of $\mathbf{E}$. However, the variable term in ϵ is proportional to E^2 and, therefore, of the same order as terms that have already been neglected in Eq. (1.3). Accordingly, ϵ will hereafter be treated as a constant, independent of position, for a given fluid at a given temperature.

In any region where there is no conduction charge, the electric displacement vector $\mathbf{D}=\mathbf{E}+\gamma\mathbf{P}$ satisfies $\nabla\cdot\mathbf{D}=0$. For a fluid, by Eq. (1.3), $\mathbf{D}=\epsilon\mathbf{E}$; and since ϵ is independent of position, $\nabla\cdot\mathbf{E}=0$ and $\nabla\cdot\mathbf{P}=0$ within the fluid. Since $\nabla\cdot\mathbf{P}=0$, there are no volume elements of polarization charge within the fluid; the only elements dq_p contributed by the fluid are surface elements, at the surfaces of contact of the fluid with its container and with bodies immersed in it.

Consider an arbitrarily polarized body B, bounded by a surface S_B. Let it be immersed in a fluid dielectric F; let the fluid be bounded externally, at a surface S_C,

[6] Max Abraham, *The Classical Theory of Electricity and Magnetism*, revised by Richard Becker, translated by John Dougall (G. E. Stechert and Company, New York, 1932), pp. 72 ff.

[7] See *The Teaching of Electricity and Magnetism at the College Level* (Report of the Coulomb's Law Committee of the A.A.P.T.), Am. J. Phys. **18**, 1–25 and 69–88 (1950).

[8] Reference 6, pp. 91–100.

[9] William Fuller Brown, Jr., Am. J. Phys. **19**, 290–304, 333–350 (1951), Sec. 2.3.

by a very large container C (Fig. 1). Within F, the potential Φ at any point P can be calculated by Eq. (1.2). Charge elements dq on and outside the external surface S_C contribute a term Φ_e; charge elements dq on and inside the internal surface S_B contribute a term Φ_i; there are no charge elements between S_B and S_C.

At distances R that are large in comparison with the dimensions of B, the term Φ_i is of dipole form,[10,11]

$$\Phi_i=\frac{\gamma}{4\pi}\frac{\mathbf{m}_q\cdot\mathbf{R}_0}{R^2}, \tag{1.4}$$

with

$$\mathbf{m}_q=\int_{B\text{ and }S_B}\mathbf{r}dq. \tag{1.5}$$

In Eq. (1.4), $\mathbf{R}_0$ is a unit vector along $\mathbf{R}$, which is now drawn from an arbitrary origin in B to the field point P. In Eq. (1.5), $\mathbf{r}$ is drawn from 0 to the charge element dq. In the integral, the charge elements dq are of three kinds: (1) volume elements $-\nabla\cdot\mathbf{P}_B d\tau$ within B; (2) surface elements $\mathbf{n}\cdot\mathbf{P}_B dS$ on S_B, contributed by the normal component of polarization $\mathbf{P}_B$ *of the immersed body* ($\mathbf{n}$ is now drawn outward from the body); (3) surface elements $-\mathbf{n}\cdot\mathbf{P}_F dS$ on S_B, contributed by the normal component of polarization $\mathbf{P}_F(=\gamma^{-1}(\epsilon-1)\mathbf{E})$ *of the fluid*.

In Eq. (1.5), the two terms contributed by polarization $\mathbf{P}_B$ of the immersed body can be combined to give

$$\mathbf{m}=\int_B\mathbf{P}_B d\tau; \tag{1.6}$$

this is the electric moment of the polarized matter of the body B. Then

$$\mathbf{m}_q=\mathbf{m}-\int_{S_B}\mathbf{r}\mathbf{n}\cdot\mathbf{P}_F dS; \tag{1.7}$$

this is the electric moment that appears in the potential formula (1.4). A formula directly relating $\mathbf{m}_q$ to $\mathbf{m}$ can be derived if the body B is a uniformly polarized ellipsoid.[11] For a thin needle-ellipsoid polarized along its long axis, $\mathbf{m}_q=\mathbf{m}/\epsilon$; for a thin disk-ellipsoid polarized along its short axis, $\mathbf{m}_q=\mathbf{m}$.

Under certain restrictions, the force and couple exerted on a small polarized body B, immersed in a fluid of dielectric constant ϵ, are[11]

$$\mathbf{F}=\epsilon\mathbf{m}_q\cdot\nabla\mathbf{E},\quad \mathbf{L}=\epsilon\mathbf{m}_q\times\mathbf{E}; \tag{1.8}$$

both can be calculated by differentiation (at constant $\mathbf{E}$) of a potential energy

$$W=-\epsilon\mathbf{m}_q\cdot\mathbf{E}. \tag{1.9}$$

In these formulas, $\mathbf{E}$ is the field intensity computed at the position of the body B but with the body absent. One of the restrictions is that the container must be very large in comparison with the dimensions of the body B; for the "image" field, i.e., the field of polarization charges induced on the outer surface S_C of the fluid when the body B is introduced, must be negligibly small. In general, $\mathbf{m}_q$ must be evaluated when the body B is under the influence of the field; but in the application to be made here, all that is required is an expression for W correct to the first order in $\mathbf{E}$, and therefore $\mathbf{m}_q$ may be replaced by its value $\mathbf{m}_{q0}$ when $\mathbf{E}=0$.

We can imagine a fictitious class of bodies that carry permanent distributions of conduction charge and have, in addition, a dielectric constant equal to that of the fluid.[12] An actual polarized body immersed in the fluid, under specified conditions, is equivalent to such a body with $\int dq_c=0$ and with $\int\mathbf{r}dq_c=\epsilon\mathbf{m}_q$; $\mathbf{m}_q$ must be evaluated for the actual body under the specified conditions. This equivalence will now be used to establish an important relation.

Consider an actual small polarized body B, immersed in a fluid in a large ellipsoidal vessel; the vessel is to be nonconducting and nonpolarizable. Let the whole be subjected to a uniform applied electric field of intensity $\mathbf{E}_a$. With the body B absent, the field intensity within the container has a uniform value $\mathbf{E}$; the uniformity is a consequence of the ellipsoidal shape. The value $\mathbf{E}$ can be calculated from $\mathbf{E}_a$ and from the depolarizing factors of the bounding ellipsoid.[13–15] With the body B present but the applied field $\mathbf{E}_a$ absent, the moment $\mathbf{m}_q$ has a certain value $\mathbf{m}_{q0}$. In the first of these situations, the potential Φ_1 inside and outside the fluid can be attributed to conduction charges dq_1 far outside the vessel and to polarization charges induced by them on the external fluid surface. In the second, the potential Φ_2 can be attributed to conduction charges dq_2 in an equivalent body of the fictitious class just described, with $\int\mathbf{r}dq_2=\epsilon\mathbf{m}_{q0}$, and to polarization charges induced by them on the external fluid surface and within the body. Under these conditions, the reciprocity theorem of electrostatics[16] asserts that

$$\int_{\text{space}}\Phi_1 dq_2=\int_{\text{space}}\Phi_2 dq_1. \tag{1.10}$$

But for the special charge distributions considered,

$$\int_{\text{space}}\Phi_1 dq_2=-\mathbf{E}\cdot\int\mathbf{r}dq_2=-\epsilon\mathbf{m}_{q0}\cdot\mathbf{E}, \tag{1.11}$$

[10] Reference 6, pp. 23 and 73.

[11] Reference 9, Sec. 2.5. In the present application the magnetic quantities $\mathbf{m}$, $\mathbf{m}_p$, $\mathbf{H}$, $\mathbf{B}$, $\mathbf{M}$, and $(\kappa_m)_A$ are to be replaced by the analogous electric quantities $\mathbf{m}$, $\mathbf{m}_q$, $\mathbf{E}$, $\mathbf{D}$, $\mathbf{P}$, and $\epsilon(=(\kappa_\epsilon)_A)$, respectively.

[12] Reference 7, Appendix A.

[13] Julius Adams Stratton, *Electromagnetic Theory* (McGraw-Hill Book Company, Inc., New York, 1941), first edition, pp. 207–217.

[14] J. A. Osborn, Phys. Rev. **67**, 351–357 (1945).

[15] Edmund C. Stoner, Phil. Mag. **36**, 803–821 (1945).

[16] J. H. Jeans, *The Mathematical Theory of Electricity and Magnetism* (Cambridge University Press, Cambridge, 1925), fifth edition, p. 163.

and

$$\int_{\text{space}} \Phi_2 dq_1 = \frac{\gamma}{4\pi} \int \frac{\mathbf{M}_0 \cdot \mathbf{R}_0}{R^2} dq_1$$
$$= \mathbf{M}_0 \cdot \frac{\gamma}{4\pi} \int \frac{\mathbf{R}_0 dq_1}{R^2} = -\mathbf{M}_0 \cdot \mathbf{E}_a, \quad (1.12)$$

where $\mathbf{M}_0$ is the moment of the entire system when the body B is present but the sources of the external field are absent; $\mathbf{R}$ is drawn from an arbitrary fixed point in the fluid to the distant charges. Therefore

$$-\epsilon \mathbf{m}_{q0} \cdot \mathbf{E} = -\mathbf{M}_0 \cdot \mathbf{E}_a. \quad (1.13)$$

The left member of Eq. (1.13) is the energy W of Eq. (1.9), evaluated to the first order in the field intensity. The right member, therefore, is another expression for this energy. For given $\mathbf{m}_{q0}$ and $\mathbf{E}_a$, the energy depends on the shape of the vessel. In the left member of Eq. (1.13), this shape dependence is contained in the factor $\mathbf{E}$; in the right, it is contained in the factor $\mathbf{M}_0$. The moment $\mathbf{M}_0$ is partly due to polarization charges induced on the external surface of the fluid by the field of the body B. These are the same charges that produce the image field. Their contribution to the total moment $\mathbf{M}_0$ remains finite as the size of the vessel increases.

Equation (1.13) will be useful in the discussion of Kirkwood's theory. It can, of course, be established directly, by evaluation of $\mathbf{E}$ for given $\mathbf{E}_a$ and of $\mathbf{M}_0$ for given $\mathbf{m}_{q0}$. This requires solution of two potential problems in ellipsoidal coordinates.

2. MOLECULAR THEORY

Consider a large ellipsoidal container of fluid in a uniform applied field $\mathbf{E}_a$; the macroscopic field intensity in the fluid then has a uniform value $\mathbf{E}$. Select a particular molecule, whose history is to be followed. About this molecule construct a surface S with the following properties: (1) it moves and rotates with the molecule, as if rigidly attached to it; (2) its distance from the molecule is everywhere large in comparison with molecular dimensions; (3) its largest dimension is small in comparison with the dimensions of the container. Apart from these restrictions, the size and shape of S are arbitrary.

From the history of the molecule, select those times when it has a specified position, described by Cartesian coordinates (x, y, z), to within $d\tau = dxdydz$, and a specified orientation, described by Eulerian angles (ϕ, θ, ψ), to within $d\Omega = \sin\theta d\phi d\theta d\psi$. We wish to evaluate the mean couple exerted on the molecule during these parts of its history.

For calculation of this mean, the molecules other than the selected one are equivalent to a certain continuum. Its properties could be found by averaging the properties of the actual molecular assembly over the specified states; this is a problem in the statistical mechanics of interacting systems. The continuum outside S is, to within completely negligible error, simply a fluid with dielectric constant ϵ. The continuum inside S, and especially in the immediate neighborhood of the selected molecule, has more complicated properties; for here short-range molecular interactions are important. It is precisely at this point that the Onsager-Böttcher model oversimplifies the situation.[17] Nevertheless, the equivalent continuum inside S has *some* definite distribution of density and of polarization; and in its mechanical and electrical interactions with the continuum outside S, it behaves like any macroscopic body. Furthermore, the molecules that it represents are in statistical equilibrium under the joint action of external matter and of the central molecule. Therefore, instead of computing the mean couple on the central molecule, we may compute the mean couple on all the matter inside S: for the part of this couple that is not exerted directly on the central molecule is exerted on other molecules inside S and is transmitted by them to the central molecule. (The central molecule itself is not in statistical equilibrium under the conditions specified; for the maintenance of the specified orientation would require the application of a couple to equilibrate the one being computed.) Finally, the mean couple on the matter in S is given by Eq. (1.8), with $\mathbf{m}_q$ given by Eq. (1.7), and with $\mathbf{m}$ equal to the mean electric moment of all the molecules inside S; the mean is taken over statistical states consistent with the specified orientation of the central molecule.

This argument makes plausible (a rigorous proof will be outlined in Sec. 3) that the molecule's statistical behavior is the same as if it were an isolated particle of moment $\epsilon \mathbf{m}_q$ in a field of intensity $\mathbf{E}$. The couple is derivable from a potential energy $-\epsilon \mathbf{m}_q \cdot \mathbf{E}$. The weighting factor to be used in the Boltzmann formula, in averaging any molecular quantity over orientations, is therefore $e^{\epsilon \mathbf{m}_q \cdot \mathbf{E}/kT}$.

For calculation of the dielectric constant, the quantity to be averaged is the component along $\mathbf{E}$ of the moment $\boldsymbol{\mu}$ of a single molecule. Take $\mathbf{E}$ along the z axis: then for given orientation, the mean is

$$\mu_z = \mu'_{0z} + \alpha' E, \quad (2.1)$$

where μ_{0z}' and α' are functions of ϕ, θ, and ψ but are independent of E. This formula assumes only that terms of higher order than the first in E are negligible; there is no implication that μ_{0z}' and α' have any simple relation to the permanent moment and polarizability of an *isolated* molecule. The mean moment over the whole statistical history of the molecule is

$$\langle \mu_z \rangle_{Av} = \int \mu_z e^{\epsilon m_{qz} E/kT} d\Omega \Big/ \int e^{\epsilon m_{qz} E/kT} d\Omega. \quad (2.2)$$

[17] For a critical analysis of the error in the nonpolar case, see William Fuller Brown, Jr., J. Chem. Phys. **18**, 1193–1200 (1950), Sec. 7.

The result is required only to the first order in E. Therefore $e^{\epsilon m_{qz}E/kT}$ may be replaced by $1+\epsilon m_{q0z}E/kT$ in the coefficient of μ_{0z}' in the numerator and by 1 in the coefficient of $\alpha' E$ and in the denominator. Thus,

$$\langle \mu_z \rangle_{Av} = \epsilon E[\mu_{0z}' m_{q0z}]_{Av}/kT + [\alpha']_{Av} E. \quad (2.3)$$

The square-bracket averages are over all orientations with equal weights. By symmetry, the subscript z in the first such average can be replaced by x or y without affecting the result. On taking $\frac{1}{3}$ the sum of the three expressions and noting that $\boldsymbol{\mu}_0' \cdot \mathbf{m}_{q0}$ must be independent of orientation, we get

$$\epsilon - 1 = \gamma n \langle \mu_z \rangle_{Av}/E = \gamma n\{[\alpha']_{Av} + \epsilon \boldsymbol{\mu}_0' \cdot \mathbf{m}_{q0}/3kT\}. \quad (2.4)$$

Here n is the number of molecules per cm^3.

Equation (2.4) is presented as a generally valid equation, involving no serious approximations except neglect of quantum effects and of quadrupole and higher multipole interactions. It does not solve the problem, because the quantities α', $\boldsymbol{\mu}_0'$, and $\mathbf{m}_{q0}$ still have to be evaluated. But it does provide a starting point for a wide class of approximations, based on approximate evaluation of these quantities by various methods.

In Eq. (2.4), $\boldsymbol{\mu}_0'$ is the mean vector moment of a single molecule in any specified orientation in the fluid, when $\mathbf{E}=0$; $\mathbf{m}_{q0}$ is the corresponding mean vector moment defined by Eq. (1.7), when $\mathbf{m}$ represents the mean moment of the molecules inside S and when the fluid outside S is treated macroscopically. The surface S is molecularly large, macroscopically small, and of arbitrary shape. It is easily shown that if S has been chosen large enough to justify macroscopic treatment of the fluid outside it, then replacement of S by any larger surface surrounding it produces no change in the value of $\mathbf{m}_{q0}$.

3. RELATION TO KIRKWOOD'S THEORY

Kirkwood's formula [reference 5, Eq. (13)] contains the moment $\mathbf{m}_{s0}$ (Kirkwood's $\overline{\boldsymbol{\mu}}$) of a macroscopic sphere surrounding the selected molecule; this moment is evaluated at $\mathbf{E}=0$. To relate $\mathbf{m}_{q0}$ to $\mathbf{m}_{s0}$, let S in Sec. 2 be a sphere. Then $\mathbf{m}_{s0}$ is the moment of the contents of the sphere and is the $\mathbf{m}$ of Eq. (1.7), so that

$$\mathbf{m}_{q0} - \mathbf{m}_{s0} = -\int_S \mathbf{r}(P_r)_F dS = [(\epsilon-1)/\gamma]\int_S \mathbf{r}(\partial\Phi/\partial r) dS. \quad (3.1)$$

The potential Φ is to be evaluated for $\mathbf{E}=0$. It consists of a dipole term $(\gamma/4\pi)\mathbf{m}_{q0}\cdot\mathbf{r}_0/r^2$ and of terms containing spherical harmonics of higher order. In the integration, these other terms drop out because of the orthogonality properties of spherical harmonics. The result is

$$\mathbf{m}_{q0} - \mathbf{m}_{s0} = -\tfrac{3}{2}(\epsilon-1)\mathbf{m}_{q0}. \quad (3.2)$$

Upon substitution of the value of $\mathbf{m}_{q0}$ from Eq. (3.2), Eq. (2.4) becomes

$$\epsilon - 1 = \gamma n\{[\alpha']_{Av} + \epsilon \boldsymbol{\mu}_0' \cdot \mathbf{m}_{s0}/(2\epsilon+1)kT\}. \quad (3.3)$$

This reduces to Kirkwood's formula when the approximation used by him is introduced in the first term. If α is the polarizability of an isolated molecule and if F is the local field, $\alpha' = \alpha F/E$; Kirkwood sets $F/E = 3\epsilon/(2\epsilon+1)$, an approximation borrowed from Onsager.

Since Eq. (2.4) is equivalent to Kirkwood's formula and since Kirkwood's formula was derived by rigorous methods of statistical mechanics, Eq. (2.4) can also be derived by such methods. This can be done, for instance, by repeating Kirkwood's derivation and then reversing the argument just given. A shorter method is the following. Kirkwood begins by showing, in effect, that the energy to be used in the Boltzmann formula is $-\mathbf{M}_0\cdot\mathbf{E}_a$, where $\mathbf{M}_0$ is the mean moment of the whole body of fluid (at $\mathbf{E}=0$) for states consistent with a specified orientation of the chosen molecule. (Kirkwood proved this only for a spherical vessel, but the result holds also for an ellipsoid.) If the surface S is now introduced as in Sec. 2, Eq. (1.13) leads directly to Eq. (2.2) and therefore to Eq. (2.4).

4. RELATION TO ONSAGER'S THEORY

Kirkwood showed that his formula reduces to Onsager's formula if his spherical surface is assumed to contain only a single molecule; such an assumption implies the legitimacy of treating everything except the chosen molecule macroscopically. The same reduction to Onsager's formula follows from Eq. (2.4), by introduction of the same assumption, when S is a sphere. But in this equation, S can have an arbitrary shape. Therefore a more general class of approximations can be obtained by choosing S so that it contains a single molecule of any desired shape.

The calculation is simple for an ellipsoidal molecule, with its moment distributed as uniform (microscopic) polarization throughout its volume. Let the moment of an isolated molecule, in zero field, have components $\mu_{0i}(i=1,2,3)$ along the principal axes of the ellipsoid. Let the induced moment be taken into account by ascribing to the polarizable molecule (σ) an internal (microscopic) dielectric constant $\epsilon\sigma$ (Onsager's n^2). Then[13,18]

$$[\alpha']_{Av} = \frac{1}{3}V(\epsilon\sigma - 1)\gamma^{-1}\epsilon \sum_{i=1}^{3} [\epsilon + D_i(\epsilon\sigma - \epsilon)]^{-1}, \quad (4.1)$$

where V is the volume of the ellipsoid and where D_1, D_2, and D_3 are the depolarizing factors (so defined that $D_1+D_2+D_3=1$). The components of $\boldsymbol{\mu}_0'$ and $\mathbf{m}_{q0}$ along the ellipsoid axes are

$$\mu_{0i}' = \mu_{0i}[\epsilon - D_i(\epsilon-1)] \times [1 + D_i(\epsilon\sigma - 1)]/[\epsilon + D_i(\epsilon\sigma - \epsilon)], \quad (4.2)$$

$$m_{q0i} = \mu_{0i}[1 + D_i(\epsilon\sigma - 1)]/[\epsilon + D_i(\epsilon\sigma - \epsilon)]. \quad (4.3)$$

[18] Th. G. Scholte, Physica **15**, 437–449 (1949).

Equation (2.4) becomes

$$\epsilon-1=n\Big\{\frac{1}{3}V\epsilon(\epsilon\sigma'-1)\sum_{i=1}^{3}[\epsilon+D_i(\epsilon\sigma'-\epsilon)]^{-1}$$
$$+\frac{1}{3}\gamma(kT)^{-1}\epsilon\sum_{i=1}^{3}\mu_{0i}^2[\epsilon-D_i(\epsilon-1)]$$
$$\times[1+D_i(\epsilon\sigma'-1)]^2[\epsilon+D_i(\epsilon\sigma'-\epsilon)]^{-2}\Big\}. \quad (4.4)$$

If numerical values are assigned to the molecular parameters, the density can be found as a function of dielectric constant and temperature by direct numerical calculation.

For a sphere, $D_1=D_2=D_3=\frac{1}{3}$, and Eq. (4.4) reduces to

$$\epsilon-1=\gamma n\{\alpha'+\epsilon\mu_0^2(2\epsilon+1)\times(\epsilon\sigma'+2)^2/9(\epsilon\sigma'+2\epsilon)^2kT\}, \quad (4.5)$$

with

$$\alpha'=3V(\epsilon\sigma'-1)\epsilon/\gamma(2\epsilon+\epsilon\sigma'). \quad (4.6)$$

To obtain Onsager's formula, it is necessary to introduce his additional approximation $nV=1$. Equation (4.5) without this approximation is Böttcher's modification of Onsager's formula;[19] when $\mu_0=0$ it becomes Böttcher's formula for the dielectric constant of a nonpolar liquid.

The "external moment" ($\mathfrak{y}^*$ or $\mathbf{m}^*$) defined by Onsager for his spherical molecule is $\epsilon\mathbf{m}_q$.

5. SUMMARY

A complete theory would produce a rigorous formula for the dielectric constant in terms of known molecular quantities. In the present state of the theory, the best that can be done is to produce an approximate formula in terms of known quantities or a rigorous formula in terms of unknown quantities. The formulas developed in Böttcher's book are of the former type; they are useful but subject to errors. Equation (2.4) is of the latter type; it is free from these errors but not directly useful. From it, however, one can derive useful formulas, such as those of Sec. 4, by introducing approximations. In this way, the introduction of approximations is delayed until the last possible moment, and a single rigorous formula can serve as the basis of a number of different approximate formulas.

As compared with Kirkwood's formula (and the variants of it proposed by Fröhlich[2]), Eq. (2.4) has the advantage that it uses, instead of a sphere, a surface of arbitrary shape; it can, therefore, be used as a starting point for approximations of a more general class. As compared with Kirkwood's derivation, the one given in Sec. 2 will, it is hoped, be more easily followed and understood by persons primarily concerned with analysis of data and not with liquid state theory.

Finally, the application of electrostatic theory made in Sec. 2 demonstrates the importance of some of the points made in the Report of the Coulomb's Law Committee of the American Association of Physics Teachers.[7] This application requires a departure from the traditional textbook way of thinking, according to which all problems concerning dielectrics are taken care of by merely inserting a factor $1/\epsilon$.[20] It is hoped that this paper will stimulate, in those who are interested in dielectrics, a critical attitude toward the traditional presentation, and a demand for textbooks that do not merely reiterate the errors of their predecessors.

[19] C. J. F. Böttcher, Physica **9**, 937–944 (1942), and reference 3.

[20] If a body with zero net charge but with an electric moment $\mathbf{m}$, independent of applied field, is immersed in a fluid of dielectric constant ϵ, the result is not, in general, a simple decrease of the field about the body in the ratio $1/\epsilon$. The reason is that the $1/\epsilon$ theorem holds only when the fluid fills all regions where there is a field; the interior of the immersed body is such a region and is not filled by the fluid.

From the literature on dielectrics it appears that some authors are unaware of this fact. Equations are presented that are correct only if the moment in them is $\epsilon\mathbf{m}_q$, and yet no distinction is drawn between this moment and $\mathbf{m}$. It is because of this prevalent confusion that, in this paper, the quantity $\epsilon\mathbf{m}_q$ has deliberately *not* been represented by a single symbol.

The Effect of Isotopic Substitution on the Entropy, Enthalpy, and Heat Capacity of Ideal Gases. I. Systems in Thermal Equilibrium. II. Chemically Reacting Systems*

JACOB BIGELEISEN
Chemistry Department, Brookhaven National Laboratory, Upton, Long Island, New York
(Received March 4, 1953)

The formulas of Bigeleisen and Mayer for the free energy difference between isotopic compounds are used to derive formulas for the similar differences in entropy, enthalpy, and heat capacity. Tables of these functions are calculated. The analogous quantities in the "thermodynamics of reaction rates" are discussed. Several useful formulas for the entropy differences of isotopic molecules are derived.

INTRODUCTION

IN two previous publications the effects of isotopic substitution on the free energy change[1] and on the rate and activation energies[2] of chemical reactions have been treated in detail. A table has been presented which permits rapid calculation of chemical exchange equilibria from vibrational data alone.[1] From these formulas one can, by standard thermodynamic methods, derive formulas for the effect of isotopic substitution on the entropy, enthalpy, and heat capacity of ideal gases and the analogous quantities in the "thermodynamics" of reaction rates.

I. SYSTEMS IN THERMAL EQUILIBRIUM

It has been pointed out previously that in the calculation of the difference in free energies or in the equilibrium constants of isotopic exchange reactions it is most convenient to use the function f, defined by the relation

$$f=(Q/Q')\pi_i(m_i'/m_i)^{\frac{3}{2}}, \tag{1}$$

where Q and Q' are the total partition functions of a pair of isotopic molecules with the isotopic atoms of mass m_i and m_i', respectively. This amounts to calculating as the ratio of partition functions, the equilibrium constant for the isotopic exchange reaction between some molecule and the free gaseous atoms.

Since the free energy is related to the partition function, Q, by the equation

$$F=-RT\ln Q/N, \tag{2}$$

the difference in the choice of standard states will appear in the free energy and entropy but not in the enthalpy or heat capacity. The usual thermodynamic quantities tabulated in the literature are related to those derived from Eq. (1), which are designated by the subscript r, by the following equations

$$F^0-F^{0\prime}=F_r^0-F_r^{0\prime}-\tfrac{3}{2}RT\textstyle\sum_i\ln m_i/m_i', \tag{3}$$

$$S^0-S^{0\prime}=S_r^0-S_r^{0\prime}+\tfrac{3}{2}R\textstyle\sum_i\ln m_i/m_i', \tag{4}$$

$$H^0-H^{0\prime}=H_r^0-H_r^{0\prime}, \tag{5}$$

$$C_p^0-C_p^{0\prime}=C_p^0{}_r-C_p^{0\prime}{}_r. \tag{6}$$

Inasmuch as the atomic species are conserved in all chemical reactions, it is obvious from the above equations that the functions with the subscript r are most convenient for the study of chemical thermodynamics.

From Eqs. (10) and (15) of B-M, one obtains

$$\frac{F_r^0-F_r^{0\prime}}{RT}=\ln s/s'-\ln\Big[1+\frac{\sigma-\sigma'}{3}+\frac{(\sigma-\sigma')^2}{18}+\frac{\sigma^2-\sigma'^2}{90}\Big]-\textstyle\sum_i[\ln u_i/u_i'+\Delta u_i/2+\ln(1-e^{-u_i'})/(1-e^{-u_i})], \tag{7}$$

$$=\ln s/s'-(\sigma-\sigma')/3-(\sigma^2-\sigma'^2)/90-\textstyle\sum_i[\ln u_i/u_i'+\Delta u_i/2+\ln(1-e^{-u_i'})/(1-e^{-u_i})], \tag{8}$$

$$\frac{S_r^0-S_r^{0\prime}}{R}=\ln s'/s-(\sigma^2-\sigma'^2)/90+\textstyle\sum_i[\ln u_i/u_i'+\ln(1-e^{-u_i'})/(1-e^{-u_i})+u_i/(e^{u_i}-1)-u_i'/(e^{u_i'}-1)], \tag{9}$$

$$\frac{(H^0-H_0^0)-(H^{0\prime}-H_0^{0\prime})}{RT}=-(\sigma-\sigma')/3-(\sigma^2-\sigma'^2)/45+\textstyle\sum_i[u_i/(e^{u_i}-1)-u_i'/(e^{u_i'}-1)], \tag{10}$$

$$\frac{C_p^0-C_p^{0\prime}}{R}=(\sigma^2-\sigma'^2)/45+\textstyle\sum_i[u_i^2e^{u_i}/(e^{u_i}-1)^2-u_i'^2e^{u_i'}/(e^{u_i'}-1)^2]. \tag{11}$$

When $\Delta u=u'-u$ is small and the rotational corrections are negligible, one obtains analogous to B-M (11'a).

$$\frac{F_r^0-F_r^{0\prime}}{RT}=\ln s/s'-\textstyle\sum_i G(u_i)\Delta u_i, \tag{12}$$

where

$$G(u_i)\equiv(\tfrac{1}{2}-1/u_i+1/(e^{u_i}-1)), \tag{13}$$

$$\frac{S_r^0-S_r^{0\prime}}{R}=\ln s'/s-\textstyle\sum_i S(u_i)\Delta u_i, \tag{14}$$

* Research carried out under the auspices of the U. S. Atomic Energy Commission.

[1] J. Bigeleisen and M. G. Mayer, J. Chem. Phys. **15**, 261 (1947), hereinafter referred to as B-M.

[2] J. Bigeleisen, J. Chem. Phys. **17**, 675 (1949).

TABLE I. Functions for the calculation of the effect of isotopic substitution on the entropy, enthalpy, and heat capacity of ideal gases.

u	$S(u)$	$\Delta S/\Delta u$	$H(u)$	$\Delta H/\Delta u$	$C(u)$	$\Delta C/\Delta u$
0.00	0.00000		0.50000		0.00000	
		0.0833		0.1666		0.1666
0.05	0.004166		0.49167		0.008331	
		0.0832		0.1666		0.1664
0.10	0.008329		0.48334		0.01665	
		0.0830		0.1664		0.1658
0.15	0.01248		0.47502		0.02494	
		0.0830		0.1662		0.1652
0.20	0.01663		0.46671		0.03320	
		0.0828		0.1658		0.1642
0.25	0.02077		0.45842		0.04141	
		0.0824		0.1654		0.1628
0.30	0.02489		0.45015		0.04955	
		0.0820		0.1650		0.1614
0.35	0.02899		0.44190		0.05762	
		0.0816		0.1642		0.1596
0.40	0.03307		0.43369		0.06560	
		0.0810		0.1638		0.1576
0.45	0.03712		0.42550		0.07348	
		0.0806		0.1630		0.1554
0.50	0.04115		0.41735		0.08125	
		0.0798		0.1620		0.1528
0.55	0.04514		0.40925		0.08889	
		0.0792		0.1610		0.1502
0.60	0.04910		0.40120		0.09640	
		0.0784		0.1602		0.1474
0.65	0.05302		0.39319		0.10377	
		0.0780		0.1596		0.1446
0.70	0.05692		0.38521		0.11100	
		0.0772		0.1584		0.1416
0.75	0.06078		0.37729		0.11808	
		0.0762		0.1570		0.1386
0.80	0.06459		0.36944		0.12501	
		0.0756		0.1556		0.1352
0.85	0.06835		0.36166		0.13177	
		0.0742		0.1544		0.1318
0.90	0.07206		0.35394		0.13836	
		0.0732				0.1282
0.95	0.07572		0.34628	0.1532	0.14477	
		0.0726				0.1242
1.00	0.07935		0.33862		0.15098	
		0.0706				0.1202
1.05	0.08288		0.33119	0.1486	0.15699	
		0.0704				0.1160
1.10	0.08640		0.32376		0.16279	
		0.0682				0.1100
1.15	0.08981		0.31641	0.1463	0.16829	
		0.0676				0.1050
1.20	0.09319		0.30913		0.17354	
		0.0664				0.1014
1.25	0.09651		0.30194	0.1429	0.17861	
		0.0650				0.0958
1.30	0.09976		0.29484		0.18340	
		0.0636				0.0938
1.35	0.10294		0.28784	0.1393	0.18809	
		0.0624				0.0878
1.40	0.10606		0.28091		0.19248	
		0.0612				0.0830
1.45	0.10912		0.27408	0.1356	0.19663	
		0.0596				0.0788
1.50	0.11210		0.26735		0.20057	
		0.0582				0.0734
1.55	0.11501		0.26071	0.1318	0.20424	
		0.0568				0.0688
1.60	0.11785		0.25417		0.20768	
		0.0556				0.0638
1.65	0.12063		0.24773	0.1278	0.21087	
		0.0540				0.0596
1.70	0.12333		0.24139		0.21385	
		0.0524				0.0544
1.75	0.12595		0.23519	0.1237	0.21657	
		0.0510				0.0494
1.80	0.12850		0.22902		0.21904	
		0.0496				0.0450
1.85	0.13098		0.22299	0.1196	0.22129	
		0.0482				0.0406
1.90	0.13339		0.21706		0.22332	
		0.0464				0.0354
1.95	0.13571		0.21123	0.1155	0.22509	
		0.0452				0.0314
2.00	0.13797		0.20551		0.22666	
		0.0436				0.0266
2.05	0.14015		0.19989	0.1112	0.22799	
		0.0422				0.0226
2.10	0.14226		0.19439		0.22912	
		0.0406				0.0178
2.15	0.14429		0.18900	0.1074	0.23001	
		0.0392				0.0138
2.20	0.14625		0.18365		0.23070	
		0.0374				0.0090
2.25	0.14812		0.17851	0.1023	0.23115	
		0.0362				0.0060
2.30	0.14993		0.17342		0.23145	
		0.0348				0.0016
2.35	0.15167		0.16844	0.0985	0.23153	
		0.0334				−0.0018
2.40	0.15334		0.16357		0.23144	
		0.0316				0.0056
2.45	0.15492		0.15880	0.0944	0.23116	
		0.0306				0.0078
2.50	0.15644		0.15413		0.23077	
		0.0290				0.0148
2.55	0.15789		0.14958	0.0902	0.23003	
		0.0278				0.0162
2.60	0.15928		0.14511		0.22922	
		0.0260				0.0192
2.65	0.16058		0.14076	0.0864	0.22826	
		0.0250				0.0228
2.70	0.16183		0.13647		0.22712	
		0.0234				0.0256
2.75	0.16300		0.13235	0.0821	0.22584	
		0.0222				0.0286
2.80	0.16411		0.12826		0.22441	
		0.0210				0.0312
2.85	0.16516		0.12433	0.0780	0.22285	
		0.0196				0.0336
2.90	0.16614		0.12046		0.22117	
		0.0182				0.0362
2.95	0.16705		0.11666	0.0743	0.21936	
		0.0172				0.0386
3.00	0.16791		0.11303		0.21743	
		0.0160				0.0408
3.05	0.16871		0.10946	0.0706	0.21539	
		0.0146				0.0428
3.10	0.16944		0.10597		0.21325	
		0.0136				0.0450
3.15	0.17012		0.10257	0.0670	0.21100	
		0.0124				0.0466
3.20	0.17074		0.09927		0.20867	
		0.0112				0.0484
3.25	0.17130		0.09606	0.0635	0.20625	
		0.0102				0.0500
3.30	0.17181		0.09292		0.20375	
		0.0092				0.0516
3.35	0.17227		0.08968	0.0601	0.20117	
		0.0082				0.0530
3.40	0.17268		0.08691		0.19852	
		0.0070				0.0540
3.45	0.17303		0.08403	0.0567	0.19582	
		0.0060				0.0554
3.50	0.17333		0.08124		0.19305	
		0.0054				0.0560
3.55	0.17360		0.07850	0.0536	0.19025	
		0.0042				0.0574
3.60	0.17381		0.07588		0.18738	
		0.0034				0.0580
3.65	0.17398		0.07332	0.0506	0.18448	
		0.0024				0.0588

TABLE I.—*Continued.*

u	$S(u)$	$\Delta S/\Delta u$	$H(u)$	$\Delta H/\Delta u$	$C(u)$	$\Delta C/\Delta u$
3.70	0.17410		0.07082		0.18154	
		0.0016				0.0596
3.75	0.17418		0.06841	0.0476	0.17856	
		0.0008				0.0598
3.80	0.17422		0.06606		0.17557	
		−0.0002				0.0604
3.85	0.17421		0.06379	0.0448	0.17255	
		0.0008				0.0608
3.90	0.17417		0.06158		0.16951	
		0.0016				0.0610
3.95	0.17409		0.05944	0.0422	0.16646	
		0.0022				0.0614
4.00	0.17398		0.05736		0.16339	
		0.0030				0.0614
4.05	0.17383		0.05535	0.0395	0.16032	
		0.0038				0.0614
4.10	0.17364		0.05341		0.15725	
		0.0042				0.0614
4.15	0.17343		0.05152	0.0372	0.15418	
		0.0048				0.0614
4.20	0.17319		0.04969		0.15111	
		0.0058				0.0612
4.25	0.17290		0.04791	0.0348	0.14805	
		0.0060				0.0608
4.30	0.17260		0.04621		0.14501	
		0.0068				0.0608
4.35	0.17226		0.04456	0.0327	0.14197	
		0.0072				0.0606
4.40	0.17190		0.04294		0.13894	
		0.0078				0.0598
4.45	0.17151		0.04140	0.0305	0.13595	
		0.0082				0.0596
4.50	0.17110		0.03989		0.13297	
		0.0086				0.0590
4.55	0.17067		0.03843	0.0286	0.13002	
		0.0092				0.0586
4.60	0.17021		0.03703		0.12709	
		0.0096				0.0582
4.65	0.16973		0.03567	0.0267	0.12418	
		0.0100				0.0574
4.70	0.16923		0.03436		0.12131	
		0.0104				0.0570
4.75	0.16871		0.03309	0.0250	0.11846	
		0.0108				0.0562
4.80	0.16817		0.03186		0.11565	
		0.0110				0.0554
4.85	0.16762		0.03066	0.0232	0.11288	
		0.0116				0.0550
4.90	0.16704		0.02954		0.11013	
		0.0116				0.0540
4.95	0.16646		0.02843	0.0218	0.10743	
		0.0122				0.0534
5.00	0.16585		0.02736		0.10476	
		0.0124				0.0526
5.05	0.16523		0.02633	0.0202	0.10213	
		0.0126				0.0518
5.10	0.16460		0.02534		0.09954	
		0.0128				0.0508
5.15	0.16396		0.02436	0.0188	0.09700	
		0.0130				0.0502
5.20	0.16331		0.02346		0.09449	
		0.0134				0.0492
5.25	0.16264		0.02253	0.0175	0.09203	
		0.0136				0.0486
5.30	0.16196		0.02171		0.08960	
		0.0138				0.0476
5.35	0.16127		0.02090	0.0164	0.08722	
		0.0138				0.0466
5.40	0.16058		0.02007		0.08489	
		0.0142				0.0460
5.45	0.15987		0.01925	0.0151	0.08259	
		0.0142				0.0450
5.50	0.15916		0.01856		0.08034	
		0.0144				0.0442
5.55	0.15844		0.01778	0.0141	0.07813	
		0.0146				0.0432
5.60	0.15771		0.01715		0.07597	
		0.0146				0.0424
5.65	0.15698		0.01642	0.0131	0.07385	
		0.0148				0.0414
5.70	0.15624		0.01584		0.07178	
		0.0148				0.0408
5.75	0.15550		0.01517	0.0121	0.06974	
		0.0150				0.0398
5.80	0.15475		0.01463		0.06775	
		0.0150				0.0388
5.85	0.15400		0.01401	0.0113	0.06581	
		0.0152				0.0380
5.90	0.15324		0.01350		0.06391	
		0.0152				0.0372
5.95	0.15248		0.01294	0.0104	0.06205	
		0.0152				0.0362
6.00	0.15172		0.01246		0.06024	
		0.0153				0.0352
6.10	0.15019		0.01150	0.0093	0.05672	
		0.0153				0.0334
6.20	0.14866		0.01060		0.05338	
		0.0154				0.0318
6.30	0.14712		0.00977	0.0079	0.05020	
		0.0154				0.0303
6.40	0.14558		0.00901		0.04717	
		0.0154				0.0287
6.50	0.14404		0.00830	0.0069	0.04430	
		0.0153				0.0273
6.60	0.14251		0.00764		0.04157	
		0.0152				0.0258
6.70	0.14099		0.00703	0.0058	0.03899	
		0.0152				0.0244
6.80	0.13947		0.00648		0.03655	
		0.0151				0.0232
6.90	0.13796		0.00596	0.0050	0.03423	
		0.0149				0.0217
7.00	0.13647		0.00548		0.03206	
		0.0149				0.0207
7.10	0.13498		0.00504	0.0042	0.02999	
		0.0147				0.0194
7.20	0.13351		0.00464		0.02805	
		0.0146				0.0183
7.30	0.13205		0.00426	0.0036	0.02622	
		0.0144				0.0172
7.40	0.13061		0.00392		0.02450	
		0.0143				0.0163
7.50	0.12918		0.00360	0.0031	0.02287	
		0.0141				0.0152
7.60	0.12777		0.00331		0.02135	
		0.0139				0.0143
7.70	0.12638		0.00304	0.0026	0.01992	
		0.0137				0.0135
7.80	0.12501		0.00279		0.01857	
		0.0136				0.0126
7.90	0.12365		0.00266	0.0022	0.01731	
		0.0134				0.0118
8.00	0.12231		0.00235		0.01613	
		0.0131				0.0114
8.10	0.12100		0.00220	0.0019	0.01499	
		0.0131				0.0101
8.20	0.11969		0.00198		0.01398	
		0.0127				0.0097
8.30	0.11842		0.00181	0.0016	0.01301	
		0.0126				0.0091
8.40	0.11716		0.00166		0.01210	
		0.0124				0.0085
8.50	0.11592		0.00153	0.0013	0.01125	
		0.0122				0.0079
8.60	0.11470		0.00140		0.01046	
		0.0121				0.0074
8.70	0.11349		0.00128	0.0011	0.00972	
		0.0118				0.0069

TABLE I.—*Continued.*

u	$S(u)$	$\Delta S/\Delta u$	$H(u)$	$\Delta H/\Delta u$	$C(u)$	$\Delta C/\Delta u$
8.80	0.11231		0.00118		0.00903	
		0.0116				0.0065
8.90	0.11115		0.00107	0.0009	0.00838	
		0.0115				0.0060
9.00	0.11000		0.00099		0.00778	
		0.0113				0.0056
9.10	0.10887		0.00091	0.0008	0.00722	
		0.0110				0.0052
9.20	0.10777		0.00083		0.00670	
		0.0109				0.0049
9.30	0.10668		0.00076	0.0007	0.00621	
		0.0108				0.0045
9.40	0.10560		0.00070		0.00576	
		0.0105				0.0042
9.50	0.10455		0.00064	0.0006	0.00534	
		0.0103				0.0040
9.60	0.10352		0.00058		0.00494	
		0.0102				0.0036
9.70	0.10250		0.00053	0.0005	0.00458	
		0.0100				0.0034
9.80	0.10150		0.00049		0.00424	
		0.0099				0.0032
9.90	0.10051		0.00045	0.0004	0.00392	
		0.0096				0.0029
10.00	0.09955		0.00041		0.00363	
		0.0095				
10.10	0.09860		0.00038	0.0004		0.0026
		0.0094				
10.20	0.09766		0.00034		0.00311	
		0.0092				
10.30	0.09674		0.00032	0.0003		0.0023
		0.0091				
10.40	0.09583		0.00029		0.00266	
		0.0088				
10.50	0.09495		0.00026	0.0003		0.0020
		0.0087				
10.60	0.09408		0.00024		0.00227	
		0.0086				
10.70	0.09322		0.00022	0.0002		0.0017
		0.0084				
10.80	0.09238		0.00020		0.00194	
		0.0084				
10.90	0.09154		0.00018	0.0002		0.0015
		0.0082				
11.00	0.09072		0.00017		0.00165	
		0.0080				
11.10	0.08992		0.00015	0.0002		0.0012
		0.0078				
11.20	0.08914		0.00014		0.00141	
		0.0078				
11.30	0.08836		0.00013	0.0001		0.0011
		0.0077				
11.40	0.08759		0.00012		0.00120	
		0.0075				
11.50	0.08684		0.00011	0.0001		0.0009
		0.0074				
11.60	0.08610		0.00010		0.00102	
		0.0073				
11.70	0.08537		0.00009	0.0001		0.0008
		0.0071				
11.80	0.08466		0.00008		0.00087	
		0.0071				
11.90	0.08395		0.00007	0.0001		0.0007
		0.0069				
12.00	0.08326		0.00007		0.00074	
		0.0068				
12.10	0.08258		0.00006	0.0001		0.0006
		0.0067				
12.20	0.08191		0.00006		0.00063	
		0.0067				
12.30	0.08124		0.00006	0.0000		0.0005
		0.0065				
12.40	0.08059		0.00005		0.00053	
		0.0064				
12.50	0.07995		0.00005	0.0000		0.0004
		0.0063				
12.60	0.07932		0.00004		0.00045	
		0.0062				
12.70	0.07870		0.00004	0.0000		0.0004
		0.0061				
12.80	0.07809		0.00003		0.00038	
		0.0060				
12.90	0.07749					0.0003
		0.0060				
13.00	0.07689		0.00003		0.00032	
		0.0058				
13.10	0.07631					0.0003
		0.0057				
13.20	0.07574		0.00002		0.00027	
		0.0057				
13.30	0.07517					0.0002
		0.0056				
13.40	0.07461		0.00002		0.00023	
		0.0055				
13.50	0.07406					0.0002
		0.0054				
13.60	0.07352		0.00002		0.00020	
		0.0054				
13.70	0.07298					0.0002
		0.0053				
13.80	0.07245		0.00001		0.00016	
		0.0052				
13.90	0.07193					0.0001
		0.0051				
14.00	0.07142		0.00001		0.00014	
		0.0051				
14.10	0.07091					0.0001
		0.0050				
14.20	0.07041		0.00001		0.00012	
		0.0049				
14.30	0.06992					
		0.0048				
14.40	0.06944		0.00001		0.00010	
		0.0048				
14.50	0.06896					
		0.0047				
14.60	0.06849		0.00001		0.00008	
		0.0047				
14.70	0.06802					
		0.0046				
14.80	0.06756		0.00001		0.00007	
		0.0045				
14.90	0.06711					
		0.0045				
15.00	0.06666		0.00000		0.00006	
		0.0044				
15.10	0.06622					
		0.0043				
15.20	0.06579				0.00005	
		0.0043				
15.30	0.06536					
		0.0043				
15.40	0.06493				0.00004	
		0.0042				
15.50	0.06451					
		0.0041				
15.60	0.06410				0.00004	
		0.0041				
15.70	0.06369					
		0.0040				
15.80	0.06329				0.00003	
		0.0040				
15.90	0.06289					
		0.0039				
16.00	0.06250				0.00003	
		0.0039				
16.10	0.06211					
		0.0038				

TABLE I.—*Continued.*

u	$S(u)$	$\Delta S/\Delta u$	$H(u)$	$\Delta H/\Delta u$	$C(u)$	$\Delta C/\Delta u$
16.20	0.06173				0.00002	
		0.0038				
16.30	0.06135					
		0.0037				
16.40	0.06098				0.00002	
		0.0037				
16.50	0.06061					
		0.0037				
16.60	0.06024				0.00001	
		0.0036				
16.70	0.05988					
		0.0036				
16.80	0.05952				0.00001	
		0.0035				
16.90	0.05917					
		0.0035				
17.00	0.05882				0.00001	
		0.0034				
17.10	0.05848					
		0.0034				
17.20	0.05814				0.00001	
		0.0034				
17.30	0.05780					
		0.0033				
17.40	0.05747				0.00001	
		0.0033				
17.50	0.05714					
		0.0032				
17.60	0.05682				0.00001	
		0.0032				
17.70	0.05650					
		0.0032				
17.80	0.05618				0.00001	
		0.0031				
17.90	0.05587					
		0.0031				
18.00	0.05556				0.00000	
		0.0031				
18.10	0.05525					
		0.0031				
18.20	0.05494					
		0.0030				
18.30	0.05464					
		0.0030				
18.40	0.05434					
		0.0029				
18.50	0.05405					
		0.0029				
18.60	0.05376					
		0.0028				
18.70	0.05348					
		0.0029				
18.80	0.05319					
		0.0028				
18.90	0.05291					
		0.0028				
19.00	0.05263					
		0.0028				
19.10	0.05235					
		0.0027				
19.20	0.05208					
		0.0027				
19.30	0.05181					
		0.0027				
19.40	0.05154					
		0.0026				
19.50	0.05128					
		0.0026				
19.60	0.05102					
		0.0026				
19.70	0.05076					
		0.0026				
19.80	0.05050					
		0.0025				
19.90	0.05025					
		0.0025				
20.00	0.05000					
		0.0025				
20.10	0.04975					
		0.0025				
20.20	0.04950					
		0.0024				
20.30	0.04926					
		0.0024				
20.40	0.04902					
		0.0024				
20.50	0.04878					
		0.0024				
20.60	0.04854					
		0.0023				
20.70	0.04831					
		0.0023				
20.80	0.04808					
		0.0023				
20.90	0.04785					
		0.0023				
21.00	0.04762					
		0.0023				
21.10	0.04739					
		0.0022				
21.20	0.04717					
		0.0022				
21.30	0.04695					
		0.0022				
21.40	0.04673					
		0.0022				
21.50	0.04651					
		0.0022				
21.60	0.04629					
		0.0021				
21.70	0.04608					
		0.0021				
21.80	0.04587					
		0.0021				
21.90	0.04566					
		0.0021				
22.00	0.04545					
		0.0020				
22.10	0.04525					
		0.0020				
22.20	0.04505					
		0.0021				
22.30	0.04484					
		0.0020				
22.40	0.04464					
		0.0020				
22.50	0.04444					
		0.0020				
22.60	0.04424					
		0.0019				
22.70	0.04405					
		0.0019				
22.80	0.04386					
		0.0019				
22.90	0.04367					
		0.0019				
23.00	0.04348					
		0.0019				
23.10	0.04329					
		0.0019				
23.20	0.04310					
		0.0018				
23.30	0.04292					
		0.0018				
23.40	0.04274					
		0.0019				
23.50	0.04255					
		0.0018				

TABLE I.—*Continued.*

u	$S(u)$	$\Delta S/\Delta u$	$H(u)$	$\Delta H/\Delta u$	$C(u)$	$\Delta C/\Delta u$
23.60	0.04237					
		0.0018				
23.70	0.04219					
		0.0018				
23.80	0.04201					
		0.0017				
23.90	0.04184					
		0.0017				
24.00	0.04167					
		0.0018				
24.10	0.04149					
		0.0017				
24.20	0.04132					
		0.0017				
24.30	0.04115					
		0.0017				
24.40	0.04098					
		0.0017				
24.50	0.04081					
		0.0016				
24.60	0.04065					
		0.0016				
24.70	0.04049					
		0.0017				
24.80	0.04032					
		0.0016				
24.90	0.04016					
		0.0016				
25.00	0.04000					

where

$$S(u_i)\equiv(1/u_i-u_ie^{u_i}/(e^{u_i}-1)^2), \quad (15)$$

$$\frac{(H^0-H_0^0)-(H^0-H_0^0)'}{RT}=\sum_i H(u_i)\Delta u_i, \quad (16)$$

where

$$H(u_i)\equiv(u_ie^{u_i}/(e^{u_i}-1)^2-1/(e^{u_i}-1)), \quad (17)$$

$$\frac{C_p^0-C_p^{0\prime}}{R}=\sum_i C(u_i)\Delta u_i, \quad (18)$$

where

$$C(u_i)\equiv(2u_i^2e^{2u_i}/(e^{u_i}-1)^3 - u_i(u_i+2)e^{u_i}/(e^{u_i}-1)^2). \quad (19)$$

These equations are valid for the isotopes of all elements except hydrogen and helium. The latter has no chemistry.

When u is small in addition to Δu, then

$$G(u_i)=(1-u_i^2/60)u_i/12, \quad (20)$$

$$S(u_i)=(1-u_i^2/20)u_i/12, \quad (21)$$

$$H(u_i)=\tfrac{1}{2}-(1-u_i^2/30)u_i/6, \quad (22)$$

$$C(u_i)=(1-u_i^2/10)u_i/6. \quad (23)$$

At $u=1$ Eqs. (20)–(23) deviate from (12)–(19) by the following amounts. (20) is low by 0.05 percent; (21) is low by 0.23 percent; (22) is high by 0.08 percent; and (23) is low by 0.67 percent. The deviation increases rapidly as u increases and therefore Eqs. (20)–(23) have been used only below $u=0.60$ in the calculation of the accompanying tables of $S(u)$, $H(u)$, and $C(u)$.

As one would anticipate the difference between C_p^0 and $C_p^{0\prime}$ is given directly as the difference between the standard formulas for the heat capacity of a rotor and an oscillator (see Mayer and Mayer, Chapter 7).[3]

The function $G(u)$ has been evaluated and tabulated previously[1] as a function of u. In Table I we present an evaluation of $S(u)$, $H(u)$, and $C(u)$ as a function of u. The behavior of these functions is shown in Fig. 1.

The entries in the columns for the entropy and heat capacity functions were obtained by direct calculations. The enthalpy function was evaluated in part from Eqs. (17) and (22) and in part from the relation $H(u)=\frac{1}{2}-(G(u)+S(u))$. Entries calculated by the latter method are less precise and have not been used in the evaluation of $\Delta H/\Delta u$. They are identified in the table by an adjacent entry for $\Delta H/\Delta u$. In accord with expectation $H(u)$ goes from $\frac{1}{2}$ to zero as u goes from 0 to ∞.

Several interesting relations can be derived from the entropy Eqs. (9) and (14). At high temperatures $S(u)$ and Δu go to zero and

$$\frac{S^0-S^{0\prime}}{R}=\ln s'/s+\sum_i \tfrac{3}{2}\ln m_i/m_i'. \quad (24)$$

This relation can also be derived simply from classical statistics and the product rule. When u is large, $S(u)$ becomes equal to $1/u$ and Eq. (9) leads to

$$\frac{S^0-S^{0\prime}}{R}=\ln s'/s-(\sigma^2-\sigma'^2)/90 + \sum_i \ln u_i/u_i'+\sum_i \tfrac{3}{2}\ln m_i/m_i'. \quad (25)$$

Several additional relations can be derived for the behavior of diatomic molecules at temperatures such that $hc\omega>7kT$. For homonuclear diatomic molecules where both atoms are replaced isotopically,

$$u/u_i'=(m'/m)^{\frac{1}{2}}$$

and

$$\frac{S^0-S^{0\prime}}{R}=5/2\ln m_i/m_i'-(\sigma^2-\sigma'^2)/90. \quad (26)$$

We may also consider the effect on the entropy of the successive substitution of the isotope A for A' in the

[3] J. E. Mayer and M. G. Mayer, *Statistical Mechanics* (John Wiley & Sons, Inc., New York, 1940).

homonuclear diatomic molecule $A'A'$.

$$\frac{S_{A-A'}{}^0-S_{A'-A'}{}^0}{R}=\ln 2-(\sigma^2-\sigma'^2)/90+\tfrac{3}{2}\ln m_A/m_{A'}+\tfrac{1}{2}\ln(m_A+m_{A'})/2m_A, \quad (27)$$

$$\frac{S_{A-A}{}^0-S_{A-A'}{}^0}{R}=-\ln 2-(\sigma^2-\sigma'^2)/90+\tfrac{3}{2}\ln m_A/m_{A'}+\tfrac{1}{2}\ln 2m_{A'}/(m_A+m_{A'}). \quad (28)$$

For the substitution of A' by A in the heteronuclear diatomic molecule AB one obtains the entropy difference

$$\frac{S_{AB}{}^0-S_{A'B}{}^0}{R}=\ln m_A/m_{A'}+\tfrac{1}{2}\ln(m_A+m_B)/(m_{A'}+m_B). \quad (29)$$

In this case when m_B/m_A is either greater than 10^2 or less than 10^{-2}

$$\frac{S_{AB}{}^0-S_{A'B}{}^0}{R}=\ln m_A/m_{A'}. \quad (30)$$

Equation (30) leads to a very simple relation for the difference in entropies of DI and HI. Between 10° and 300°K the entropy of DI is greater than HI by $R\ln 2 = 1.38$ e.u. From Eq. (26) one finds the entropy difference between D_2 and H_2 (less nuclear spin) to be 3.44 e.u. in the temperature range 300°–800°K. This is in good agreement with the extensive calculations of Woolley, Scott, and Brickwedde.[4]

Application of Eqs. (14), (16), and (18) to the vibrational data for $B^{11}F_3$ and $B^{10}F_3$ yield $S^0{}_{B^{11}F_3}-S^0{}_{B^{10}F_3}=0.004$ e.u., $(H^0-H_0{}^0)_{B^{11}F_3}-(H^0-H_0{}^0)_{B^{10}F_3}=10.4$ cal mole^{-1}, and $C_p{}^0{}_{B^{11}F_3}-C_p{}^0{}_{B^{10}F_3}=0.093$ cal deg^{-1} mole^{-1} all at 300°K.

The question arises about the corrections necessary for anharmonicity of the vibrations and the interaction of rotation and vibration. These corrections are greatest for molecules containing hydrogen. A detailed analysis shows that it is sufficient to use the zero-order frequencies, for which the product rule is valid, throughout, except for the zero point energy term which should be calculated after application of the anharmonic corrections. The errors introduced by this procedure are then less than 0.1 percent in f and therefore negligible.

Thermodynamics of Reaction Rates

In the discussion of the relative rates of reaction of a pair of isotopic molecules A_1 and A_2 it has been shown that the ratio of rate constants, k_1/k_2, is given by[2]

$$\frac{k_1}{k_2}=\frac{K_1}{K_2}\left(\frac{m_2{}^*}{m_1{}^*}\right)^{\frac{3}{2}}\frac{f}{f^\ddagger}. \quad (31)$$

[4] Woolley, Scott, and Brickwedde, J. Research Natl. Bur. Standards **41**, 379 (1948).

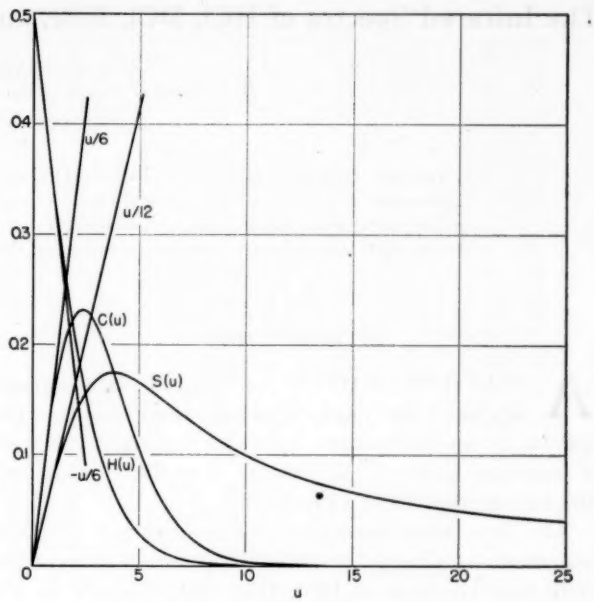

FIG. 1. Effect of isotopic substitution on the entropy, enthalpy, and heat capacity per unit of $\Delta u=hc\Delta\omega/kT$.

The above equation can also be written in terms of the equilibrium constant for the exchange reaction

$$A_1+A_2{}^\ddagger=A_2+A_1{}^\ddagger, \quad (32)$$

since

$$K_{32}=f/f^\ddagger. \quad (33)$$

The formulas derived for the difference in the experimental activation energies, $d\ln(k_1/k_2)/dT$, differ from $H^0-H^{0\prime}$ in the previous section by the temperature coefficients of K_1/K_2 and the tunnel effects.

The only other quantity which we should consider is the effect of isotopic substitution on the entropy of activation. From (31), (33), and the usual thermodynamic relationships we can write

$$\frac{k_1}{k_2}=\frac{K_1}{K_2}\left(\frac{m_2{}^*}{m_1{}^*}\right)^{\frac{3}{2}}\exp(S_2-S_1)/R-(S_2{}^\ddagger-S_1{}^\ddagger)/R \times\exp-(E_2-E_1)/RT+(E_2{}^\ddagger-E_1{}^\ddagger)/RT. \quad (34)$$

The entropy differences, S_2-S_1 and $S_2{}^\ddagger-S_1{}^\ddagger$, can be calculated from the formulas for $S_r{}^0-S_r{}^{0\prime}$ in the preceding section. Comparison with experiment can be made after dividing k_1/k_2 by all the other terms on the right-hand side of (34).

ACKNOWLEDGMENT

The computation of Table I was carried out in part by Mr. Arthur Levy and Miss Jean Snover. Mr. Clayton Weaver kindly assisted in the compilation of the table.

The Infrared Spectra of HCl, DCl, HBr, and NH_3 in the Region from 40 to 140 Microns*

R. L. HANSLER† AND R. A. OETJEN
Department of Physics, Ohio State University, Columbus, Ohio
(Received November 25, 1952)

The pure rotation spectra of HCl, DCl, HBr, and NH_3 in the region from 40 to 140 microns as measured with an automatic-recording grating spectrometer are presented in tabular and graphical form. A photograph of a recorded spectrogram provides an indication of the quality of the data. A comparison of the experimental results with figures based on accepted values of the molecular constants shows substantial agreement.

INTRODUCTION

A SELF-RECORDING far-infrared spectrograph described previously[1] has been used to obtain the spectra of several halogen hydrides and ammonia with a resolving power $\lambda/\Delta\lambda$ greater than 100 throughout the region from 40 to 140 microns.

The first far-infrared study of the halogen hydrides was made by Czerny[2] in 1925. He observed most of the pure rotation lines of HCl, HBr, HF, and HI in the region from 40 to 125 microns. In 1950, McCubbin and Sinton[3] observed the first five pure rotation lines of HCl, the first line occurring near 500 microns. Subsequently, McCubbin[4] reported new data characterized by higher resolving power. No previous measurement of the pure rotation spectrum of DCl has been reported.

The far-infrared spectrum of ammonia has been observed by several investigators.[5,6] The first high-resolution studies were carried out by Wright and Randall,[7] in which they observed the inversion doubling of the lines near 100, 120, and 140 cm^{-1}. Later Foley and Randall[8] observed the fine structure of the lines near 216, 236, 256, 273, and 293 cm^{-1}. McCubbin and Sinton[3] observed the lines near 20, 40, 60, 80, and 100 cm^{-1}, and McCubbin[4] clearly showed the inversion doubling in the line near 60 cm^{-1}.

EXPERIMENTAL PROCEDURE

The gases studied were introduced into the optical path of the spectrograph in a cell equipped with two polyethylene windows 0.004 inch thick. The cell provided a ½-inch optical path. The pressure in the cell could be changed at will and measured by means of a mercury manometer connected to the system. The rest of the instrument was evacuated to a pressure of about 50 microns Hg. The gas was at room temperature for all measurements. The cell was placed directly in front of the entrance slit of the spectrograph.

With the exception of the DCl, the gases were obtained commercially. The DCl was produced by the action of heavy sulfuric acid on NaCl. The DCl was passed slowly through a $CaCl_2$ drying tube to remove any water formed.

In obtaining the data, each line was scanned several times at different pressures and with different slit widths and gain in order to locate line centers with the greatest accuracy.

RESULTS

Diatomic Molecules

Figure 1 is a reproduction of a portion of the spectrum as it appeared on the recorder chart, when gas from a cylinder reportedly containing HBr, but which was contaminated with HCl, was introduced into the absorption cell. In this and in Fig. 2, absorption is indicated by a rise in the curve. The HBr absorption lines are marked with arrows from above; the HCl lines are marked with arrows from below. The approximately equal spacing (in frequency) of each set of lines, characteristic of the pure rotation spectra of diatomic molecules, is clearly seen. The variation in the intensity of the background is due to the variation in the efficiency of the filters, windows, and of the grating. This reproduction of an automatically recorded spectrogram, as it comes from the instrument, has been included to give some indication of the quality of the data obtained with this far-infrared spectrograph. It required about one hour to record the spectrogram in Fig. 1.

In Tables I, II and III are listed, respectively, data obtained for HCl, DCl, and HBr. For comparison, the values of the frequencies, computed on the basis of the constants for the molecules as compiled by Herzberg,[9] are shown in the fifth column, with the difference between the observed and computed values being shown in the last two columns. The larger differences, observed

* The construction and maintenance of the instrument with which these data were obtained was sponsored by the Air Research and Development Command through a contract with The Ohio State University Research Foundation.

† Eastman Kodak Fellow 1951–1952. Now with the General Electric Company, Nela Park, Cleveland, Ohio.

[1] Oetjen, Haynie, Ward, Hansler, Schauwecker, and Bell, J. Opt. Soc. Am. **42**, 559 (1952).
[2] M. Czerny, Z. Physik **34**, 227 (1925); **44**, 235 (1927).
[3] T. K. McCubbin and W. W. Sinton, J. Opt. Soc. Am. **40**, 537 (1950).
[4] T. K. McCubbin, Jr., J. Chem. Phys. **20**, 668 (1952).
[5] R. M. Badger and C. H. Cartwright, Phys. Rev. **33**, 692 (1929).
[6] R. B. Barnes, Phys. Rev. **47**, 658 (1935).
[7] N. Wright and H. M. Randall, Phys. Rev. **44**, 391 (1933).
[8] H. M. Foley and H. M. Randall, Phys. Rev. **59**, 171 (1941).
[9] G. Herzberg, *Molecular Spectra and Molecular Structure I. Spectra of Diatomic Molecules* (D. Van Nostrand Company, Inc., New York, 1950), second edition.

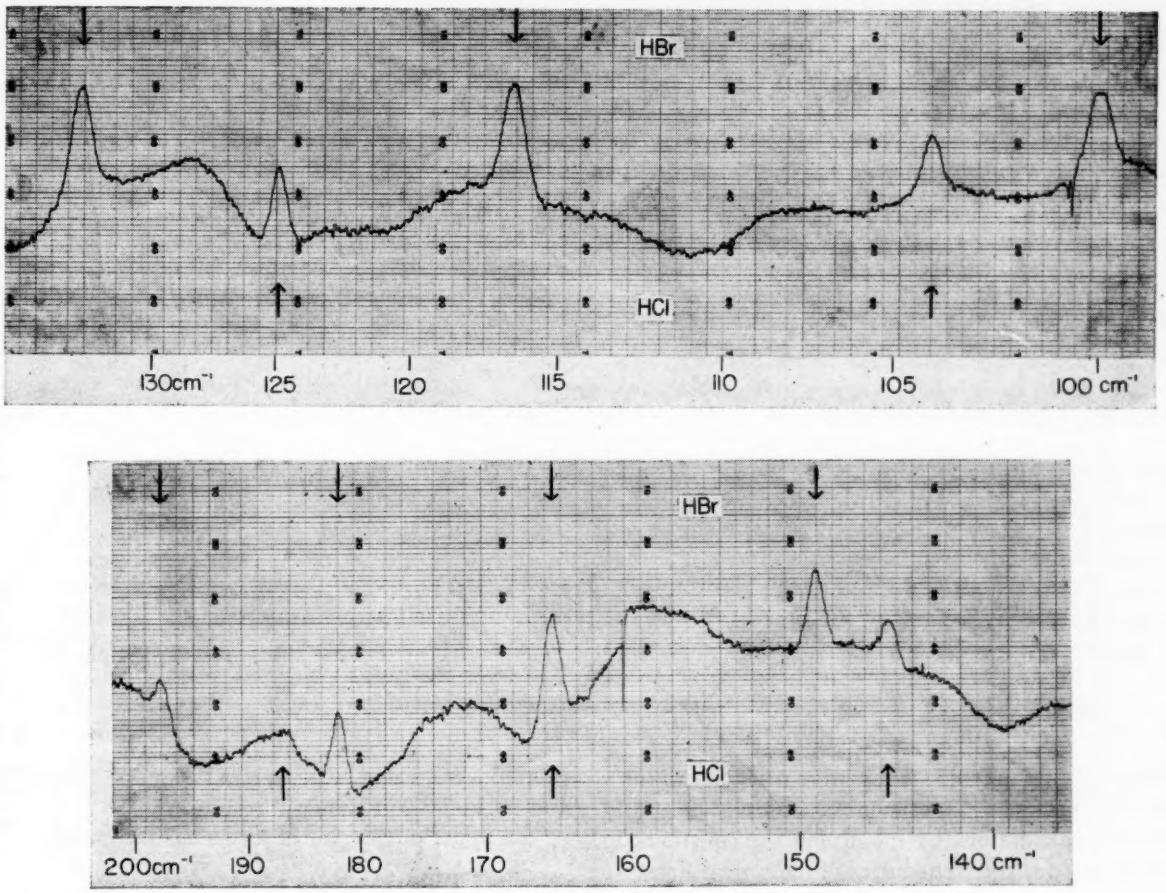

FIG. 1. Far-infrared spectrum of HCl and HBr. Absorptions resulting from HCl are indicated by arrows below the curves. Absorptions resulting from HBr are indicated by arrows above the curves.

for high values of the rotational quantum number J, are due to the fact that relatively high gas pressures were necessary in order to obtain sufficient absorption when using a $\frac{1}{2}$-inch cell at room temperature. This caused some pressure broadening which resulted in a loss of accuracy in locating the line centers.

Ammonia

The far-infrared spectrum of ammonia was obtained by introducing commercially obtained gas into the $\frac{1}{2}$-inch cell and adjusting the pressure to give the best spectrum. Too high a pressure resulted in complete absorption over the entire breadth of the line, while too low a pressure resulted in insufficient absorption. The observed contours of each line are shown in Fig. 2. The spectrograph was evacuated, but no effort was made to dry the ammonia. The portions of the observed spectrum which are in some doubt because of the occurrence of water vapor absorption at those places are indicated by broken rather than solid lines.

Interpretation of Ammonia Data

It is of interest to note briefly the history of the rotational spectrum of ammonia and its interpretation.

Wright and Randall,[7] in addition to verifying experimentally the inversion doubling of the rotational lines, showed that the frequency may be represented by a cubic equation in the quantum number J, which indicates the total angular momentum. The slight departure from a linear equation is caused by a centrifugal deformation of the molecule.

Slawsky and Dennison,[10] in a theoretical study of axial molecules, showed that the centrifugal distortion produces fine structure, so that for ammonia-like molecules, instead of there being two energy levels associated with each value of J, there are $(2J+1)$ levels. The quantum number K, giving the angular momentum about the symmetry axis, was introduced by these authors. They developed an expression for calculating the intensities of the components. They further indicated that, for higher values of J the fine structure should broaden, so that the shapes of the absorptions would differ from those observed previously for low J values.

Foley and Randall[8] observed the effect predicted by Slawsky and Dennison[10] for absorptions corresponding

[10] Z. I. Slawsky and D. M. Dennison, J. Chem. Phys. **7**, 509 (1939).

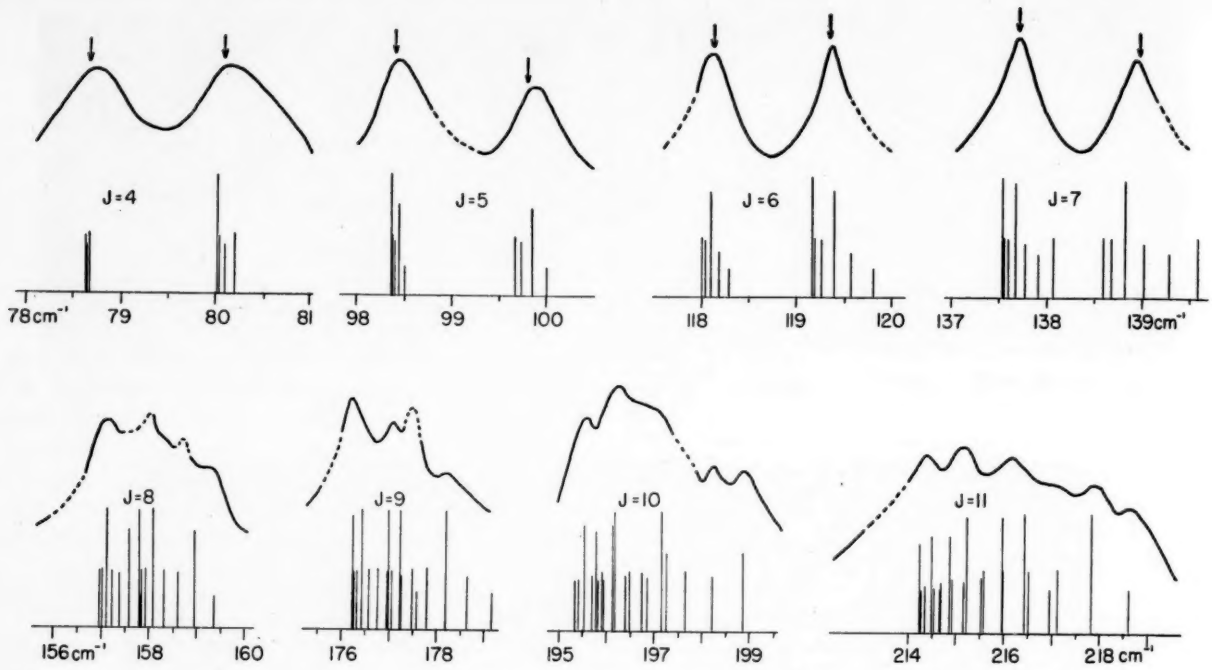

FIG. 2. Far-infrared spectrum of ammonia.

to $J=11$ through $J=15$. They were able to obtain a better fit between experimental observations and theoretical calculations by modifying the constants in the equation for the frequencies of individual lines.

Using microwave techniques, Good[11] showed that all inversion doubled pairs of energy levels do not have the same separation, but rather that the separation is a function of J and K. This means that the inversion frequency is altered by centrifugal distortion of the molecule.

When the results of Good[11] are taken into account, it is found that frequencies calculated from expressions developed previously do not fit the experimentally observed absorption curves. Through the use of different constants, fairly good correspondence between calculated values and experimental values reported here and by Foley and Randall[8] results.

The upper of the pair of levels has the energy

$$E_{JK}^{-}=19.88\frac{(J^2+J)}{2}+AK^2-0.00324\frac{(J^2+J)^2}{4}$$

$$+0.00310\frac{(J^2+J)K^2}{2}+BK^4$$

$$+0.7935-0.00505(J^2+J)+0.00704K^2,$$

TABLE I. HCl rotational lines

Quantum numbers associated with energy levels		Location of absorption observed		calculated	Difference	
Lower	Upper	Microns	cm⁻¹	cm⁻¹	cm⁻¹	Microns
3	4	120.02	83.32	83.38	−0.06	−0.09
4	5	96.03	104.13	104.13	0.00	0.00
5	6	80.17	124.73	124.82	−0.09	−0.06
6	7	68.79	145.37	145.43	−0.06	−0.03
7	8	60.28	165.89	165.95	−0.06	−0.02
8	9	53.70	186.23	186.37	−0.14	−0.04
9	10	48.40	206.60	206.67	−0.06	−0.01
10	11	44.08	226.86	226.85	+0.01	+0.00

TABLE II. DCl rotational lines.

Quantum numbers associated with energy levels		Location of absorption observed		calculated	Difference	
Lower	Upper	Microns	cm⁻¹	cm⁻¹	cm⁻¹	Microns
6	7	133.07	75.15	75.24	−0.09	−0.16
7	8	116.41	85.90	85.92	−0.02	−0.03
8	9	103.62	96.51	96.57	−0.06	−0.06
9	10	93.34	107.14	107.19	−0.05	−0.04
10	11	84.88	117.81	117.77	+0.04	+0.03
11	12	77.97	128.26	128.31	−0.05	−0.03
12	13	72.05	138.80	138.81	−0.01	−0.01
13	14	67.00	149.26	149.26	0.00	0.00
14	15	62.61	159.71	159.67	+0.04	+0.02
15	16	58.80	170.06	170.02	+0.04	+0.01
16	17	55.44	180.39	180.31	+0.08	+0.02
17	18	52.44	190.69	190.54	+0.15	+0.04
18	19	49.75	200.99	200.73	+0.26	+0.07
17	20	47.38	211.07	210.81	+0.26	+0.06

[11] W. E. Good, Phys. Rev. **70**, 213 (1946).

and the lower level has the energy

$$E^{+}_{JK}=19.88\frac{(J^2+J)}{2}+AK^2-0.00324\frac{(J^2+J)^2}{4}$$
$$+0.00310\frac{(J^2+J)K^2}{2}+BK^4,$$

where A and B are constants which do not enter into the frequencies in which we are interested. The frequencies are

$$\nu^J_{J-1-\to+}=19.88J-0.00324J^3+0.00310JK^2$$
$$-0.7935+0.00505(J^2+J)-0.00704K^2,$$

and

$$\nu^J_{J-1+\to-}=19.88J-0.00324J^3+0.00310JK^2$$
$$+0.7935-0.00505(J^2+J)+0.00704K^2.$$

Calculated values for $J=4$ through $J=11$ based on these expressions are shown as vertical straight lines below the corresponding curves in Fig. 2. The lengths of the lines, within one J value, are proportional to the intensities computed from the rules given by Slawsky and Dennison.[10] The arrows above the first four pairs indicate the "center of mass" of the calculated spectrum. It will be observed that the separation of these, for increasing values of J are 1.41, 1.39, 1.21, and 1.26 cm^{-1}. These values are smaller than the $2\cdot0.7935=1.587$ cm^{-1}, which would be expected from the microwave data if the effects of centrifugal distortion were ignored. For values of J greater than seven, the spread of the fine structure is so large that it masks the inversion doubling. For values of J less than four, the separation would be larger, thus approaching the microwave value of 1.587 cm^{-1}.

TABLE III. HBr rotational lines.

Quantum numbers associated with energy levels		Location of absorption observed		calculated	Difference	
Lower	Upper	Microns	cm^{-1}	cm^{-1}	cm^{-1}	Microns
4	5	119.99	83.34	83.41	−0.07	−0.10
5	6	100.13	99.87	99.99	−0.12	−0.12
6	7	85.85	116.48	116.54	−0.06	−0.04
7	8	75.26	132.88	133.02	−0.14	−0.08
8	9	66.98	149.30	149.44	−0.14	−0.06
9	10	60.35	165.69	165.78	−0.09	−0.03
10	11	55.01	181.78	182.03	−0.25	−0.08
11	12	50.47	198.13	198.20	−0.07	−0.02
12	13	46.72	214.03	214.27	−0.24	−0.05
13	14	43.50	229.89	230.23	−0.34	−0.06

Grateful acknowledgement is made of comments by Professor D. M. Dennison upon reading our manuscript. Acknowledgement is also made of the help of Professor E. E. Bell, which was given throughout this investigation.

Diffusion in Binary Systems*

STEPHEN PRAGER†
Department of Chemistry, Cornell University, Ithaca, New York
(Received March 18, 1953)

The Onsager-Fuoss equation for the concentration dependence of the diffusion coefficient is derived from a kinetic picture, taking into account the asymmetry in the Brownian motion induced by concentration gradients. Mass flow is introduced by considering diffusion in the presence of a pressure gradient. Systems exhibiting volume changes on mixing are discussed, and a modification of the Matano procedure for calculating diffusion coefficients is suggested. It is shown that diffusion coefficients obtained from steady-state permeability measurements and those obtained from interdiffusion data differ by a factor of $\bar{V}_2 c_2$, the volume fraction of the nonpermeating component.

IT has been found by Johnson[1] that the diffusion coefficient measured in a two-component system with a chemical concentration gradient differs from that obtained when the diffusion of radioactively tagged molecules is observed in the absence of any gradient in the *total* concentration of either component. Seitz[2] has explained this on the basis that in the former case the frequency with which a molecule jumps to the right is not the same as that with which it jumps to the left, whereas in the latter case the two frequencies are identical. The nature of this asymmetry will here be related to thermodynamic considerations; at the same time mass flow will be automatically introduced by considering diffusion in the presence of a pressure gradient. The concept of mass flow will then be extended to include systems which exhibit volume changes on mixing and systems in which one component is prevented from moving (steady-state permeation).

THEORY

Imagine a diffusion column of unit cross-sectional area with a concentration gradient in the x direction, divided into compartments of width λ by imaginary planes perpendicular to the x axis (λ to be chosen macroscopically small but microscopically large). The average frequency ν with which a given molecule jumps from one compartment to an adjacent one will depend in general not only on the concentrations α_1 and α_2 of the components in the original compartment, but also on the concentrations β_1 and β_2 in the final one, and should therefore be written

$$\nu_i=\nu_i(\alpha_1, \alpha_2; \beta_1, \beta_2), \quad (i=1 \text{ or } 2).$$

The *net* number P of molecules of each component permeating in unit time from one compartment to its neighbor is thus given by

$$P_i=\lambda[\alpha_i\nu_i(\alpha_1, \alpha_2; \beta_1, \beta_2)-\beta_i\nu_i(\beta_1, \beta_2; \alpha_1, \alpha_2)], \quad (1)$$

which may, if the concentration gradients are not too large, be written in the following differential form:

$$P_i=-\lambda^2\sum_j\left[\left(\frac{\partial}{\partial\alpha_j}-\frac{\partial}{\partial\beta_j}\right)(a_i\nu_i)\right]_{\substack{\alpha_1=\beta_1=c_1\\ \alpha_2=\beta_2=c_2}}\frac{\partial c_j}{\partial x}, \quad (1a)$$

where c_1 and c_2 are the mean concentrations in the two compartments, and all subscripts are understood to take on the values 1 or 2. Equation 1(a) is similar to one previously derived by Seitz.[2]

If the concentration gradients $\partial c_1/\partial x$ and $\partial c_2/\partial x$ are such that a pressure gradient $\partial p/\partial x$ results, hydrodynamic flow will take place, giving rise to an additional contribution to the permeation rates,

$$P_i=-\lambda^2\sum_j\left[\left(\frac{\partial}{\partial\alpha_j}-\frac{\partial}{\partial\beta_j}\right)(\alpha_i\nu_i)\right]_{c_1, c_2}\frac{\partial c_j}{\partial x}+v(x, t)c_i, \quad (1b)$$

where v is the flow velocity, assumed to be in the x direction and dependent only on the x coordinate and the time t. A pressure gradient may thus relieve itself in two ways: by interdiffusion of the two components and by expansion or contraction of the mixture as a whole; of these, the latter is so much more rapid, at least in liquids and solids, that the former may, for all practical purposes, be neglected in comparison.

In the absence of a chemical concentration gradient the rate of permeation of radioactive material is given by

$$P_i^*=-\lambda^2\nu_i(c_1, c_2; c_1, c_2)(\partial c_i^*/\partial x), \quad (2)$$

where c_1 and c_2 represent the *total* concentrations, and c_i^* the concentration of labeled molecules of the ith component. The problem now is to relate $\nu_i(\alpha_1, \alpha_2; \alpha_1, \alpha_2)$ to $\nu_i(\alpha_1, \alpha_2; \beta_1, \beta_2)$.

For this purpose the dependence of ν_i on still another variable, namely, the external force f_i acting in the x direction on each mole of component i, will be investigated. Such a force must in general remain imaginary, although it can be realized in the case of ions by the use of an electrostatic field; this lack of reality detracts nothing from the validity of the subsequent derivation, however. Under the action of such forces a concentra-

* This work was carried out as part of a research project sponsored by U. S. Army Ordnance.
† Present address: School of Chemistry, University of Minnesota, Minneapolis, Minnesota.
[1] W. A. Johnson, Trans. Am. Inst. Mining Met. Engrs. **147**, 331 (1942).
[2] F. Seitz, Phys. Rev. **74**, 1513 (1948).

tion gradient will in general result; at equilibrium the relations

$$\alpha_i\nu_i(\alpha_1, \alpha_2; \beta_1, \beta_2; f_i)=\beta_i\nu_i(\beta_1, \beta_2; \alpha_1, \alpha_2; -f_i) \quad (3)$$

must be valid for any pair of adjacent compartments; rewritten in differential form these become

$$\lambda\sum_i\left[\left(\frac{\partial}{\partial\alpha_j}-\frac{\partial}{\partial\beta_j}\right)(\alpha_i\nu_i)\right]_{\substack{\alpha_1=\beta_1=c_1\\ \alpha_2=\beta_2=c_2\\ f_i=0}}\frac{\partial c_j}{\partial x}$$

$$=2c_if_i\left[\frac{\partial\nu_i}{\partial f_i}\right]_{\substack{\alpha_1=\beta_1=c_1\\ \alpha_2=\beta_2=c_2\\ f_i=0}}. \quad (3a)$$

Thermodynamics gives the force f_i as

$$f_i=\partial\mu_i/\partial x, \quad (4)$$

where μ_i is the chemical potential of component i.

To find $[\partial\nu/\partial f]_{c_1,c_2,0}$ a force f_i^* is imagined to act on labeled i molecules in a system with no over-all concentration gradient, a force f_i' being applied to the nonradioactive i molecules so that the total force acting on component i at each point is zero. Again, at equilibrium

$$\alpha_i^*\nu_i(\alpha_1, \alpha_2; \alpha_1, \alpha_2, f_i^*)$$
$$=\beta_i^*\nu_i(\alpha_1, \alpha_2; \alpha_1, \alpha_2, -f_i^*), \quad (5)$$

or, in differential form,

$$\lambda\nu_i(\alpha_1, \alpha_2; \alpha_1, \alpha_2; 0)\partial c_i^*/\partial x$$
$$=2c_i^*f_i^*[\partial\nu_i/\partial f]_{c_1,c_2,0}, \quad (5a)$$

where f_i^* is given by

$$f_i^*=\frac{\partial\mu_i^*}{\partial x}=\frac{RT}{c_i^*}\frac{\partial c_i^*}{\partial x}, \quad (6)$$

because of the ideality of the system being considered. Combination of Eqs. (1b), (3a), (4), (5a), and (6) yields

$$P_i=-\frac{D_i^*(c_1, c_2)}{RT}c_i\frac{\partial\mu_i}{\partial x}+vc_i, \quad (7)$$

which is very like the formula derived by Onsager and Fuoss[3] by a somewhat more rigorous method. Here D_i^* is the diffusion coefficient in the absence of any total concentration gradient, given by

$$D_i^*(c_1, c_2)=\lambda^2\nu_i(c_1, c_2; c_1, c_2; 0). \quad (8)$$

From thermodynamics we have

$$\frac{\partial\mu_i}{\partial x}=\left(\frac{\partial\mu_i}{\partial c_i}\right)_{P,T}\frac{\partial c_i}{\partial x}+\left(\frac{\partial\mu_i}{\partial P}\right)_{c_i,T}\frac{\partial P}{\partial x}$$
$$=\left(\frac{\partial\mu_i}{\partial c_i}\right)_{P,T}\frac{\partial c_i}{\partial x}+\left(\bar{V}_i-kc_i\left(\frac{\partial\mu_i}{\partial c_i}\right)_{P,T}\right)\frac{\partial P}{\partial x}, \quad (9)$$

so that Eq. (7) becomes

$$P_i=vc_i-\frac{D_i^*c_i}{RT}\left\{\left(\frac{\partial\mu_i}{\partial c_i}\right)_{P,T}\frac{\partial c_i}{\partial x}\right.$$
$$\left.+\left(\bar{V}_i-kc_i\left(\frac{\partial\mu_i}{\partial c_i}\right)_{P,T}\right)\frac{\partial P}{\partial x}\right\}, \quad (10)$$

where $\bar{V}_i$ is the partial molal volume of component i, and k is the compressibility of the mixture at constant composition. Actually, since the system was presumably at a uniform pressure to begin with, and since, as already mentioned, any pressure gradient built up by differences in the diffusion rates of the two components will be quickly smoothed out by the term vc_i in Eq. (10) with almost no contribution from the $\partial P/\partial x$ term, the latter may be neglected. Equation (10) may thus be closely approximated by

$$P_i=vc_i-\frac{D_i^*c_i}{RT}\left(\frac{\partial\mu_i}{\partial c_i}\right)_{P,T}\frac{\partial c_i}{\partial x}. \quad (11)$$

INTERDIFFUSION OF TWO COMPONENTS

The rates at which the concentrations change at a point are thus given by

$$\frac{\partial c_1}{\partial t}=-\frac{\partial P_1}{\partial x}=\frac{\partial}{\partial x}\left(D_1\frac{\partial c_1}{\partial x}\right)-\frac{\partial}{\partial x}(vc_1),$$
$$\frac{\partial c_2}{\partial t}=-\frac{\partial P_2}{\partial x}=\frac{\partial}{\partial x}\left(D_2\frac{\partial c_2}{\partial x}\right)-\frac{\partial}{\partial x}(vc_2), \quad (12)$$

where D_1 and D_2 are defined as

$$D_i=\frac{c_iD_i^*}{RT}\left(\frac{\partial\mu_i}{\partial c_i}\right)_{P,T}, \quad (i=1, 2). \quad (13)$$

Equations (12) were derived in a recent paper by Darken.[4]

To Eqs. (12) must be added a third equation, namely, the dependence of P on c_1 and c_2 at temperature T, or, since P is essentially constant, the relation between c_1 and c_2 at pressure P and temperature T,

$$c_2=f(c_1)=(1-\bar{V}_1c_1)/\bar{V}_2. \quad (14)$$

Introduction of (14) into the second of Eqs. (12) and use of the relation

$$(\partial c_2/\partial c_1)_{P,T}=-\bar{V}_1/\bar{V}_2 \quad (15)$$

leads to

$$-\frac{\bar{V}_1}{\bar{V}_2}\frac{\partial c_1}{\partial t}=-\frac{\partial}{\partial x}\left(D_2\frac{\bar{V}_1}{\bar{V}_2}\frac{\partial c_1}{\partial x}\right)-f(c_1)\frac{\partial v}{\partial x}+\frac{\bar{V}_1}{\bar{V}_2}\frac{\partial c_1}{\partial x}, \quad (16)$$

which, when combined with the first of Eqs. (12),

[3] L. Onsager and R. M. Fuoss, J. Phys. Chem. **36**, 268 (1932).

[4] L. S. Darken, Trans. Am. Inst. Mining Met. Engrs. **175**, 184 (1948).

yields

$$\frac{\partial v}{\partial x}=\bar{V}_1\frac{\partial}{\partial x}\left(D_1\frac{\partial c_1}{\partial x}\right)-\bar{V}_2\frac{\partial}{\partial x}\left(D_2\frac{\bar{V}_1}{\bar{V}_2}\frac{\partial c_1}{\partial x}\right). \quad (17)$$

Integration by parts from $-\infty$ to x transforms (17) into

$$\partial=\bar{V}_1(D_1-D_2)\frac{\partial c_1}{\partial x}+\int_{-\infty}^{x}\frac{c_2}{c_1}\times\left(D_1+D_2\frac{\bar{V}_1c_1}{\bar{V}_2c_2}\right)\left(\frac{\partial\bar{V}_2}{\partial c_1}\right)_{P,T}\left(\frac{\partial c_1}{\partial x}\right)^2dx, \quad (18)$$

∂ and $\partial c_1/\partial x$ having been assumed to be zero at $x=-\infty$. Substituting (18) into (12), we get

$$\frac{\partial c_1}{\partial t}=\frac{\partial}{\partial x}\left(D\frac{\partial c_1}{\partial x}\right)-\frac{\partial}{\partial x}\left(c_1\int_{-\infty}^{x}\frac{D}{\bar{V}_2c_1}\times\left(\frac{\partial\bar{V}_2}{\partial c_1}\right)_{P,T}\left(\frac{\partial c_1}{\partial x}\right)^2dx\right),$$

$$\frac{\partial c_2}{\partial t}=\frac{\partial}{\partial x}\left(D\frac{\partial c_2}{\partial x}\right)-\frac{\partial}{\partial x}\left(c_2\int_{-\infty}^{x}\frac{D}{\bar{V}_2c_1}\times\left(\frac{\partial\bar{V}_2}{\partial c_1}\right)_{P,T}\left(\frac{\partial c_1}{\partial x}\right)^2dx\right), \quad (19)$$

where

$$D=D_1\bar{V}_2c_2+D_2\bar{V}_1c_1 \quad (20)$$

is the mutual diffusion coefficient of Hartley and Crank.[5] The second terms on the right in (18) and (19) arise because of volume changes on mixing, and vanish when such changes do not occur, i.e., when $(\partial\bar{V}_1/\partial c_1)_{P,T}$ is zero, in which case Eqs. (19) reduce to the usual diffusion relations.

If the initial distribution of material is such that

$$c_1(x,0)=\begin{cases}0 & -\infty<x<0\\ c_1^{\infty} & 0<x<\infty\end{cases}, \quad (21)$$

then Eqs. (19) can be treated by the Boltzmann method[6] even if $(\partial\bar{V}_1/\partial c_1)_{P,T}$ is not zero. Thus if we suppose c_1 to be a function of $\lambda=x/t^{\frac{1}{2}}$ alone, the first of Eqs. (19) becomes

$$-\tfrac{1}{2}\lambda\frac{dc_1}{d\lambda}=\frac{d}{d\lambda}\left(D\frac{dc_1}{d\lambda}\right)-\frac{d}{d\lambda}\left(c_1\int_{-\infty}^{\lambda}\frac{D}{\bar{V}_2c_1}\times\left(\frac{\partial\bar{V}_2}{\partial c_1}\right)_{P,T}\left(\frac{dc_1}{d\lambda}\right)^2d\lambda\right), \quad (22)$$

with boundary conditions

$$c_1(-\infty)=0,\quad c_1(\infty)=c_1^{\infty}. \quad (23)$$

If $c_1(\lambda)$ is known from experiment, Eq. (22) can be solved for $D(c_1)$ to give

$$D(c_1)=-\tfrac{1}{2}\frac{d\lambda}{dc_1}\left[\int_0^{c_1}\lambda dc_1+c_1\bar{V}_2\times\int_0^{c_1}\frac{\left(\int_0^{c_1}\lambda dc_1\right)}{c_1\bar{V}_2^2}\left(\frac{\partial\bar{V}_2}{\partial c_1}\right)_{P,T}dc_1\right]. \quad (24)$$

The first term in (24) is the usual expression for calculating $D(c_1)$ from $c_1(\lambda)$; the second term is a small correction to this, which Matano[7] approximates by a constant times c_1,

$$D(c_1)=-\tfrac{1}{2}\frac{d\lambda}{dc_1}\left(\int_0^{c_1}\lambda dc_1+Ac_1\right), \quad (25)$$

where A is obtained from the requirement that at $c_1=c_1^{\infty}$, where $d\lambda/dc_1$ becomes infinite, D must remain finite, so that

$$A=\frac{1}{c_1^{\infty}}\int_0^{c_1^{\infty}}\lambda dc_1. \quad (26)$$

A better approximation would be to treat $\bar{V}_2$ and $(1/c_1)(\partial\bar{V}_2/\partial c_1)_{P,T}$ as constants, in which case (24) becomes

$$D(c_1)=-\tfrac{1}{2}\frac{d\lambda}{dc_1}\left[\int_0^{c_1}\lambda dc_1+Bc_1\times\int_0^{c_1}\left(\int_0^{c_1}\lambda dc_1\right)dc_1\right], \quad (27)$$

where B is given by

$$B=\frac{\int_0^{c_1^{\infty}}\lambda dc_1}{c_1^{\infty}\int_0^{c_1^{\infty}}\left(\int_0^{c_1}\lambda dc_1\right)dc_1}; \quad (28)$$

this procedure, like Matano's, requires no data on the partial molal volumes.

STEADY-STATE PERMEATION

When the diffusion coefficient is measured by a steady-state permeation method, Eq. (11) can be used directly. If component 2 is the one which is not moving, then P_2 is zero,

$$P_1=vc_1-D_1(dc_1/dx),$$
$$0=vc_2-D_2(dc_2/dx), \quad (29)$$

where P_1 is a measurable, constant quantity.

[5] G. S. Hartley and J. Crank, Trans. Faraday Soc. **45**, 801 (1949).

[6] L. Boltzmann, Ann. Physik **53**, 960 (1894).

[7] L. Matano, J. Phys. (Japan) **8**, 109 (1933).

Combining Eqs. (29) and (15) we have

$$v=-\frac{D_2\bar{V}_1}{c_2\bar{V}_2}\frac{dc_1}{dx} \tag{30}$$

and

$$P_1=-\frac{D}{c_2\bar{V}_2}\frac{dc_1}{dx}. \tag{31}$$

From (31) it appears that the diffusion coefficients obtained from the Boltzmann method and the steady-state method differ by a factor $\bar{V}_2c_2$, which is close to unity when c_1 is small, but goes to zero as the concentration of the permeating component increases. Equation (31) does not, of course, predict an infinite value of P_1 as c_2 goes to zero, since dc_1/dx also approaches zero in that limit.

THE JOURNAL OF CHEMICAL PHYSICS VOLUME 21, NUMBER 8 AUGUST, 1953

Thermal Diffusion in Binary Systems

STEPHEN PRAGER* AND HENRY EYRING
University of Utah, Salt Lake City, Utah

(Received March 31, 1953)

Just as is the case with ordinary diffusion, thermal diffusion is accompanied by a mass flow, which does not vanish even after the steady state has been reached. As a result of this mass motion the thermal diffusion coefficients of *both* components in a binary mixture enter into the expression for the steady-state mole fraction gradient of either one, so that a knowledge of the latter is not sufficient, in general, to resolve the total heat of activation for diffusion into a heat of hole formation and a heat of activation for jumping. Mass flow should exist even in pure liquids in the presence of a temperature gradient, and this gives rise to the interesting possibility that the heat of activation for self-diffusion can be resolved into its components.

IN a previous paper[1] (hereafter referred to as *I*) the mutual diffusion coefficient of two interdiffusing components was discussed in terms of the Brownian motion of the individual particles. The existence of concentration gradients introduced an asymmetry into this motion, which was related to thermodynamic quantities, leading to the equations of Onsager and Fuoss.[2] Consideration of diffusion in the presence of a pressure gradient then introduced the mass flow concept discussed by Darken[3] as well as by Hartley and Crank.[4] In the present work these ideas will be extended to thermal diffusion.

THEORY

If, as in *I*, the diffusion column is mentally divided up into slices of thickness λ and unit cross-sectional area, then the average frequency ν_i with which molecules of a species i jump from one compartment to another will depend in general on the mole fraction† η_i of component i and the temperature γ in the original compartment, as well as on ξ_i and δ, the corresponding values of these quantities in the final one:

$$\nu_i=\nu_i(\eta_i, \gamma; \xi_i, \delta) \quad (i=1, 2). \tag{1}$$

In writing (1) we have tacitly assumed that the pressure p is the same in both compartments. The net rate at which each component permeates from one compartment to the next is therefore

$$P_i=\lambda[\alpha_i\nu_i(\eta_i, \gamma; \xi_i, \delta)-\beta_i\nu_i(\xi_i, \delta; \eta_i, \gamma)], \tag{2}$$

where α_i and β_i are the concentrations of i which correspond to mole fractions η_i and ξ_i, respectively. Equation (2) can be rewritten in terms of derivatives of c_i, n_i, and T, the mean local concentration, mole fraction, and temperature, with respect to x, the coordinate in the direction of diffusion:

$$P_i=-\lambda^2\Bigg\{\nu_i(n_i, T; n_i, T)\frac{\partial c_i}{\partial x}+c_i\left[\left(\frac{\partial}{\partial\eta_i}-\frac{\partial}{\partial\xi_i}\right)\nu_i\right]_{\substack{\eta_i=\xi_i=n_i\\ \gamma=\delta=T}}\frac{\partial n_i}{\partial x}+c_i\left[\left(\frac{\partial}{\partial\gamma}-\frac{\partial}{\partial\delta}\right)\nu_i\right]_{\substack{\eta_i=\xi_i=n_i\\ \gamma=\delta=T}}\frac{\partial T}{\partial x}\Bigg\}. \tag{3}$$

Bearing in mind that dn_1/dx can be expressed in terms of $\partial c_1/\partial x$, $\partial T/\partial x$, the partial molal volume $\bar{V}_2$ of component 2, and the expansion coefficient α of the mixture, by the relation

$$\frac{\partial n_1}{\partial x}=\frac{1}{(c_1+c_2)^2\bar{V}_2}\left[\frac{\partial c_1}{\partial x}+\alpha c_1\frac{\partial T}{\partial x}\right], \tag{4}$$

* Present address: School of Chemistry, University of Minnesota, Minneapolis, Minnesota.

[1] S. Prager, J. Chem. Phys. **21**, 1344 (1953).

[2] L. Onsager and R. M. Fuoss, J. Phys. Chem. **36**, 268 (1932).

[3] L. S. Darken, Trans. Am. Inst. Mining Met. Engrs. **175**, 184 (1948).

[4] G. S. Hartley and J. Crank, Trans. Faraday Soc. **45**, 801 (1949).

† The concentrations used in *I* are replaced here by the mole fractions so as to facilitate the later interpretation of the dependence of ν on γ and δ.

we can, by defining

$$D_1^*=\lambda^2\nu_1(n_1T;n_1T),$$

$$D_1'=\lambda^2\frac{c_1}{(c_1+c_2)^2\bar{V}_2}\left[\left(\frac{\partial}{\partial\eta_1}-\frac{\partial}{\partial\xi_1}\right)\nu_1\right]_{\substack{\eta_1=\xi_1=n_1\\ \gamma=\delta=T}},$$

$$\mathfrak{D}_1^*=\lambda^2\left[\left(\frac{\partial}{\partial\gamma}-\frac{\partial}{\partial\delta}\right)\nu_1\right]_{\substack{\eta_1=\xi_1=n_1\\ \gamma=\delta=T}},$$

transform (3) into

$$P_1=-(D_1^*+D_1')\frac{\partial c_1}{\partial x}-c_1(\mathfrak{D}_1^*+\alpha D_1')\frac{\partial T}{\partial x}, \quad (5)$$

a similar relation being valid for the other component. By comparison of (5) when $\partial T/\partial x=0$ with the results of I, it becomes apparent that

$$D_1^*+D_1'=D_1=\frac{D_1^*}{RT}c_1\left(\frac{\partial\mu_1}{\partial c_1}\right)_{p,T}$$

$$=D_1^*\frac{(\bar{V}_1n_1+\bar{V}_2n_2)}{\bar{V}_2}\left(\frac{\partial\ln a_1}{\partial\ln n_1}\right)_{p,T}, \quad (6)$$

where μ_1 is the chemical potential of 1 and a_1 its activity.

If, as before, we assume the rates of permeation of the two components to be independent, then pressure gradients will arise which are rapidly smoothed out by mass flow. Denoting the flow velocity by $v(x,t)$, we get for the actual rates of permeation $P_i^\ddagger$

$$P_i^\ddagger=-D_i\frac{\partial c_i}{\partial x}-[\mathfrak{D}_i^*+\alpha(D_i-D_i^*)]c_i\frac{\partial T}{\partial x}+vc_i. \quad (7)$$

If a steady state has been reached with P_1 and P_2 both equal to zero, then

$$v=D_1\frac{\partial\ln c_1}{\partial x}+[\mathfrak{D}_1^*+\alpha(D_1-D_1^*)]\frac{\partial T}{\partial x}$$

$$=D_2\frac{\partial\ln c_2}{\partial x}+[\mathfrak{D}_2^*+\alpha(D_2-D_2^*)]\frac{\partial T}{\partial x}, \quad (8)$$

which can, with the aid of (4) and (6) be rearranged to give

$$v=\frac{D_2^*D_1^*}{(D_1^*n_2+D_2^*n_1)}\left\{\frac{\mathfrak{D}_1^*}{D_1^*}n_1+\frac{\mathfrak{D}_2^*}{D_2^*}n_2-\alpha\right\}\frac{\partial T}{\partial x} \quad (9)$$

and

$$\frac{\partial\ln n_1}{\partial T}=n_2\left[\frac{(\mathfrak{D}_2^*-\mathfrak{D}_1^*)-\alpha(D_2^*-D_1^*)}{(D_1^*n_2+D_2^*n_1)}\right]\times\left(\frac{\partial\ln a_1}{\partial\ln n_1}\right)_{T,p}^{-1},$$

$$\frac{\partial\ln n_2}{\partial T}=-n_1\left[\frac{(\mathfrak{D}_2^*-\mathfrak{D}_1^*)-\alpha(D_2^*-D_1^*)}{(D_1^*n_2+D_2^*n_1)}\right]\times\left(\frac{\partial\ln a_1}{\partial\ln n_1}\right)_{T,p}^{-1} \quad (10)$$

or

$$\frac{\partial\ln(n_2/n_1)}{\partial T}=-\left[\frac{(\mathfrak{D}_2^*-\mathfrak{D}_1^*)-\alpha(D_2^*-D_1^*)}{(D_1^*n_2+D_2^*n_1)}\right]\times\left(\frac{\partial\ln a_1}{\partial\ln n_1}\right)_{T,p}^{-1}. \quad (11)$$

The general treatment of nonsteady-state diffusion is considerably more difficult, and results will only be given for the case where there is no change in total volume on mixing the two components in any proportion, and where thermal expansion can be neglected ($\bar{V}_i$ constant and $\alpha=0$). For such a situation it can be shown, by a method analogous to that used in I, that

$$v=\bar{V}_1(D_1-D_2)\frac{\partial c_1}{\partial x}+(\mathfrak{D}_1^*\bar{V}_1c_1+\mathfrak{D}_2^*\bar{V}_2c_2)\frac{\partial T}{\partial x} \quad (12)$$

and

$$\frac{\partial c_1}{\partial t}=\frac{\partial}{\partial x}\left(D\frac{\partial c_1}{\partial x}\right)-\frac{\partial}{\partial x}\left(\bar{V}_2c_1c_2[\mathfrak{D}_2^*-\mathfrak{D}_1^*]\frac{\partial T}{\partial x}\right),$$

$$\frac{\partial c_2}{\partial t}=\frac{\partial}{\partial x}\left(D\frac{\partial c_2}{\partial x}\right)+\frac{\partial}{\partial x}\left(\bar{V}_1c_1c_2[\mathfrak{D}_2^*-\mathfrak{D}_1^*]\frac{\partial T}{\partial x}\right), \quad (13)$$

where

$$D=D_1\bar{V}_2c_2+D_2\bar{V}_1c_1=(D_1^*n_2+D_2^*n_1)\left(\frac{\partial\ln a_1}{\partial\ln n_1}\right)_{p,T}$$

is the mutual diffusion coefficient.[1,3,4]

DISCUSSION

Wirtz and Hiby[5] have obtained an expression for $\mathfrak{D}_i^*$ by setting

$$\nu_i=A_i\exp\left(-\frac{H_i'}{R\gamma}\right)\exp\left(-\frac{H_i}{R\delta}\right), \quad (14)$$

where H_i is that portion of the total heat of activation

[5] K. Wirtz and J. W. Hiby, Physik. Z. 44, 369 (1943).

$\Delta H_i^{\ddagger}$ necessary to form a hole for a molecule of species i to jump into, H_i' the portion required to permit that molecule to enter the hole, and A_i is the frequency factor, assumed here to be independent of both γ and δ. Equation (14) expresses the idea that H_i is furnished at the temperature δ prevailing at the end of the jump, whereas H_i' is furnished at the temperature γ maintained at the starting point. Substitution of (14) into the definition of $\mathfrak{D}_i^*$ leads to

$$\mathfrak{D}_i^*/D_i^*=\frac{H_i'-H_i}{RT^2}. \tag{15}$$

Wirtz[6] has also discussed the possibility that, in addition to H_i and H_i', a heat H_i'' may have to be supplied at a point half-way between the initial and final points of the jump, in order to get the molecules in that vicinity into a favorable configuration. This heat will be furnished with equal probability at the initial or the final temperature, so that ν_i is given by

$$\nu_i=\tfrac{1}{2}A_i\left\{\exp\left[-\frac{(H_i'+H_i'')}{R\gamma}\right]\exp\left(-\frac{H_i}{R\delta}\right)+\exp\left(-\frac{H_i}{R\gamma}\right)\exp\left(-\frac{H_i+H_i''}{R\delta}\right)\right\}, \tag{16}$$

which leads once more to Eq. (15); thus the existence of H_i'' does not affect $\mathfrak{D}_i^*/D_i^*$, although it enters into the expression for $\Delta H_i^{\ddagger}$:

$$\Delta H_i^{\ddagger}=H_i+H_i'+H_i''. \tag{17}$$

If mass flow is ignored, i.e. if we arbitrarily set v equal to zero in Eq. (8), we get, assuming ideality and using (4),

$$\frac{\partial \ln n_i}{\partial T}=\alpha-\frac{\mathfrak{D}_i^*}{D_i^*}, \tag{18}$$

which is an equation used by Denbigh,[7] who also pointed out that in the limit of pure component i $\partial \ln n_i/\partial T$ is zero, so that, according to (18) and (15),

$$\alpha=(H_i'-H_i)/RT^2. \tag{19}$$

Since the expansion coefficient α is in general positive, Eq. (19) implies that, for self diffusion at least, H_i' must be greater than H_i, which is in direct contradiction to Eyring,[8] who concludes from Bridgman's measurements on viscosities at high pressures[9] that H_i' is usually only 10–20 percent of the total heat of activation.

No such difficulties are encountered if (18) is replaced by (10); combining the latter with (15) we get

$$\frac{\partial \ln n_1}{\partial T}=-\frac{n_2}{RT^2}\left(\frac{\partial \ln a_1}{\partial \ln n_1}\right)^{-1}_{T,p}\times\left[\frac{D_1^*(H_1'-H_1-RT^2\alpha)-D_2^*(H_2'-H_2-RT^2\alpha)}{D_1^*n_2+D_2^*n_1}\right],$$
$$\frac{\partial \ln n_2}{\partial T}=\frac{n_1}{RT^2}\left(\frac{\partial \ln a_1}{\partial \ln n_1}\right)^{-1}_{T,p}\times\left[\frac{D_1^*(H_1'-H_1-RT^2\alpha)-D_2^*(H_2'-H_2-RT^2\alpha)}{D_1^*n_2+D_2^*n_1}\right], \tag{20}$$

or

$$\frac{\partial \ln(n_2/n_1)}{\partial T}=\frac{1}{RT^2}\left(\frac{\partial \ln a_1}{\partial \ln n_1}\right)^{-1}_{T,p}\times\left[\frac{D_1^*(H_1'-H_1-RT^2\alpha)-D_2^*(H_2'-H_2-RT^2\alpha)}{D_1^*n_2+D_2^*n_1}\right]. \tag{21}$$

As the mole fraction of component i approaches unity, the mole fraction of the other component becomes zero, and therefore the requirement that $\partial \ln n_i/\partial T$ must vanish in the limit $n_i=1$ is automatically fulfilled by (20), without giving rise to relations such as (19). Furthermore, unless the mass flow velocity v can be determined (e.g., by following the motion of a non-diffusing particle suspended in the solution), it will in general be impossible to resolve the contributions of $H_2'-H_2$ and $H_1'-H_1$ to the observed composition gradient.

Equation (20) can be used to express the heats of transport Q_i^* in terms of $H_i'-H_i$. If we assume ideality, Q_i^*, as defined by Denbigh,[7] is given by

$$\frac{\partial \ln n_i}{\partial x}=-\frac{Q_i^*}{RT^2}\frac{\partial T}{\partial x}, \tag{22}$$

so that

$$Q_1^*=n_2\times\left[\frac{D_1^*(H_1'-H_1-RT^2\alpha)-D_2^*(H_2'-H_2-RT^2\alpha)}{D_1^*n_2+D_2^*n_1}\right],$$
$$Q_2^*=-n_1\times\left[\frac{D_1^*(H_1'-H_1-RT^2\alpha)-D_2^*(H_2'-H_2-RT^2\alpha)}{D_1^*n_2+D_2^*n_1}\right]. \tag{23}$$

Inspection shows that the Q_i^* given by (23) satisfy the identity

$$Q_1^*n_1+Q_2^*n_2=0, \tag{24}$$

which can readily be derived from (22).

[6] K. Wirtz, Physik. Z. 44, 221 (1943).
[7] K. G. Denbigh, Trans. Faraday Soc. 48, 1 (1952).
[8] Roseveare, Powell, and Eyring, J. Appl. Phys. 12, 669 (1941).
[9] P. M. Bridgman, *The Physics of High Pressure* (Macmillan Company, New York, 1931).

Equations (9) and (10) give rise to the very interesting possibility of obtaining $H_i'-H_i$ for the pure components. A sufficiently large particle (2) suspended in a pure liquid (1) should follow any mass flow of the liquid without undergoing any appreciable Brownian motion of its own. The velocity of mass motion of the pure liquid is given by (9) with n_2 set equal to zero:

$$v=(\mathfrak{D}_1^*-\alpha D_1^*)\frac{\partial T}{\partial x}=\frac{D_1^*}{RT^2}(H_1'-H_1-RT^2\alpha)\frac{\partial T}{\partial x}. \quad (25)$$

For ordinary liquids a reasonable set of values for the quantities involved in (25) is $H_1'=1$ kcal/mole, $H_1=6$ kcal/mole, $D_1^*=10^{-5}$ cm^2/sec, $\alpha=10^{-3}/°C$; thus, if we are working at room temperature with a temperature gradient of 10°C/cm, v would have a value of about -0.1 mm/hr, which can readily be observed with a traveling microscope.

Alternatively we can allow the system to reach a steady state and measure $\partial \ln n_2/\partial T$. If n_2 is very low and $D_2^*\ll D_1^*$, then the second of Eq. (20) becomes

$$\frac{\partial \ln n_2}{\partial T}=\frac{D_1^*}{D}\left(\frac{H_1'-H_1}{RT^2}-\alpha\right). \quad (26)$$

Both D_1^* and D can be measured independently, the former being the self-diffusion coefficient of pure component 1, while the latter is the observed mutual interdiffusion coefficient for the mixture; thus $H_1'-H_1$ can be calculated if $\partial \ln n_2/\partial T$ is known.

If we assume H_1' to be less than H_1, Eq. (26) predicts that the slowly diffusing component will tend to concentrate in the colder regions, and that this effect will be the more pronounced the lower the value of D. These qualitative predictions seem to be born out by the data of Debye and Bueche[10] on polystyrene-toluene solutions.

In conclusion it may be worth pointing out that there is one case for which Eqs. (10) reduce to (18), and that is when we are dealing with a very dilute solution of a small molecule component (1) in a polymer (2). Here we have again that $D_2^*\ll D_1^*$, but now it is n_1 that is very low, so that, if the solution is sufficiently dilute to be ideal, the first of Eqs. (10) becomes

$$\frac{\partial \ln n_1}{\partial T}=\alpha-\frac{\mathfrak{D}_1^*}{D_1^*}=\alpha-\frac{H_1'-H_1}{RT^2}. \quad (27)$$

ACKNOWLEDGMENT

One of us (S. P.) wishes to express his gratitude to Bell Telephone Laboratories, Inc. for the award of a Frank B. Jewett fellowship, which made this work possible.

[10] P. Debye and A. M. Bueche in *High Polymer Physics* (Remsen Press, Brooklyn, 1948).

Intermolecular Potentials from Dielectric Polarization in Polar Gases

FRANK E. HARRIS* AND BERNI J. ALDER
Department of Chemistry and Chemical Engineering, University of California, Berkeley, California
(Received March 6, 1953)

A theory which relates the dielectric polarization of polar gases to the intermolecular potential is formulated. In it occurs an expansion in powers of $1/V$, analogous to the virial expansion. The convergence of this series is briefly discussed, and the impossibility of rotational transitions in the gas phase is shown. Evaluation is limited to the leading term of the expansion, which involves interactions of a pair of molecules only and which is calculable from a knowledge of the intermolecular potential. Various intermolecular potentials consistent with virial data are introduced, and the results are compared with experiment for ammonia, methyl fluoride, and hydrogen fluoride. In view of the unsatisfactory precision of the experimental data, the agreement is as good as can be expected and is qualitatively in agreement with previous concepts of the strength and nature of the hydrogen bond.

I

IT has been possible to calculate the intermolecular force by means of equations which relate it to such experimental data for dilute gases as the equation of state and the viscosity. However, these determinations of the intermolecular force do not depend strongly on its angular component, and an alternative source of information based on a directionally dependent phenomenon would be desirable. The dielectric polarization is an equilibrium property possessing this characteristic.

In view of the development by Kirkwood,[1] and the authors,[2] of a theory of dielectric polarization in polar substances, the relationship between the macroscopic phenomenon and directionally dependent molecular interactions has been established, and dielectric measurements may therefore be employed to study more critically orientationally dependent forces. It is shown in this paper that the correlation parameter which determines the dielectric constant may be expanded, analogously to the virial expansion, in a sum in which successive terms depend upon the interaction between pairs, triplets, and consecutively larger numbers of molecules. The leading term of this series, involving pair interaction only, will represent the contribution to the correlation parameter in the limit of large volumes and may be calculated from a knowledge of the intermolecular potential. The choice of the intermolecular potential must be such as to yield correct values for both the second virial coefficient and the dielectric constant. This added restriction on the choice of the potential, plus the more critical determination of its angular dependence by means of the dielectric constant, allows for its more precise evaluation than heretofore.

The experimental data presently available do not justify extensive calculations. We have therefore concentrated our efforts upon presentation of the general theory by which the intermolecular potential may be evaluated. The method will be illustrated by application to the few polar gases for which sufficient experimental data have been reported.

II

The equation for the dielectric constant ϵ of an isotropic polar substance is[2]

$$\left(\frac{\epsilon-n^2}{n^2+2}\right)\left(\frac{2\epsilon+1}{\epsilon}\right)=4\pi\frac{N}{V}\frac{\mu^2 g}{3kT}, \tag{1}$$

where N/V is the number of molecules per unit volume, and n and μ are the refractive index and dipole moment, respectively. The correlation parameter g can be evaluated from the formula obtained by Kirkwood,[1]

$$g=1+\frac{N}{\Omega V}\int \cos\gamma n(\mathbf{r},\omega)d\mathbf{r}(d\omega), \tag{2}$$

in which γ is the angle between a dipole at the origin directed along the polar axis and another dipole at the configuration of integration. $n(\mathbf{r},\omega)$ is the distribution function depending on the distance $\mathbf{r}$ and on all angles ω necessary to specify the relative position and orientation of the pair of molecules involved. Ω is a normalization coefficient such that $\Omega=\int(d\omega)$. Equation (2) will be evaluated by the methods of classical statistical mechanics because quantum effects are small in the present applications. However, under conditions where quantum effects are important the appropriate distribution function must be substituted.

μ represents the moment of a molecule in the medium, which differs from the vacuum moment because of the field of its neighbors. In the limit of large volumes, μ can be expressed in terms of μ_0, the vacuum moment, by the use of Onsager's equation for the reaction field:

$$\mu=\mu_0\left(\frac{n^2+2}{3}\right)\left(\frac{2\epsilon+1}{2\epsilon+n^2}\right). \tag{3}$$

Equation (1) differs from the frequently used Debye equation[3] for polar gases. If we introduce the molar

* Predoctoral Fellow, National Science Foundation.
[1] J. G. Kirkwood, J. Chem. Phys. 7, 911 (1939).
[2] F. E. Harris and B. J. Alder, J. Chem. Phys. (to be published).
[3] P. Debye, *Polar Molecules* (The Chemical Catalog Company, Inc., New York, 1929).

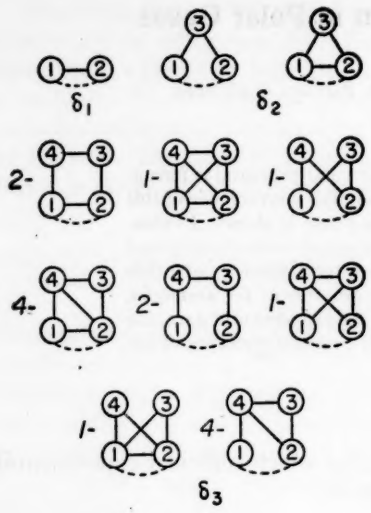

FIG. 1. Representation of the first three irreducible integrals δ_k. The number to the left of each diagram in δ_3 indicates the number of times that diagram occurs in the integrand.

polarization, $P=(\epsilon-1/\epsilon+2)V_m$, in which V_m is the molar volume, (1) becomes

$$P=\frac{4\pi N_0}{3}\left[\alpha+\frac{\mu_0^2}{3kT}\frac{g\epsilon(2\epsilon+1)}{\epsilon+2}\left\{\frac{n^2+2}{2\epsilon+n^2}\right\}^2\right]. \quad (4)$$

N_0 denotes Avogadro's number and α the molecular polarizability. Equation (4) will reduce to the Debye equation in the limit of large volume since g and $[\epsilon(2\epsilon+1)/(\epsilon+2)][(n^2+2)/(2\epsilon+n^2)]^2$ become unity. Thus, dipole moments determined by extrapolation of vapor phase measurements to zero density will retain their validity; however, Eq. (4) must be used to determine the dependence of P upon density.

III

We now proceed to evaluate g. Equation (2) is equivalent to the expression

$$g=1+\frac{N\int\cos\gamma_{12}\exp\left[-\frac{1}{kT}V_N(\mathbf{r}_1,\cdots\mathbf{r}_N;\omega_1,\cdots\omega_N)\right]d\mathbf{r}_1\cdots d\mathbf{r}_N(d\omega_1)\cdots(d\omega_N)}{\int e^{-V_N/kT}d\mathbf{r}_1\cdots d\mathbf{r}_N(d\omega_1)\cdots(d\omega_N)}, \quad (5)$$

where $V_N(\mathbf{r}_1,\cdots\mathbf{r}_N;\omega_1,\cdots\omega_N)$ is the total energy of interaction between N molecules, and γ_{12} is the angle between the dipoles of two arbitrary molecules, 1 and 2. If it is assumed that V_N may be approximated by a sum of interactions between pairs of molecules,

$$V_N=\sum_{i>j}V_{ij},$$

and the definition $e^{-V_{ij}/kT}-1=f_{ij}$ is introduced, Eq. (5) can be expanded in a manner similar to that employed in the expansion of the partition function in order to obtain the virial coefficients. We plan to discuss the expansion for g in a subsequent publication. The resulting development in powers of $1/V$ is

$$g=1+\left(\frac{N}{V}\right)\delta_1+\left(\frac{N}{V}\right)^2\delta_2+\cdots+\left(\frac{N}{V}\right)^k\delta_k+\cdots. \quad (6)$$

δ_1, δ_2, etc. represent "irreducible" integrals comparable to the β's of the Mayer theory.[4] The integrand of δ_k contains pair interaction terms involving $k-1$ molecules in addition to molecules 1 and 2, which are always present by virtue of the $\cos\gamma_{12}$ terms. The δ's are irreducible in the sense that they cannot be expressed in terms of δ's of lower k value and β's. As with the β's, the number and kinds of pair interactions represented by a δ can be counted by the aid of a diagram. A circle is used to represent each molecule, and a line drawn between a pair of molecules indicates that a corresponding f_{ij} is present in the integral. A dashed line is always drawn between molecules 1 and 2 to represent the $\cos\gamma_{12}$ factor. The δ's will then have the following characteristics for $k>1$: (1) All circles must be multiply connected when both solid and dashed lines are counted as connections. (2) If there is a solid line in addition to the dashed line between circles 1 and 2, the diagram must remain totally multiply connected when the dashed line is not counted as a connection.

δ_1 is represented by a diagram with both a solid and a dashed line between circles 1 and 2. The first two δ's and their general form are given by

$$\delta_1=\frac{1}{\Omega^2V}\int\cos\gamma_{12}f_{12}d\mathbf{r}_1d\mathbf{r}_2(d\omega_1)(d\omega_2), \quad (7)$$

$$\delta_2=\frac{1}{\Omega^3V}\int\cos\gamma_{12}[f_{23}f_{13}+f_{12}f_{23}f_{13}]\times d\mathbf{r}_1d\mathbf{r}_2d\mathbf{r}_3(d\omega_1)(d\omega_2)(d\omega_3), \quad (8)$$

and

$$\delta_k=\frac{1}{(k-1)!\Omega^{k+1}V}\times\int\cos\gamma_{12}\sum_{k+1>i>j}\prod f_{ij}d\mathbf{r}_1\cdots d\mathbf{r}_{k+1}(d\omega_1)\cdots(d\omega_{k+1}).$$

Diagrams for the first three δ's are shown in Fig. 1.

In the limit of large volumes, Eq. (6) reduces to its first term. Replacing f_{12} by its definition, and using the

[4] J. E. Mayer and M. G. Mayer, *Statistical Mechanics* (John Wiley and Sons, Inc., New York, 1940), Chap. XIII (and Appendices).

fact that $\int \cos\gamma_{12}(d\omega_1)$ vanishes,

$$g=1+\frac{N}{\Omega V}\int \cos\gamma_{12}e^{-V_{12}/kT}d\mathbf{r}_{12}(d\omega_{12}), \qquad (9)$$

where we have changed to relative coordinates $\mathbf{r}_{12}$, ω_{12}. Equation (9) may alternatively be derived directly from (2) by virtue of the fact that $n(\mathbf{r},\omega)$ is given, for large volumes, by $n(\mathbf{r},\omega)=\exp(-V_{12}/kT)$.

The convergence of the series (6) may be investigated by methods parallel to those useful in the study of the virial expansion; we plan to present the results of such an investigation with the forthcoming discussion of the expansion. However, some pertinent remarks may be made at this time. The denominator of Eq. (5) representing the normalization factor is simply the partition function, which, when expanded in powers of $1/V$, is known to yield an absolutely convergent series for conditions corresponding to the gas phase. The series in the numerator of (5) may be put into one-to-one correspondence with the series of the denominator. Each term of the numerator is, in absolute value, smaller than or equal to the corresponding term of the denominator by virtue of the fact that $|\cos\gamma_{12}|\leq 1$. The numerator then must also converge when the denominator converges. Since (6) may be obtained by division of the two absolutely convergent series, it too must converge for values of $1/V$ corresponding to the gas state. This fact precludes the existence of a "gaseous crystal" analogous to a liquid crystal in the liquid phase. The above considerations do not require, however, that (6) diverge whenever the virial expansion is divergent; in fact, it is not unreasonable to surmise that (6) may continue to converge into the liquid, or even into the solid state. If in the rotational phase space there is no state analogous to the short-range order in translational phase space (liquid), the expansion would then diverge in some materials at the point of formation of liquid crystals, and for many substances at their melting points. If, however, the molecules are still free to rotate below the melting point, the expansion would diverge at the point of the first rotational transition. In any case, orientational condensation would be expected to correspond to the point of divergence of the expansion of the dielectric correlation parameter.

IV

Solutions may now be determined for Eq. (9) using various forms of V_{12}. We shall consider intermolecular potentials composed of a spherically symmetric repulsive term, dependent upon an inverse power of r; an attractive term, also spherically symmetric, which will represent the dispersion (van der Waals) energy and which will have an r^{-6} dependence; and further terms, which will represent the interactions of all electric multipoles, both permanent and induced. The potential of any arbitrary charge distribution in a molecule can be expressed by such a multipole expansion. This potential may therefore be written

$$V=\lambda r^{-s}-cr^{-6}+\Phi(\mathbf{r},\omega), \qquad (10)$$

where s is the exponent of the repulsive term, λ and c are constants, and $\Phi(\mathbf{r},\omega)$ represents the electrostatic potential.

The leading term of $\Phi(\mathbf{r},\omega)$ is the dipole-dipole interaction, which depends on r^{-3}. The r^{-4} term consists of the dipole-quadrupole energy, and the r^{-5} term contains the quadrupole-quadrupole and dipole-octupole interactions. The r^{-6} term includes not only the quadrupole-octupole and dipole-24-pole interactions, but also the permanent dipole-induced dipole interaction energy. Terms in powers of $1/r$ higher than six will not be considered here since their effect can be safely neglected.

It is evident that for spherically symmetric potentials g is equal to unity. This, however, is only true for monatomic gases. For other gases, even if μ were zero, the quadrupole moment might not be, and moreover the van der Waals forces would not be strictly symmetric since the polarizability is not the same in all directions. This would result in unequally favored relative orientations possessing net induced dipole moments. Since the repulsive potential is not, in these cases, radially symmetric, it will also contribute to this effect.

Since our procedure will be to attempt to satisfy both dielectric and virial coefficient data, and since there exists no satisfactory alternative method for calculating the coefficients λ and c of the repulsion and van der Waals attraction, we shall determine these coefficients from the virial data, and introduce the potential thereby obtained into the equations describing the dielectric polarization. Therefore, all terms of the electrostatic potential omitted from consideration will be partially compensated for by the adjustment to optimum values of the parameters c and λ. This means that any electrostatic term omitted will be replaced by a spherically symmetric term of the same average effect. Clearly this approximation will be most seriously in error for terms of strong angular dependence, and will be better for more nearly spherically symmetric terms. These latter terms in the multipole expansion are those which have some degree of symmetry with respect to the operation of rotation of one molecule of an interacting pair such as, for example, the two fold symmetry of the dipole-quadrupole interaction. Thus, since the evaluation of all significant terms is laborious, and furthermore since the quadrupole moment is not known in many instances, those terms which will be kept as a first approximation are those representing a polarizable point dipole, namely, the dipole-dipole and dipole-induced dipole interactions. Higher multipoles will contribute significantly, but even the dipole-induced dipole term in the gases treated is found to be small relative to the total energy. This indicates that the probable errors resulting from an

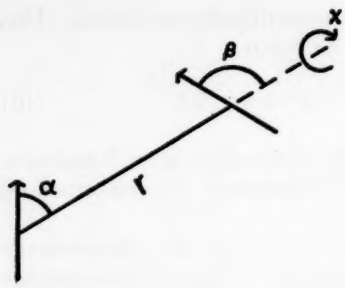

FIG. 2. The coordinate system used to evaluate dipole interactions.

inexact treatment of further terms will not be more important than the approximations already made of spherical symmetry of the repulsive and van der Waals terms.

In describing the dipole-dipole and dipole-induced dipole contributions, we shall use a coordinate system in which one molecule is placed at the origin with its dipole oriented along the polar axis. The configuration will be described by the intermolecular distance r and the angles α, β, and χ, as illustrated in Fig. 2. The range of α and β is 0 to π, while that of χ is 0 to 2π. γ_{12} is related to the above angles by

$$\cos\gamma_{12}=\cos\alpha\cos\beta+\sin\alpha\sin\beta\cos\chi. \tag{11}$$

In these coordinates, the dipole-dipole interaction energy is

$$\Phi_1=\frac{-\mu_0^2}{r^3}(2\cos\alpha\cos\beta-\sin\alpha\sin\beta\cos\chi), \tag{12}$$

and the permanent dipole-induced dipole interaction, for molecules of spherically symmetric polarizability α, is

$$\Phi_2=\frac{-\alpha\mu_0^2}{r^6}(3\cos^2\alpha+3\cos^2\beta+2). \tag{13}$$

In both (12) and (13), the dipole moment to be used is the vacuum moment. No allowance has been made for the additional dipole moment induced at the first molecule by the induced dipole of the second molecule. This additional correction is, for the present purposes, negligible.

TABLE I. Ammonia.

	Second virial coefficient $\frac{+N_0B_1}{2}$ (cc/mole)				
Temp. °K	calc. I[a,e]	calc. II[b,i]	calc. III[e]	calc. IV[d]	expt.[h]
285.7	317	...	...	...	...
300	...	274	270	261	270
400	120.4	121	119.5	123	119
500	66.1	68	65.8	68.2	66.6
600	38.7	...	39.0	39.3	40.6

	Second dielectric correlation coefficient $N_0\delta_1$ (1/mole)					
Temp. °K	calc. I[a]	calc. II[b]	calc. III[c]	calc. IV[d]	expt.[f]	expt.[g]
323	0.0193	0.0595	0.0178	0.0190	0.021	0.0096
373	0.0095	0.0303	0.0088	0.0103	0.021	...
423	0.0054	0.0176	0.0049	0.0063	0.031	...
473	0.0034	0.0112	0.0030	0.0042	0.022	...

[a] Rigid dipoles, hard sphere core. $c=1.055\times10^{-58}$ erg/cm^6, $\sigma=3.18$A, $\mu_0=1.48$D., $\alpha=0$, $s=\infty$.
[b] Rigid dipoles, 12th power repulsion. $c=0.5165\times10^{-58}$ erg/cm^6, $\sigma=2.58$A, $\mu_0=1.47$D., $\alpha=0$, $s=12$.
[c] Rigid dipoles, hard sphere core, altered μ_0. $c=1.028\times10^{-58}$ erg/cm^6, $\sigma=3.15$A, $\mu_0=1.436$D., $\alpha=0$, $s=\infty$.
[d] Polarizable dipoles, hard sphere core. $c=1.637\times10^{-58}$ erg/cm^6, $\sigma=3.50$A, $\mu_0=1.48$D., $\alpha=2.24\times10^{-24}$ cm^3, $s=\infty$.
[e] See reference 5b.
[f] See reference 6.
[g] See reference 7.
[h] See reference 8.
[i] See reference 11.

V

Equation (9) is to be used with the potential (10) to obtain values of g. In order to gain additional information regarding the effect of the various terms of the potential, and to perform a simpler preliminary calculation, a solution was first sought using only the dipole-dipole term of the electrostatic potential. Upon expanding the exponential in (9) into a power series, it may be shown by the method employed for the calculation of the second virial coefficient[5] that

$$\delta_1=2^5\pi\sigma^3y^{6/s}\sum_{n=1}^{\infty}\sum_{t=0}^{(\leq n-1/2)}y^{(ns-6n+6t)/s}p^{2t+1}C_{nt}, \tag{14}$$

where C_{nt} is defined in Appendix I. y, σ, and p are defined by

$$\sigma^{s-6}=\frac{\lambda}{c},\quad y=\frac{c}{kT\sigma^6},\quad p=\frac{\mu_0^2\sigma^3}{c}.$$

In the limit $s\to\infty$, $\lambda\to\infty$, σ constant, the repulsive potential corresponds to a hard sphere core of diameter σ. This limiting case is discussed in Appendix I.

In addition, we shall need Stockmayer's result for the second virial coefficient:[5b]

$$\frac{-\beta_1}{2}=\frac{2\pi\sigma^3}{3}y^{3/s}\times\left\{\Gamma\left(\frac{s-3}{s}\right)-\sum_{n=1}^{\infty}\sum_{l=0}^{\leq n/2}y^{(ns-6n+6l)/s}p^{2l}D_{nl}\right\}. \tag{15}$$

D_{nl} is listed in Appendix I.

Next, calculations of both δ_1 and β_1 were made, including in the potential the dipole-induced dipole energy (13). By processes entirely similar to those employed in the derivation of (14) and (15), the following results were obtained.

$$\delta_1=2^6\pi\sigma^3y^{6/s}\times\sum_{n=1}^{\infty}\sum_{k=1}^{n}\sum_{l=0}^{\leq(k-1/2)}y^{(ns-6n+6l)/s}p^kq^{k-2l-1}J_{nkl}. \tag{16}$$

$$\frac{-\beta_1}{2}=\frac{2\pi\sigma^3}{3}y^{3/s}\left\{\Gamma\left(\frac{s-3}{s}\right)-\sum_{n=1}^{\infty}\sum_{k=0}^{n}\sum_{l=0}^{\leq k/2}y^{(ns-6n+6l)/s}p^kq^{k-2l}F_{nkl}\right\}. \tag{17}$$

[5a] J. E. Lennard-Jones, Proc. Roy. Soc. (London) **A106**, 463 (1924).
[5b] W. H. Stockmayer, J. Chem. Phys. **9**, 398 (1941).

Expressions for J_{nkl} and F_{nkl} are given and tabulated in Appendix II. q is defined by the equation $q=\alpha/\sigma^3$.

All the series expansions in this section were examined and found to be convergent for all values of the variables y, p, and q.

VI

The only substances for which sufficient measurements were found on both the dielectric polarization and the equation of state were ammonia, methyl fluoride, and hydrogen fluoride. For each of these substances, experimental values of g were computed by means of Eq. (1). The experimental second virial coefficient was then used to determine optimum values of the parameters c and λ. Finally, these values of c and λ were inserted into the expressions for δ_1, and the results compared with experiment.

1. Ammonia

The dielectric constant of gaseous ammonia has been measured as a function of pressure by Uhlig, Kirkwood, and Keyes,[6] and by Van Itterbeek and de Clippeleir.[7] The second virial coefficient has been determined experimentally by Keyes,[8] and the experimental data fitted to the rigid dipole model by Stockmayer[5b] and Rowlinson.[11] Myers[9] refined this calculation by partial inclusion of terms involving the quadrupole moments according to methods outlined by Margenau and Myers.[10] His calculations indicate that the quadrupole terms are of about the same magnitude as the dipole-induced dipole term, and that these terms are each less than 25 percent of the dipole-dipole interaction. Because of the symmetry considerations mentioned earlier, it is seen that omission of the quadrupole term and subsequent replacement by its average value should not seriously influence calculated values of g.

Four calculations were carried out for ammonia. The results are shown in Table I. The first was for a hard sphere core with a rigid dipole interaction potential, and the second for the same potential, except with an inverse twelfth-power repulsive term. The $s=12$ calculation resulted in an increase in the computed value of $g-1$ mainly because of the smaller value of σ, which causes the angular interaction to be placed closer in, and therefore to be increased. In succeeding calculations the hard sphere core potential was used as a reference point to investigate the effect of changing various terms. The effect of the small uncertainty in the experimentally determined dipole moment was studied, by making a calculation with a moment $\mu_0=1.436$ D. (D. represents Debye units) the lowest probable value, in contrast to the value here adopted of 1.48 D. This calculation showed that the values of δ_1 were not sensitive to the uncertainty in μ_0. Finally, a calculation including induced dipole interactions was made. It increased the value of δ_1 by about 20 percent at 473°K, but did not alter it greatly at 323°K. From the change brought about by including the induced dipole interactions, it may be concluded that the probable effect of inclusion of further directionally dependent terms in the energy will be to decrease the temperature dependence somewhat without greatly altering the order of magnitude of $g-1$.

TABLE II. Experimental values of the second dielectric correlation coefficient for ammonia.

Temp. °K	$1/V$ (moles/l)	$N_0\delta_1$* (l/mole)
473	0.536	0.0224
	1.427	0.0154
	2.095	0.0138
	3.234	0.0148
423	0.611	0.0311
	1.704	0.0170
	2.61	0.0180
	4.48	0.0152
373	0.722	0.0208
	1.393	0.0158
	2.27	0.0163
	2.649	0.0147
323	0.650	0.0215

* See reference 6.

The experimental results are not sufficiently accurate to enable more than an order of magnitude comparison to be made, as can be seen from the scattering of the experimental values of δ_1 in Table II, and the disagreement between the two sets of experimental data. The experimental results and the calculated ones for $s=12$ are seen to be in rough agreement except for the temperature dependence of δ_1. It is doubtful that the inclusion of further directionally dependent terms in the energy can change the calculated temperature dependence to near the experimental one. Besides, the experimental temperature coefficient must be wrong since δ_1 has to be a monatonically decreasing function of temperature due to the fact that the angular interaction must decrease as the temperature is increased.

2. Methyl Fluoride

The dielectric constant of methyl fluoride has been measured at 50° to 75°C by David, Hamann, and Pearse.[12] These authors also report values of the second virial coefficient at the same temperatures.[13] Their data, all obtained at elevated pressures, extrapolate to the same value of the dipole moment as that obtained by Smyth and McAlpine,[14] namely, $\mu_0=1.81$ D.

[6] Uhlig, Kirkwood, and Keyes, J. Chem. Phys. **1**, 155 (1933).
[7] A. Van Itterbeek and K. de Clippeleir, Physica **14**, 349 (1948).
[8] F. G. Keyes, J. Am. Chem. Soc. **60**, 1761 (1938).
[9] V. Myers, Phys. Rev. **75**, 1620 (1949).
[10] H. A. Margenau and V. W. Myers, Phys. Rev. **66**, 1761 (1938).
[11] J. S. Rowlinson, Trans. Faraday Soc. **45**, 974 (1949).
[12] David, Hamann, and Pearse, J. Chem. Phys. **20**, 969 (1952).
[13] S. D. Hamann and J. Pearse, Trans. Faraday Soc. **48**, 101 (1952).
[14] C. P. Smyth and K. B. McAlpine, J. Chem. Phys. **2**, 499 (1934).

TABLE III. Methyl fluoride.

Temp. °K	Second virial coefficient (cc/mole) calc.[a]	expt.[c]	Second dielectric correlation coefficient (1/mole) calc.[a]	expt.[b]
323.2	−172	−171	0.0038	<0.005
348.2	−140	−141	0.0030	<0.005

[a] Rigid dipoles, hard sphere core. $c=5.733\times10^{-58}$ ergs/cm^6, $\sigma=4.51$A, $\mu_0=1.81$D., $\alpha=0$, $s=\infty$.
[b] See reference 12.
[c] See reference 13.

Calculation of experimental values of g on the basis of Eq. (1), and the use of (3) to account for the change of dipole moment with environment yield conclusions at variance with those reported by David, Hamann, and Pearse. These authors failed to make the correction represented by (3), and therefore claimed the data indicated restricted rotation at temperatures and pressures above the critical values. We find that the extent of correlation is below the experimentally detectable limit up to the highest pressures studied.

Calculations for the hard sphere core and rigid dipole model yield values of $g-1$ too small to be detected by the above experiments. Since decreasing s and the addition of the induced dipole term should not change the order of magnitude of δ_1, it was concluded that this calculated result was consistent with experiment. Data for methyl fluoride are given in Table III.

3. Hydrogen Fluoride

Neither the equation of state nor dielectric data have been as precisely determined for hydrogen fluoride as for ammonia and methyl fluoride. Therefore the experimental values of β_1 and δ_1 contain large uncertainties. The dielectric polarization of hydrogen fluoride was measured in the range below atmospheric pressure by Oriani and Smyth,[15] and the second virial coefficient was calculated from the equation of state data of Briegleb,[16] Simons and Hildebrand,[17] Long, Hildebrand, and Morrell,[18] and Fredenhagen.[19]

All that can be expected is the order of magnitude agreement in δ_1 shown in Table IV. σ and the energy of the hydrogen bond are in rough agreement with experiment.[17,20] It is to be noted that δ_1 is much larger for HF than for NH_3 or CH_3F, because of the strong directionally dependent hydrogen bond.

TABLE IV. Hydrogen fluoride.

Temp. °K	Second virial coefficient (cc/mole) calc.[a]	expt.	Second dielectric correlation coefficient (1/mole) calc.[a]	expt.[b]
311	−500	−400	0.4	0.7

[a] Rigid dipoles, hard sphere core. $c=0.05\times10^{-58}$ ergs/cm^6, $\sigma=2.70$A, $\mu_0=1.91$D., $\alpha=0$, $s=\infty$.
[b] See reference 15.

APPENDIX I

Expansion of δ_1 and β_1 for rigid dipole interaction.

The coefficient C_{nt} occurring in Eq. (14) is

$$C_{nt}=\frac{A_t}{(n-2t-1)!\,(2t+1)!}\cdot\frac{1}{s}\Gamma\left(\frac{6n-6t-6}{s}\right), \quad \text{(A1.1)}$$

where

$$A_t=\frac{2^{2t}(t+2)!\,t!}{(2t+4)!\,(2t+3)}\sum_{u=0}^{t}\frac{(2u)!}{(u!)^2}(3u-t). \quad \text{(A1.2)}$$

The expression for D_{nl} of Eq. (15) is

$$D_{nl}=\frac{G_l}{(n-2l)!\,(2l)!}\cdot\frac{3}{s}\Gamma\left(\frac{6n-6l-3}{s}\right), \quad \text{(A1.3)}$$

where

$$G_l=\frac{2^{2l+1}l!\,(l+1)!}{(2l+1)(2l+2)!}\sum_{t=0}^{l}\frac{(2t)!}{(t!)^2}. \quad \text{(A1.4)}$$

The relations for the corresponding coefficients for the hard core potential can be derived from the more general forms (A1.1) and (A1.3) by use of the relation

$$\lim_{x\to0}x\Gamma(x)=1.$$

Equation (A1.4) may be transformed into Stockmayer's result[5b] by application of the identity

$$\frac{2^{2l+1}(l+1)!}{(2l+2)!}\sum_{t=0}^{l}\frac{(2t)!}{(t!)^2}=\sum_{t=0}^{l}\frac{3^t}{t!\,(l-t)!\,(2t+1)}. \quad \text{(A1.5)}$$

Numerical values of these coefficients have not been tabulated here, as they may be obtained from coefficients given in Appendix II by methods described there.

APPENDIX II

Expansion of δ_1 and β_1 for polarizable dipole interaction.

The coefficient J_{nkl} occurring in Eq. (16) is

$$J_{nkl}=\frac{T_{kl}}{(n-k)!}\cdot\frac{1}{s}\Gamma\left(\frac{6n-6l-6}{s}\right), \quad \text{(A2.1)}$$

where

$$T_{kl}=\sum_{t=0}^{l}\sum_{j=0}^{k-2l-1}\sum_{p=0}^{j}\frac{3^j2^{k-j}[(2l-2t+2p+1)(2l-2t+2j-2p+1)-(t+1)(2l-2t-1)]}{(k-2l-j+1)!\,p!\,(j-p)!\,(2l-2t+1)!}$$
$$\times\left[\frac{(2l-2t+2p)!\,(l+p+2)!\,(2l-2t+2j-2p)!\,(l+j-p+2)!}{(l-t+p)!\,(2l+2p+4)!\,(l-t+j-p)!\,(2l+2j-2p+4)!}\right]. \quad \text{(A2.2)}$$

[15] R. A. Oriani and C. P. Smyth, J. Am. Chem. Soc. **70**, 125 (1948).
[16] G. Briegleb, Naturwissenschaften **29**, 420 (1941).
[17] J. Simons and J. H. Hildebrand, J. Am. Chem. Soc. **46**, 2183 (1924).
[18] Long, Hildebrand, and Morrell, J. Am. Chem. Soc. **65**, 182 (1943).
[19] K. Fredenhagen, Z. anorg. u. allgem. Chem. **218**, 161 (1934).
[20] Bauer, Beach, and Simons, J. Am. Chem. Soc. **61**, 19 (1939).

TABLE V. The coefficients F_{nkl} and J_{nkl} for $s=\infty$.

F_{nkl}

k,l \ n	1	2	3	4	5	6	7	8
0,0	1	1/6	1/30	1/168	1/1080	1/7920	1/65520	1/604800
1,0	4	4/3	2/5	2/21	1/54	1/330	1/2340	1/18900
2,0		44/15	44/25	22/35	22/135	1/30	11/1950	11/13500
2,1		1/3	1/9	1/30	1/126	1/648	1/3960	1/28080
3,0			1472/525	1472/735	736/945	736/3465	184/4095	184/23625
3,1			8/15	8/25	4/35	4/135	1/165	1/975
4,0				9424/3675	9424/4725	4712/5775	4712/20475	1178/23625
4,1				2224/2625	2224/3675	1112/4725	1112/17325	278/20475
4,2				1/75	1/125	1/350	1/1350	1/6600
5,0					16064/7425	16064/9075	8032/10725	8032/37125
5,1					2528/2205	2528/2835	1264/3465	1264/12285
5,2					116/2625	116/3675	58/4725	58/17325
...						...	...	...
6,2						2404/25725	2404/33075	1202/40425
6,3						29/55125	29/77175	29/198450
...							...	...
7,3							176/77175	176/99225
...								...
8,4								11/694575
...								...

J_{nkl}

k,l \ n	2	3	4	5	6	7	8
2,0	1/180	1/360	1/1080	1/4320	1/21600	1/129600	1/907200
3,0		157/12600	157/18900	157/50400	157/189000	157/907200	157/5292000
3,1		1/3600	1/7200	1/21600	1/86400	1/432000	1/2592000
4,0			94/4725	47/3150	47/7875	47/28350	47/132300
4,1			2/1575	4/4725	1/3150	2/23625	1/56700
5,0				18353/727650	36706/1819125	18353/2182950	18353/7640325
5,1				23/7350	23/9800	23/24500	23/88200
5,2				1/44100	1/66150	1/176400	1/661500
6,0					635204/23648625	317602/14189175	317602/33108075
6,1					3973/727650	7946/1819125	3973/2182950
6,2					1/8820	1/11760	1/29400
...						...	...
7,3						1/952560	1/1270080
...						...	...

The expression for F_{nkl} of Eq. (17) is

$$F_{nkl}=\frac{H_{kl}}{(n-k)!}\cdot\frac{1}{s}\Gamma\left(\frac{6n-6l-3}{s}\right), \tag{A2.3}$$

where

$$H_{kl}=\sum_{t=0}^{l}\sum_{j=0}^{k-2l}\sum_{p=0}^{j}3^{j+1}2^{k-j+2}\cdot\frac{1}{(2l-2t)!(k-2l-j)!p!(j-p)!}\times\left[\frac{(2l-2t+2p)!(l+p+1)!(2l-2t+2j-2p)!(l+j-p+1)!}{(l-t+p)!(2l+2p+2)!(l-t+j-p)!(2l+2j-2p+2)!}\right]. \tag{A2.4}$$

These coefficients are tabulated in Table V for the case of a potential with a hard sphere core. It is possible by use of (A2.1) and (A2.3) to obtain from the tabulated coefficients the corresponding quantities for a $1/r^s$ repulsive potential, without the necessity of performing additional summations. The coefficients C_{nl} and D_{nl} given in Appendix I may be obtained from those listed by picking out the values of the subscripts for which the exponent of q in (16) or (17) vanishes.

Diffusion in the System CH_4-TCH_3 to 300 Atmospheres Pressure*

Q. R. JEFFRIES AND H. G. DRICKAMER
Department of Chemistry, University of Illinois, Urbana, Illinois

(Received March 16, 1953)

Diffusion coefficients have been measured in the system CH_4-TCH_3 to 300 atmospheres pressure. In general the results are consistent with the predictions of Enskog's dense gas theory. At the highest densities, the diffusion coefficients are lower than the theory predicts. This is expected as, at these densities, unevaluated terms in the dense gas correction become significant.

DIFFUSION has been studied in the system CH_4-TCH_3 to 300 atmospheres pressure, using the method described in one of our previous publications.[1] The tritiated methane was obtained from Tracerlab.

The kinetic theory of diffusion in dilute gases has been developed by Enskog[2] and the collision cross-section integral for the Lennard-Jones model have been evaluated by Hirschfelder *et al.*[3] When Enskog's dense gas correction[4] is appended, the equation takes the form

$$D=\frac{3}{16}\left(\frac{kT}{\pi\mu}\right)^{\frac{1}{2}}\frac{1}{r_0^2 W_{(1)}{}^{(1)} n\chi},$$

where μ = reduced mass, r_0 = collision diameter, n = number of molecules per unit volume, $W_{(1)}{}^{(1)}$ = collision cross-section integral, $\chi=1+5/12\pi n\sigma^3+0.1275\ (\pi n\sigma^3)^2+\cdots$, and σ = collision diameter for solid elastic spheres assumed equal to r_0.

The experimental diffusion coefficients are listed in Table I and Fig. 1 and compared with theory. The p-v-t data of Kvalnes and Gaddy[5] were used. It can be seen that the agreement is excellent except at the highest pressures. In this region the experimental coefficients are 10–20 percent lower than predicted by Eq. (1). In this density region (one and one-half times the critical density), the higher terms in χ would be significant. The deviation is thus in the direction to be expected.

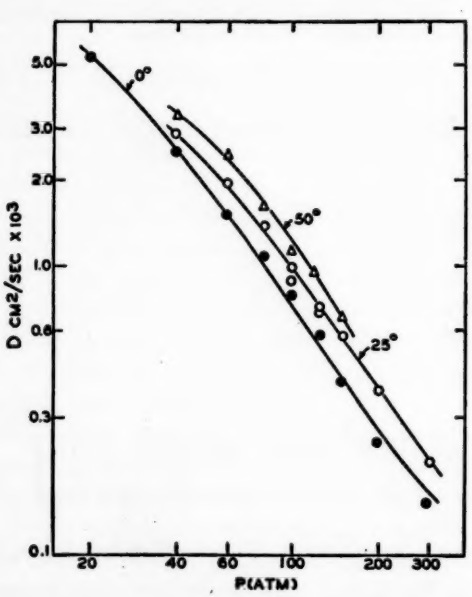

FIG. 1. Diffusion coefficients in the system CH_4-TCH_3. The points are experimental data; the lines are calculated from Eq. (1).

TABLE I. Diffusion data CH_4-TCH_3.

P atmos	T°C	P g/cc	X	$D_{expt}\times10^3$ cm²/sec	$D_{theor}\times10^3$ cm²/sec
40	50°	0.026	1.079	3.65	3.50
60	50°	0.0392	1.124	2.46	2.36
80.3	50°	0.0532	1.172	1.60	1.64
100	50°	0.0686	1.229	1.13	1.22
124.8	50°	0.085	1.293	0.94	0.93
150	50°	0.103	1.368	0.664	0.715
40.5	25°	0.030	1.09	2.91	2.91
60	25°	0.044	1.14	1.98	1.90
80	25°	0.0596	1.195	1.38	1.36
100	25°	0.0828	1.283	0.98	0.91
100	25°	0.0828	1.283	0.87	0.91
125	25°	0.099	1.349	0.69	0.715
125	25°	0.099	1.349	0.71	0.715
150	25°	0.1192	1.436	0.57	0.56
200	25°	0.1585	1.62	0.368	0.374
300	25°	0.214	1.912	0.21	0.231
20	0°	0.0156	1.047	5.3	5.5
40.2	0°	0.0322	1.095	2.48	2.55
60	0°	0.051	1.164	1.51	1.52
81	0°	0.0716	1.240	1.09	1.02
100	0°	0.0916	1.329	0.75	0.734
125	0°	0.1184	1.431	0.575	0.535
150	0°	0.1445	1.550	0.40	0.413
200	0°	0.188	1.770	0.248	0.270
300	0°	0.242	2.071	0.150	0.177

These results are in contrast to the previously published results for CO_2[1] which showed marked deviations from theory well below the critical density. This emphasizes the role of orientation in CO_2 diffusion. Since methane is essentially spherically symmetrical no such effects would be expected.

Q. R. Jeffries would like to acknowledge financial assistance from the U. S. Atomic Energy Commission.

* This work was supported in part by the U. S. Atomic Energy Commission.

[1] W. L. Robb and H. G. Drickamer, J. Chem. Phys. **19**, 1504 (1951).

[2] S. Chapman and T. G. Cowling, *The Mathematical Theory of Non Uniform Gases* (Cambridge University Press, Cambridge, 1939).

[3] Hirschfelder, Curtiss, Bird, and Spotz, J. Chem. Phys. **16** 968 (1948).

[4] Reference 2, pp. 273–295.

[5] H. M. Kvalnes and V. L. Gaddy, J. Am. Chem. Soc, **53**, 394 (1931).

The Effect of Pressure on Diffusion in the System CCl_4-SnI_4*

E. P. Doane and H. G. Drickamer
Department of Chemistry, University of Illinois, Urbana, Illinois

(Received March 16, 1953)

Diffusion coefficients have been measured for the system CCl_4-SnI_4 using I^{131} tagged SnI_4. Isotherms were obtained at 50°C and 75°C to 2000 atmospheres pressure. The results are interpreted in terms of the activation enthalpy, entropy, and volume. Below 1000 atmospheres the diffusion mechanism differs only slightly from that in effect at atmospheric pressure. At higher pressures orientational effects are observed.

In a series of previous papers[1–4] a method was presented for measuring diffusion in liquids under pressure. This method was applied to organic liquid mixtures involving CS_2 as one of the components, and to aqueous solutions. The results were interpreted in terms of the activation enthalpy $\Delta H^{\ddagger}$, the activation volume $\Delta V^{\ddagger}$, and the activation entropy above that at atmospheric pressure $\Delta S^{\ddagger}-\Delta S_0^{\ddagger}$.

This paper presents the results of measurements of diffusion of a very dilute solution of SnI_4 (I^{131} tagged) in CCl_4. The system was chosen because of the simple symmetry of the molecules. The tagged SnI_4 was prepared from iodine received as NaI from the Oak Ridge National Laboratory. I_2 was generated by heating with $K_2Cr_2O_7$, and this was reacted with metallic tin in CCl_4 solution as described by McDermott.[5] The nonradioactive solution was matched colorimetrically with the tagged solution. All mixtures were carefully shielded from light to retard decomposition of the iodine. Two isotherms were obtained, at 50°C and 75°C. The pressure range was limited to 2000 atmospheres because of freezing of CCl_4. The results are presented in Table I and Fig. 1.

Table I. Diffusion coefficients SnI_4^{131} in CCl_4-SnI_4 in CCl_4.

Temperature (°C)	Pressure (atmos)	Observed $D\times10^5$ (cm²/sec)
50	200	3.30
50	400	2.66
50	600	2.17
50	600	2.08
50	1200	1.12
50	2000	0.70
75	200	4.66
75	500	3.27
75	600	3.08
75	1000	1.97
75	1000	1.93
75	1500	1.24
75	2000	1.18
75	2000	1.06

The plot of D *versus* pressure shows a relatively constant decrease up to 1000 atmos. Beyond this point the rate of decrease slows gradually. In the plots of the ratio of the activation volume to the molal volume, $\Delta V^{\ddagger}/\bar{V}$, the activation enthalpy $\Delta H_p^{\ddagger}$, and the increase in activation entropy from 1 to P atmospheres $\Delta S_p^{\ddagger}-\Delta S_0^{\ddagger}$ *versus* pressure (Figs. 2 and 3), this apparent change at about 1000 atmos is much more pronounced. It should be noted here that because only two isotherms were determined, the values of ΔH_p are average values at an intermediate temperature of about 62.5°C. The values of $\Delta S_p^{\ddagger}-\Delta S_0^{\ddagger}$ calculated from $\Delta H_p^{\ddagger}$ are given at 50°C, those at 75°C are the same within the accuracy of the calculation. The plots of $\Delta V^{\ddagger}/\bar{V}$ for the two temperatures are nearly level up to this point. This indicates that in effect the amount a SnI_4 molecule must push back its surroundings in order to diffuse is nearly constant over this range despite the considerable change in free volume. Furthermore, the nearly constant

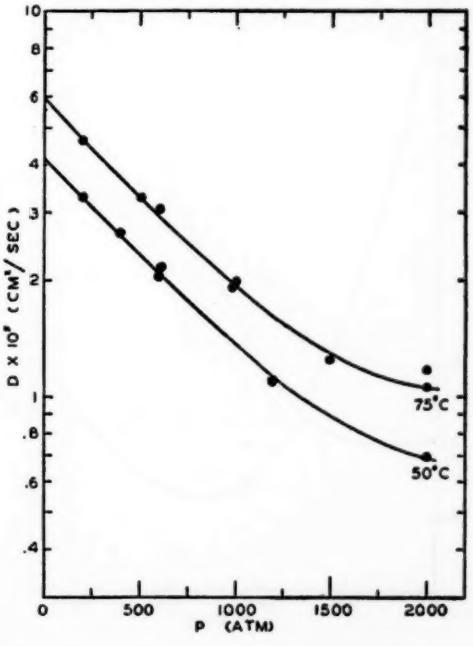

Fig. 1. Diffusion coefficients *versus* pressure—CCl_4-SnI_4.

* This work was supported in part by the U. S. Atomic Energy Commission.

[1] R. C. Koeller and H. G. Drickamer, J. Chem. Phys. **21**, 267 (1953).
[2] R. C. Koeller and H. G. Drickamer, J. Chem. Phys. **21**, 575 (1953).
[3] Cuddeback, Koeller and Drickamer, J. Chem. Phys. **21**, 589 (1953).
[4] R. B. Cuddeback, and H. G. Drickamer, J. Chem. Phys. **21**, 597 (1953).
[5] F. A. McDermott, J. Am. Chem. Soc. **33**, 1963 (1911).

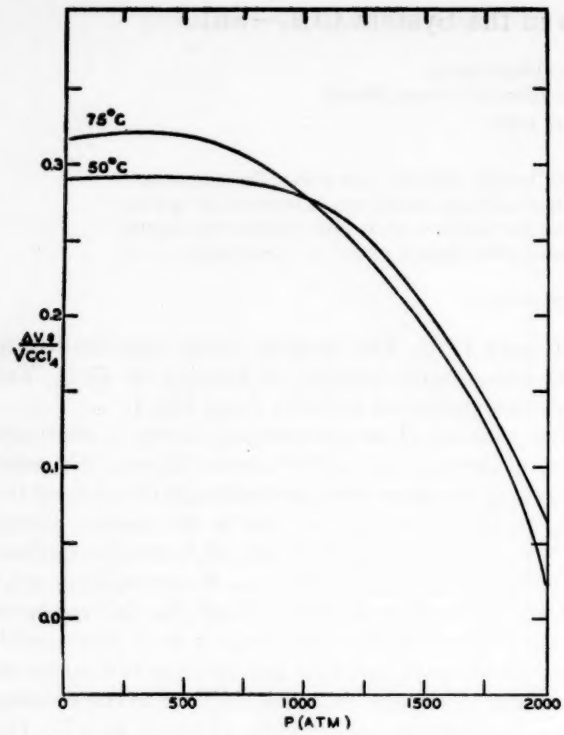

FIG. 2. $\Delta V^{\ddagger}/V$ *versus* pressure—CCl_4-SnI_4.

low value of ΔH_p shows that the enthalpy of the activated state does not increase relative to that of the normal state. Or, in other words, little energy is expended in accomplishing this volume increase. While

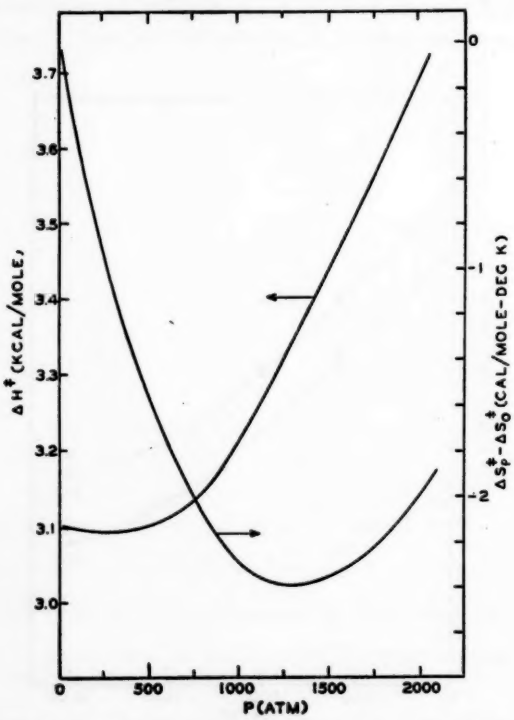

FIG. 3. $\Delta H^{\ddagger}$ *versus* pressure—CCl_4-SnI_4. $\Delta S^{\ddagger}-\Delta S_0^{\ddagger}$ *versus* pressure—CCl_4-SnI_4.

both $\Delta V^{\ddagger}/\bar{V}$ and $\Delta H_p^{\ddagger}$ are changed little, however, D decreases considerably. The reason is found in the $\Delta S_p^{\ddagger}-\Delta S_0^{\ddagger}$ curve, which falls rapidly over this region. This means that the entropy of the normal state does not decrease as rapidly as does that of the activated state; that is, the number of degrees of freedom of the activated state are reduced relative to the normal state. Thus the increasing resistance to diffusion over the region below 1000 atmos is apparently caused by the requirement that as pressure increases the SnI_4 molecules must be more stringently oriented in the activated state. This conclusion becomes plausible if we consider the SnI_4 molecules as tetrahedra moving through spheres, or rotating CCl_4 molecules. It is obvious that

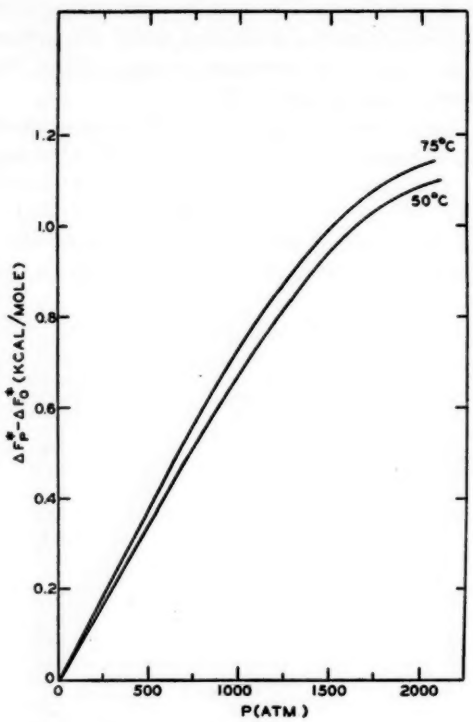

FIG. 4. $\Delta F^{\ddagger}-\Delta F_0^{\ddagger}$ *versus* pressure—CCl_4-SnI_4.

in order to diffuse through a medium of closely packed spheres a tetrahedral molecule can move with less distortion of the spheres, on the average, if it is oriented than if it moves without any orientation.

Above 1000 atmos the $\Delta V^{\ddagger}/\bar{V}$ drops sharply, showing that the amount of distortion needed to move is decreasing. The sudden rise in $\Delta H_p^{\ddagger}$, however, shows that the energy expended to accomplish this smaller distortion is much greater than at lower pressures. The curve of $\Delta S_p^{\ddagger}-\Delta S_0^{\ddagger}$ levels and begins to rise, indicating that the degree of order imposed upon the normal state increases faster than that required of the activated state. The sharp decline in $\Delta V^{\ddagger}/\bar{V}$ with increasing pressure shows that diffusion is taking place more and more through existing holes, and accordingly indicates

that some sort of quasi-static arrangement is appearing in the CCl_4 which allows the formation of holes larger than those existing at lower pressures. The most likely explanation seems to be that rotation in the CCl_4 molecules surrounding the SnI_4 molecules begins to be inhibited to some extent at about 1000 atmos at these temperatures. This does not mean that any sharp transition corresponding to the case for the solid at one atmosphere takes place. On the contrary, the nature of the liquid state is such that a sharp transition would not be expected. The intermolecular distances in a liquid are much less uniform than those in a solid. Hence, any such inhibition of rotation would be expected to be a localized phenomenon whose occurrence increases gradually with increasing density. In addition, the present work furnishes no clue as to whether such an inhibition takes place only around SnI_4 molecules or whether it would take place even in pure CCl_4. In either event the structure resulting from such an inhibition of the rotation would be expected to be harder to distort, a conclusion supported by the higher values of $\Delta H_p^{\ddagger}$.

The plots of $\Delta F_p^{\ddagger}-\Delta F_0^{\ddagger}$ are shown in Fig. 4. These values are not truly values at 50° and 75°, since they were calculated from the "average" values of $\Delta H_p^{\ddagger}-\Delta H_0^{\ddagger}$. The curve shows an increasing value of $\Delta F_p^{\ddagger}-\Delta F_0^{\ddagger}$ with P, qualitatively paralleling the decrease in D. This is, of course, to be expected from the manner in which $\Delta F_p^{\ddagger}-\Delta F_0^{\ddagger}$ was obtained.

E. P. Doane would like to acknowledge financial assistance from the Visking Corporation and from the U. S. Atomic Energy Commission.

Diffusion in Liquid Sulfur*

R. L. Saxton and H. G. Drickamer
Department of Chemistry, University of Illinois, Urbana, Illinois

(Received March 16, 1953)

Diffusion coefficients have been measured in liquid sulfur over the range 120°C–320°C. Two varieties of sulfur, both treated to remove organic impurities, were used. No essential difference was found between them. The break in the diffusion rate occurs at a lower temperature than does the break in the viscosity curve, and the total drop in diffusion rate is much smaller than the rise in viscosity. The effect of added impurity is also less important for diffusion than for flow. This is attributed to the smaller effective moving segment in molecular motion.

SULFUR is an unusual and interesting liquid. Below about 160°C the molecules form eight-membered rings. Near this temperature the rings apparently break up and long chains form. This change is accompanied by a tremendous increase in viscosity which has been thoroughly studied.

In this work the diffusion of S^{35} into ordinary sulfur was studied. The S^{35} was obtained from the Oak Ridge National Laboratory of the U. S. Atomic Energy Commission. Two varieties of untagged sulfur were used, the first from the shelf; and the second, a sample of Worland sulfur was obtained through the courtesy of Dr. E. W. Duecker of the Texas Gulf Sulfur Company. This second sample was especially low in metallic impurities. Both samples were treated by the method of Bacon and Fanelli[1] to remove organic impurities. No essential difference between the two kinds of sulfur was obtained.

The diffusion coefficients were measured in the following manner. Cylinders of coarse fritted glass were pumped full of sulfur. These cylinders were placed in a close fitting stainless steel cell, and the edges were filled with sulfur. The cell was inserted in a furnace. The setup is shown in Fig. 1. The furnace and cell were then heated to temperature, and a little S^{35} was injected on the surface. The temperature was measured to 1°C by chromel-alumel thermocouples. After a fixed period (20–90 minutes) the cell was removed and quenched. The analysis consisted in sanding off samples of the frit on pieces of emery cloth and counting these slices under a Geiger counter. Measuring the frit with a micrometer before and after each sample was removed gave the slice thickness, and the position of the sample

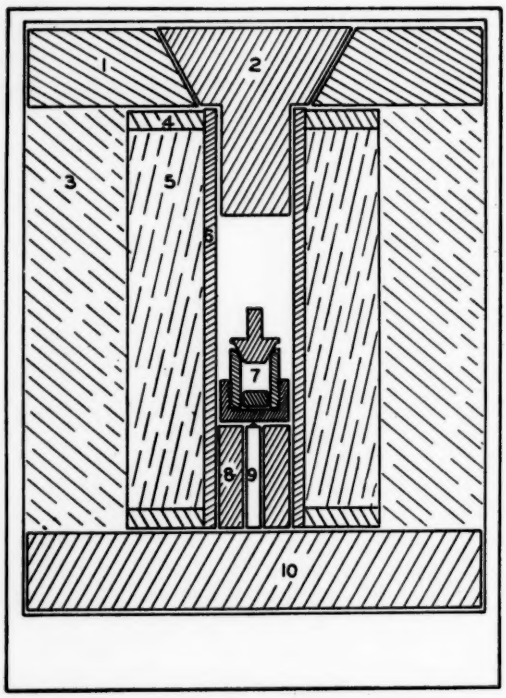

Fig. 1. Apparatus for sulfur diffusion. (1) Marionite top, (2) Marionite plug, (3) Rock wool, (4) Transite annulus, (5) Chromel heating strip in glass wool and alundum cement, (6) Alundum tube, (7) Stainless steel diffusion cell, (8) Marionite plug, (9) Alundum thermocouple tube, (10) Marionite bottom.

Table I.

Temp °C	Diffusion coefficient cm²/sec ×10⁶	Temp °C	Diffusion coefficient cm²/sec ×10⁶
122.5	1.05	201.0	0.837[a]
123.0	1.20[a]	206.0	0.871
125.0	1.45	215.0	0.946
126.0	1.52[a]	231.0	0.804
139.0	2.52	236.0	0.826
139.0	2.47	240.0	0.905[a]
141.5	2.80[a]	268.0	1.55[a]
148.0	3.90	273.0	1.52
149.0	3.85	274.0	1.23[a]
149.0	2.42[a]	278.0	2.05[a]
153.0	2.45	292.0	1.90[a]
154.5	2.90	307.0	2.34[a]
155.0	3.22[a]	307.0	2.10[a]
158.5	1.45	316.0	2.26
163.0	1.31		
163.4	1.24[a]	194.0	1.29[a] iodine
167.5	1.17	195.0	1.25 oil
170.0	1.53		
180.0	1.03		
183.0	0.90		
185.0	0.863		
192.0	0.714		
199.0	0.710		

[a] Worland sulfur.

* This work was supported in part U. S. Atomic Energy Commission.

[1] R. F. Bacon and R. Fanelli, Ind. Eng. Chem. **34**, 1043 (1942).

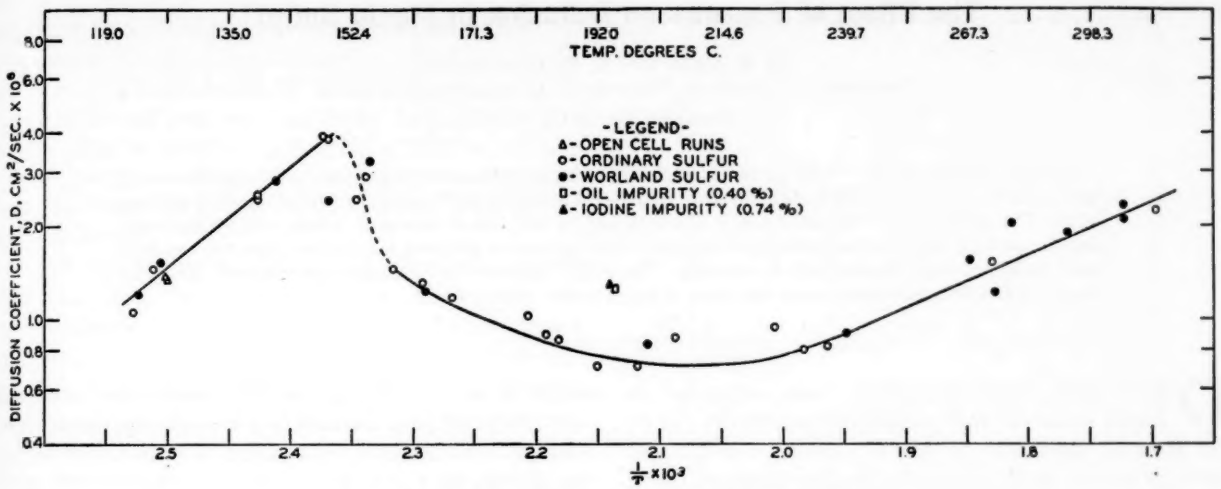

FIG. 2. Diffusion coefficient *versus* $1/T$ for S^{35} in sulfur.

in the frit. Considerable care was taken to obtain reproducible counting geometry on the slices.

The equation for diffusion from an instantaneous source is

$$C=\frac{Q}{(\pi Dt)^{\frac{1}{2}}}\exp\left(-\frac{Dt}{4X^2}\right),$$

where C=concentration, Q=intensity of source, D=diffusion coefficient, t=time, X=distance. A plot of ln C *versus* $t/4X^2$ gives a slope of $-D$.

The effective path length of the fritted glass was obtained by measuring D in an open column of 127°C liquid sulfur in an apparatus similar to that used by Tung[2] for organic liquids. This could not be extended to higher temperatures because of the temperature sensitivity of the scintillation crystals used in the continuous concentration measurement. The results are shown in Table I and Fig. 2.

The diffusion coefficients were particularly sensitive to temperature in the region 148–152°C, and the least reproducible results were obtained in this range.

In the low-temperature range below the transition point the diffusion coefficients could be expressed in the form

$$D=204.7\exp(-14\,900/RT).$$

Above 240°C the equation for D is

$$D=1.13\times10^{-3}\exp(-7250/RT).$$

In the intermediate region no simple expression for D was obtainable.

There are several significant features. The discontinuity in the diffusion coefficient occurs near 150°C, about ten degrees below the discontinuity in the viscosity curve. The drop in D is by a factor of about 20, while the viscosity rises by a factor of nearly 14 000. It is well known that certain impurities inhibit chain length and limit the large rise in viscosity. However, two different samples of sulfur were used, and both were prepared by the recommended method. No difference in the coefficients were obtained.

Viscosity measurements were made on the purified sulfur by the falling ball method, and these gave viscosities in the high-temperature range (160–200°C) which agreed in magnitude with those obtained on highly purified sulfur by Bacon and Fanelli.[3] As a further check, samples containing 1 percent heavy oil and 1 percent iodine were run at 195°C. These gave practically identical results, about 20 percent above those for pure sulfur. We attribute the smaller change in D to the fact that the unit of chain length for molecular motion may be smaller than the unit for flow in the polymeric sulfur. Molecular motion would then be less affected than viscous flow by chain length or by impurities which inhibit chain length.

[2] L. H. Tung and H. G. Drickamer, J. Chem. Phys. **20**, 13 (1953).

[3] R. F. Bacon and R. Fanelli, J. Am. Chem. Soc. **65**, 639 (1943).

The Effect of Pressure on Diffusion in Liquid Sulfur*

D. R. Cova and H. G. Drickamer
Department of Chemistry, University of Illinois, Urbana, Illinois
(Received March 16, 1953)

Diffusion coefficients have been measured in liquid sulfur to 2500 atmospheres pressure for isotherms at 140°C, 150°C, 175°C, and 210°C. One isotherm was also obtained at 195°C for sulfur containing 0.75 percent iodine. The motion in the viscous region is characterized by very small activation volumes which indicates that the moving segment is very small. This shows why the drop in diffusion rate in the transition region is small compared with the increase in viscosity. The iodine reduces the "effective temperature" 10–15°C. Above 1200–1500 atmospheres only one form of liquid sulfur seems to exist.

DIFFUSION coefficients have been measured in liquid sulfur to 2500 atmospheres pressure (or to the freezing pressure) at 140°C, 150°C, 175°C, and 210°C. One isotherm (195°C) was also obtained using sulfur containing 0.75 percent iodine. The method used was quite similar in principle to that described in a previous paper for atmospheric pressure work.[1] The diffusion of S^{35} (obtained from Oak Ridge National Laboratory) into ordinary sulfur was measured in cylindrical fritted glass pellets of coarse porosity. The concentration gradient was measured by sanding off slices and counting the activity under carefully controlled geometrical conditions. The pellet thickness was measured by micrometer after each slice was taken. The sulfur was purified by the method of Bacon and Fanelli[2] as in the atmospheric pressure work.

The inside of the bomb used in the high pressure work is shown in Fig. 1. Thin-walled lead capsules which fit the fritted glass pellets closely were stamped out. The pellet was inserted in a capsule, the edges were filled with sulfur, and a thin layer of radioactive sulfur was placed on the surface. The top was covered with heavy silicone grease and the capsules placed in a steel supporting sleeve which prevented lateral de-

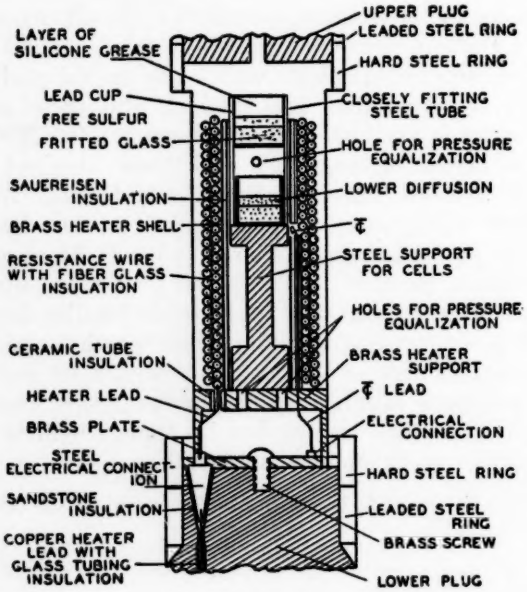

FIG. 1. Interior view of high pressure bomb with furnace.

TABLE I.

Temperature °C	Pressure atmos	Diffusion coefficient $cm^2/sec \times 10^7$
140	0	24.0
140	440	13.8
140	760	8.10
150	0	39.3
150	1100	24.2
175	0	9.70
175	520	6.02
175	1000	3.93
175	2000	2.10
210	0	6.70
210	20	6.40
210	300	4.60
210	560	4.30
210	900	4.06
210	1200	4.13
210	2000	3.73
210	2400	3.52
195[a]	0[a]	13.1[a]
195[a]	500[a]	6.95[a]
195[a]	1200[a]	4.58[a]
195[a]	2000[a]	3.60[a]

[a] For the system, sulfur-iodine. All points are the average of two determinations agreeing within ±10 percent.

formation. The pressure transmitting fluid (silicone oil) was added, the connections were tightened, the system was pumped to pressure, and heat was applied. (It took 10–40 seconds to get to temperature.) Pressure was applied with a hand pump and was measured with a Bourdon gauge calibrated against a dead-weight gauge. The temperatures were measured with thermocouples placed inside the bomb. In the region where the capsules were, the temperature was uniform to ±1°–2°C. At the end of the run (30–120 minutes) the heat was cut off. It usually took about 20 to 40 seconds to cool below freezing. The pellets were removed and analyzed as described previously. All runs were made in duplicate. The diffusion coefficients are shown in Table I and Fig. 2, the activation volumes divided by the atomic volume, in Fig. 3. Compressibilities were

* This work was supported in part by the U. S. Atomic Energy Commission.

[1] R. L. Saxton and H. G. Drickamer, J. Chem. Phys. **21**, 1361, (1953).

[2] R. F. Bacon and R. Fanelli, Ind. Eng. Chem. **34**, 1043 (1942).

estimated from Bridgman's[3] data for solid sulfur. At atmospheric pressure it was assumed that the liquid had twice the compressibility of the solid, and at 2000 atmospheres one and one half times solid sulfur. The possible error in calculating D or the activation volume is very small no matter what reasonable assumption is made. (About 5 percent for 100 percent error in the compressibility.)

In the mobile region (below 150°C) the activation volume is 1–3 atomic volumes: i.e., one-eighth to three-eighths of the molar volume of the eight-membered ring and are independent of pressure. This corresponds closely to the results obtained in many simple liquids in the same pressure range.[4] In the viscous region the activation volume starts at 2–6 atomic volumes and rapidly decreases to an atomic volume or less. As sulfur is generally considered to exist in long chains in this region, it is apparent that the segment involved in a single move is a very small fraction of the chain.

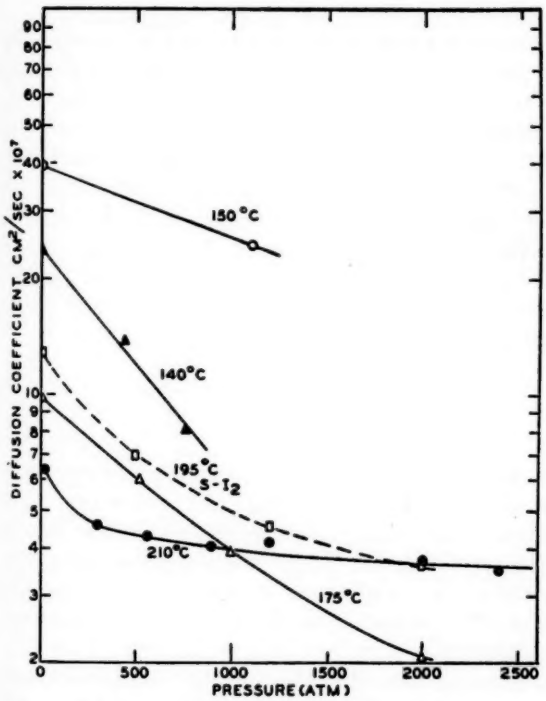

FIG. 2. Diffusion coefficients *versus* pressure S^{35} in sulfur.

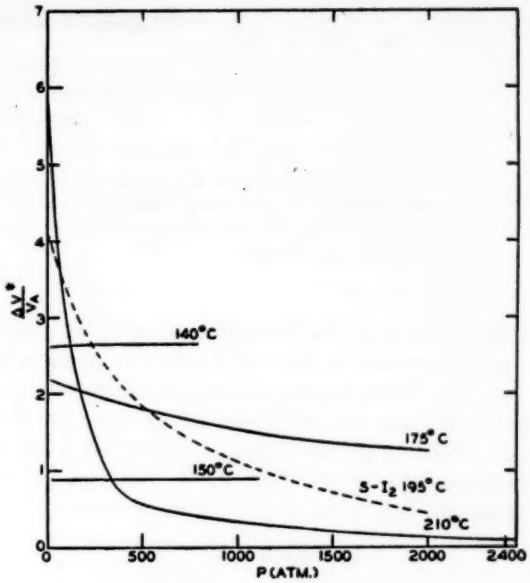

FIG. 3. Activation volume *versus* pressure.

Since the moving segment is so small, the motion is not greatly affected by the length of the sulfur chain. Therefore it is easy to see why the diffusion coefficient does not drop off rapidly in the region of greatly increasing viscosity.

The 195° isotherm containing iodine is intermediate in slope between the 175° and 210° isotherms run on pure sulfur, but the curve is displaced about 20 percent higher. In general, it can be said that the effect of the iodine is to lower the effective temperature of the melt 10–15°C.

The runs made at 20 atmospheres correspond closely to the result obtained by a different method[1] at atmospheric pressure, which gives greater confidence in the data.

The change of structure in liquid sulfur takes place with a decrease in volume and should therefore be displaced towards lower temperatures at high pressure. Since the melting point increases with pressure, it is evident that above some pressure only the "high pressure" liquid should exist. Our data indicate that above 1200–1500 atmospheres D increases with temperature at all temperatures, which is consistent with the above conclusion.

[3] P. W. Bridgman, *Physics of High Pressure* (Macmillan Company, New York, 1931).
[4] R. C. Koeller and H. G. Drickamer, J. Chem. Phys. **21**, 575 (1953).

Negative Cluster Concentrations

JOHN E. KILPATRICK
Department of Chemistry, The Rice Institute, Houston, Texas
(Received March 20, 1953)

The number of clusters of a given size in a real gas frequently turns out to be negative. Nevertheless a model based upon the cluster idea leads to the correct virial expansion. This model is tested further by a direct calculation of the gas imperfection entropy from the possibly complex entropy of formation and of mixing of these clusters.

IN a recent issue of this journal Woolley[1] has exploited a novel approach to the virial equation of state of a real gas. Woolley's approach can be summed up as follows. Every gas can be considered an ideal gas if the effective number of molecules is identified with the total number of clusters of all sorts. His Eqs. (4) and (5) are equivalent to the well-known equations[2]

$$PV=kT\sum n_j, \tag{1}$$

$$N=\sum jn_j, \tag{2}$$

where n_j is the number of clusters of j molecules. He then introduces an equilibrium constant K_j for the formation of a j cluster from j separate molecules. By a perfectly straight forward path he proceeds to obtain the pressure virial expansion and the density virial expansion, with the two sets of virial coefficients given as polynomials in the K_j.

This procedure provides a very satisfying derivation of the virial equation and is particularly well suited for presentation to undergraduate students in that the basic assumption is plausible and no statistical mechanics is used. However, one disconcerting point is rather obvious. Any gas with a positive second-virial coefficient must have a negative K_2, a negative partial pressure of binary clusters and a negative number of binary clusters.

Now is this a valid interpretation of the equations and if so, what does it mean? Our feeling is that there is nothing wrong with the concept of negative concentration; on the contrary, it may be a very useful concept.

The usual derivation of the virial equation begins with the assumption that the n_j are an actual count of the number of j-clusters. The implication is that all of the n_j are zero or positive. Equations (1) and (2) are then deduced, together with an expression for n_j, $n_j=Vg_jz^j$. When it develops later that the n_j (for $j>1$) can be negative, some doubt is thrown upon the whole derivation, if one is prejudiced against negative concentrations.

Fortunately however, the virial equation does not have to rest upon this foundation. The fundamental equations of the expansion

$$P=kT\sum g_jz^j, \tag{3}$$

$$x=N/V=\sum jg_jz^j, \tag{4}$$

can be obtained[3] from the grand partition function in a way that is correct classically or quantum mechanically and in which no mention need ever be made of the "number of j clusters." If one defines n_j as $n_j=Vg_jz^j$ (V, g_j and z being previously rigorously defined), Eqs. (3) and (4) at once transform into Eqs. (1) and (2). The latter two equations are then exact; however no physical meaning need necessarily be attached to the n_j. The equilibrium constants of reference 1 can easily be shown to be related to the g_j of reference 2 by the equation

$$K_j=\frac{g_j}{g_1{}^j}(kT)^{j-1}. \tag{5}$$

The quotient $g_j/g_1{}^j$ is just Mayer's[2] cluster integral b_j. The polynomials for α_n [Eq. (30), reference 2] are identical with the polynomials given by Woolley [reference 1, Eq. (12)]. The relation given in Eq. (5) is surprising. One might have expected that K_j would be just $Z_j/Z_1{}^j$, where Z_j is the partition function for j molecules.

It occurred to us that the "reality" of the numbers of clusters (possibly one should say, the usefulness of a model in which one attaches physical significance to the numbers of clusters) might be tested by making another application of them. For example, the gas imperfection entropy might be given by the entropy of mixing of the clusters of different sizes, together with the entropy of formation of these clusters from separate molecules. This proves to be true. The complex logarithms of negative n_j's do appear but in such a way that the imaginary parts all cancel identically.

The equilibrium constant for the formation of a j cluster is

$$K_j=P_j/P_1{}^j, \tag{6}$$

where P_j is the partial pressure of the j cluster and is given by

$$P_j=n_jP/\sum n_j=n_jkT/V. \tag{7}$$

[1] H. W. Woolley, J. Chem. Phys. **21**, 236 (1953).
[2] G. S. Rushbrooke, *Statistical Mechanics* (Oxford University Press, London, 1949), p. 266; J. E. Mayer and M. G. Mayer, *Statistical Mechanics* (John Wiley & Sons, Inc., New York, 1940), pp. 277 and 292.
[3] J. E. Kilpatrick, J. Chem. Phys. **21**, 274 (1953).

The standard entropy of formation of a j cluster is

$$\Delta S_j^0 = S_j^0 - jS_1^0 = R \ln K_j + RT\left(\frac{\partial \ln K_j}{\partial T}\right)_P. \quad (8)$$

The gas imperfection entropy is then

$$S_{\text{real}} - S_{\text{ideal}} = \Delta S = -k \sum n_j \ln P_j + Nk \ln P$$

$$+ k \sum n_j \left(\ln K_j + T\frac{\partial \ln K_j}{\partial T}\right). \quad (9)$$

By the use of Eqs. (1, 2, 6, 7), this expression readily reduces to

$$\Delta S/R = \ln P - \left(\frac{\partial}{\partial T}(T \ln P_1)\right)_P. \quad (10)$$

On the other hand, we can calculate this same entropy difference directly from the equation of state. The most convenient starting point is Woolley's[1] Eq. (8) which is mathematically equivalent to his final virial expansion. We have already shown his virial expansion is rigorously valid, even down in the quantum-mechanical region. Woolley gives

$$\frac{PV}{RT} = \frac{P}{P_1}\frac{dP_1}{dP} \quad (11)$$

from which one can deduce

$$\left(\frac{\partial S}{\partial P}\right)_T = -\left(\frac{\partial V}{\partial T}\right)_P = -R\frac{\partial}{\partial T}\left(T\frac{\partial \ln P_1}{\partial P}\right)$$

$$= -R\frac{\partial}{\partial P}\frac{\partial}{\partial T}(T \ln P_1). \quad (12)$$

The gas imperfection entropy is then

$$\Delta S/R = \ln P - \left(\frac{\partial}{\partial T}(T \ln P_1)\right)_P, \quad (13)$$

which is identical with Eq. (10).

It may be objected that these two paths are mathematically and thermodynamically equivalent. So they are. Our point is that thermodynamic and physical reasoning based upon a model with negative concentrations of clusters leads to correct results and is internally self-consistent.

Rotation Vibration Bands of Some Symmetric Top Molecules Under High Resolution*

T. A. WIGGINS, E. R. SHULL, AND D. H. RANK
Department of Physics, The Pennsylvania State College, State College, Pennsylvania

(Received February 3, 1953)

The fine structure of some parallel bands of the symmetric top molecules CH_3I, CD_3Br, CHF_3, and $CHCl_3$ has been investigated in the 1.6 and 2.2μ regions. The double-pass plane grating spectrograph was capable of achieving a resolving power in excess of 100 000. For most of these bands the "line" nature of the sub-bands in the P, Q, and R branches was demonstrated. In the case of CH_3I the resolution was complete enough to demonstrate conclusively the complicated fine structure of the P and R "lines." Molecular constants have been derived from the bands of CH_3I, CD_3Br, and CHF_3. The theoretically expected relationship between the zeta's has been shown to hold in perpendicular CH_3I bands.

USE of PbS detectors in conjunction with a large grating spectrograph allows observation of much of the finer detail in the rotation-vibration spectra of symmetric top molecules. We shall report on our observations and analysis of some of the bands of CH_3I, CD_3Br, CHF_3, and $CHCl_3$ in the 1.6 and 2.2μ regions.

Recently,[1,2] we have described a method of double-passing a plane grating. This optical system was used in the present work in the double-pass configuration employing a PbS cell as detector. A Brown Electronik recorder is operated by the same amplifier used in our first work[3] on CH_3Br. The wavelength measurements were made by use of previously measured methane absorption lines[4] or higher-order neon emission lines as standard wavelengths.

In our first work[3] on CH_3Br using the grating in the single-pass configuration, the PbS cell had a sensitive area of 1 mm×5 mm and a resistance of approximately 1.5 megohms. We have now obtained PbS cells, "Eastman Ektron detectors," which have a sensitive area of 0.2 mm×2.0 mm and a resistance of 30 000 ohms. These new detectors produced a 20-fold increase in signal-to-noise ratio when used with the same amplifier as formerly, when compared to the older 1×5-mm high-resistance cells. We have now been able to obtain better traces of spectra in the double-pass configuration, with its consequent doubling of the resolution, than was possible at half the resolution with the single-pass and the larger high-resistance detectors.

The gases investigated were contained in a sealed Pyrex absorption tube of one meter length. The pressures used varied through a range of from 1 to 20 cm of Hg. The fine structure work on the parallel bands was done making use of pressures of from 1 to 5 cm. The 1-cm pressure was used in the case of $CHCl_3$.

TABLE I. Frequencies in vacuum wave numbers in perpendicular bands of CH_3I.

K	$2\nu_4$ $\nu_0=6102.4$	$\nu_4+\nu_1$ $\nu_0=5942.4$
	P_{Q_K}	
11		5839.0
10		849.3
9		859.0
8	6017.9	868.4
7	29.9	877.8
6	41.2	887.9
5	52.6	897.9
4	64.0	907.8
3	75.2	917.3
2	86.4	926.9
1	97.2	936.2
	R_{Q_K}	
0	6108.1	5945.7
1	119.0	955.0
2	129.4	964.5
3	139.9	974.3
4	151.0	984.8
5	160.6	994.4
6	170.8	6003.0
7	180.7	10.8
8	189.5	19.9
9	200.5	
10	209.0	
11	218.1	
12	227.3	

METHYL IODIDE

Two perpendicular and two parallel bands near 6000 cm^{-1} were observed. The perpendicular bands have been assigned as $\nu_1+\nu_4$ and a component of $2\nu_4$ on the basis of fundamentals as given by Bennett and Meyer[5] and Lagemann and Nielsen.[6] Quantum numbers were assigned to the Q branches on the basis of intensity and alternation of intensity due to the nuclear spin of the three hydrogen atoms. The frequencies of the Q branches are tabulated in Table I.

A least-squares solution for the coefficients in the equation[7] for the sub-band origins was made. Values

* This research was assisted by support from Contract N6onr-269, Task V, of the U. S. Office of Naval Research.

[1] D. H. Rank and T. A. Wiggins, J. Opt. Soc. Am. **42**, 983 (1952).

[2] Rank, Shull, and Wiggins, J. Opt. Soc. Am. **43**, 214 (1953).

[3] Rank, Rix, and Wiggins, J. Opt. Soc. Am. **43**, 157 (1953).

[4] Rank, Bennett, and Wiggins, J. Opt. Soc. Am. **43**, 213 (1953).

[5] W. H. Bennett and C. F. Meyer, Phys. Rev. **32**, 888 (1928).

[6] R. T. Lagemann and H. H. Nielsen, J. Chem. Phys. **10**, 668 (1942).

[7] G. Herzberg, *Infra-red and Raman Spectra of Polyatomic Molecules* (D. Van Nostrand Company, Inc., New York, 1945), p. 429.

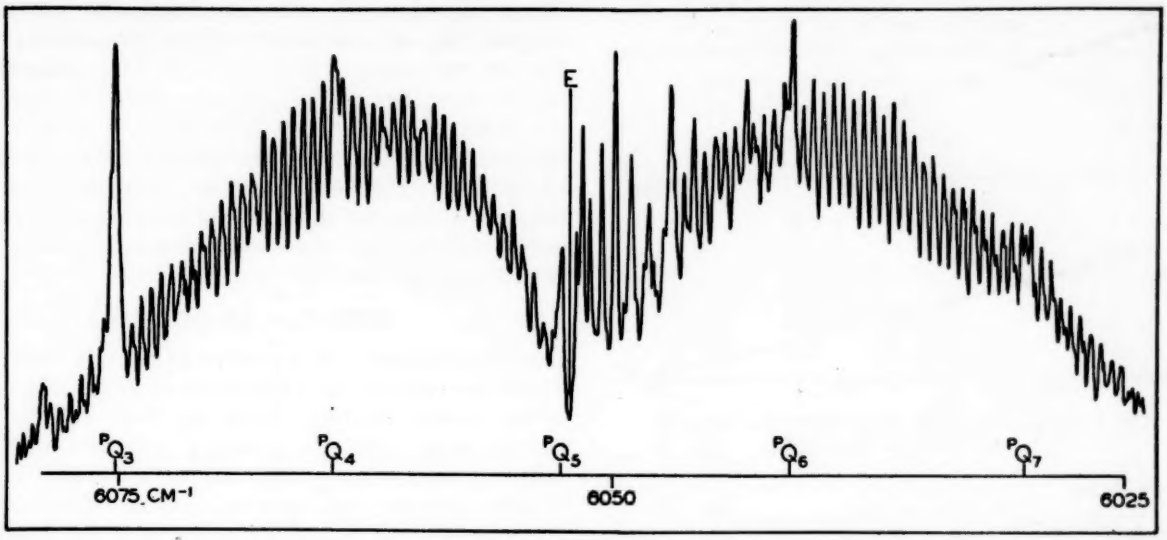

FIG. 1. The parallel component of $2\nu_4$ of methyl iodide with some Q branches of the perpendicular component indicated. E denotes a zirconium emission line.

for the band origin and δ were then computed to be: 5942.4 cm^{-1} and 0.060 ($\nu_1+\nu_4$); and 6102.4 cm^{-1} and -0.119 ($2\nu_4$). It is noted that the former value of δ is nearly the same as the value given[8] for the ν_4 fundamental while the latter is of opposite sign and of twice the magnitude. These results are in conformity with the theory presented by Johnston and Dennison.[9]

The parallel bands observed are assigned as $2\nu_1$ and a component of $2\nu_4$. The former is weak and partially obscured by the $\nu_1+\nu_4$ band. The band center is at 5890 cm^{-1}. The separation of the P and R maxima is 23 cm^{-1}.

The parallel component of $2\nu_4$ is shown in Fig. 1. Some Q branches of the perpendicular component and a zirconium emission line are indicated. The Q branch and several P-branch lines of the parallel band are shown in Fig. 2. The intensity alternation is easily seen, the lines corresponding to $K=3$, 6, and 9 being strong; $K=0$ corresponds to a forbidden transition. A plot of the frequencies in the Q branch *versus* K^2 is shown in Fig. 3A. Frequencies for lines in the P, Q, and R branches are tabulated in Table II.

Since the Q branch was resolved, quantum numbers could be assigned in the P and R branches. Least-squares solutions for the slope and intercept of the Q-branch plot and the usual methods of analysis using Δ_2F'' and band-origin plots enabled the computation of the following constants:

$$\nu_0=6051.94 \text{ cm}^{-1}$$
$$B'-B''=0.000211 \text{ cm}^{-1}$$
$$B''=0.2499 \text{ cm}^{-1},\ B'=0.25044 \text{ cm}^{-1}$$
$$A'-A''-B'-B''=-0.0601 \text{ cm}^{-1}$$
$$A'=5.01_7 \text{ cm}^{-1} \text{ (using Herzberg's value[10] of } A''=5.07_7 \text{ cm}^{-1}).$$

[8] Reference 7, p. 438.
[9] M. Johnston and D. M. Dennison, Phys. Rev. **48**, 868 (1935).
[10] See reference 7, page 437.

The value for B'' given above can be compared with the microwave measurement of Gordy, Simmons, and Smith[11] of 0.25023 cm^{-1}. These data indicate an increase in the HCH angle for the $2\nu_4$ vibration.

The spreading of the Q branch indicates that the P and R branch "lines" are complicated and should show fine structure under sufficient resolution. This structure can be seen in Fig. 4A showing three P branch lines. To a first approximation frequencies in these branches

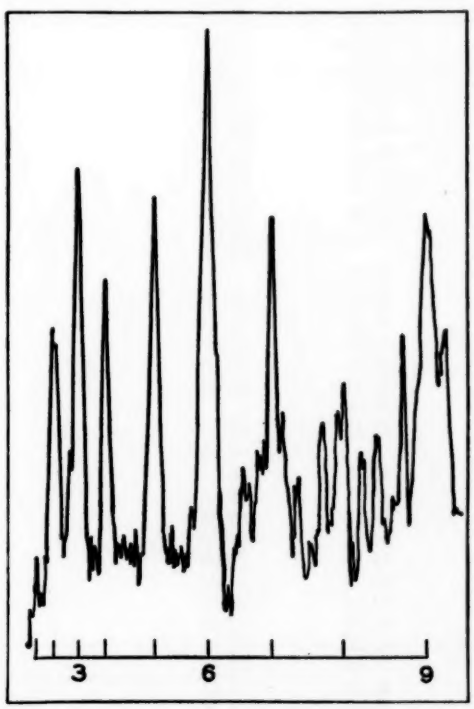

FIG. 2. The Q branch of the parallel component of $2\nu_4$ of CH_3I.

[11] Gordy, Simmons, and Smith, Phys. Rev. **74**, 243 (1948).

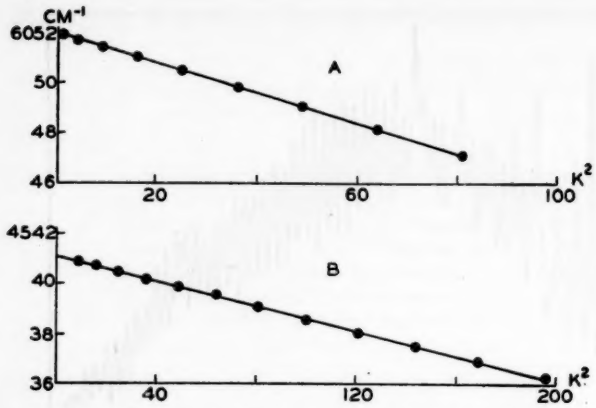

FIG. 3. Frequencies in the Q branch plotted *versus* K^2 for (a) CH_3I and (b) CD_3Br.

are given by

$$\nu=\nu_0\pm(B'+B'')m+(A'-A''-B'+B'')K^2,$$
$$m\geqslant 1, \quad K\geqslant 0.$$

TABLE II. Frequencies in vacuum wave numbers in the parallel component of $2\nu_4$ of CH_3I. $\nu_0=6051.94$ cm^{-1}.

J	$Q_{P(J)}$	$Q_{R(J)}$	K	Q_K
			1	6051.88
2		6053.43	2	51.66
3		53.88	3	51.37
4		54.48	4	51.00
5		54.70	5	50.44
6		55.44	6	49.80
7	6048.48	55.99	7	48.98
8	47.97	56.48	8	48.13
9	47.47		9	47.06
10		57.50		
11	46.41	57.97		
12	45.96	58.46		
13	45.46	59.00		
14	44.92	59.53		
15	44.43	60.03		
16	43.97	60.56		
17	43.41	61.02		
18	42.97	61.56		
19	42.51	62.14		
20	42.00	62.60		
21		63.07		
22		63.65		
23	40.59			
24	40.08	64.59		
25	39.56	65.13		
26	39.09	65.64		
27	38.60	66.10		
28	38.11	66.62		
29	37.64			
30	37.11	67.59		
31		68.16		
32	36.18	68.67		
33	35.64	69.15		
34	35.18	69.63		
35	34.75	70.16		
36	34.21	70.69		
37	33.70	71.22		
38	33.25	71.75		
39	32.76	72.32		
40	32.30	72.83		
41	31.80	73.31		
42	31.32	73.83		
43	30.82	74.36		
44	30.33			

Using this equation and considering the statistical weights, Fig. 4B was constructed, to the same scale as Fig. 4A, for values of K from 0 to 9. The values for J and K, from left to right, for the "line" assigned as $J=25$ are: 17, 8; 15, 9; 19, 7; 23, 4; 22, 5; 25, 0; 24, 3; 25, 1; 21, 6; 25, 2. Since the line for $J=25$, $K=0$ is nearly at the middle of the "line," and since the B'' value is nearly the same as the microwave value, it can be assumed that the other molecular constants reported also are correct.

METHYL-d_3 BROMIDE

A perpendicular and a parallel band were observed. These are assigned as components of $2\nu_4$ on the basis of the fundamentals as given by Noether.[12] In the parallel band only the Q branch was resolved. The failure to resolve the other branches is due to the two bromine isotopes and the closely packed K structure. Since the nuclear spin of deuterium is 1, the intensity alternation of 8:11, rather than 1:2 for molecules containing three hydrogens, yields lines in the fine structure of more uniform intensity.

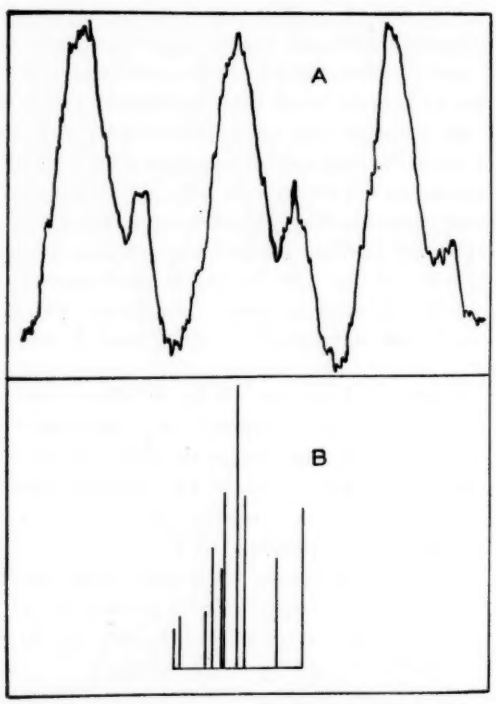

FIG. 4. (A) Fine structure of lines in the P branch of $2\nu_4$ of CH_3I. (B) Predicted structure of a P branch line.

A plot of the frequencies in the Q branch *versus* K^2 is shown in Fig. 3B. The intercept is $\nu_0=4541.05$ cm^{-1}, the slope is $(A'-A''-B'+B'')=-0.0243$ cm^{-1}. The origin of the perpendicular band was found to be 4576.9 cm^{-1} using $B''=0.26$ cm^{-1} from microwave measurements of Simmons and Goldstein[13] and A'' as

[12] H. O. Noether, J. Chem. Phys. **10**, 664 (1942).
[13] J. W. Simmons and J. H. Goldstein, J. Chem. Phys. **20**, 122 (1952).

2.54 cm^{-1}, one-half the value given by Herzberg[10] for CH_3Br. Measured frequencies are tabulated in Table III.

FLUOROFORM

The parallel band shown in Fig. 5 has been assigned as $2\nu_1$ on the basis of the fundamental measured by Price[14] and Rix.[15] The most prominent feature of the band is the strong Q branch. The insert in the figure is the continuation of the Q branch, shown in two sections

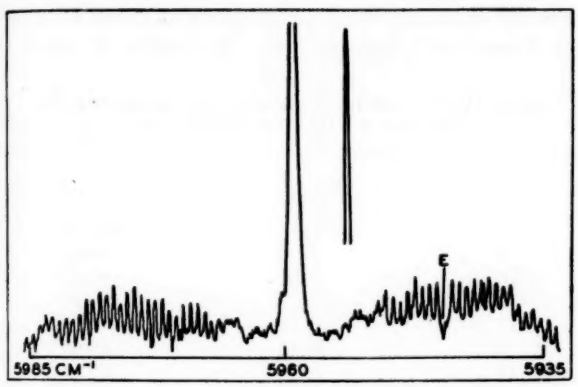

FIG. 5. The $2\nu_1$ band of CHF_3. The insert is the continuation of the Q branch. E denotes a zirconium emission line.

for ease in photographic reproduction. Figure 6A shows this Q branch at maximum resolution and dispersion. Choosing the band origin at the sharp edge of the Q branch as observed at low pressure, quantum numbers for the lines in the P and R branches were assigned. A value of $B''=0.3453$ cm^{-1} is found. The results conform with the Δ_2F'' values listed by Bernstein and Herzberg.[14] From a band origin plot it was found that $\nu_0=5959.46$ cm^{-1} and $B'-B''=-0.000325$ cm^{-1}. Using the microwave measurement of $B''=0.34522$ cm^{-1} from measurements by Gilliam, Edwards, and Gordy,[16] $B'=0.34489$ cm^{-1}.

TABLE III. Frequencies in vacuum wave numbers in the $2\nu_4$ bands of CD_3Br.

	Perpendicular component $\nu_0=4576.9$		Parallel component $\nu_0=4541.05$
K	$P\ Q_K$	$R\ Q_K$	$Q\ Q_K$
0		4580.8	
1	4574.5	87.2	
2	68.1	93.4	
3	61.6	99.5	4540.82
4	55.1	605.9	40.69
5	48.6	12.0	40.45
6	42.0	18.1	40.15
7	35.4	25.3	39.88
8	28.4	30.7	39.54
9	21.5	36.4	39.09
10	14.9	42.2	38.62
11	8.5	47.9	38.08
12	1.1	53.8	37.50
13			36.93
14			36.34

The tightness of the Q branch indicates that the P and R "lines" are also very narrow so that no ambiguity is present in the assignment of quantum numbers. The measured frequencies are tabulated in Table IV.

CHLOROFORM

The parallel band shown in Fig. 7 has been assigned as $2\nu_1$ on the basis of the fundamental as measured by

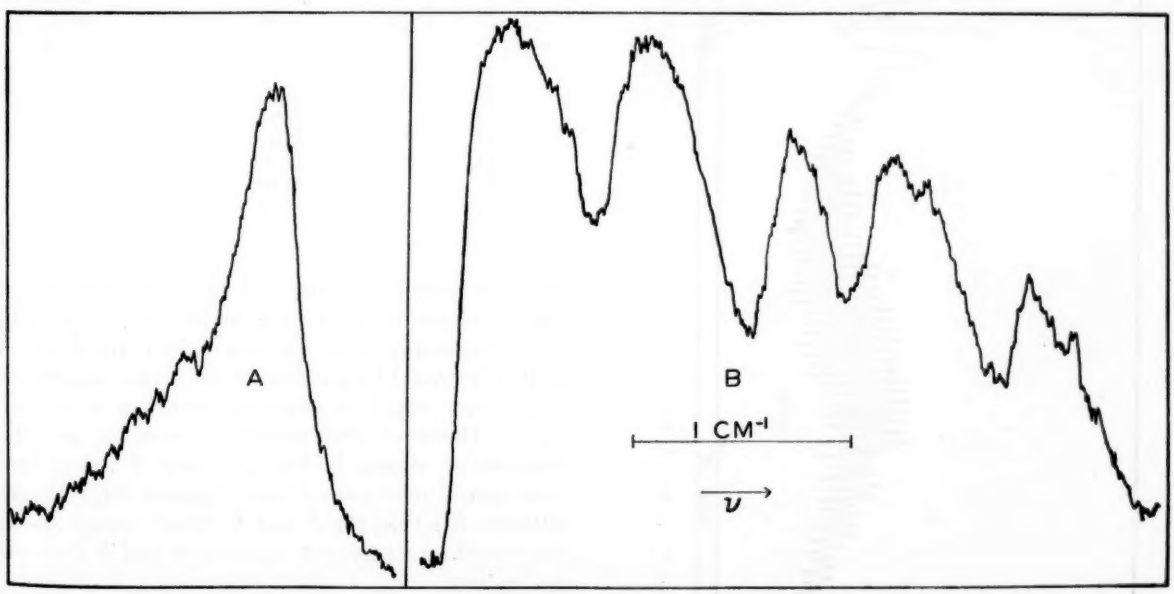

FIG. 6. The Q branches of (A) CHF_3, (B) $CHCl_3$ under maximum resolution.

[14] W. C. Price, unpublished work quoted by H. J. Bernstein and G. Herzberg in J. Chem. Phys. **16**, 30 (1948).
[15] H. D. Rix, J. Chem. Phys. **21**, 1077 (1953).
[16] Gilliam, Edwards, and Gordy, Phys. Rev. **75**, 1014 (1949).

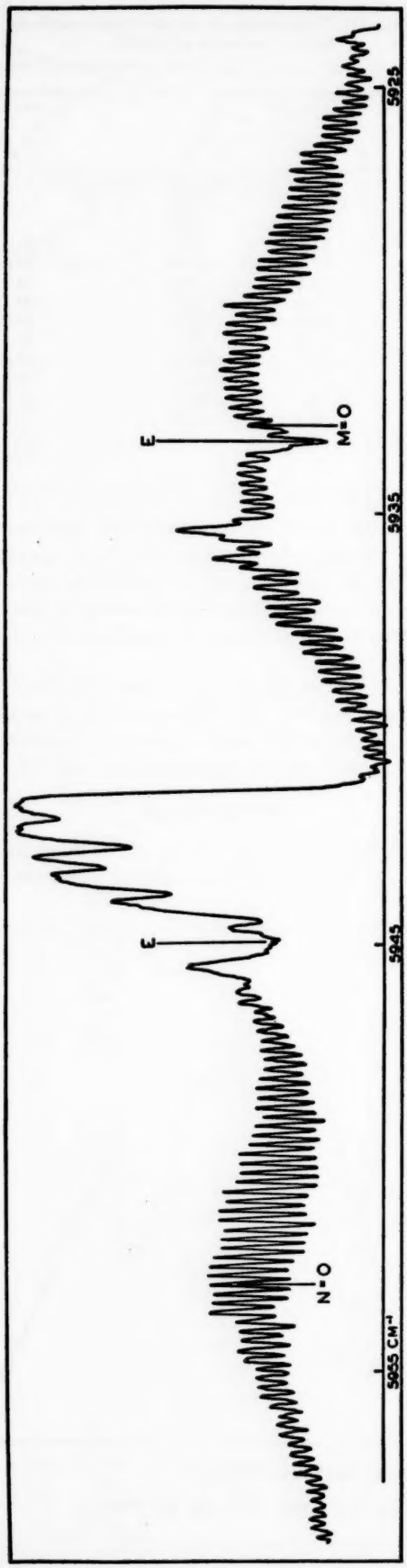

FIG. 7. The $2\nu_1$ band of $CHCl_3$. The lines labeled $M=0$ and $N=0$ refer to empirical Eqs. (1) and (2). E denotes a zirconium emission line.

Ginsburg.[17] As in fluoroform there is a strong Q branch. This branch is shown in Fig. 6B to the same scale as the fluoroform Q branch. It is resolved into several components which degrade toward short wavelengths, opposite to the Q branch of fluoroform. The components do not seem to fit any simple relation.

Several of these components have an appearance similar to the Q branch of fluoroform as might be expected from the similarity of the molecules. Two of these components could be accounted for as Q branches of the molecules $CHCl_3^{35}$ and $CHCl_2^{35}Cl^{37}$ which occur in nearly equal abundance.[18] Equations given by Voge and Rosenthal[17] indicate that the origins of these Q branches would be separated by about 0.2 cm^{-1}, the heavier molecule having the higher frequency. This is about the separation of the lines in the P and R branches so that it would be possible to have two superimposed bands that result in resolved branches as shown in Fig. 7. However, this would not account for all the components shown in Fig. 6B since if the Q branch were spread over such a wave-number interval due to different K levels, the P and R "lines" would also have this broad structure and separate P and R lines would not appear.

TABLE IV. Frequencies in vacuum wave numbers in the $2\nu_1$ band of CHF_3. $\nu_0=5959.46$ cm^{-1}.

J	$Q_{P(J)}$	$Q_{R(J)}$
8		5965.79
9		66.42
10		67.07
11		67.74
12	5951.16	68.47
13	50.43	69.08
14		69.78
15	49.03	70.43
16	48.32	71.13
17	47.62	71.76
18	46.93	72.47
19	46.18	73.13
20	45.52	73.84
21		74.51
22	44.09	75.15
23	43.39	75.81
24	42.70	76.49
25	41.97	77.20
26	41.32	77.84
27	40.56	78.52
28	39.90	79.17
29	39.16	79.84
30		80.53
31		81.23
32	37.08	81.79
33	36.42	82.42
34	35.70	
35	34.98	83.85
36	34.20	84.49

[17] N. Ginsburg, the result quoted by H. H. Voge and J. E. Rosenthal in J. Chem. Phys. 4, 137 (1936).

[18] D. H. Rank and J. A. Van Horn, J. Opt. Soc. Am. 36, 454 (1946).

TABLE V. Frequencies in vacuum wave numbers in the $2\nu_1$ band of $CHCl_3$.

P Branch		*R* Branch	
5940.74	5930.75	5946.04	5956.19
40.54	30.53	46.28	56.41
40.32	30.29	46.51	56.64
	30.12	46.71	56.87
39.88	29.91	46.95	57.07
39.67	29.69	47.18	57.31
39.44	29.48	47.43	57.53
39.26	29.24	47.65	57.76
39.05	29.01	47.90	57.97
38.81	28.82	48.11	58.22
38.58	28.63	48.30	58.43
	28.41	48.54	58.66
	28.20	48.76	58.92
	28.00	48.97	59.13
37.71	27.78	49.19	59.42
37.50	27.58		59.70
37.29	27.37		
37.06	27.18	49.82	
36.85	26.95	50.07	
36.63		50.30	
36.42		50.52	
36.19		50.74	
36.00	26.09	50.96	
35.79	25.86	51.15	
35.53	25.68	51.36	
35.31	25.48	51.59	
35.08		51.78	
34.84		52.00	
34.64		52.23	
34.44		52.44	
34.23		52.63	
34.02		52.93	
33.76		53.09	
33.56		53.31	
		53.54	
		53.77	
32.92		53.99	
32.70		54.19	
32.47		54.43	
32.25		54.61	
32.01		54.85	
31.80		55.06	
31.64		55.31	
31.39		55.50	
31.16		55.72	
30.96		55.98	

The chloroform sample was purified by fractional distillation through a glass-helices packed column of about 30 effective plates. Samples taken throughout the process showed no differences in the Q branch so that the wide Q branch cannot be attributed to impurities. It is concluded that the Q branch is due to the asymmetric molecule $CHCl_2{}^{35}Cl^{37}$. This molecule could have a strong Q branch but weak P and R branches. The irregular absorption in the P branch can be assigned to difference bands involving the low fundamental ν_3 and ν_6.

About 120 rotational lines were measured. The frequencies are tabulated in Table V. Since the band origin could not be determined it was not possible to assign quantum numbers. Even with the microwave measurement of $B''=0.110147$ cm^{-1} by Ghosh, Trambarulo, and Gordy[19] no unique assignment could be made due to the small value of B'' and the undoubtedly small $B'-B''$. It was possible to fit equations by least squares to the two branches. They are

$$P \text{ branch: } \nu=5932.93\pm0.21601M +0.00007M^2, \quad M<35, \quad (1)$$

$$R \text{ branch: } \nu=5952.89\pm0.22056N +0.00007N^2, \quad N<30. \quad (2)$$

The average deviation between computed and measured frequencies is ±0.02 cm^{-1}. The lines for $M=0$ and $N=0$ are indicated in Fig. 7.

Acknowledgments are due Dr. W. H. Pearlson of the Minnesota Mining and Manufacturing Company and Dr. R. C. McHarness of the Jackson Laboratory of E. I. du Pont de Nemours and Company, Inc. for making available the samples of fluoroform.

[19] Ghosh, Trambarulo, and Gordy, J. Chem. Phys. **20**, 605 (1952).

The Detection of Atoms and Free Radicals in Flames by Mass Spectrometric Techniques*

S. N. Foner and R. L. Hudson
Applied Physics Laboratory, The Johns Hopkins University, Silver Spring, Maryland
(Received Februrary 13, 1953)

A mass spectrometric method employing a molecular beam gas sampling system has been developed for the detection of atoms and radicals in chemical reactions. Background signals have been virtually eliminated by mechanically modulating the molecular beam and applying phase detection to the ion signal. The application of the method is illustrated by examples of low-pressure flames. In the hydrogen-oxygen flame H, O, and OH have been positively identified. The mass spectrum of a simple hydrocarbon flame, such as the methane-oxygen flame, is complicated by the presence of a large number of stable components generated in the flame. In the methane-oxygen flame the stable intermediates include C_2H_2, CO, CH_2O or C_2H_6, CH_4O, and C_4H_2. The methyl radical has been clearly identified in the methane-oxygen flame. A search for the HO_2 radical in the hydrogen-oxygen flame was made without obtaining positive results. The HO_2 detection problem is discussed in detail.

I. INTRODUCTION

ALTHOUGH there is little doubt that most chemical reactions proceed as chain processes involving atoms and free radicals as intermediates, the specific elementary reactions which take place have been unambiguously established in only a few cases. In the case of combustion reactions the experimental evidence for the existence of atoms and radicals has been fragmentary. Optical spectroscopy of flames has been applied with success to atoms and a number of diatomic radicals such as OH, CH, C_2, and NH. The spectroscopic situation in regard to polyatomic radicals is not very satisfactory because of serious identification difficulties.[1] The spectroscopic method does, however, supply data, unattainable by any other method, on the excited states of the components which it is able to identify.

The difficulties encountered by spectroscopic methods both in detecting radicals and in deriving concentrations from the observed spectral intensities has led to the exploration of other experimental techniques. These include (1) Paneth mirror method, (2) molecular beam methods, (3) mass spectrometry, and (4) microwave spectroscopy.

Of all the methods that have been proposed for studying reaction intermediates, the mass spectrometric method because of inherently high sensitivity, analytical response to all components, and capability of supplying quantitive determinations, appears to offer the greatest promise. The capabilities of the mass spectrometer were explored by Eltenton[2] in studies of the reaction intermediates in the thermal decomposition of some lower hydrocarbons and in low-pressure flames. A number of short-lived intermediates in flames were successfully detected in the pioneering experiments of Eltenton. However, certain expected radicals, such as OH, whose presence is substantiated by prolific spectroscopic data, were not found.

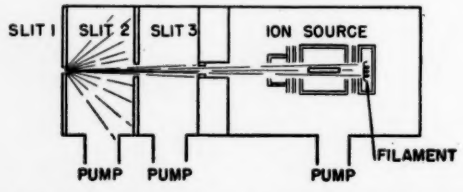

FIG. 1. Schematic diagram of the molecular beam gas sampling system.

II. PRINCIPLE OF THE METHOD

The high reactivity of intermediates occurring in flames places special requirements on the mass spectrometer gas sampling system: (1) the gas sample must be removed from the reaction zone as rapidly as possible; (2) collisions of the gas molecules with the walls of the instrument must be avoided. A hybrid molecular beam type gas sampling system was designed for this purpose and is shown schematically in Fig. 1. Gases from the reaction zone, to the left of Slit 1, stream through the first orifice as a sonic jet, at the usual reaction vessel pressures, with the flow rapidly changing in character from viscous to molecular as the pressure drops. The second slit selects the central portion of the gas stream emerging from the first orifice thereby selecting a sample of gas molecules which had the least likelihood of colliding with the walls of the inlet orifice. Slit 3 by providing additional collimation of the molecular beam is effective in preventing scattered gas molecules in the first gap from entering the ionization chamber of the mass spectrometer. Diffusion pumps evacuate the three sections of the apparatus. The electron beam in the ion source is made coaxial with the molecular beam to increase the probability of ionizing the incoming gas molecules. In certain respects the sampling system resembles the molecular beam system used by Fraser and Jewitt[3] in studying the ionization potentials of the methyl and ethyl radicals. In that investigation,

* This work was supported by the U. S. Navy Bureau of Ordnance. A report on this work was presented at the Washington meeting (May, 1952) of the American Physical Society.

[1] A. G. Gaydon, *Spectroscopy and Combustion Theory* (Chapman and Hall, Ltd., London, 1948).

[2] G. C. Eltenton, J. Chem. Phys. **15**, 455 (1947).

[3] R. G. T. Fraser and T. N. Jewitt, Proc. Roy. Soc. (London), **A160**, 563 (1937).

however, lower source pressures were involved and detection of radicals was made with an ionization gauge.

The presence of atoms and free radicals in the molecular beam can be determined by appearance potential measurements[4,5] since their ionization potentials will be lower than the corresponding appearance potentials of electron dissociation products. If $A(X)$ is the appearance potential of the ion X^+ formed by dissociative ionization of the molecule XY by the electron impact process,

$$XY+e\rightarrow X^++Y+2e, \quad (1)$$

then

$$A(X)=D(XY)+I(X)+E, \quad (2)$$

where $D(XY)$ is the dissociation energy of XY, $I(X)$ is the ionization potential of the radical X, and E is the sum of the kinetic and electronic excitation energies of X^+ and Y. Since dissociation energies are of the order of a few electron volts, it is possible, in principle at least, to detect radicals by employing electron energies slightly below the value required for the dissociative ionization process. In practice the thermal spread in energy of the bombarding electrons causes all observed ionization curves to vanish exponentially as the voltage is decreased. To resolve radicals from dissociative ionization products requires then that the electron voltage be chosen so that contributions from the tail of the dissociative ionization curve can be neglected. A consequence of operating at low electron energies is that the effective sensitivity of the mass spectrometer for radical detection may be reduced by perhaps a hundredfold from the sensitivity that is obtained if one operates at the maxima of the ionization efficiency curves, a situation which is approximated at conventional ionizing voltages (50 to 75 volts).

Another possible means of detecting free radicals, which avoids the difficulties due to dissociation effects at high electron energies, is to form negative ions by electron attachment. This method is not favored in the mass spectrometer because collisional stabilization of the excited negative ions is ruled out as a possible mechanism at the prevailing pressures in the ion source, and radiative capture of an electron is an inefficient process, the probability of capture in the case of atoms being about 10^{-7} per collision.[6] In the experiments to be described, no effort was made to detect radicals by the electron capture mechanism.

III. EXPERIMENTAL ARRANGEMENT

Figure 2 shows the actual physical arrangement of the gas inlet system employed in the flame studies. The burner section and the disk mounting the sampling orifice are clamped to the mass spectrometer with teflon gaskets employed for vacuum seals. To reduce scattering of the molecular beam in the first region,

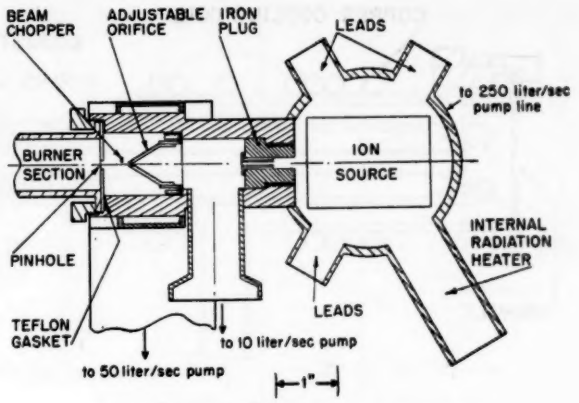

FIG. 2. Cross section of mass spectrometer gas inlet system.

the second orifice (diameter 0.0286 in.) is drilled in a hollow conical brass piece which is threaded for movement in an axial direction. A magnetically driven beam chopper mounted ahead of the second orifice serves an important role in a scheme for discriminating against background signals. The second region is a noncritical transition section between the moderately high pressure (5×10^{-3} mm) in the first region and the high vacuum ($\sim10^{-6}$ mm) in the ion source. The third slit is a rectangular channel, with entrance dimensions 0.052 in. $\times$0.099 in., which diverges to prevent specular reflection of beam molecules into the ion source.

A circular sampling aperture rather than a conventional narrow rectangular slit having the same gas capacity was adopted in these experiments to minimize reactions on the slit surfaces. It is likely that gas sampling systems designed in the future will utilize the recently described technique of producing a high intensity molecular beam[7,8] by placing the first slit in the supersonic stream of a miniature nozzle. The observed beam intensity, in our present design, is also considerably larger than expected for a conventional molecular beam design in which the slit width is limited to one mean free path.[9] The beam definition required in our case is much less than in most molecular beams so that cloud formation, which adversely affects the intensity of highly collimated beams, is not a serious factor. The simple sampling design employed here to study chemical reactions causes the reaction to be quenched very rapidly ($\sim10^{-6}$ sec) as the gas expands so that very active intermediates should survive extraction from the reaction zone.

The burner assembly is shown in Fig. 3. The reactants may be premixed or, as is indicated in the figure, sent in separately. The central burner tube is insulated from the rest of the assembly by a Teflon sleeve and can be moved by a micrometer drive mechanism. The

[4] J. A. Hipple and D. P. Stevenson, Phys. Rev. **63**, 121 (1943).
[5] D. P. Stevenson, Disc. Faraday Soc. No. 10, 35 (1951).
[6] H. S. W. Massey, *Negative Ions* (Cambridge University Press, Cambridge, 1950).
[7] A. Kantrowitz and J. Grey, Rev. Sci. Instr. **22**, 328 (1951).
[8] G. B. Kistiakowsky and W. P. Slichter, Rev. Sci. Instr. **22**, 333 (1951).
[9] R. G. J. Fraser, *Molecular Rays* (Cambridge University Press, Cambridge, 1931).

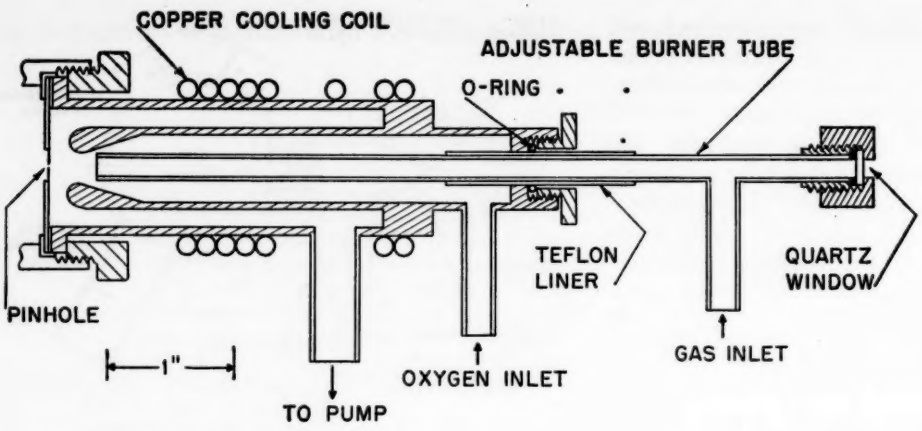

FIG. 3. Burner assembly.

flame is ignited by an electrical discharge between the center tube and the metal burner housing. A quartz window is used to observe the flame and to monitor the temperature of the diaphragm to prevent melting. The construction of the sampling orifice is shown in detail in Fig. 4. The diaphragm was usually a disk of gold foil 0.001 in. thick spotwelded, sandwich style, between the nickel welding ring and the monel plate. Approximately 50 spotwelds around the nickel ring were used to make a strong vacuum-tight joint. The entrance orifice was punched with a tungsten needle after the welding operation. Depending on the range of burner pressures to be explored the orifice diameter varied from 0.001 in. to 0.0045 in. The variation of ion beam intensity with pressure in the burner section is illustrated in Fig. 5 for oxygen entering through the 0.0045-in. pinhole. Since the scattering pressure in the first section is proportional to the burner pressure, and the unscattered molecular beam intensity is likewise proportional to the burner pressure, the ion intensity might be expected to follow the simple relationship $I \alpha p e^{-p/c}$, where I is the ion intensity, p is the burner pressure, and c is a constant. The theoretical curve shown was computed for $c=3.3$ cm Hg pressure. The maximum molecular beam intensity is normally obtained when the mean free path in the scattering region is just equal to the distance between the slits. Scattering of the beam near the entrance orifice will reduce the mean free path below the value computed from kinetic theory. In our case the distance between slits is 0.454 cm and the maximum intensity occurs at a chamber pressure of 4 microns. The mean free path for oxygen molecules from kinetic theory is 1.3 cm at 4 microns pressure, so that scattering in the beam and near the entrance slit has cut the effective mean free path by a factor of 3. It should be noted that the maximum beam intensity is obtained when the ratio of orifice diameter to mean free path in the burner, D/λ, is 70 rather than unity, which is the optimum value for conventional molecular beams.

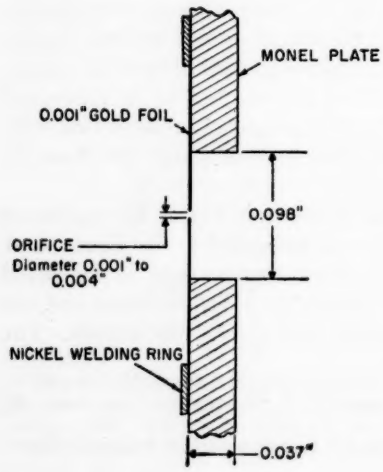

FIG. 4. Sampling orifice construction.

The operation of the mass spectrometer in obtaining data will be explained by referring to the block diagram of the instrument shown in Fig. 6. For exploratory work the beam chopper is not used, the ion accelerating energy is automatically swept with a sawtooth waveform, and the ion spectrum is displayed on an oscilloscope screen. A magnetically operated gate permits the selection of either a conventional electrometer amplifier (VX-41) detector, with a feedback circuit to reduce the input circuit time constant, or an electron multiplier detector. The electron multiplier detector with 13 stages of Be-Cu electrodes was patterned after the design by Allen[10] and shortly after installation had an over-all multiplication of 10^7. A molybdenum helix heater and a radiation shield surrounded the multiplier to permit bakeout while on the system. Comparison of the ion spectra obtained with the two detectors serves to determine (1) the relative sensitivity of the electron multiplier for different ions and (2) the current gain of the multiplier, a parameter which slowly decreased with time. Weak ion intensities are recorded by a conventional scaler circuit connected to the electron multiplier. The presence of background ion signals which arise from the diffusion pump oil, pyrolysis products generated by the filament, and diffusely scattered or reacted beam molecules seriously limit the useful sensitivity

[10] J. S. Allen, Rev. Sci. Instr. **18**, 739 (1947).

of the detecting system thus far described. Dissociation products generated at the hot filament, even when an oxide cathode is used, are particularly annoying in experiments on atom and radical detection. By incorporating a molecular beam chopper between the first and second slits and employing phase detection of the ion current signal, the background problem is virtually eliminated. The beam chopper is a vibrating reed magnetically driven at a frequency of about 200 cps with amplitude stabilization derived from a capacity pickup in the feedback loop of the driver oscillator. A sylphon bellows allows some lateral displacement of the chopper to obtain a symmetrical wave form of the ion signal. The time constant of the phase detector recording circuit is 8 seconds. With the high pulsing rate of the molecular beam used here, the background pressure in the ion source, and consequently the background ion intensity, does not change materially between bursts. A moderately high chopping frequency is necessary to assure adequate discrimination against pyrolysis products of the molecular beam constituents. If the molecular beam is harmonically modulated at an angular frequency ω, the volume of the ion source housing and pumping line is V liters, and the speed of the diffusion pump is S liters/sec and if $\omega V \gg S$, one finds that the ion source pressure is fractionally modulated by $S/\omega V$ and the phase angle Φ is given by $\tan\Phi = \omega V/S$. The in-phase component of the pressure variation which is observed by the phase detector is thus $S^2/\omega^2 V^2$. In our case $\omega \sim 1200$/sec, $V \sim 5$ liters, and $S \sim 100$ liters/sec so that $\omega V \sim 60S$ and the in-phase component of the background pressure variation is about 3×10^{-4}. The effect of pressure modulation can be further reduced, if required, by slightly adjusting the phasing of the detector. Statistical fluctuation in the background signal level is generally a more important factor, particularly for small ion intensities.

In an experiment to determine the background discrimination which is actually realized by the beam modulation technique, an argon beam from the burner section which gave a detector signal of 3 millivolts, corresponding to about 400 ions/sec, was observed while a background pressure of argon was developed in the ion source by sending argon directly into the ion source through a needle valve. The modulated beam could be measured in the presence of a 40-volt dc background signal so that a discrimination factor of 10^4 was obtained. In the important practical case where the background arises from scattered beam molecules, including decomposition products formed on the filament, the collimation of the molecular beam introduces an additional discrimination factor of 10 because the molecular density in the beam is about 10 times the scattered molecular density in this apparatus. The signal-to-noise voltage ratio S/N for a system using a modulated beam when the noise results from statistical fluctuations in the background intensity is given

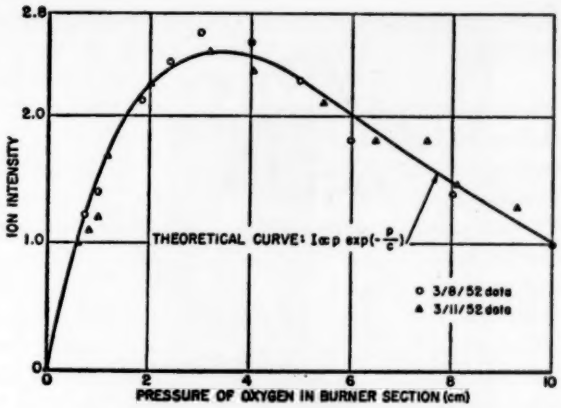

FIG. 5. Beam intensity as a function of pressure in the burner section.

approximately by

$$S/N = n(T)^{\frac{1}{2}}/(n_s)^{\frac{1}{2}}, \tag{3}$$

where n= the number of ions/sec from modulated beam, n_s= the number of disturbing ions/sec from the background, and T= observation time in seconds. If the background noise is developed primarily by scattering and reaction of certain beam constituents whose density in the primary beam is R times the density of the desired component and if each reaction generates α disturbing atoms or radicals, then

$$S/N \geq (nTc/\alpha R)^{\frac{1}{2}}, \tag{4}$$

where c is the beam collimation factor, with the equality sign representing complete conversion of the primary beam constituents. Experiments were performed with gases, such as hydrogen and oxygen which are known to react on the filament to produce hydrogen atoms and carbon monoxide, respectively, to see if the pyrolysis products would be observed with the chopped

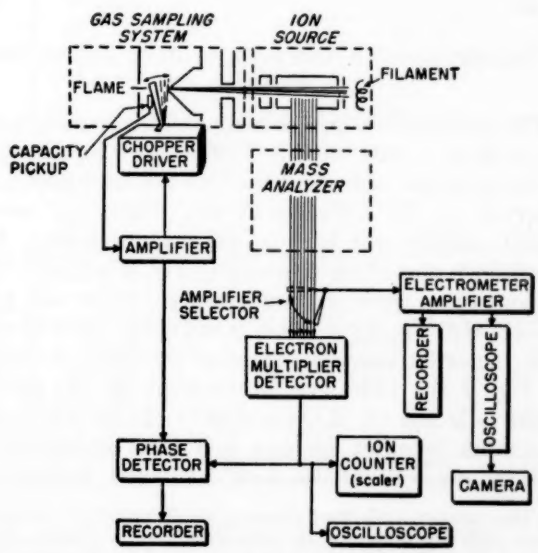

FIG. 6. Block diagram of the mass spectrometer.

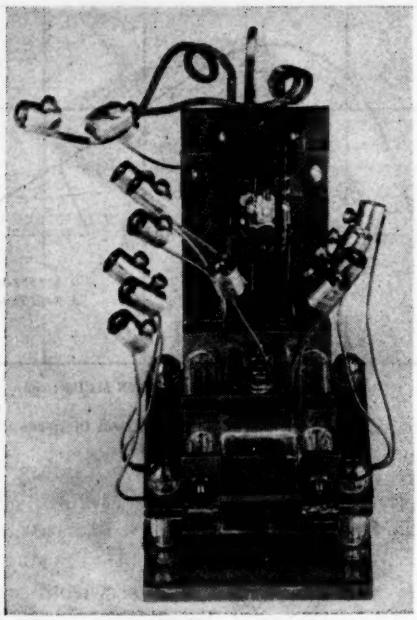

FIG. 7. Photograph of the ion source assembly showing the aperture through which the molecular beam enters.

beam method. No indications of decomposition products were observed.

The electron gun assembly with a view of the entrance hole in the last plate for the molecular beam is shown in Fig. 7. Because the electron and molecular beams are coaxial in the present design, the electron collector box was fabricated of mu-metal to cause the magnetic lineup field to vanish inside the collector box. The electrons are constrained to follow the magnetic field lines and run into the walls of the collector.

Mass analysis was performed in a 90° sectored magnetic field, using a 5-inch radius of curvature, and employing slits which gave a resolution of about 1 part in 130.

IV. EXAMPLES OF ATOM AND RADICAL DETECTION: H, OH

The appearance potential method for detecting atoms and radicals is illustrated in Figs. 8 and 9 for the cases of the hydrogen atom and the OH radical which were observed in the hydrogen-oxygen flame. An oxide-coated cathode was used as an electron source. The logarithmic plot of ion intensity in Fig. 8 indicates that H^+ ions come from two processes: (1) $H+e\rightarrow H^++2e$, and (2) $H_2O+e\rightarrow H^++OH+2e$ or $H_2+e\rightarrow H^++H+2e$, with the onset energies separated by about 5 volts.† In Fig. 9 the OH^+ ions are formed by (1) $OH+e\rightarrow OH^++2e$ and (2) $H_2O+e\rightarrow OH^++H+2e$. The rough separation in onset energies is 5 volts in agreement with the theoretical lower limit, 5.17 volts, corresponding to the dissociation energy of the H_2O molecule. The appearance potential data taken with unstabilized flames as radical sources are not good enough for exact energy determinations. The same technique applied to atoms and radicals generated in high concentrations by a discharge tube source or by pyrolysis of compounds such as $Pb(CH_3)_4$ should yield results comparable to those normally obtained with stable molecules. It was not felt, however, that such measurements were required for the present investigation. It is evident that for electron energies at or below 18 volts the contributions from dissociation processes are negligible for both OH and H.

† The experimental onset energy separation agrees somewhat better with the value for H_2 ionization [H. D. Smyth, Revs. Modern Phys. 3, 347 (1931)], 18.6−13.53=5.1 volts, than with the value for H_2O ionization, 6.0 volts.

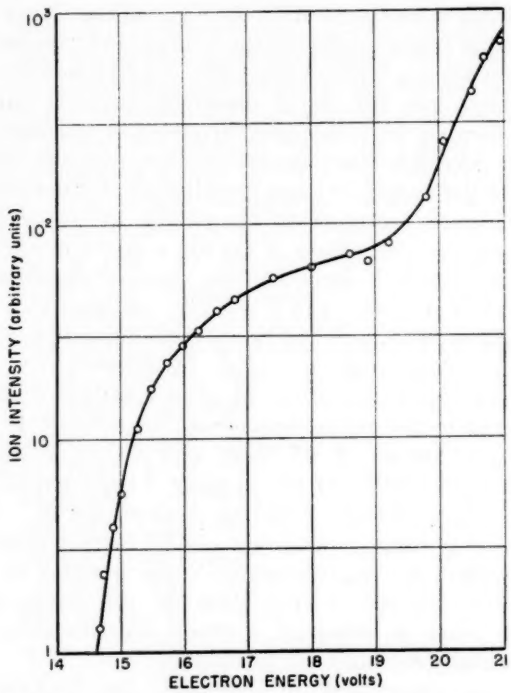

FIG. 8. Appearance potential curve for hydrogen atoms in the hydrogen-oxygen flame. Voltages are uncorrected for contact potentials, space charge, etc.

V. ANALYSIS OF FLAMES

Hydrogen-Oxygen Flame

The reaction of hydrogen and oxygen has been studied extensively[11,12] both experimentally and theoretically. Since a relatively small number of chemical entities can be present in the hydrogen-oxygen reaction, positive identification of the constituents can be obtained by mass analysis and appearance potential studies.

Low-pressure hydrogen-oxygen flames have been explored with the burner assembly previously described

[11] C. N. Hinshelwood and A. T. Williamson, *The Reaction between Hydrogen and Oxygen* (Oxford University Press, New York, 1934).

[12] B. Lewis and G. von Elbe, *Combustion, Flames and Explosions of Gases* (Cambridge University Press, New York, 1938).

(Fig. 3) in an effort to identify the reaction intermediates. The gases were admitted separately, hydrogen entering through the central burner tube and oxygen flowing in the surrounding annular space. Analyses of the mass spectra obtained with the modulated beam method clearly indicated the presence of H, O, and OH as intermediates. The intensities of these intermediates were in fact adequate to permit profile mapping of the flame as the central burner tube was moved away from the pinhole.

The observed ion intensities for a hydrogen-oxygen flame at 6 cm pressure with flow rates at NTP of 300 cc/min H_2 and 860 cc/min O_2 are given in Fig. 10. The stable components H_2, O_2, and H_2O are treated

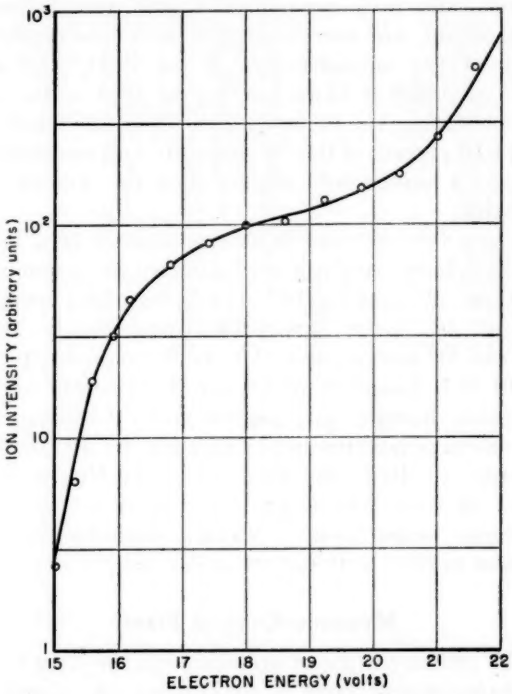

FIG. 9. Appearance potential curve for the OH radical in the hydrogen-oxygen flame. Voltages are uncorrected for contact potentials, space charge, etc.

in the upper graph, while the intermediates are shown in the lower graph. The electron accelerating voltages were 48 volts for the stable components and 18 volts for the intermediates. The abscissa is the relative displacement of the burner tube from the pinhole with the origin corresponding to a minimum spacing of about 0.050 in. enforced by a mechanical stop to prevent the burner tube from being driven accidentally into the gold diaphragm.

The interpretation of the data is complicated by diffusion effects, turbulent mixing, and changes in the flame front configuration as the central tube is displaced. These curves are not, therefore, to be confused with the concentration profiles in a flame with premixed gases. Moreover, the diaphragm affects the hydrodynamic flow of the gases, a circumstance which is difficult to avoid and is probably the most serious deficiency of the gas sampling system design.

The discontinuities in the H_2 and H_2O curves at 0.025 in. were quite reproducible and accompanied by a change in the appearance of the flame. This probably means that the flame front has two stable positions and flips from one to the other at the discontinuity. The region 0.025 in. to 0.075 in. shows the classical behavior: H_2 and O_2 being consumed, H_2O being produced, and H, O, and OH going through maxima. The behavior of the various concentrations in region 0.075 to 0.250 in. may be interpreted as the result of continuous variation in the shape of the flame front as the burner tube is retracted. The O_2 and H_2O concentrations are almost mirror images, an increase in one accompanied by a decrease in the other. Since the atom and radical concentrations do not follow the concentration changes of the stable components, we conclude that they are produced primarily by chemical kinetic mechanisms rather than by dissociation of the stable components at the flame temperature.

The determination of absolute concentrations of H, O, and OH would require that the mass spectrometer be calibrated with sources of these intermediates in which the concentrations could be computed from thermodynamic data (for example, thermal dissociation of H_2O at high temperatures) or measured by inde-

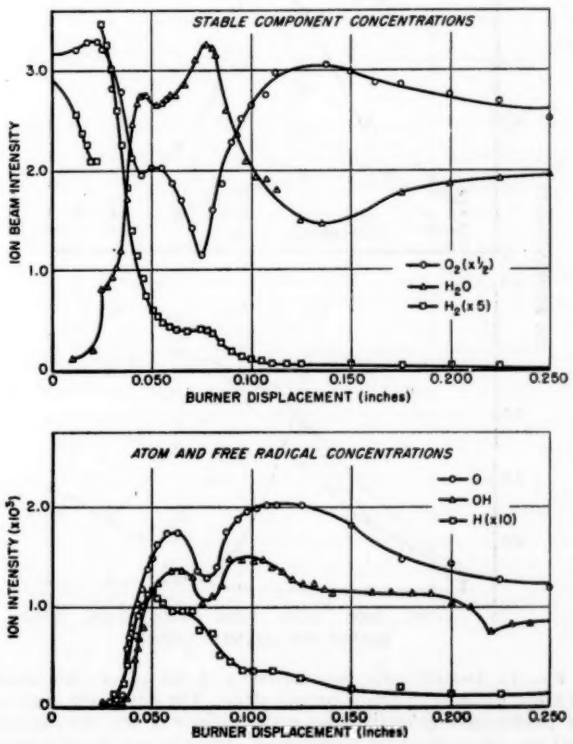

FIG. 10. Ion intensity measurements of stable components and intermediates in the low pressure hydrogen-oxygen flame. The abscissa is the relative displacement of the central burner tube from the pinhole.

pendent means (for example, absorption spectroscopy for OH). In the absence of such a calibration in our work to date, an order of magnitude estimate of the radical concentrations may be made by assuming that their ionization cross-section curves are similar to those of their associated stable molecules. On this basis the intensities of the curves in the lower graph of Fig. 10 should be multiplied by about a factor of 10 when compared with the upper graph to compensate for the decreased sensitivity at the lower electron energy. The maximum atom and radical concentrations are thus estimated to be of the order of 1 percent.

One of the principal reasons for studying the H_2-O_2 flame was the possibility of obtaining direct experimental evidence of the existence of the HO_2 radical[13,14] which has been postulated as a reaction intermediate to explain the second and third explosion limits. In principle, the experimental conditions for HO_2 detection are much better than for the detection of the other intermediates, since the only interfering peaks at mass 33 are $O^{16}O^{17}$ present as 0.078 percent of the O_2 concentration and possibly HO_2^+ from dissociative ionization of H_2O_2. Under experimental conditions in low pressure flames which afforded a generous yield of H, O, and OH a search was made for HO_2 at mass 33 and H_2O_2 at mass 34. In these experiments no excess in the 34 peak above the expected $O^{16}O^{18}$ intensity was observed so that H_2O_2 dissociation did not contribute to the 33 peak. Under these conditions observations can be made both at high electron energies to see if there is an excess of mass 33 above the $O^{16}O^{17}$ value and at low electron energies to see if an ion current is obtained below the appearance potential of the molecular oxygen ion on the assumption that $I(HO_2)<I(O_2)$. The results of the low electron energy experiments were negative. At high electron energies there was a small increase in the 33 peak intensity, although the change was not outside the limits of error in our measurement of the 33/32 ratio. Attempts to adjust flame parameters such as burner position, burner pressure, and hydrogen-oxygen ratio to increase the 33 peak were uniformly unsuccessful. For some unknown reason the reproducibility of the measurements of the $O^{16}O^{17}/O_2^{32}$ ratio made at different times was not so good as for other isotopic ratios. The excess in mass 33 was definitely less than 0.01 percent of the O_2^{32} intensity and was therefore at least a hundredfold smaller than the observed OH intensity.

It was felt that our failure to observe HO_2 in low pressure flames could be explained by the requirement of triple collisions for HO_2 formation which would be favored by higher pressures. Consequently a few experiments were made with a smaller sampling pinhole (0.001-inch diameter) which permitted higher burning pressures. Burning at pressures up to 0.5 atmosphere did not give positive indications for the HO_2 radical. In order to clarify the situation of the HO_2 radical a series of experiments are being planned in which hydrogen atoms from a Wood's discharge tube are allowed to react with oxygen molecules.‡

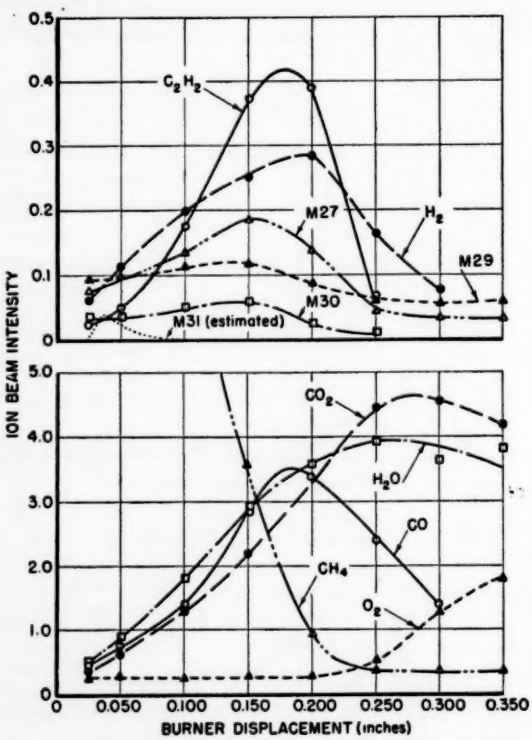

FIG. 11. Ion intensity measurements of the major components in a low pressure methane-oxygen flame. The data were obtained by photographing oscilloscope presentations of the mass spectra and are uncorrected for background. The abscissa is the relative displacement of the burner tube from the pinhole.

Methane-Oxygen Flame

The primary purpose in presenting the data for the methane-oxygen flame is to indicate the complexity of the reaction system which obtains in a hydrocarbon flame and to point out some of the analytical difficulties which result from this situation. In studying the methane-oxygen flame, one essentially investigates the general problem of hydrocarbon combustion because a number of the intermediates found are higher mass hydrocarbons, alcohols, etc. Whereas the identification of a component by mass number is quite adequate in simple reactions, such a procedure is insufficient and can easily lead to incorrect results in hydrocarbon flames. The detection of radicals is also made difficult because a large number of molecules are potential sources of the radical ion in dissociative ionization processes.

The combustion of methane, the simplest hydrocarbon, was used in our early experiments to check out

[13] C. N. Hinshelwood, Proc. Roy. Soc. (London) **A188**, 1 (1946).
[14] G. J. Minkoff, Disc. Faraday Soc. **2**, 151 (1947).

‡ *Note added in proof.*—These experiments are reported in a letter to be published in this journal entitled "The Detection of the HO_2 Radical by Mass Spectrometry."

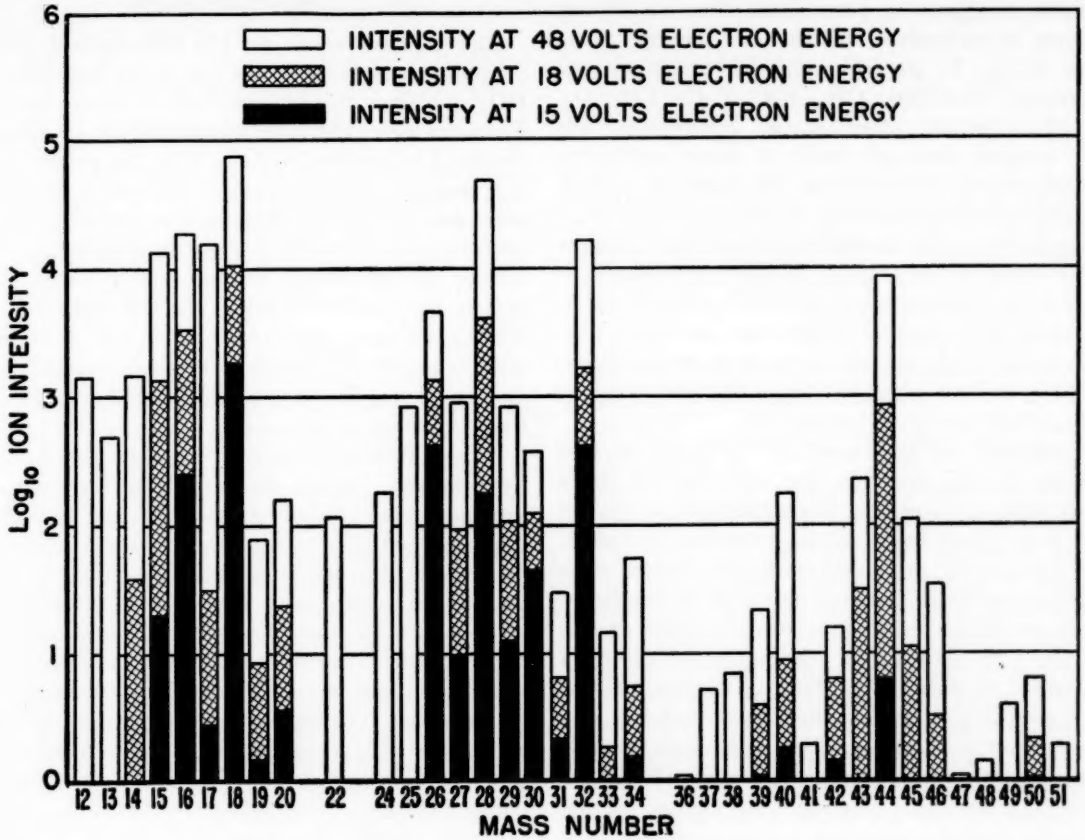
INTENSITY AT 48 VOLTS ELECTRON ENERGY
INTENSITY AT 18 VOLTS ELECTRON ENERGY
INTENSITY AT 15 VOLTS ELECTRON ENERGY
Log10 ION INTENSITY
0
1
2
3
4
5
6
12 13 14 15 16 17 18 19 20 22 24 25 26 27 28 29 30 31 32 33 34 36 37 38 39 40 41 42 43 44 45 46 47 48 49 50 51
MASS NUMBER

FIG. 12. Mass spectra of the methane-oxygen flame obtained at different values of electron energy. A range of 10^5 in intensities is covered by the logarithmic scale. The actual electron energies are lower than the indicated voltages by about 1.5 volts because of contact potentials, space charge, etc.

the molecular beam sampling techniques. Figure 11 shows the composition profiles for the major peaks in the CH_4-O_2 flame at 12 cm pressure when methane was admitted in the center tube and oxygen flowed in the surrounding annulus. In this particular experiment, which was made prior to the installation of the beam chopper, the sampling orifice was a 0.002-in. hole in an 0.002-in. platinum diaphragm, and the ion spectra were displayed on an oscilloscope screen and photographed. As the burner tube is displaced from the pinhole the decrease in CH_4 is accompanied, as expected, by increases in CO_2, H_2O, and O_2. The curves for CO, C_2H_2, H_2, and components having masses 27, 29, 30, and 31 go through distinct maxima showing that they are formed in the early stages of the reaction and are consumed as the reaction goes to completion. The large amount of acetylene produced in the reaction shows that the combustion reaction is by no means simple. The ion intensities at the numbered masses have been corrected for contributions from the other components and have been tentatively identified as follows: mass 27, $C_2H_3^+$ from C_2H_4; mass 29, CHO^+ from HCHO or $C_2H_5^+$ from C_2H_6; mass 30, $C_2H_6^+$ or $HCHO^+$; mass 31, CH_3O^+ from CH_3OH.

The complexity of the methane-oxygen combustion spectrum poses some formidable analytical problems. This situation is illustrated in Fig. 12 which gives recent data for combustion at 0.1 atmosphere obtained at a single burner position with the modulated beam technique. The gas sampling orifice in this case was a 0.004-in. hole in the usual 0.001-in. thick gold diaphragm. Ion spectra were measured at different electron bombarding energies not only to furnish evidence for radicals in the flame but to provide some analytical assistance in interpreting the spectrum. Despite the assistance rendered by variations in pattern with electron energy, it has not been possible to identify the sources of all the ion peaks shown. The difficulty in making identifications stems from the following sources: (1) there are a large number of chemical compounds which could conceivably be manufactured from the reactants and give peaks at the observed mass numbers; (2) some of the molecules extracted from the flame are in excited states and therefore will have dissociative ionization spectra which are different from standardizing spectra obtained at normal temperatures; (3) unstable components whose ion spectra can only be guessed are also present.

The intensity measurements at the lowest energy (15 volts) are of particular importance because most

of the peaks correspond to parent ions, thus simplifying the picture considerably. In the low energy mass spectrum of Fig. 12 the following stable components can be readily identified: CH_4, H_2O, C_2H_2, CO_2, O_2, CO_2, C_4H_2. Certain other stable compounds are certainly present although there is some ambiguity in the assignments. For example, the mass 30 peak is contributed by formaldehyde or ethane or a mixture of both. Resolution of the formaldehyde-ethane question by examination of the 27 peak which is characteristic of ethane is not possible because other hydrocarbons in the spectrum have mass 27 dissociation products. The situation in the upper portion of the mass range shown in Fig. 12 is not too clear, although the data suggest that C_3H_4, C_3H_6 and C_3H_8 are present.

In examining the spectrum for evidence of free radicals one initially assumes that all observed peaks arise from stable compounds. There must be convincing evidence that a peak could not be generated by ionization or dissociation of stable molecules before it is attributed to a radical. The only radical in the methane-oxygen flame for which we have positive proof at this time is the CH_3 radical. In addition to observing a large intensity at mass 15 (see Fig. 12) which could not be due to anything other than the CH_3 radical, we have appearance potential data which substantiates this identification. Appearance potential curves have not been obtained for the components at masses 29, 31, and 39 which might be expected to disclose the presence of the radicals HCO or C_2H_5, CH_3O, and C_3H_3, respectively. The CH_3O^+ intensity at mass 31 ostensibly comes from methyl alcohol ionization. Although the intensity of C_3H_3 cannot come from propane[15] [$A(C_3H_3^+)=15.7\pm0.5$ volts] or propylene[15] [$A(C_3H_3^+)=14.1\pm0.2$ volts], and is too high to be expected from C_3H_4 ionization, we do not have definite proof for the presence of the C_3H_3 radical since an appearance potential curve for the ion was not obtained. A similar situation exists in the case of the mass 29 peak.

The intensity of mass 33 at 15 volts (too small to appear on the graph, Fig. 12) was higher than the $O^{16}O^{17}$ contribution from oxygen, while the mass 34 peak checked the expected $O^{16}O^{18}$ intensity. The isotopic contribution from methyl alcohol is probably not sufficient to account for the discrepancy. We are reluctant to ascribe the small intensity difference to the HO_2 radical, particularly in view of our essentially negative results for this radical in the hydrogen-oxygen flame. In the complicated methane-oxygen flame it is possible that the small excess in the ion peak at mass 33 could even be CH_5O^+ which occurs as a large peak in the spectrum of isobutyl alcohol.[16]

[15] J. Delfosse and W. Bleakney, Phys. Rev. **56**, 256 (1939).

[16] Mass Spectral Data, API Research Project 44, National Bureau of Standards Serial No. 369.

VI. DISCUSSION

The negative result for the HO_2 radical in the hydrogen-oxygen flame is not due to an instability of the HO_2^+ ion since this ion occurs in the mass spectrum of hydrogen peroxide. The interpretation of Eltenton's[17] observed intensities at mass 33 in the methane-oxygen and propane-oxygen flames is not clear. Identification of his mass 33 peak as HO_2 must be treated with reservations in view of some alternative explanations for intensity at this mass number, particularly since his system was unable to detect the OH radical in flames. The experiments reported here do not, however, rule out the occurrence of the HO_2 radical in the hydrogen-oxygen flame in considerably smaller concentration than the other intermediates.

The difficulty in identifying the intermediates in hydrocarbon flames, illustrated in the case of the methane-oxygen flame, arises from the complexity of the spectrum due to the large number of compounds present in the flame, rather than from an intrinsic inability to distinguish the radicals from the stable components. In most cases where the ion intensities are high enough to permit good determinations of appearance potentials, the ambiguity between radicals could be resolved. The appearance potentials of the free radicals would, of course, have to be determined by other experiments, such as electron impact studies of stable molecules. It should be noted that the appearance potential method for detection can not be applied if the ionization potential of the atom or radical is greater than that of a stable constituent of the system which is present in high concentration. For example, oxygen atoms ($I.P.=13.63$ volts) would not be detected in the presence of methane ($I.P.=13.1$ volts). A practical solution to this problem lies in utilization of mass spectrometers with higher mass resolution. The use of an instrument with higher resolving power would also solve some of the analytical problems in identifying the stable components in complex reactions.

At the present time it appears that the most profitable applications of the mass spectrometric techniques for detecting atoms and free radicals will be in elucidating the mechanisms of simple gas phase reactions. There are a number of interesting reactions between atoms and molecules which have been studied with less definitive analytical methods.[18] Among the elementary reactions which we propose to investigate in detail is the reaction of hydrogen atoms with oxygen molecules.

The authors are indebted to Dr. F. T. McClure, Dr. W. H. Avery, and Dr. A. Kossiakoff for advice and encouragement during the course of the investigation and to Mr. B. H. Nall for building the electron multiplier detector.

[17] Reference 2, page 478.

[18] E. W. R. Steacie, *Atom and Free Radical Reactions* (Reinhold Publishing Corporation, New York, 1946).

Thermal Expansion of Zirconium between 298°K and 1600°K*

GORDON B. SKINNER† AND HERRICK L. JOHNSTON
The Cryogenic Laboratory and the Department of Chemistry, Ohio State University, Columbus, Ohio
(Received March 31, 1952)

The average coefficients of thermal expansion of hexagonal zirconium between 298°K and 1143°K are 5.5×10^{-6} deg^{-1} along the a axis, 10.8×10^{-6} deg^{-1} along the c axis, and 7.2×10^{-6} deg^{-1} for a randomly oriented polycrystalline sample. The average value of the linear coefficient of expansion of cubic zirconium between 1143°K and 1600°K is 9.7×10^{-6} deg^{-1}. At the transition there is a decrease in volume of 0.66 percent.

INTRODUCTION

THE fact that zirconium crystallizes in the close-packed hexagonal lattice at room temperature and in the body-centered cubic lattice in the temperature range above the transition (at about 1143°K) has been known for some time.[1] Owing to the anisotropic crystal structure at lower temperatures, there is some question as to the meaning of measurements reported by Zwikker,[2] by Squire and Kaufmann,[3] and by Adenstadt,[4] of the thermal expansion of bulk samples of zirconium.

In an attempt to clarify these measurements, we have determined the two expansion coefficients of hexagonal zirconium, using the x-ray diffraction method, and have also measured the (isotropic) expansion of cubic zirconium, using the conventional comparator method.

MATERIALS

The zirconium used for these experiments was described in a previous paper.[5] It was prepared by the iodine method, and contained about 1 atom percent hafnium. Specimens for x-ray diffraction were in the form of rods about 0.05 cm in diameter. The specimen used for measurements of bulk thermal expansion was about 25.4 cm long and 0.62 cm in diameter and had two blackbody holes, each 0.099 cm in diameter, drilled 5 cm from each end.

TABLE I. Thermal expansion of α zirconium (reference temperature = 298.16°K).

T°, K	a_0, kX	c_0, kX	V, kX^3	$\Delta V/3V_0=\Delta l/l_0$
950	3.2393	5.1741	47.019	0.0051
1032	3.2393	5.1751	47.033	0.0052
1042	3.2406	5.1816	47.125	0.0058
1119	3.2400	5.1803	47.095	0.0056
1164	3.2413	5.1856	47.181	0.0062

APPARATUS AND PROCEDURE

The x-ray diffraction apparatus described by Edwards, Speiser and Johnston[6] was used. A few modifications were made, the most important being the insertion of a liquid-air trap between the oil diffusion pump and the camera. Nevertheless, it was not possible to obtain, in the apparatus, a vacuum much better than 10^{-5} mm, and considerable trouble was experienced due to contamination of the zirconium specimens. This became most serious at the higher temperatures, so that the x-ray method was not used above 1252°K.

The zirconium rod used for the measurement of the expansion of cubic zirconium was supported inside a 1.27-cm diameter tantalum tube 38.1 cm long, which in turn was supported within an evacuated Pyrex tube of about 5 cm diameter. An evenly wound rf work coil of 0.62-cm copper tubing was placed around the outside of this Pyrex tube. The tantalum tube had two small holes, and the Pyrex tube two plane windows, opposite the blackbody holes in the zirconium rod. Through these openings measurements of temperature were made with a Leeds and Northrop disappearing-filament optical pyrometer, and measurements of position (using the edges of the blackbody holes as reference marks) were made with two telescopes mounted on a traveling carriage whose position could be read to within 0.001 mm.

Lattice parameters were calculated from the x-ray diffraction patterns using the method of Cohen,[7] and two corrections were then applied. The first of these corrections was made to account for the impurities (chiefly hafnium) which were initially in the zirconium. On the assumption that the impurities effect both

TABLE II. Thermal expansion of β zirconium.

T°, K	$\Delta l/l_0$	T°, K	$\Delta l/l_0$
1166	0.0040	1408	0.0066
1251	0.0051	1492	0.0073
1289	0.0053	1533	0.0079
1387	0.0063	1584	0.0080

* This work was supported in part by the U. S. Office of Naval Research under contract with the Ohio State University Research Foundation.
† Monsanto Chemical Company Fellow, 1950–1951.
[1] R. W. G. Wyckoff, *Crystal Structures* (Interscience Publishers, Inc., New York, 1948).
[2] C. Zwikker, Physica **6**, 361 (1926).
[3] C. F. Squire and A. R. Kaufmann, J. Chem. Phys. **9**, 673 (1941).
[4] H. K. Adenstedt, Trans. Am. Soc. Metals **44**, 949 (1952).
[5] Skinner, Edwards, and Johnston, J. Am. Chem. Soc. **73**, 174 (1951).
[6] Edwards, Speiser, and Johnston, Rev. Sci. Instr. **20**, 343 (1949).
[7] M. U. Cohen, Rev. Sci. Instr. **6**, 68 (1935).

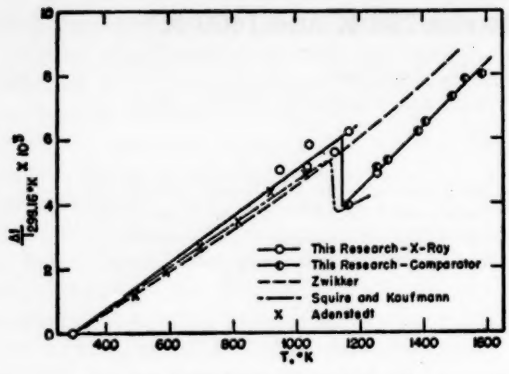

FIG. 1. Thermal expansion of zirconium.

parameters, a_0 and c_0, in the same proportion and in the ratio of their concentrations and atomic radii, experimental values were multiplied by a factor of 1.00027 to give the parameters of pure zirconium. The second correction was made to account for the observation that the parameters at room temperature were usually larger after a high-temperature measurement than before, owing to the absorption of impurities (chiefly oxygen and nitrogen gases) by the sample. Half the increase was subtracted from the measured parameters at high temperature, on the assumption that the impurities were absorbed at a uniform rate throughout the high-temperature measurement. Experimental data were rejected in a few cases where parameters at room temperature increased by excessive amounts. However, this second correction was not always necessary, since in some of the experiments the specimens were protected from these residual gases by a thin-walled beryllium tube.

EXPERIMENTAL RESULTS

The lattice parameters of pure zirconium at 25°C were found to be $a_0=3.2265\pm0.0010kX$ and $c_0=5.1371\pm0.0015kX$. The axial ratio c_0/a_0 is 1.5922 ± 0.0007. The unit cell volume is $46.314\pm0.037kX^3$, and the density, 6.501 ± 0.005 g/cm³. The experimental lattice parameters, with cell volumes and expansions for α-zirconium at high temperatures, are listed in Table I.

From these data, the average coefficient of linear expansion between 298°K and 1143°K, is 5.5×10^{-6} deg^{-1} along the a axis and 10.8×10^{-6} deg^{-1} along the c axis. The mean coefficient of linear expansion is 7.2×10^{-6} deg^{-1}, being intermediate between the above two values. The assumption of a constant expansion coefficient over the temperature range appears to be justified, within the experimental error, since Squire and Kaufmann[3] obtained a linear expansion curve by measurement of the gross thermal expansion of a rod over this same range.

The measurement of the lattice parameter of β-zirconium gave $a_0=3.6089\pm0.0020kX$ at 1252°K. The unit cell volume is $47.00\pm0.08kX$, which gives $\Delta V/V_0=0.0149$ and $\Delta l/l_0=0.0050$. Relative to this figure, the values of $\Delta l/l_0$ obtained by direct measurement of thermal expansion are listed in Table II. The density of β-zirconium at 1252°K is 6.406 ± 0.011 g/cm³.

The $\Delta l/l_0$ values are shown graphically in Fig. 1. The curves obtained by Squire and Kaufmann[3] and Adenstedt[4] fall somewhat lower than ours. Zwikker's[2] curve is lower than ours for α zirconium but higher for β zirconium.

ERRORS

We have estimated that the maximum uncertainties in the parameters at room temperature are $0.0010kX$ in a_0 and $0.0015kX$ in c_0. For the high-temperature patterns the corresponding uncertainties are $0.0020kX$ and $0.0040kX$, while the uncertainty in a_0 for the β phase is $0.0020kX$. In terms of thermal expansion coefficients, the maximum uncertainty is 10 percent along the a axis and 14 percent along the c axis.

The thermal expansion measurements of β zirconium with the comparator arrangement were considerably more precise, the maximum uncertainty in the coefficient of expansion, as estimated from the scatter of the experimental points from a straight line, being about 4 percent. However, these measurements had to be related to room temperature through the x-ray diffraction measurement of β zirconium, which could have been in error by as much as 7 percent. If this error existed, the whole curve for β zirconium would be shifted vertically (see Fig. 1).

In view of these comparatively large errors in measuring distances, errors introduced in temperature measurements may safely be neglected.

Phase Equilibrium in the System Calcite-Aragonite†

JOHN C. JAMIESON*
Department of Geology, University of Chicago, Chicago, Illinois
(Received March 26, 1953)

The equilibrium curve for two of the phases of $CaCO_3$, calcite-aragonite, has been determined as a function of temperature and pressure over the range 25–80°C and several thousand kg/cm², using the electrical conductivity of aqueous solutions of each form. Aragonite is proved to be the high pressure modification. From the determined equilibrium curve, various thermodynamic quantities are obtained in a more accurate fashion than previously possible. All normal natural occurrences of aragonite must be due to metastable formation rather than equilibrium, since the geothermal gradient lies completely in the calcite field.

INTRODUCTION

THE direct determination of the actual equilibrium curve with respect to temperature and pressure, of polymorphic forms exhibiting an irreversible transition, is difficult if not impossible. Hence an indirect approach must be made in terms of fundamental thermodynamic quantities. At any point on the (P, T) equilibrium curve, the Gibbs free energies of the two forms must be equal, so a determination of the free energy surfaces from thermal data gives immediately the equilibrium curve. Equally, the determination of any other property of the two forms, which is a single-valued function of their free energies, will give the equilibrium curve.

Two of the forms of $CaCO_3$, calcite and aragonite, are among the earliest known examples of a polymorphic pair, both having widespread geologic occurrence, but their actual stability fields have not previously been determined beyond the fact that aragonite is unstable with respect to calcite at all temperatures and moderate pressures, except possibly at low temperatures.

The method used to obtain the equilibrium curve for this polymorphic pair is the measurement of the electrical resistance of aqueous solutions of each form at high pressures and several temperatures. Then from these measurements the curve is extrapolated with the aid of thermal data.

THEORETICAL BACKGROUND

Let G be the Gibbs free energy of a pure phase, S its entropy, V its volume, c_p its heat capacity at constant temperature, all in units per mole. Then

$$\left(\frac{\partial G}{\partial T}\right)_P = -S \quad \text{and} \quad S = \int_0^T \frac{c_p}{T} dT, \tag{1}$$

where there are no phase transitions in the interval $(0, T)$, and the integral is taken at constant pressure. Then for $P = P_0$,

$$G(P_0, T) - G(P_0, 0) = -\int_0^T S dT. \tag{2}$$

If the expression for c_p is known, then the function

$$\frac{G(P_0, T) - G(P_0, 0)}{T},$$

may be evaluated. This gives the Gibbs free energy of a phase as a function of temperature for a given pressure, but contains an as yet undetermined constant, namely $G(P_0, 0)$, the free energy at P_0 and the absolute zero of temperature. For the case of polymorphism, it is obvious that if the difference in free energy of the various forms is known for any one given temperature, then the difference in free energy is known for all temperatures, at the given pressure, for which adequate c_p data are available.

Anderson[1] has determined c_p for calcite and aragonite over the range 55–294°K, and lately these data have been extended by Kobayashi[2,3] up to a little under 800°K. It is of interest to calculate a point for calcite-aragonite equilibrium from these data first and then to compare it with the experimental results. It must be emphasized that these calculations bear only on the relative stability of the two forms and say nothing about the possibility of a third phase being the actual stable form of $CaCO_3$. This possibility must be taken care of by additional knowledge of the system.

Anderson[1] gives the two following expressions for the respective c_p in terms of combinations of Debye functions and Einstein functions:

$$c_p \text{ (calcite)} = D\left(\frac{180}{T}\right) + 2E\left(\frac{370}{T}\right) + 2E\left(\frac{1210}{T}\right),$$

$$c_p \text{ (aragonite)} = D\left(\frac{244}{T}\right) + 2E\left(\frac{342}{T}\right) + 2D\left(\frac{1897}{T}\right).$$

† A dissertation submitted to the Faculty of the Division of the Physical Sciences in candidacy for the degree of Doctor of Philosophy, University of Chicago.

* Now Postdoctoral Fellow, National Science Foundation, Department of Geology, University of Chicago.

[1] C. T. Anderson, J. Am. Chem. Soc. **56**, 340 (1934).
[2] K. Kobayashi, Science Rept. Tôhoku Univ., First Ser. **35**, 103 (1951).
[3] K. Kobayashi, Science Rept. Tôhoku Univ., First Ser. **35**, 111 (1951).

TABLE I. Free energy data for calcite-aragonite at 1 kg/cm².

T°K	$1/T(G_c-G_{co})$	G_c-G_{co} cal/mole	$1/T(G_a-G_{ao})$	(G_a-G_{ao}) cal/mole
298.1	−10.68	−3184	− 9.69	−2889
300	−10.75	−3225	− 9.76	−2928
320	−11.53	−3690	−10.53	−3370
340	−12.28	−4175	−11.27	−3832
360	−13.02	−4687	−12.00	−4320

Kelley and Anderson[4] give $\Delta G(1, 298.1)=G_c(1, 298.1)-G_a(1, 298.1)=-273$ cal/mole. The pressure is in kg/cm², the temperature in °K, the subscript "c" denotes calcite, and "a" denotes aragonite. (The calculations done before experimentation were based on these data.) More recently Kobayashi[2,3] has given values of

$$\frac{G(1, T)-G(1, 0)}{T}$$

obtained from his c_p measurements and those of Anderson[1] as reproduced partially in Table I. Kobayashi[2,3] also gives $\Delta G(1, 298.1)=-311$ cal/mole, and $\Delta G(1, 0)=-16$ cal/mole. From these data the equilibrium curve for calcite-aragonite could be calculated as in the following paragraphs.

For a pure phase $\partial G/\partial P)_T=V(P, T)$, hence

$$G(P, T)-G(1, T)=\int_1^P V(P, T)dP,$$

where $V(P, T)$ is the molal volume. For calcite-aragonite we have

$$\Delta G(P, T)-\Delta G(1, T)=\int_1^P \Delta V(P, T)dP.$$

For the two forms to be in equilibrium at (P, T), $\Delta G(P, T)=0$, hence

$$-\Delta G(1, T)=\int_1^P \Delta V(P, T)dP. \qquad (3)$$

This equation, when solved for P at a given T, gives the (P, T) point at which aragonite and calcite are in equilibrium. To solve the equation, it is necessary to know the molal volume of each form as a function of pressure and temperature.

Birch *et al.*[5] give $\Delta V/V_0$ for calcite as follows: (The pressure has been converted from bars to kg/cm²)

$$-\frac{\Delta V}{V_0}=1.319(10)^{-6}P-4.08(10)^{-12}P^2 \quad \text{at} \quad 303.1°\text{K},$$

$$-\frac{\Delta V}{V_0}=1.344(10)^{-6}P-4.30(10)^{-12}P^2 \quad \text{at} \quad 348.1°\text{K},$$

and for aragonite

$$-\frac{\Delta V}{V_0}=1.52(10)^{-6}P \quad \text{at} \quad 273.1°\text{K}.$$

The former was determined by Bridgman,[6] while the latter was determined from measurements by Madelung and Fuchs[7] only to a few hundred atmospheres. The change in compressibility of aragonite with temperature may be approximated by using Bridgman's[6] value for celestite ($SrSO_4$), which is orthorhombic as is aragonite and possesses a compressibility of the same order of magnitude as that of aragonite. It seems better to use these more modern values rather than values such as are given by Voigt[8] which are calculated from elastic moduli, since the former are from actual measurements made under hydrostatic pressure. Thermal expansion data are given by Kozu and Kani[9] and Kozu *et al.*[10] for atmospheric pressure. The values for the specific gravities may be found in Dana[11] as $\rho_c=2.7102\pm.0002$ at 20°C, $\rho_a=2.947\pm.002$, no temperature given. Thus from the above, plus Kobayashi's[2,3] value of $\Delta G(1, 298.1)=-311$ cal/mole, we obtain the equilibrium pressure of 4660 kg/cm² for 298.1°K. Calcite is the low-pressure modification and aragonite is the high-pressure modification of $CaCO_3$. This compares with an actually determined value of 3920 kg/cm², an error of 20 percent. The major contribution to the error in this calculation is the uncertainty in the value of $\Delta G(1, 298.1)$ because of lack of knowledge of $\Delta G(0, 0)$, which may be of the order of 10–15 percent, hence this figure gives only a clue to the order of magnitude of pressure required, rather than a quantitative result. However in many situations, especially when dealing with substances of geologic interest, such a value may be the best obtainable. In the present case, similar calculations were carried out before experimental work was begun, in order to ascertain what range of pressure equipment would be needed.

EXPERIMENTAL PROCEDURE

In order to determine experimentally the equilibrium curve between calcite and aragonite, the indirect approach of measuring the resistance of aqueous solutions of each form was used. This method can succeed only when the rate of transition from one form to the other is extremely slow, so that the unstable form can actually come to "equilibrium" with its solution. This point will be mentioned later in the description of the experimental results. At equilibrium of the two phases,

[4] K. K. Kelley and C. T. Anderson, U. S. Bur. Mines, Bull. 384 (1935).

[5] Birch, Schairer, and Spicer, Geol. Soc. Am., Spec. Paper, No. 36 (1942).

[6] P. W. Bridgman, Am. J. Sci. Ser. 5, **10**, 483 (1925).

[7] E. Madelung and R. Fuchs, Ann. phys. **65**, 289 (1921).

[8] W. Voigt, *Lehrbuch der Kristallphysik* (Teubner, Berlin, 1928).

[9] S. Kozu and K. Kani, Proc. Imp. Acad. (Tokyo) **10**, 222 (1934).

[10] S. Kozu, M. Masuda, and J. Veda, Science Rept. Tohoku Univ., Third Ser. **3**, 247 (1929).

[11] Palache, Berman, and Frondel, *Dana's System of Mineralogy* (John Wiley and Sons, Inc., New York, 1951), seventh edition, Vol. 2.

the solubilities of each in water are equal, and hence, making the plausible assumption that the ions released by each are the same, with the same mobilities, the electrical conductivity of a solution of calcite is equal to that of a solution of aragonite at their (P, T) point of equilibrium. Since the conductivity is a function of the mobility of the ions, their charge and number, it is possible that the conductivities should be equal at more than one pressure on each isotherm. However for slightly soluble salts, the mobilities should be independent of which solid phase is present. In this case the difference of the conductivities is a function only of the number of ions which are present.

It is to be noted that this method involves equilibrium of the two solid phases of $CaCO_3$ in a different thermodynamic environment; hence this equilibrium curve is not necessarily the same as that of the system without water. There are two factors to be taken into consideration; one is the possibility of H_2O entering into the calcite and aragonite lattices, the other is the effect of a change in amount of CO_2 present in the H_2O. It is easily shown that for the case of H_2O entering into the solid phase in ideal solution, $P-P_0=RT/\Delta\bar{V}\ \ln C_c/C_a$, where P is the equilibrium pressure of the transition with H_2O in the respective lattices; P_0 is the transition pressure of the two phases in the absence of H_2O; $\Delta\bar{V}$ is the difference in fictive molal volume between calcite and aragonite; C_c is the concentration of $CaCO_3$ in the calcite phase; C_a is the concentration of $CaCO_3$ in the aragonite phase; and the temperature is constant. Numerically we have for 300°K, $P-P_0\cong 8500\ \ln C_c/C_a$ kg/cm², so even if there exists, say 2 percent of H_2O in the calcite phase and 1 percent H_2O in the aragonite phase, the equilibrium pressure is changed only 85 kg/cm². It is estimated that the effect is actually much smaller than this.

In studying the second factor, Gibbs' phase rule informs us that with undersaturated CO_2 present in the liquid phase there are two degrees of freedom, i.e., the equilibrium curve is affected, while for CO_2 in excess, a fourth phase forms and there is a unique (P, T) equilibrium curve, but not necessarily that of the system in the absence of CO_2. However the equilibrium curve is affected only to the extent that CO_2 is dissolved in the two $CaCO_3$ solid phases, which is governed by the amount of CO_2 in the H_2O. The change in equilibrium pressure for a constant temperature is again $P-P_0=RT/\Delta\bar{V}\ \ln C_c/C_a$ with the notation as previously defined except that P is the equilibrium pressure with CO_2 in the lattices. This effect is negligible in the present case, since the amount of CO_2 in the H_2O is quite small.

The pressure was applied by the typical Bridgman apparatus for the range up to 15 000 atmospheres as has been described elsewhere by Kurnick,[12] except that an oil bath surrounding the bomb was used to maintain the temperature. The pressure was measured with a manganin gauge which has been calibrated against the freezing point of Hg and a Wheatstone bridge to an absolute accuracy of 0.2 percent. The temperature was measured with a Leeds and Northrup type K potentiometer, using a chromel P-alumel thermocouple inserted into a $\frac{3}{4}$-in. deep hole drilled in the top of the bomb. The thermocouple was calibrated against the boiling point of H_2O. A calibration run, using an experimental plug with a thermocouple mounted in a hole drilled in the experimental plug to $\frac{1}{4}$ in. of the experimental cavity, plus another junction in series with the first, extending to the middle of the chamber (Kurnick[12]) gave agreement to 0.1°C with the bomb couple when the system was in thermal equilibrium. Hence an absolute accuracy of 0.5°C was obtained. The oil bath was regulated by a thermostat. At equilibrium the temperature of the bomb was held ±0.1°C; however there was as much as a degree difference from run to run even with the thermostat setting untouched. This was ascribed to the change in temperature of the tap water circulating in the connecting pipe, which served to keep the manganin pressure gauge at a uniform temperature.

The cell (Fig. 1) was machined entirely from white virgin Teflon (polytetrafluoroethylene). It was constructed in the style of a hypodermic syringe, with a sliding section to separate the hexane used as a pressure transmitting fluid from the carbonate solutions, and to compensate for the differential compressibilities of the two fluids. The electrodes were supported by screwed-in plugs, which once in place were never removed. The tapped hole in the top of the slide was for a threaded chrome steel rod used in filling and handling the cell. The Pt electrodes were platinized. The theory of the cell was that at equal pressures solutions of calcite and aragonite would have the same compressibility and hence have the same "cell constant" for a given pressure. The slide was always started out from the same position. Reproducibility of results and smoothness

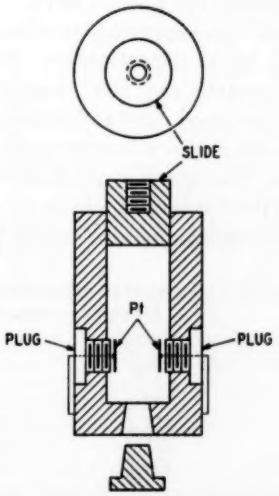

FIG. 1. Conductivity cell for use at high pressures.

[12] S. W. Kurnick, J. Chem. Phys. **20**, 218 (1952).

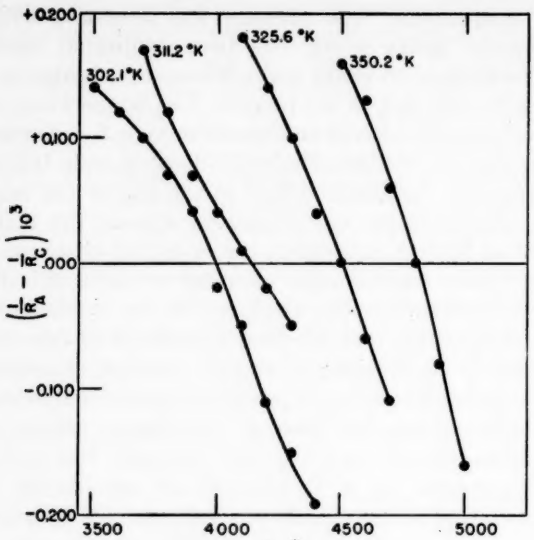

FIG. 2. Difference plot to determine equilibrium pressures as a function of temperature.

of curves were used as the proof of this hypothesis. After two early runs the cell gave results reproducible to 1 percent. Since the isothermal curves were made up of points from several runs, their smoothness attested to no great variation in the cell itself from run to run. No effect was noted from the possible phase transition in Teflon at these pressures. By using difference plots the water correction canceled out.

After platinization, several attempts were made to clean the cell by boiling in HNO_3. The cell was found to be still contaminated and a steady fall in conductivity of a given solution with time was noticed. Alternate boilings of the cell in Methanol and double-distilled water for a few days, followed by placing the cell under a 2-micron vacuum at room temperature for 12 hours and then at 90°C for 12 hours, prepared the cell for use. After each run the cell was cleaned by soaking in Methanol for an hour and then boiled in double-distilled water for 1 to 2 hours.

The cell was supported on the experimental plug by two thin brass pieces and a phosphor-bronze spring which also made electrical connections.

The water used was prepared by double distillation in a Pyrex still and was stored in Pyrex flasks sealed with Parafilm. The specific conductivity of the water was about $2(10)^{-6}$ mhos. A check of the *p*H of the water was maintained, measurements being made with a Beckman *p*H meter immediately preceding the filling of the cell. The *p*H was maintained at 6.3±0.1, indicating a fairly constant CO_2 percentage in the water. Unfortunately there did not seem to be any way of maintaining a really rigorous control of CO_2 pressure in this series of experiments.

TABLE II. Experimentally determined equilibrium points for calcite-aragonite.

T°K	*P* kg/cm²
302.1	3980
311.2	4130
325.6	4500
350.1	4800

The calcite was prepared from freshly cleaned and ground Iceland Spar, sieved through 100-mesh screen, with the fine dust left in to compensate for the fineness of the aragonite. The aragonite was prepared by slowly dropping 1*N* $CaCl_2$ into 1*N* Na_2CO_3 (both C.P. grade) at 100°C after the method of de Keyser and Dequeldre.[13] Analysis by x-ray spectrometer failed to show any trace of calcite in this preparation.

Analysis by x-ray spectrometer of the end products of several runs of both aragonite and calcite at various temperatures and pressures showed traces of vaterite. This was regarded as being only incidentally due to the pressure applied. Since these carbonates become more soluble at high pressures when pressure is released, they precipitate partially in metastable forms. For this reason measurements were made only after increases in pressure, minor fluctuations in the apparatus of course being tolerated.

Electrical measurements were made on a Brown Electro-Measurement Corporation Universal Impedance Bridge, Model 250-C, using a General Radio Corporation null detector, type 1231B, for the balance. The bridge was isolated from the 1000-cps generator by a General Radio Corporation transformer, type 578-A. The absolute accuracy of the bridge readings was 0.5 percent. However for these experiments the important accuracy of the bridge was that of duplication, namely, 0.02 percent. This figure was established by checking the bridge against a resistance box on several occasions. Capacitance was balanced out with a 500$\mu\mu$f variable air condenser in shunt. No correction was made for this capacitance since again the important consideration was duplication.

Each run on one filling of the cell lasted from 2 to 4 days. In that tine 3 or 4 points were set on an isothermal curve as a function of pressure. Time for equilibrium after a pressure change varied from 7 to 24 hours. In general the higher the pressure, the longer the time to reach equilibrium. Readings of the bridge were made as a function of time until a constant value of the resistance was obtained. No disturbance of the system by the readings was noticed. No signs were found during measurements of an actual transition proceeding.

EXPERIMENTAL RESULTS

Runs were made at four temperatures, 29.0, 38.1, 52.6, and 77.1°C. Two runs were made with aragonite in the cell at 103°C and 2900 kg/cm², but no signs of reaching an equilibrium were observed in 26 hours on

[13] W. L. de Keyser and L. Dequeldre, Bull. soc. chim. Belges **59**, 40 (1950).

either and the runs were abandoned. It is not known whether this lack of equilibrium is to be attributed to the slowness of solution of the aragonite, to some other factor, or to the cell itself, which had not been seasoned to that temperature.

The data were corrected for minor temperature deviations, plotted as the reciprocals of the measured resistance, fitted to smooth curves, and then the differences between the calcite curve and the aragonite curve for the same temperature were noted at several pressures. These differences are plotted as in Fig. 2, and the intersection of the isothermal curve with the zero axis gives the equilibrium pressure. Table II gives the results of this plot. R_A is the resistance of the cell containing H_2O and aragonite, R_C that of H_2O and calcite.

In order to obtain other thermodynamic quantities, the data from Table II were fitted by the method of least squares to the following equation:

$$P=17.864T-1405 \quad (P \text{ in kg/cm}^2,\ T \text{ in °K}). \qquad (4)$$

The fit is accurate to 2 percent. In Table III and Table IV are collected the thermal data which may be derived from this equilibrium curve ($\Delta H=H_c-H_a$ etc.). The

TABLE III. Derived thermal data along the equilibrium curve.

T°K	$\Delta H(P, T)$ cal/mole	$\Delta S(P, T)$ cal/mole	ΔC_p cal/mole
302.1	+375	+1.24	−0.13
311.2	385	1.24	−0.13
325.6	401	1.23	−0.17
350.2	426	1.22	−0.19

Clapeyron relation (5)

$$\frac{dP}{dT}=\frac{\Delta H}{T\Delta V}=\frac{\Delta S}{\Delta V}, \qquad (5)$$

was used to obtain $\Delta H(P, T)$ and $\Delta S(P, T)$. In Table IV, $\Delta G(1, T)$ was computed from Eq. (3) using the values for the thermal expansion and compressibility, referred to previously. These values for $\Delta G(1, T)$ together with Kobayashi's[2,3] values for $\Delta G(1, T)-\Delta G(1, 0)$ give the next column $\Delta G(1, 0)$. ΔC_p was obtained from Eq. (6) and finally $\Delta H(1, T)$ was derived from Eq. (7),

$$\Delta C_p(P, T)=\frac{d(\Delta H)}{dT}-\Delta S(P, T), \qquad (6)$$

$$\Delta H(P, T)-\Delta H(1, T)$$
$$=-\Delta G(1, T)+T\Delta S(P, T)-T\Delta S(1, T). \qquad (7)$$

DISCUSSION AND CONCLUSIONS

For all practical purposes $\Delta G(1, 0)=\Delta G(0, 0)$. From Table IV, the average $\Delta G\langle(0, 0)_{Av}\rangle=\Delta G_0=+22.6$ cal/mole, with an accuracy of ±3 cal/mole. This value,

TABLE IV. Derived thermal data at 1 kg/cm².

T°K	$\Delta G(1, T)$ cal/mole	$\Delta G(1, 0)$	$\Delta H(1, T)$ cal/mole
302.1	−278	+21.6	+66
311.2	−288	21.8	68
325.6	−305	21.9	73
350.2	−331	25.2	80

together with Kobayashi's[2,3] free energy data, leads to a value of -272.5 ± 3 cal/mole for $\Delta G(1, 298.1)$. This value is in excellent agreement with Kelley and Anderson's[4] older value of $\Delta G(1298.1)=-273$ cal/mole. It is in fair agreement with Kobayashi's[2,3] value of -311 ± 23 cal/mole, the most recent determination by calorimetric means. Other older values of $\Delta G(1, 298.1)$ are discussed by these authors. The only disagreement with Kobayashi's[2,3] value is in the determination of ΔG_0. Again in the case of $\Delta H(1, T)$, the only disagreement with Kobayashi's[2,3] value is in the determination of ΔG_0. The negative sign for ΔC_p signifies that the heat capacities of the two forms have interchanged in magnitude, since at room pressure, calcite has the higher heat capacity. The increase in $\Delta S(P, T)$ from $\Delta S(1, T)$, namely, about 0.1 eu, is of the right order of magnitude to satisfy Maxwell's equation $\partial S/\partial P)_T=-aV$, where a is the coefficient of thermal expansion.

Using the value $\Delta G_0=+22.6$ cal/mole and Anderson's free energy data, we can extrapolate the measured curve of equilibrium as shown in Fig. 3. The other phases of $CaCO_3$ in the diagram are the other two forms of calcite observed by Bridgman.[14] Also indicated is the geothermal gradient for this range. Preliminary investigations on aragonite with a shearing apparatus as described by Bridgman[15] gave inconclusive results over the range up to 30 000 kg/cm². The best that can be said is that there are possibly two transitions at 30°C, one at about 20 000 kg/cm², the other at 26 000 kg/cm². Further investigation with more sensitive apparatus is needed at this point. For this reason these data have not been included.

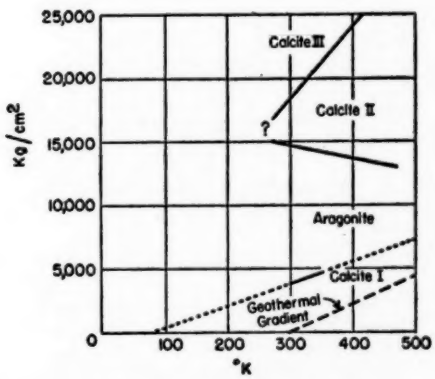

FIG. 3. Phase diagram of $CaCO_3$.

[14] P. W. Bridgman, Am. J. Sci., Fifth Ser. **237**, 7 (1939).
[15] P. W. Bridgman, Phys. Rev. **48**, 825 (1935).

It will be noted from Fig. 3 that the usually accepted values of the geothermal gradient (e.g., Yoder[16]) lie completely in the calcite$_I$ phase of $CaCO_3$ with the possible exception that if the temperature of disassociation is raised sufficiently high by pressure, calcite$_{II}$ or aragonite may become stable. Thus probably, except for peculiar local conditions of high hydrostatic pressure and moderate temperatures, the only known form of $CaCO_3$ which is stable under natural geologic conditions is that of calcite. This fact has been widely accepted for many years, but this is the first time that a physico-chemical proof has been offered. In order to explain the occurrence of aragonite, both organic and inorganic, the conditions for metastable precipitation must be considered rather than those of equilibrium. Backström's[17] hypothesis that aragonite has a low-temperature stability field seems to be verified since the extrapolated curve intersects the $P=0$ axis at about 80°K. The actual stability field (if any) of vaterite, the third atmospheric pressure form of $CaCO_3$, is still undetermined.

The experimental method of determining $\Delta G(1, 298.1)$ seems to have certain advantages. Since the measurement of the conductivity of a solution can be considerably refined, the value of this standard free energy change for polymorphic forms may be obtained quite precisely as compared to that obtained by calorimetric methods. The value for $\Delta G(1, 298.1)$ is less dependent on pressure errors than on heat measurements, while the values for compressibility and thermal expansion can be made very precise. The main uncertainty lies in the frequent lack of determination of compressibility and thermal expansion, and in the case of most minerals the variation in reported densities creates a major difficulty. Of course the method is not suited for any transitions which are at all rapid. These are capable of being directly determined.

The use of a cell constructed from Teflon for conductivity work seems quite feasible, at least for moderate temperatures. The temperature limits of this type of cell have not as yet been explored. The work of calibrating the cell to determine conductivities and solubilities at high pressure is at present in progress. The intention is to explore the possibilities of obtaining the solubilities of silicates at high pressures. There is data in existence at present from Zisman[18] by which the cell could be calibrated, but it has been decided that an independent check would be desirable.

The author wishes to express his thanks to Doctor H. Ramberg, Doctor A. W. Lawson, and Doctor J. R. Goldsmith for their encouragement, suggestive questions, and constructive criticism throughout the course of this research. Doctor N. H. Nachtrieb and Doctor A. H. Smith made many helpful suggestions. N. D. Nachtrieb constructed the cell and did much other machine work. Thanks are due the Geology Department for its grant of the R. D. Salisbury Memorial Fellowship for the course of this work, and to the staff of the Institute for the Study of Metals where the work was performed for the interest they have shown.

This work was supported in part by funds from the U. S. Office of Naval Research.

[16] H. S. Yoder, Jr., Trans. Am. Geophys. Union **31**, 827 (1950).
[17] H. L. J. Backström, Z. physik. Chem. **97**, 179 (1921).
[18] W. A. Zisman, Phys. Rev. **39**, 151 (1932).

Cooperative Orientation in Solutions. The Accuracy of the Quasi-Chemical Approximation

J. A. BARKER
Division of Industrial Chemistry, Commonwealth Scientific and Industrial Research Organisation, Melbourne, Australia

(Received March 12, 1953)

The accuracy of the quasi-chemical approximation used in the theoretical treatment of a lattice model for solutions in which cooperative orientation of molecules takes place is examined. The quasi-chemical method of Guggenheim and the modified quasi-chemical method of Kikuchi are used to find higher approximations. It is found that the quasi-chemical approximation for pairs is satisfactory for lattices which are not close-packed, though it may be seriously in error for closepacked lattices.

I. INTRODUCTION

IN a previous publication[1] the author proposed a simple lattice model for solutions in which cooperative orientation of molecules takes place, such as solutions of associated liquids. In this model the continuous range of possible orientations of a molecule was replaced by a number of discrete orientations such that a number of "contact points" on the molecule were in contact with neighboring molecules. This is exactly analogous to the procedure in the lattice theory of nonpolar solutions which limits the translational possibilities to a discrete set by constraining the molecules to lie on lattice sites. Thus the new model is a straightforward extension of the lattice model to deal with orientation-dependent forces.

A theoretical treatment of the model based on the quasi-chemical approximation for pairs of lattice sites was given. This theory has been applied with some success to interpret the thermodynamic properties of solutions containing alcohols,[1,2] and to give a qualitative interpretation of the occurrence of both upper and lower critical solution temperatures in some liquid systems.[3] It therefore appeared desirable to examine the accuracy of the quasi-chemical approximation on which the theory was based.

A further reason for this examination was that a study of the two systems ethanol+carbon tetrachloride and methanol+carbon tetrachloride indicated[2] that the effective hydrogen bond strengths were different in the two systems. Since this is unlikely to be the case, a weakness was suggested in some aspect of the model, or of the theoretical treatment, or of the experimental results. It will be shown in this paper that the quasi-chemical approximation is not seriously in error.

In the theory of regular mixtures the accuracy of the quasi-chemical approximation has been tested by extending the method to consider larger groups of sites than pairs,[4] and has been found to be satisfactory. However in regular mixtures the deviations from randomness are always small, otherwise a second phase separates. The very large deviations from randomness of *orientation* which can occur in the type of solution considered here make necessary a fresh examination of the question.

II. THEORETICAL CONSIDERATIONS

The theoretical results derived previously[1] were based on the quasi-chemical approximation for pairs of lattice sites. There are two methods which can be used to give more accurate results, each of which may be regarded as a generalization of the quasi-chemical approximation, allowing consideration of larger groups of sites than pairs. The first of these, originally proposed by Guggenheim,[5] will be called the quasi-chemical method (Q), while the second, originally proposed by Kikuchi,[6] will be called the modified quasi-chemical method ($M-Q$). The work in this paper will be based on a discussion of these two methods given by Barker.[7]

For present purposes the idea of configuration of a set of lattice sites must be generalized to mean, "particular arrangement of molecules of definite kinds, *each in a definite orientation*, on the lattice sites of the set." Once the generalization implied by the italicized phrase

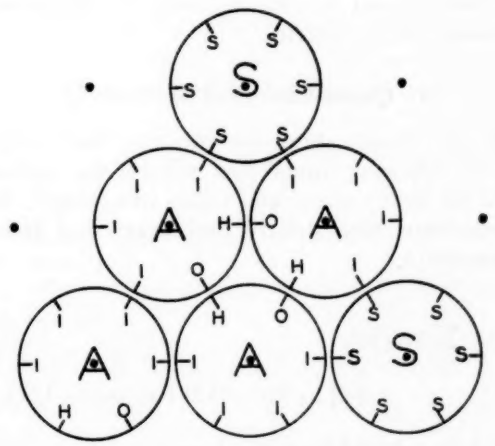

FIG. 1. The triangular lattice model.

[1] J. A. Barker, J. Chem. Phys. **20**, 1526 (1952).
[2] Barker, Brown, and Smith, on Solutions of Non-electrolytes, Disc. Faraday Soc., 1953.
[3] J. A. Barker and W. Fock, on Solutions of Non-electrolytes, Disc. Faraday Soc., 1953.
[4] E. A. Guggenheim, *Mixtures* (Oxford University Press, London, 1952).
[5] E. A. Guggenheim, Proc. Roy. Soc. (London) **A183**, 213 (1944).
[6] R. Kikuchi, Phys. Rev. **81**, 988 (1951).
[7] J. A. Barker, Proc. Roy. Soc. (London) **A216**, 45 (1953).

TABLE I.

Configuration of triangle	$H.O$ $O\ \ H$ $.H\ O.$	$I.H$ $I\ \ O$ $.O\ H.$	$I.O$ $I\ \ H$ $.I\ I.$	$I.I$ $I\ \ I$ $.I\ I.$	$O.I$ $H\ \ S$ $.I\ S.$	$I.I$ $I\ \ S$ $.I\ S.$	$S.S$ $I\ \ S$ $.I\ S.$	$S.S$ $S\ \ S$ $.S\ S.$
Fraction of triangles having configuration ($\gamma_i z_i$)	$2z_1$	$6z_2$	$36z_3$	$216z_4$	$72z_5$	$1296z_6$	$2592z_7$	$1728z_8$
Configuration of pair	$H-O$	$I-I$	$I-S$	$S-S$				
Fraction of pairs having configuration ($\beta_i y_i$)	$8y_1$	$64y_2$	$192y_3$	$144y_4$				
Configuration of lattice site	H	O	I	S				
Fraction of lattice sites having configuration	$2\times(x_A/12)$	$2\times(x_A/12)$	$8\times(x_A/12)$	$12\times(x_S/12)$				

is made, the theory of reference 7 may be applied without change.

The theory will be illustrated with reference to a particular model shown in Fig. 1, in which molecules of two kinds, A and S, are distributed on a two-dimensional triangular lattice. This model is related to a model used for solutions of alcohols in nonpolar solvents.[1] To reduce the number of configurations to manageable proportions, we will suppose that the interaction energy U_{HO} between H and O contact points is very strongly negative. It can be seen on both physical and mathematical grounds that, in the limit as $U_{HO}\rightarrow-\infty$, one can neglect all configurations in which H contact points occur unpaired with O contact points, or *vice versa*. The relation of this limiting case with the case of finite U_{HO} is discussed below. We will further suppose that the interaction energies for contacts other than $H-O$ contacts are zero.

The possible configurations of triangles, pairs, and single lattice points are shown in Table I. In counting configurations we have assumed that the molecules can turn over on the lattice, so that a single molecule has 12 possible orientations.

If the distribution of triangles among the possible configurations is known, the distributions of pairs and lattice sites among their configurations can be calculated. In fact one finds the following relations:

$$\begin{aligned}
2x_A/12&= z_1+2z_2+ 6z_3 &&+12z_5\\
8x_A/12&= 2z_2+24z_3+216z_4+24z_5+864z_6+ 864z_7 &&\qquad(1)\\
12x_S/12&= 24z_5+432z_6+1728z_7+1728z_8,
\end{aligned}$$

$$\begin{aligned}
8y_1&=2z_1+4z_2+12z_3 &&+24z_5\\
64y_2&= 2z_2+24z_3+216z_4 &&+432z_6\\
192y_3&= 48z_5+864z_6+1728z_7 &&\qquad(2)\\
144y_3&= 864z_7+1728z_8.
\end{aligned}$$

We now set out the two methods for calculating the free energy of the system.

(a) Quasi-Chemical Method (Q)

For the entropy, heat content, and free energy we take the following forms[7] (we will use the symbols H and G, for heat content and Gibbs free energy, though the equations give strictly the energy and Helmoltz free energy):

$$S/k=-\sum_{i=1}^{8}\gamma_i z_i \ln z_i + 2[x_A \ln(x_A/12)+x_S \ln(x_S/12)], \quad (3)$$

$$H=3(2z_1+4z_2+12z_3+24z_5)U_{HO}, \quad (4)$$

$$G=H-TS. \quad (5)$$

Using the method of undetermined multipliers, one seeks the values of z_1, z_2, etc., which minimize the free energy subject to Eq. (1). The results are

$$\begin{aligned}
&z_1=r^3, \quad z_2=r^2s, \quad z_3=rs^2, \quad z_4=s^3,\\
&z_5=rsl, \quad z_6=s^2l, \quad z_7=sl^2, \quad z_8=l^3,
\end{aligned} \quad (6)$$

where r, s, l are to be determined by substituting from (6) in (1) and solving the resulting equations for r, s, and l. By substituting from (6) in (3), (4), and (5) the free energy, heat content, and entropy of the system can then be determined.

If $-U_{HO}$ has a finite value, rather than being infinitely large, similar equations are found, but the equations to determine r, s, l contain more terms due to the previously neglected configurations.

(b) Modified Quasi-Chemical Method (M-Q)

For the entropy, heat content, and free energy we take the forms[7]

$$S/k=-2\sum_{i=1}^{8}\gamma_i z_i \ln z_i+3\sum_{i=1}^{4}\beta_i y_i \ln y_i - [x_A \ln(x_A/12)+x_S \ln(x_S/12)], \quad (7)$$

$$H=24y_1U_{HO}, \tag{8}$$

$$G=H-TS. \tag{9}$$

We now seek values of y_i, z_i which minimize the free energy subject to both (1) and (2). The results are

$$\begin{aligned} &y_2=u^2x^2, \quad y_3=uvy^2, \quad y_4=v^2z^2 \\ &z_1=w^3, \quad z_2=w^2x, \quad z_3=wx^2, \quad z_4=x^3 \\ &z_5=wy^2, \quad z_6=xy^2, \quad z_7=y^2z, \quad z_8=z^3, \end{aligned} \tag{10}$$

where u, v, w, x, y, z are to be determined by substituting from (10) in (1) and (2) and solving the resulting equations. Substitution in (7), (8), (9) then gives values for the free energy, heat content, and entropy of the system.

The equations for the $M-Q$ method when $-U_{HO}$ is not very large are very complicated and will not be discussed here.

We have illustrated both Q and $M-Q$ methods for a model in which each molecule occupies one lattice site. If either molecule (or both) occupies more than one lattice site the same method can be used, the only differences being in the table corresponding to Table I and the formulas corresponding to Eqs. (1), (2).

The above formulas for the limiting case with $-U_{HO}$ very large must break down for very low concentrations of the component A, for the $H-O$ contacts must then be broken, and the neglected configurations must assume overriding importance. Fortunately one can immediately write down a formula for the chemical potential in this case, *viz.*,

$$\mu_A=RT[\ln x_A-\ln 12], \quad x_A\ll 1, \tag{11}$$

in which the term $-RT\ln 12$ is due to the fact that each molecule has 12 orientations.

Results analogous to those above can be derived for any desired model. In order to obtain numerical results, it is necessary to solve rather complicated sets of simultaneous equations of high degree. Standard numerical methods were used to find the results used below.

Most of the numerical results will be given in terms of excess chemical potentials, $\mu_A{}^E$ and $\mu_S{}^E$, excess free energy of mixing $G_x{}^E$, and heat of mixing $H_x{}^M$. The derivation of these quantities from the results already given is straightforward.

TABLE II. Thermodynamic functions for triangular lattice model, equimolar mixture, calculated by pairs approximation for several values of $\eta=\exp(-U_{HO}/kT)$.

η	$\mu_A{}^E/RT$	$\mu_S{}^E/RT$	$G_x{}^E/RT$	$H_x{}^M/RT$	$S_x{}^E/R$
1	0	0	0	0	0
10	0.124	0.177	0.150	0.176	+0.0262
100	0.205	0.385	0.295	0.205	−0.0896
1000	0.233	0.490	0.361	0.117	−0.245
∞	0.247	0.547	0.397	0	−0.397

III. NUMERICAL RESULTS

(a) Triangular Lattice Model

Most of our calculations with higher approximations are based on the limiting case when $-U_{HO}$ is very large. It is therefore necessary to examine the status of this limiting case. We remark first, that it is just in this limiting case that the quasi-chemical approximation for pairs should be most in error, so that the limiting case should give us an upper limit to the error of that approximation. The way in which the limiting values are approached is shown in Table II (calculated with pairs approximation for the equimolar mixture). We note that the values of $G_x{}^E$ approach the limiting value monotonically, although $H_x{}^M$ and $S_x{}^E$ individually pass through a maximum before decreasing to the limiting value (which is zero for $H_x{}^M$). For $\eta=\exp(-U_{HO}/kT)=100$, $G_x{}^E$ has attained 74 percent of the limiting value and for $\eta=1000$ it has attained 91 percent of that value. For at least some solutions to which models of this type would apply (solutions containing alcohols) the appropriate values of η are in the region of several hundreds.[1,2] Thus the limiting case $-U_{HO}\to\infty$ is appropriate for comparing values given by different methods of approximation.

Thermodynamic functions for this limiting case, as calculated with different approximations, are shown in Table III. We note first that in regard to qualitative features, in particular the location of the maximum in the $G_x{}^E$ curve at values of x_A less than 0.5 and the change in sign of the excess entropy of mixing from

TABLE III. Thermodynamic functions for triangular lattice model in limiting case $-U_{HO}\to\infty$, as calculated by different approximations.

x_A	$\mu_A{}^E/RT$ Pair	Triangle, Q	Triangle, $M-Q$	$\mu_S{}^E/RT$ Pair	Triangle, Q	Triangle, $M-Q$	$G_x{}^E/RT$ Pair	Triangle, Q	Triangle, $M-Q$
0	$\frac{U_{HO}}{RT}-2.603$	$\frac{U_{HO}}{RT}-2.492$	$\frac{U_{HO}}{RT}-2.381$	0	0	0	0	0	0
0.125	1.354	1.130	···	0.128	0.0952	···	0.281	0.225	···
0.25	0.749	0.650	0.546	0.261	0.202	0.141	0.383	0.314	0.242
0.5	0.247	0.226	0.206	0.547	0.444	0.338	0.397	0.335	0.272
0.75	0.0521	0.0502	0.0488	0.863	0.732	0.597	0.255	0.221	0.186
0.875	0.0123	0.0121	···	1.035	0.896	···	0.140	0.123	···
1.0	0	0	0	1.216	1.077	0.937	0	0	0

TABLE IV. Triangle (Q) results for $\eta=500$, compared with pair results for $\eta=500$ and for $\eta=675.4$.

	x_A	μ_A^E/RT	μ_S^E/RT	G_x^E/RT	H_x^M/RT	S_x^E/R
Triangle (Q)	0.0	3.873	0.0	0.0	0.0	0.0
$\eta=500$	0.5	0.211	0.406	0.308	0.0859	−0.223
	1.0	0.0	0.995	0.0	0.0	0.0
Pair	0.0	3.787	0.0	0.0	0.0	0.0
$\eta=500$	0.5	0.228	0.468	0.348	0.144	−0.204
	1.0	0.0	1.088	0.0	0.0	0.0
Pair	0.0	4.064	0.0	0.0	0.0	0.0
$\eta=675.4$	0.5	0.230	0.478	0.354	0.132	−0.223
	1.0	0.0	1.105	0.0	0.0	0.0

negative values for larger x_A values to positive values for very small x_A, the different approximations are in agreement. Quantitatively, however, the differences are more marked. Thus if we adopt the triangle ($M-Q$) values as standard and consider the value of G_x^E for the equimolar mixture, the triangle (Q) value is 23 percent high, and the pair value is 46 percent high. Since the triangle ($M-Q$) values are probable fairly close to the correct values,[7] this gives an estimate of the error in the pair approximation. We will find, however, that the situation is not nearly so serious for lattices which are not closepacked.

Results for one finite value of η ($\eta=500$) have been calculated with the triangle (Q) approximation, and are shown in Table IV.

For comparison we give also values calculated with the pair approximation for the same value of η, and also for $\eta=675.4$, this latter value being chosen to give exactly the same value of the excess entropy of mixing for the equimolar mixture. The last comparison is of interest since in applications to experimental data[1,2] the value of the excess entropy of mixing for the equimolar mixture has been used to determine the interaction energy U_{HO}. In the present case, the values of U_{HO} derived using pair and triangle (Q) approximations would differ by about 5 percent (note that $-U_{HO}$ is proportional to $\ln\eta$).

(b) Simple Cubic Lattice Model

As an example of a more open lattice, we have made calculations for a model in which molecules of type A having one H, one O, and four I contact points, and of type S having six S contact points, are arranged on a simple cubic lattice. The H and O contact points on an A molecule are assumed to be adjacent to each other (so that, if A is the center of the molecule, the angle HAO is a right angle). As basic group of lattice sites the square of 4 sites was used. The $M-Q$ method was impracticably complicated, and the Q method was used, in the limiting case $-U_{HO}\to\infty$. The thermodynamic functions are shown in Table V, with the pair values for comparison. The pair values are identical with those for the triangular lattice model, since both lattices have the coordination number 6.

TABLE V. Thermodynamic functions for simple cubic lattice model, limiting case $-U_{HO}\to\infty$.

x_A	μ_A^E/RT pair	μ_A^E/RT square (Q)	μ_S^E/RT pair	μ_S^E/RT square (Q)	G_x^E/RT pair	G_x^E/RT square (Q)
0.0	$\frac{U_{HO}}{RT}-2.603$	$\frac{U_{HO}}{RT}-2.600$	0.0	0.0	0.0	0.0
0.5	0.2469	0.2474	0.5470	0.5437	0.3970	0.3956
1.0	0.0	0.0	1.216	1.217	0.0	0.0

The largest difference between pair and square (Q) values amounts to about ½ percent. We have no way of telling what results an *exact* calculation of thermodynamic functions for this model would give. However the calculations we have made are sufficient to indicate fairly definitely that the total error in thermodynamic functions calculated by the pairs approximation can hardly exceed a few percent. For a still more open lattice such as the diamond lattice, on which the smallest closed group is a hexagon, compared with square and triangle for simple cubic and triangular lattices, the error in the pairs approximation is probably completely negligible.

IV. CONCLUSIONS

It has been shown how the quasi-chemical method of Guggenheim and the modified quasi-chemical method of Kikuchi may be used to calculate higher approximations to thermodynamic functions for a lattice model of solutions in which cooperative orientation of molecules takes place. The application of these methods involves the solution of sets of simultaneous algebraic equations of high degree, and the methods are too complicated for use in the interpretation of experimental data. However sufficient numerical results have been obtained to show that the quasi-chemical pairs approximation, which was used in the original treatment of the model is sufficiently accurate for lattices which are not closepacked, though it may be very seriously in error for close-packed lattices.

Adsorption on Proteins and Interactions between Protein Molecules in Solution

TERRELL L. HILL*
Naval Medical Research Institute, Bethesda, Maryland
(Received April 28, 1953)

A theoretical approach to the problem of the interconnection between adsorption on proteins and interactions between protein molecules in solution is outlined. As an illustration, the second virial coefficient and related quantities are discussed. A more detailed account of this work will be published in the *Annals of the New York Academy of Sciences.*

THE standard treatment[1] of the adsorption of ions or molecules on proteins does not include the interconnection between adsorption and protein-protein interactions. We outline here a theoretical approach to this problem which should have applications, for example, to the nature of the average force between protein molecules, to the effect of protein concentration on adsorption isotherms and titration curves and to the influence of bound ions or molecules, or *p*H, on osmotic pressure, aggregation, solubility, etc., of proteins. The theory also applies to "adsorbent" molecules other than proteins. A more detailed and general account of this work will be published in the *Annals of the New York Academy of Sciences.*

Consider M spherically symmetrical protein molecules (each with B sites for adsorption, not necessarily all equivalent) in a volume V, m_s of which have s adsorbate molecules bound. Let q_s be the partition function of the s adsorbed molecules on a protein molecule. As a simple example[1,2] we might have

$$q_s=\frac{B!j^s}{s!(B-s)!}\exp(-\alpha s^2/B), \tag{1}$$

where j and α are functions of temperature. Let W be the potential of mean force between the M protein molecules (in the absence of other protein molecules[3]) for a given configuration. If we assume W is a sum of pair interactions $w(r)$, then $w(r)$ for any pair depends in general on the two s values. To indicate this, we shall use the notation $w_{ss'}(r)$. Then the partition function of the M protein molecules, with a total of N adsorbed molecules, is

$$Q(M,N,V,T)=\sum_{\mathbf{m}}\Big(\prod_{s=0}^{B}q_s^{m_s}\Big)\Bigg(\Big[\prod_{s=0}^{B}\frac{f_s^{m_s}}{m_s!}\Big]\int\cdots\int_V \times\exp[-W(\{\mathbf{m}\})/kT]d\{\mathbf{m}\}\Bigg), \tag{2}$$

where the sum is over all sets $\mathbf{m}=m_0, m_1, \cdots m_B$ consistent with $\sum m_s=M$ and $\sum sm_s=N$, f_s includes the internal partition function of an s protein molecule and the factor $(2\pi M_s kT/h^2)^{\frac{3}{2}}$, and $\{\mathbf{m}\}$ refers to the translational coordinates of the set $\mathbf{m}$. We employ the McMillan-Mayer notation[3] from this point on.

For the expansions below, it is much more convenient to use a grand ensemble, open with respect to both N and M. The grand partition function is

$$\Xi(V,T,\mu,\mu_a)=\sum_{M=0}^{\infty}\sum_{N=0}^{MB}\times\exp[(M\mu/kT)+(N\mu_a/kT)]Q(M,N,V,T)$$
$$=\sum_{\mathbf{m}=0}^{\infty}\Big[\prod_{s=0}^{B}\frac{(F_s z x^s)^{m_s}}{m_s!}\Big]\int\cdots\int_V \times\exp[-W(\{\mathbf{m}\})/kT]d\{\mathbf{m}\}, \tag{3}$$

where μ and μ_a are the protein and adsorbate chemical potentials, respectively, $F_s=q_s f_s$, $z=\exp(\mu/kT)$ and $x=\exp(\mu_a/kT)$.

The number of adsorbate molecules bound per protein molecule, on the average, is $\bar{N}/\bar{M}$. This ratio may be obtained from

$$\bar{N}=x(\partial\ln\Xi/\partial x)_{z,V,T}$$
$$=(1/\Xi)\sum_{\mathbf{m}=0}^{\infty}\Big(\sum_{s=0}^{B}sm_s\Big)\Big[\prod_{s=0}^{B}\frac{(F_s z x^s)^{m_s}}{m_s!}\Big]\int\cdots\int_V \times\exp[-W(\{\mathbf{m}\})/kT]d\{\mathbf{m}\} \tag{4}$$

and

$$\bar{M}=z(\partial\ln\Xi/\partial z)_{x,V,T}$$
$$=(1/\Xi)\sum_{\mathbf{m}=0}^{\infty}\Big(\sum_{s=0}^{B}m_s\Big)\Big[\prod_{s=0}^{B}\frac{(F_s z x^s)^{m_s}}{m_s!}\Big]\int\cdots\int_V \times\exp[-W(\{\mathbf{m}\})/kT]d\{\mathbf{m}\}. \tag{5}$$

The protein osmotic pressure π is given by Eq. (3) and

$$\pi V=kT\ln\Xi. \tag{6}$$

As an illustration of these general equations, let us consider the second virial coefficient and related quanti-

* Fellow of the John Simon Guggenheim Memorial Foundation, Department of Chemistry, Yale University, 1952–1953.

[1] See, for example, I. M. Klotz in *Modern Trends in Physiology and Biochemistry* (Academic Press, New York, 1952), edited by E. S. G. Barron. Also, G. Scatchard, Ann. N. Y. Acad. Sci. **51**, 660 (1949).

[2] T. L. Hill, J. Phys. Chem. **57**, 324 (1953), Eq. (7).

[3] W. G. McMillan and J. E. Mayer, J. Chem. Phys. **13**, 276 (1945).

ties. By regarding Eqs. (3), (4), and (5) as expansions in powers of z, we find easily

$$\Xi=1+zVB_1+\tfrac{1}{2}z_2VB_2+\cdots, \tag{7}$$

$$\rho=\bar{M}/V=zB_1+z^2(B_2-VB_1^2)+\cdots, \tag{8}$$

$$z=\frac{\rho}{B_1}-\frac{\rho^2}{B_1^3}(B_2-VB_1^2)+\cdots, \tag{9}$$

$$\frac{\bar{N}}{\bar{M}}=\frac{A_1}{B_1}\left[1+\frac{\rho}{B_1}\left(\frac{1}{2}\frac{A_2}{A_1}-\frac{B_2}{B_1}\right)+\cdots\right], \tag{10}$$

$$\frac{\pi}{kT}=\rho-\frac{\rho^2}{2B_1^2}(B_2-VB_1^2)+\cdots, \tag{11}$$

where

$$A_1=\sum_{s=0}^{B} sF_sx^s \tag{12}$$

$$A_2=\sum_{s,s'=0}^{B}(s+s')(F_sx^s)(F_{s'}x^{s'}) \times\int_V \exp[-w_{ss'}(r)/kT]4\pi r^2dr, \tag{13}$$

$$B_1=\sum_{s=0}^{B} F_sx^s, \tag{14}$$

$$B_2=\sum_{s,s'=0}^{B}(F_sx^s)(F_{s'}x^{s'}) \times\int_V \exp[-w_{ss'}(r)/kT]4\pi r^2dr. \tag{15}$$

In Eq. (10) the usual expression, A_1/B_1, for $\bar{N}/\bar{M}$ is obtained in the limit $\rho\to 0$, or if $w_{ss'}(r)$ is the same for all s, s'. Otherwise, Eq. (10) gives the dependence of the adsorption isotherm on protein concentration ρ for small ρ. According to Eq. (11) the second virial coefficient is

$$\beta=-\frac{1}{2}\frac{\sum_{s,s'=0}^{B}[s,s'](F_sx^s)(F_{s'}x^{s'})}{\left(\sum_{s=0}^{B}F_sx^s\right)^2}, \tag{16}$$

where

$$[s,s']=\int_0^\infty\{\exp[-w_{ss'}(r)/kT]-1\}4\pi r^2dr. \tag{17}$$

Equation (16) shows how β depends on x, which is proportional to the activity of adsorbate in solution.[4]

[4] We are neglecting here, for simplicity, interactions between adsorbate molecules and protein molecules in solution (other than actual binding).

β can be expanded in powers of x from Eq. (16):

$$-2\beta=[0,0]+2x\frac{F_1}{F_0}([0,1]-[0,0]) +x^2\left[\left(\frac{F_1}{F_0}\right)^2([1,1]+3[0,0]-4[0,1]) +2\frac{F_2}{F_0}([0,2]-[0,0])\right]+\cdots \tag{18}$$

β reduces to $-[0,0]/2$ if $x\to 0$ or if $w_{ss'}(r)$ is the same for all s, s'.

Generic distribution functions $\rho^{(\mathbf{n})}$ for a set of protein molecules $\mathbf{n}=n_0, n_1, \cdots, n_B$ in an open system can be expressed in terms of W as follows:

$$\rho^{(\mathbf{n})}=\frac{1}{\Xi}\sum_{\mathbf{m}=\mathbf{n}}^{\infty}\left[\prod_{s=0}^{B}\frac{(F_szx^s)^{m_s}}{m_s!}\right]\int\cdots\int_V \times\exp[-W(\{\mathbf{m}\})/kT]d\{\mathbf{m}-\mathbf{n}\}. \tag{19}$$

The distribution function of real interest, however, is $\rho^{(n)}$ for $n=n_0+n_1+\cdots+n_B$ protein molecules *irrespective* of s values, given by

$$\rho^{(n)}=\sum_{\mathbf{n}}\frac{n!}{n_0!\cdots n_B!}\rho^{(\mathbf{n})}, \tag{20}$$

where the sum is over sets $\mathbf{n}$ restricted by $\sum n_s=n$. The correlation function $g^{(n)}$ may then be defined by $g^{(n)}=\rho^{(n)}/\rho^n$. The simplest example is $g^{(2)}$, the radial distribution function, in the limit $\rho\to 0$. One finds from Eqs. (19) and (20),

$$g_{\rho\to 0}{}^{(2)}(r)=\frac{\sum_{s,s'=0}^{B}\exp[-w_{ss'}(r)/kT](F_sx^s)(F_{s'}x^{s'})}{\left(\sum_{s=0}^{B}F_sx^s\right)^2}, \tag{21}$$

so that

$$\beta=-\tfrac{1}{2}\int_0^\infty[g_{\rho\to 0}{}^{(2)}(r)-1]4\pi r^2dr. \tag{22}$$

If we set $g^2(\rho\to 0)$ in Eq. (21) equal to $\exp(-w^0/kT)$, it is easy to see that $w^0(r)$ is then the actual effective potential of mean force between two protein molecules, the "mean" force including here proper averaging with respect to s and s'.

Letters to the Editor

THIS section will accept reports of new work, provided these are terse and contain few figures, and especially few half-tone cuts. The Editorial Board will not hold itself responsible for opinions expressed by the correspondents. Contributions to this section should not exceed 600 words in length and must reach the office of the Editor not later than the 15th of the second month preceding that of the issue in which the Letter is to appear. No proof will be sent to the authors. A publication charge of $15.00 per Letter is made which, when honored, will entitle the Institution to 100 free reprints.

Some New Data on the $NO-N_2O_5$ Reaction*†

GEORGE R. COWAN, DAVID ROTENBERG, ARTHUR DOWNIE, BRYCE CRAWFORD, JR., AND R. A. OGG, JR.
School of Chemistry, University of Minnesota, Minneapolis 14, Minnesota, and Department of Chemistry, Stanford University, Stanford, California
(Received April 22, 1953)

WE HAVE made some preliminary studies on the reaction

$$NO+N_2O_5\rightarrow 3NO_2.$$

The reaction was investigated by Smith and Daniels,[1] who proposed a suitable mechanism. Ogg[2] incorporated these elementary steps in a mechanism which simultaneously accounted for the decomposition of N_2O_5. A further discussion of the mechanism in relation to some other reaction systems has been given by Johnston.[3] Ogg *et al.* attempted a study of the reaction with a standard spectrometer and reported evidence supporting the proposed mechanism.[4] It seemed to us that this would be a good reaction to study with our fast-scanning spectrometer modified as described elsewhere.[5]

The assumed mechanism involves the following steps:

$$N_2O_5 \underset{k_2}{\overset{k_1}{\rightleftharpoons}} NO_2+NO_3,$$

$$NO+NO_3\xrightarrow{k_6}2NO_2.$$

The rate expression is

$$-d(N_2O_5)/dt=k_1(N_2O_5)/[1+k_2(NO_2)/k_6(NO)]. \quad (1)$$

k_1 and k_2 are dependent on the total pressure, while k_1/k_2 and k_6 are independent of the pressure. Johnston and co-workers[6,7] recently reported systematic studies of the initial rates, obtaining values of k_1 as a function of pressure; under the conditions they used they reported negligible inhibition by NO_2. Determination of the inhibition constant $k'=k_2/k_6$, and demonstration of its dependence on pressure, which should be identical with that of k_1, would provide a key piece of information in support of the mechanism. The present investigation was undertaken therefore with the aim of determining both k_1 and k' as functions of total pressure.

The rate constants can be obtained from a plot based on the rearranged differential equation

$$-dt/d\ln(N_2O_5)=(1/k_1)+(k'/k_1)(NO_2)/(NO). \quad (2)$$

This method involves taking the slopes from a plot of $\ln(N_2O_5)$ *versus* time t, a procedure which was not reliable. Therefore the rate expression was integrated. For the case of interest, $(N_2O_5)>(NO)$, the result is

$$y=-[k'/(1-3k')]w+k_1/(1-3k'), \quad (3)$$

where

$$y=\ln[(N_2O_5)_0/(N_2O_5)]/(t-t_0)$$

and

$$w=[(NO_2)_\infty/(N_2O_5)_\infty]\ln[(NO)_0(N_2O_5)/(NO)(N_2O_5)_0]/(t-t_0).$$

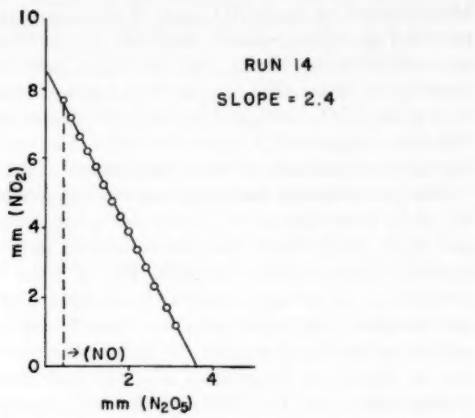

FIG. 1. Concentration (NO_2) *versus* (N_2O_5) during reaction; stoichiometry demands a straight line with a (negative) slope of 3.

A plot of y *versus* w (see Fig. 3) gives a straight-line plot. Denoting the intersection of the equation with the line $y=w/3$ by y_1, and the intercept on the w axis by w_0, we have

$$k_1=y_1, \quad k'=k_1/w_0.$$

The reaction was carried out in an 8-cm cell placed at the focal point in the fore optics. Since NO_2 causes the formation of an absorbing layer of nitrate on rocksalt, AgCl windows were used. They were butted firmly against the ground ends of the cell and cemented with a ring of Apiezon W wax on the outside. The reactants were admitted into the evacuated cell from two bulbs through opposed jet tips about 1 cm apart, by opening and closing the two stopcocks by one continuous motion of a linked crank. This method gave adequately fast mixing and filling of the reaction cell. The jet bulbs containing NO and N_2O_5, respectively, were pressurized to the same total pressure with dry nitrogen.

An examination of Eq. (3) shows that one of the species NO, NO_2, and N_2O_5 must be followed in time, and all three must simultaneously be obtained at one point in time. Use of the integrated expression also requires a low enough concentration of NO_2 so that association to N_2O_4 is small. NO_2 and N_2O_5 possess very strong infrared absorption bands which allow determination of pressures of a few mm Hg in an 8-cm cell, whereas the NO absorption band is about 100 times weaker. Therefore we used as excess of N_2O_5 over NO, in which case $(NO)=(N_2O_5)-(N_2O_5)_\infty$. After a survey of the various spectra involved we selected the strong N_2O_5 band at 1730 cm^{-1} and the strong NO_2 band at 1630 cm^{-1} for observation in time. With the alternate-exposure chopping method described elsewhere,[5] these two bands were observed together with good resolution at a scanning rate of 4.3 cps.

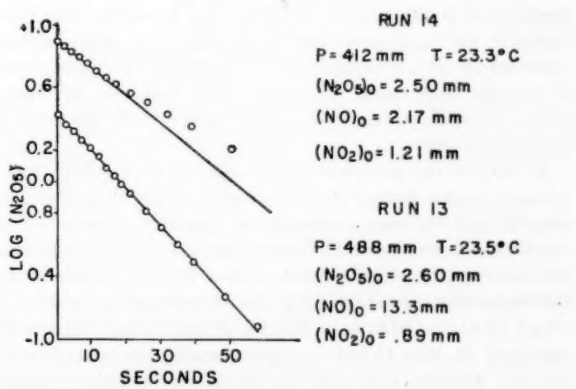

FIG. 2. Runs showing inhibition proportional to $(NO_2)/(NO)$. In Run 13 (lower plot), excess NO was used, and no inhibition appears. In Run 14 (upper plot), NO was in short supply; inhibition is shown by the deviation of the points.

Measurement of both NO_2 and N_2O_5 concentrations in time provided an internal check, simplified the problem of obtaining zero concentration blanks, and eliminated resetting of the spectrometer to obtain $(NO_2)_\infty$. The N_2O_5 band selected was overlain by a strong N_2O_4 band, and although the degree of association of NO_2 was always small, a correction to the observed optical density was required particularly in the later stages of the reaction.

The optical-density data were smoothed graphically, and about 10 points were selected for conversion to concentrations of NO_2 and N_2O_5, which were then plotted against each other. For the assumed stoichiometry a straight line of slope -3 should be obtained. In actual fact a good fit to a straight line was obtained, but the slope was found to be less than 3, about 2.4. This was attributed to a scale error in the N_2O_5 calibration curve due to loss of N_2O_5 in its preparation from NO and transfer to the cell during calibration. On this basis the N_2O_5 concentrations were scaled to give a slope of 3.

It was later discovered from spectral observation in a different region that considerable amounts of HNO_3 were present under conditions obtaining in the calibration runs where an excess of O_3 was used to prevent decomposition of N_2O_5. Since the chief source of H_2O was in the O_3 supply, the amount of HNO_3 present in the

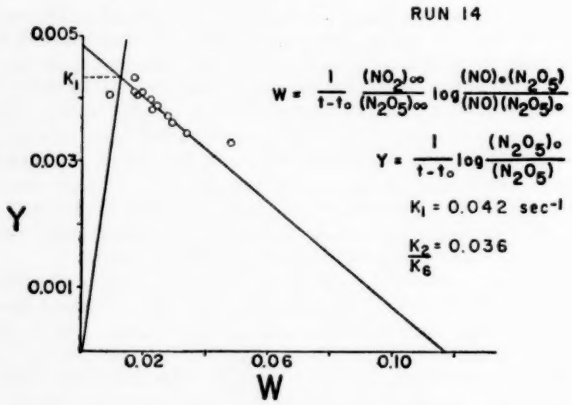

FIG. 3. Plot to determine rate constants of integrated rate expression in the form of Eq. (3).

reaction runs is believed to be small. Since HNO_3 has a strong band lying on top of the 1730 cm^{-1} N_2O_5 band, hydrolysis of N_2O_5 results in only a moderate decrease in absorption. This could account for an error in the N_2O_5 calibration but of course could also have caused mischief in the kinetic measurements. Steps were undertaken to insure absence of HNO_3 and to obtain spectroscopic evidence for its absence, the latter procedure being somewhat confused by the overlapping of the strong HNO_3 bands by strong or medium N_2O_5 bands. The work of repeating the rate measurements under these conditions was interrupted by the destruction of the laboratory.

In view of the uncertainty as to the effect of HNO_3, and also because of the damage to our records incurred in the fire, no attempt will be made to present all the data obtained. Typical results are illustrated in the figures. Figure 1 illustrates the straight line obtained by plotting (NO_2) *versus* (N_2O_5). Evidence for the inhibition effect is shown in Fig. 2 in the comparison of Run 14, in which $(N_2O_5) > (NO)$, with Run 13, in which a large excess of NO was used. In Run 13 indirect spectroscopic determination of NO was not possible, but, since inhibition here is clearly negligible, only k_1 can be determined. Figure 3 shows the plot for Run 14 of the variables occurring in the integrated equation (3), from which the rate constants are evaluated. It may be seen that k_1 is determined fairly accurately, whereas $k' = k_2/k_6$ is subject to considerable uncertainty. Sufficient runs had not been made to determine the pressure dependence of k'.

Some preliminary observations have been made on the isotopic exchange of N between NO_2 and N_2O_5, a reaction which can also provide confirmation of the dissociation of N_2O_5. The procedure involved mixing of enriched NO_2 containing 60 percent N^{15} with ordinary N_2O_5. The isotopic composition of NO_2 could be followed by observation of the 1630 cm^{-1} NO_2 band. The preliminary results indicated that the fast-scanning spectrometer is nicely suited to the study of isotopic exchange reactions.

* This work was supported by the U. S. Navy, Bureau of Ordnance, through contract with the University of Minnesota.
† This work was reported in part at the American Chemical Society Meeting held in Atlantic City, September 14 to 19, 1952.
[1] J. H. Smith and F. Daniels, J. Am. Chem. Soc. **69**, 1735 (1947).
[2] R. A. Ogg, Jr., J. Chem. Phys. **18**, 572 (1951).
[3] H. S. Johnston, J. Am. Chem. Soc. **73**, 4542 (1951).
[4] Ogg, Richardson, and Wilson, J. Chem. Phys. **18**, 573 (1950).
[5] Cowan, Vincent, and Crawford, J. Opt. Soc. Am. **43**, 710 (1953).
[6] R. L. Mills and H. S. Johnston, J. Am. Chem. Soc. **73**, 938 (1951).
[7] H. S. Johnston and R. L. Perrine, J. Am. Chem. Soc. **73**, 4782 (1951).

Application of a Fast-Scanning Infrared Spectrometer to a Kinetic Study of the $NO_2-C_2H_5OH$ Reaction*

RICHARD E. NIGHTINGALE, GEORGE R. COWAN, AND BRYCE CRAWFORD, JR.
School of Chemistry, University of Minnesota, Minneapolis 14, Minnesota
(Received April 22, 1953)

A FAST-SCANNING infrared spectrometer has been described recently[1] which was designed for the study of infrared spectra of propellant flames. This instrument was capable of scanning portions of the infrared spectrum at repetition rates of 10–20 spectra per second and so has found use in the study of fast gas reactions.[2]

The Naval Ordnance Research Laboratory in which this instrument was housed was destroyed by fire on February 9, 1953, and so it will be some months before work involving the fast-scanning spectrometer can be continued. We are therefore at this time reporting some preliminary studies concerning the application of this technique to the gas-phase reaction between nitrogen dioxide and ethyl alcohol.

This reaction has become of interest in connection with the study of the thermal decomposition of alkyl nitrates since Levy[3] discovered that ethyl nitrite is a major product in the decomposition of ethyl nitrate. A possible source of the ethyl nitrite is[4]

$$2NO_2+C_2H_5OH \rightarrow C_2H_5ONO+HNO_3. \quad (1)$$

Yoffe and Gray have reported on this reaction directly.[5] No attempt was made to study the kinetics as they report it to be very fast.

We have carried out this reaction in an 8-cm absorption cell to which AgCl windows were cemented with Apiezon W sealing compound. Rocksalt windows could not be used because of the reaction with NO_2 resulting in a nitrate coating on the windows which absorbs in the region of interest.

Rapid mixing of the reacting gases was accomplished in the same way as has been done with other studies on the oxides of nitrogen.[2] Two storage bulbs attached to the reaction cell were used to admit the gases through jet tips about 1 cm apart at the focal point of the fore optics.

During the course of the $NO_2-C_2H_5OH$ reaction we have scanned the region 1600 cm^{-1} to 1800 cm^{-1} which one would expect to be quite rich in absorption bands. With the evacuated cell in place, photographs of the spectrum displayed on an oscilloscope were taken, and the reacting gases were admitted through linked stopcocks. Spectra were taken at the rate of 4.3 per second for one minute. The rate of scan and method of recording were then

changed to medium scan, i.e., a rectified signal was put into a Sanborn recorder with the oscillator running at 16 seconds per revolution (8 seconds per spectrum). Finally the spectrum of the products was taken in the rocksalt region at slow scan (as a conventional spectrometer).

Figure 1 shows a spectrum resulting from a typical experiment in which initial concentrations were 8.3 mm of NO_2, 8.5 mm of C_2H_5OH, and 93 mm N_2. There does not appear to be any further

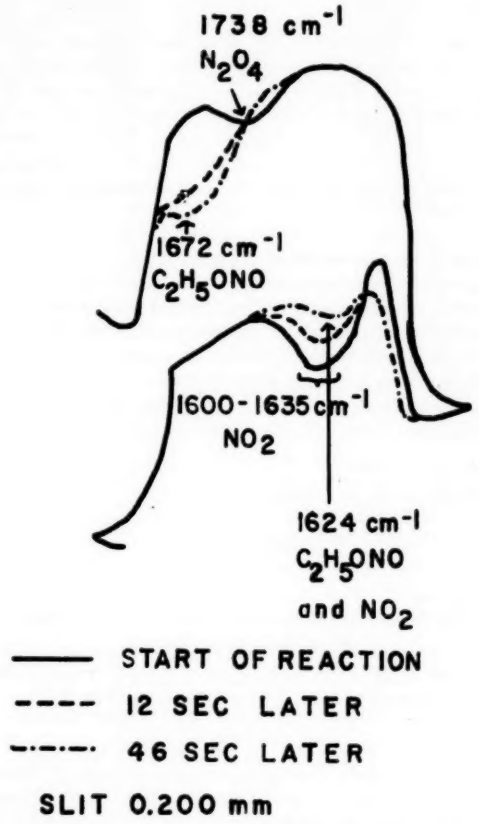

FIG. 1. Infrared spectra of the $NO_2-C_2H_5ONO$ reaction at several time intervals at 22°C.

increase in the intensity of the 1672 cm^{-1} band of C_2H_5ONO after 20 seconds. At concentrations of 14.7 mm NO_2, 17.5 mm C_2H_5OH, and 78 mm N_2 the reaction seemed to be essentially complete after about 5 seconds.

A study of the spectrum of the products of the reaction should enable one to determine if the stoichiometry of the reaction is truly as given by Eq. (1). With the help of spectra of the pure compounds we have been able to satisfactorily assign all of the bands found in the spectrum of the products. It remains to be determined whether the compounds are present in the right amounts, but there do not seem to be any large deviations from the band intensities to be expected.

We hope to report a more complete kinetic study of this reaction at a later date.

*This work was supported by the U. S. Navy, Bureau of Ordnance, through contract with the University of Minnesota.

[1] Wheatley, Vincent, Rotenberg, and Cowan, J. Opt. Soc. Am. **41**, 665 (1951).

[2] Cowan, Vincent, and Crawford, J. Opt. Soc. Am. **43**, 710 (1953).

[3] J. B. Levy, U. S. Naval Ordnance Laboratory, White Oak, Maryland, NAVORD Report 2313, June, 1952.

[4] However, see J. B. Levy, U. S. Naval Ordnance Laboratory, White Oak, Maryland, NAVORD Report 2608, December, 1952.

[5] A. D. Yoffe and P. Gray, J. Chem. Soc. **1951**, 1412.

Note on the Infrared Absorption of the Flame of a Simple Double-Base Powder*

HORACE F. WHITE, GEORGE R. COWAN, DAVID ROTENBERG, AND BRYCE CRAWFORD, JR.
School of Chemistry, University of Minnesota, Minneapolis 14, Minnesota

(Received April 22, 1953)

PRELIMINARY investigations of the infrared absorption of the flame and combustion products of a simple double-base powder indicate the presence of eight or nine strong bands in the region from 1250 to 4000 cm^{-1}. At present, however, the exact location, and hence the total number of most of these bands, is

TABLE I.

Observed bands (cm^{-1})	Possible assignments (cm^{-1})
2349	2349 CO_2
2198	R } of CO or N_2O
2053	P } of CO or R of CN

in considerable doubt and must remain so for some time due to the destruction of our equipment and records by fire in February, 1953. Nevertheless, it still seems worth while to report our findings prior to the fire.

This frequency region was scanned with the fast-scanning infrared spectrometer previously described[1] at an oscillation frequency of 4 cps and at oscillation amplitudes varying from 868 to 134 cm^{-1}.

The sample cell in which the powder strands were burned was designed to produce a laminar flow of nitrogen, parallel to the powder strand and perpendicular to the infrared beam. Two rocksalt windows (15-mm diameter), located tangent to the chamber bore permit light to pass through this high-pressure vessel. In our preliminary runs, a pressure of about 140 lb/sq in. was used.

While the spectrum seems to indicate eight or nine strong bands in the region scanned, only three of these bands have been measured with the accuracy necessary for spectral location. Of

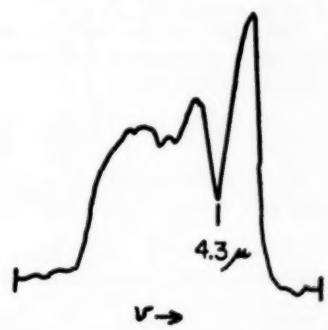

FIG. 1. Spectrum of a simple double-base powder flame in the 4.3μ region. Oscillation amplitude 300 cm^{-1}.

these three bands, only one can be assigned with any accuracy and it has been used as an internal standard. This band is the 4.3μ CO_2 band. The observed bands, as well as two alternative assignments, are listed in Table I.

Figure 1 shows one scan taken in the direction of increasing frequency (amplitude 300 cm^{-1}) and is representative of the spectra obtained.

If the alternative or CO assignment is taken, the flame temperature is found to be approximately 2000°K when the rotational constant is taken as $B=1.922$ cm^{-1}.[2]

* This work was supported by the U. S. Navy, Bureau of Ordnance, through contract with the University of Minnesota.

[1] Wheatley, Vincent, Rotenberg, and Cowan, J. Opt. Soc. Am. **41**, 665 (1951); Cowan, Vincent, and Crawford, J. Opt. Soc. Am. **43**, 710 (1953).

[2] G. Herzberg, *Spectra of Diatomic Molecules* (D. Van Nostrand Company, Inc., New York, 1950), p. 127.

Relation between Critical Temperature and Pressure of Normal Paraffins

YATENDRA PAL VARSHNI
Department of Physics, Allahabad University, Allahabad, India
(Received April 17, 1953)

TRAUTZ[1] has shown that the viscosity at the critical point η_c may be represented as a function of the molecular weight M, the critical pressure P_c, the critical temperature T_c, and the gas constant R. Dimensional analysis indicates that the form of the function should be

$$\eta_c = \text{const}\left[\frac{M^3P_c^4}{T_cR}\right]^{1/6}, \quad (1)$$

which may be written more compactly as

$$\eta_c = B\left[\frac{M^3P_c^4}{T_c}\right]^{1/6}, \quad (2)$$

where B is a constant.

If $P_cV_c/RT_c = P_cM/R\rho_cT_c = \text{constant}$, ρ_c being the critical density, then substitution for P_c in Eq. (2) gives

$$\eta_c = K\left[\frac{P_c^4T_c^3}{M}\right]^{1/6}, \quad (3)$$

where K is another constant.

This is the expression given by Grunberg and Nissan.[2] Their investigations have shown that η_c for the paraffins higher than propane is almost constant. Assuming ρ_c also to be constant, they have shown from Eq. (3) that T_c^3 is an additive property from propane to octane.

It is found that this additive relation holds good also for the higher paraffins, though only approximately as shown in Table I. There seems to be a decrease in the additive value as we go higher up in the series.

However, the fact that η_c and ρ_c are almost the same for the different n paraffins gives an important relation between the critical temperature and the critical pressure.

Assuming η_c and ρ_c to be constant and eliminating M between Eqs. (2) and (3), we get

$$T_c/P_c = C, \quad (4)$$

C being a constant.

The validity of the formula is shown in column 4 of Table II. Column 5 of the same table shows the values of the following empirical function:

$$T_c/P_c + \frac{6.4\times10^6}{T_c/P_c}. \quad (5)$$

It will be observed that if we neglect methane, the value of (4) gradually rises and becomes constant. This result is rather surprising, because in view of Grunberg and Nissan's results one could have expected the relation to hold better for the lower paraffins than for the higher paraffins. The mean value of the constant for the paraffins from pentane to nonadecane is 2832. The empirical function (5) is seen to be constant to a greater degree. Its mean value from ethane to nonadecane is 5091.

TABLE I.[a]

No. of C atoms	Paraffin	T_c in °K	$T_c^3\times10^{-5}$	Differences
1	methane	190.7	69	
				215
2	ethane	305.3	284	
				217
3	propane	368.8	501	
				273
4	butane	426.2	774	
				267
5	pentane	470.4	1041	
				270
6	hexane	508	1311	
				264
7	heptane	540	1575	
				271
8	octane	569.4	1846	
				265
9	nonane	595.4	2111	
				264
10	decane	619.3	2375	
				278
11	undecane	642.6	2653	
				272
12	dodecane	663.8	2925	
				264
13	tridecane	683.2	3189	
				256
14	tetradecane	701	3445	
				250
15	pentadecane	717.6	3695	
				264
16	hexadecane	734.3	3959	
				248
17	heptadecane	749.3	4207	
				238
18	octadecane	763.2	4445	
				228
19	nonadecane	776	4673	

[a] Data from *Landolt-Börnstein Tabellen* and Hodgman's *Handbook of Chemistry and Physics.*

TABLE II.[a]

No. of C atoms	T_c in °K	P_c in atmos.	T_c/P_c	Function (5)
1	190.7	45.8	1291	6250
2	305.3	48.8	2182	5183
3	368.8	43	2419	5066
4	426.2	36	2558	5061
5	470.4	33.04	2704	5071
6	508	29.63	2766	5081
7	540	26.89	2800	5086
8	569.4	24.66	2828	5092
9	595.4	22.86	2846	5095
10	619.3	21.24	2854	5097
11	642.6	19.92	2868	5100
12	663.8	18.59	2862	5097
13	683.2	17.55	2861	5098
14	701	16.56	2852	5096
15	717.6	15.75	2849	5096
16	734.3	15.10	2854	5097
17	749.3	14.41	2845	5095
18	763.2	13.83	2839	5093
19	776	13.43	2844	5095

[a] Data from *Landolt-Börnstein Tabellen* and Hodgman's *Handbook of Chemistry and Physics.*

The author wishes to thank Dr. K. Majumdar and Dr. R. D. Tewari for their interest in the investigation.

[1] Trautz, Ann. Physik **11**, 190 (1931); Trautz and Binkele, Ann. Physik **5**, 561 (1930); Licht and Stechert, J. Phys. Chem. **48**, 23 (1944).
[2] Grunberg and Nissan, Nature **161**, 170 (1948).

Hyperconjugation in $C_6H_7^+$ and Other Hydrocarbon Ions†

LUCY W. PICKETT, NORBERT MULLER,* AND R. S. MULLIKEN‡
Mount Holyoke College, South Hadley, Massachusetts, and Oxford University, Oxford, England
(Received June 15, 1953)

IN certain reactions of strong acids with aromatic hydrocarbons, conjugate acids of the latter can be formed.[1] Simplest is $C_6H_7^+$, which may be called benzenium ion. Using the LCAO MO method, we have calculated energy levels, charge distribution, bond orders and resonance energy of this ion.

Benzenium ion may be considered the simplest prototype of the probable reaction intermediates in electrophilic substitution reactions of aromatic hydrocarbons. Previous calculations[2] on such intermediates neglected hyperconjugation.

We treat the ion as if it had six π electrons, in orbitals made by combining the six $2p\pi_C$AO's and a quasi-π orbital ($1s_H - 1s_H$) on the H_2 pseudo-atom (see Fig. 1).

The resulting secular determinant contains diagonal elements $x_i = \alpha_i - E$, $\alpha_i = \int\psi_i H\psi_i d\tau$, and off-diagonal elements $\beta_{ij} + \frac{1}{2}S_{ij}(x_i + x_j)$, where $\beta_{ij} = \int\psi_i H\psi_j d\tau - \frac{1}{2}S_{ij}(\alpha_i + \alpha_j)$, and S_{ij} is the overlap integral $\int\psi_i\psi_j d\tau$.

We first set $x_i = x_0$ for all carbon atoms, and $x_H = x_0 + \delta\beta_0$, with $S_{CC} = 0.25$, $S_{CH} = 0.512$, and $\beta_{CH} = 2\beta_{CC}$.[3] We tried several δ values from -0.5 to $+0.5$.[4] In further calculations with $\delta = 0$, we made the β's and S's self-consistent with the calculated bond orders and corresponding distances, assuming β proportional to S.[3] Finally, we allowed for the effect on the α-values of the uneven computed distribution of charge among the several atoms by replacing each α_i by $\alpha_i + \omega\beta_0 q_i$ and repeating the computations until self-consistency was reached. Here q_i is the charge on the ith atom, calculated from the appropriately normalized coefficients of the occupied MO's. Trial values of 2 and 4 for ω were used.

The hyperconjugation energy is the difference between the energy thus computed and that similarly computed for the

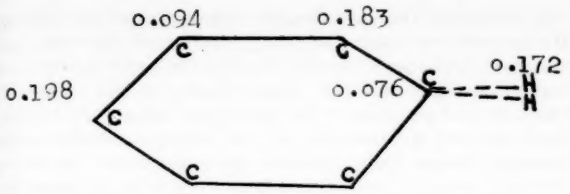

FIG. 1. Diagram of $C_6H_7^+$ showing charge distribution for $\delta=0$, $\omega=2$.

conventional model,[2] consisting here of four π electrons on five carbon atoms, plus an "inert" CH_2 group. For $\delta=0$, the computed hyperconjugation energy varies from $0.288\beta_0$, or about 17 kcal, if $\omega=0$, to $0.456\beta_0$, or about 27 kcal if $\omega=4$.§ It is larger for $\delta<0$ and smaller for $\delta>0$; empirically, it is fairly sure that $\delta<0$, perhaps about -0.5.[4]

Calculations now in progress indicate that ω is about 1.5; they involve the application of procedures like that described above to the ethyl, isopropyl, *t*-butyl and allyl free radicals and their positive ions, where the observed stabilization energies[5] become comprehensible if an ω of this magnitude is introduced.

The computations predict two electronic transitions in or near the visible for $C_6H_7^+$, a moderately strong one perhaps in the red and a strong one perhaps in the violet. Unpublished new experimental work by C. Reid at Chicago on the toluenium and xylenium ion spectra is in agreement with these predictions.

From the present calculations and from computations and observations on alkyl radicals and ions, it appears that in hyperconjugated systems containing an *odd number* of centers bearing π or quasi-π electrons, the hyperconjugation energy is of a *larger order of magnitude* than in similar systems containing an even number of such centers.[6] It should be noted especially that these results are reproduced theoretically using the same parameters[3,4] in the two cases.

† The computations on $C_6H_7^+$ were begun by L.W.P. at Chicago in the summer of 1951, continued at Mount Holyoke, and extended by N.M. in 1953.
‡ National Research Council Postdoctorate Fellow, at Oxford University.
‡ Fulbright scholar at Oxford University; permanent address, University of Chicago.
[1] M. Kilpatrick and F. E. Luborsky, J. Am. Chem. Soc. **75**, 577 (1953) and references to McCaulay and Lien, H. C. Brown and others given there.
[2] G. W. Wheland, J. Am. Chem. Soc. **64**, 900 (1942) and others. See in particular V. Gold, J. Chem. Soc. **1952**, 2184.
[3] a. Mulliken and Rieke, J. Am. Chem. Soc. **63**, 1770 (1941) and b. Mulliken and Roothaan, Chem. Rev. **41**, 219 (1947).
[4] In reference 3, δ values between 0 and +1 were used; but on the basis of empirical evidence Coulson and Crawford (in press) assume $\delta<0$, probably about -0.5.
§ These values are reduced by about 7 kcal by compressional energy corrections, but considerably raised by the use of $\delta=-0.5$. These points will be discussed in more detail in a paper in preparation.
[5] Franklin and Lumpkin, J. Chem. Phys. **20**, 745 (1952); Halpern, J. Chem. Phys. **20**, 744 (1952).
[6] Twisted ethylene (see reference 3b) containing two independent three-π-center hyperconjugated systems, also has large hyperconjugation energy.

Microwave Spectrum of HDO*†

D. W. POSENER‡ AND M. W. P. STRANDBERG
Research Laboratory of Electronics and Department of Physics, Massachusetts Institute of Technology, Cambridge, Massachusetts
(Received June 15, 1953)

IN order to improve our knowledge of the water molecule we have attempted to analyze the HDO microwave spectrum, guided by the behavior of the frequencies calculated theoretically from infrared data on H_2O and D_2O.

It is found that the frequencies of *Q*-branch transitions calculated in this manner bear a very simple relationship to those actually observed; the ratio (observed/calculated) is very nearly constant for transitions with a given value of K (i.e., K_{-1}, the index denoting the K value of the limiting prolate symmetric top) but with different J values, and the ratios for different families, i.e., different K's, are also simply related. By extrapolating the process one can predict additional *Q*-branch frequencies with very good accuracy; in Table I we give three such predictions, and the frequencies observed for the two lines that were searched for.

TABLE I. HDO predicted Q-branch transitions.

Transition	Frequency (Mc/sec) Predicted	Observed
$6_{24}\rightarrow 6_{23}$	64 417	...
$10_{56}\rightarrow 10_{55}$	8 836	8 836.95 ±0.1
$11_{57}\rightarrow 11_{56}$	22 577	22 581.1 ±0.2

It may be inferred from these results that the theoretical distortion parameters are very close to the true values. For this and for other reasons, we have attempted to fit the spectrum by adjusting only the theoretical effective reciprocal moments of inertia.

In all our frequency calculations, the actual rotational energies were computed directly by an extension of the continued-fraction method described by King, Hainer, and Cross[1] for the rigid rotor case. The $(K|K\pm1)$ and $(K|K\pm3)$ elements appear in the HDO rotational matrix, which, after application of the Wang transformation, factors into two submatrices only. We have included the effects of these elements in the fitting process, since they cannot be neglected for higher J and K transitions; in the extreme case considered, the $11_{57}\rightarrow 11_{56}$ transition, the theoretical values of these elements contribute about 32 Mc/sec to the frequency.

The known *P*- and *R*-branch lines are best fitted by adjusting both $(a+c)/2$ and the remaining distortion parameter D_J; the latter has to be changed from its theoretical value by some 25 percent, which is not consistent with the earlier assumption of the reliability of the theoretical distortion constants. However, this adjusted D_J should be considered as including some correction for the inaccuracy of the *Q*-branch parameters and so is not a good approximation to the true molecular D_J.

TABLE II. HDO microwave transitions.

Transition	Frequency (Mc/sec) Calculated	Distortion (Calculated minus rigid)	Observed	Observed minus calculated	Reference
		Q Branch			
$2_{21}\rightarrow 2_{20}$	10 275.660	− 50.170	10 278.99	3.330	a
$3_{22}\rightarrow 3_{21}$	50 232.692	− 322.228	50 236.90	4.208	a
$4_{32}\rightarrow 4_{31}$	5 701.757	− 79.716	5 702.78	1.023	b
$5_{33}\rightarrow 5_{32}$	22 307.350	− 387.214	22 309 ±5		c
			22 307.67±0.05	0.320	d
$6_{43}\rightarrow 6_{42}$	2395.019	− 71.180	2394.61	−0.419	e
$7_{44}\rightarrow 7_{43}$	8582.081	− 303.910	8576.89		b
			8577.7 ±0.1	−4.381	This work
$8_{45}\rightarrow 8_{44}$	24 865.250	−1084.806	24 884.77±0.05	19.520	This work
			24 884.85±0.1		f
$9_{55}\rightarrow 9_{54}$	3041.952	− 193.638	3044.71	2.748	e
$10_{56}\rightarrow 10_{55}$	8829.125	− 651.649	8836.95±0.1	7.825	This work
$11_{57}\rightarrow 11_{56}$	22 538.263	−1940.704	22 581.1 ±0.2	42.837	This work
$12_{67}\rightarrow 12_{66}$	2961.394	− 345.654	2961	−0.394	e
		P and *R* Branch			
$4_{22}\rightarrow 5_{05}$	2983	5038	2887.4	−95	e
$7_{07}\rightarrow 6_{24}$	12 198	−11 597	...	...	...
$4_{14}\rightarrow 3_{21}$	20 516	−4446	20 460.40	−56	a
			26 880.44		g
$6_{24}\rightarrow 7_{17}$	26 844	12 164	26 880.38±0.05	36	This work
			26 880.47±0.1		f
$5_{24}\rightarrow 4_{31}$	62 447	−20 086	...	...	...
$5_{23}\rightarrow 6_{06}$	69 602	7232	...	...	...
$6_{42}\rightarrow 7_{35}$	74 778	41 083	...	...	...
$6_{33}\rightarrow 7_{16}$	117 710	15 629	...	...	...
$8_{53}\rightarrow 9_{46}$	183 710	82 512	...	...	...

[a] M. W. P. Strandberg, J. Chem. Phys. **17**, 901 (1949).
[b] Microwave Spectroscopy Laboratory, Research Laboratory of Electronics, M.I.T., unpublished work.
[c] C. H. Townes and F. R. Merritt, Phys. Rev. **70**, 558 (1946).
[d] Strandberg, Wentink, Hillger, Wannier, and Deutsch, Phys. Rev. **73**, 188 (1948).
[e] S. Weisbaum, private communication; Weisbaum, Beers, and Herrmann, Phys. Rev. **90**, 338 (1953). We are grateful to S. Weisbaum and Y. Beers for allowing us to use their results prior to publication.
[f] Jen, Bianco, and Massey, J. Chem. Phys. **21**, 520 (1953).
[g] K. B. McAfee, Jr., Doctoral thesis, Harvard (1949).

Several other methods of adjusting the parameters to fit the observed spectrum have been tried, and we find the one described above to give the most satisfactory results, shown in Table II. The discrepancy between calculated and observed frequencies amounts to a few percent of the distortion correction, at worst, and we believe that it is not possible to improve the fit further without going to higher approximations in the theory of vibration-rotation interaction.[2] In particular, we find that the linear form[3]

TABLE III. HDO parameters.

	Theoretical	Observed
$(a+c)/2$	4.4487 $\times 10^5$ Mc/sec	4.484 $\pm 0.002 \times 10^5$ Mc/sec
$(a-c)/2$	2.5301 $\times 10^5$ Mc/sec	2.555 $\pm 0.005 \times 10^5$ Mc/sec
κ	−0.68120	−0.6841 ±0.0002
D_J	9.1418 Mc/sec	11.6 ±2.0 Mc/sec
D_{JK}	36.8132 Mc/sec	36.8 ±0.5 Mc/sec
D_K	287.0893 Mc/sec	287 ±5 Mc/sec
δ_J	3.3331 Mc/sec	3.333 ±0.005 Mc/sec
R_5	−7.8772 Mc/sec	−7.877 ±0.010 Mc/sec
R_6	−0.5722 Mc/sec	−0.572 ±0.005 Mc/sec
$R_7^{(a)}$	3.1160 Mc/sec	3.12 ±0.05 Mc/sec
$R_8^{(y)}$	−8.1994 Mc/sec	−8.20 ±0.05 Mc/sec
$R_9^{(y)}$	49.9173 Mc/sec	50.0 ±0.5 Mc/sec

of the Q-branch distortion correction, which is only a first-order approximation, cannot be used *per se* to adjust the distortion parameters to give a better fit. Any attempt to do so results in a set of numbers which fail to give a satisfactory approximation to the exact calculations and which should be considered constants in a semiempirical formula, rather than significant approximations to the true molecular parameters. Although such a solution can be useful in predicting further Q-branch lines, its extension to P- and R-branch transitions will be of limited validity.

Our theoretical calculations placed the $6_{24} \rightarrow 7_{17}$ line at 28 134 Mc/sec, some 1253 Mc/sec above the frequency of an observed transition which was believed, from the Stark effect, to be this line.[4] It is apparent from Table II that our tentative identification is strongly supported by the analysis.

Table III shows the parameters finally obtained for this molecule, after rounding off to the estimated accuracy.

Further work is being carried out, and a full report will be published later.

* This work was supported in part by the Signal Corps, the Air Materiel Command, and the U. S. Office of Naval Research.

† Portion of a Ph.D. thesis, Department of Physics, M.I.T. The content of this thesis, substantially unabridged, will be published as Technical Report No. 255, Research Laboratory of Electronics, M.I.T.

‡ Australian Commonwealth Scientific and Industrial Research Organization Studentship holder.

[1] King, Hainer, and Cross, J. Chem. Phys. **11**, 27 (1943).

[2] H. H. Nielsen, Revs. Modern Phys. **23**, 90 (1951); our distortion parameters in Table III are expressed in terms of the phase choice of reference 1.

[3] R. E. Hillger and M. W. P. Strandberg, Phys. Rev. **83**, 575 (1951); D. Kivelson and E. Bright Wilson, Jr., J. Chem. Phys. **20**, 1575 (1952).

[4] D. W. Posener, M.I.T. Research Laboratory of Electronics, Quarterly Progress Report, January 15 (1953); Jen, Bianco, and Massey, J. Chem. Phys. **21**, 520 (1953).

Extension of the N_2^+ (C→X) Bands in the Far Ultraviolet Region*

YOSHIO TANAKA†

Laboratory of Molecular Structure and Spectra, Department of Physics, The University of Chicago, Chicago 37, Illinois

(Received June 3, 1953)

REINVESTIGATION of the N_2^+ (C→X) bands was made using an 84-cm normal-incidence vacuum spectrograph. Two types of discharge tubes were used: one (Π-shape) for an uncondensed and the other (straight type) for a condensed discharge. Not only were pure N_2 and pure NO gases used in both tubes, but also mixtures of a trace of these with a large amount of helium were fed into the tubes. In each case the gas was pumped continuously through the spectrograph, while the pressure inside the tube was several mm.

In the case of the uncondensed discharge of pure N_2 and pure NO, we could not obtain the N_2^+ (C→X) bands. However, in the condensed discharge of these pure gases, the bands appeared very weakly; furthermore, they appeared only in the range $v' < 3$. When we used mixtures of the gases with helium, the system of bands appeared quite strongly in both the condensed and uncondensed discharges. Only the bands due to the transitions between $v' \geqslant 3$ and various v'' were present, as was previously observed by Watson and Koontz[1] in the condensed discharge of (N_2+He). In these cases, we can make an extension of the system below about 1300A. The results are shown in Table I, compared with the values of Watson and Koontz.

Setlow,[2] from a consideration of the intensity distribution, had proposed an alternative v' assignment, and his suggestion has recently been confirmed by Miescher and Baer[3] from measurements of the isotope shifts due to $(N_2^{15})^+$, $(N^{15}N^{14})^+$, and $(N_2^{14})^+$ ionized molecules. Thus the corrected v' assignment has been adopted in Table I.

As we have mentioned, in the case of the mixture of gases (N_2+He, NO+He), we could not observe the bands which are the result of the transitions $(v' < 3) \rightarrow v''$, and in each sequence the bands $(v' = 3) \rightarrow v''$ were the strongest. This feature, which had already been observed by Watson and Koontz, was attributed by them to the resonance excitation of the $v' = 3$ level by He^+. If we take Gaydon's value[4] of the dissociation energy of N_2, (9.764 ev), then the energy of the $v' = 3$ level of the C state, (24.330 ev), is nearly equal to the dissociation limit ($N\,^4S + N^+\,^3P$), (24.304 ev), of the N_2^+ ground state. Douglas[5] recently proposed the possibility of inverse predissociation at $v' = 3$ to explain an anomalously

TABLE I. $C^2\Sigma_u^+ \rightarrow X^2\Sigma_g^+$ bands of N_2^+.

v'	v''	ν observed (cm^{-1}) present	I	ν (cm^{-1}) Watson and Koontz	I
3	11	48551.7	3	48553.7	4
4	12	48727.7	2	48729.5	3
5	13	48907.8	1	48912.5	2
6	14	49089.9	0	49097.6	1
7	15	49280.3	0		
1	8	50127.8[a]	0	50134.6	0
2	9	50248.7[a]	0	50257.6	1
3	10	50387.2	7	50391.5	10
4	11	50526.4	6	50530.6	8
5	12	50672.0	5	50675.7	6
6	13	50821.7	3	50824.2	4
7	14	50965.3	1	50975.2	1
8	15	51126.6	0	51127.0	1
9	16			51285.2	0
10	17			51426.8	0
0	6	51991.5[a]	0	51996.4	1
1	7	52063.5[a]	0	52073.1	2
2	8	52154.5[a]	0	52160.5	2
3	9	52259.6	6	52261.7	9
4	10	52366.4	5	52363.1	7
5	11	52474.6	4	52472.6	5
6	12	52586.9	3	52585.3	3
7	13	52700.5	0	52695.0	0
8	14	52810.3	0	52809.1	0
0	5	53997.7[a]	0	54006.1	2d
1	6	54040.3[a]	0	54046.9	2
2	7	54095.0[a]	0	54100.2	1
3	8	54166.1	6	54165.3	6
4	9	54234.8	3	54233.4	3
5	10	54306.5	0	54308.6	1
0	4	56042.8[a]	1	56050.4	1d
1	5				
2	6			56074.0	1
4	8	56134.0	0	56138.7	1
5	9	56178.5	0	56180.6	1
6	10	56216.7	0	56224.2	0
3	6	58079.9	6	58078.9	3d
4	7				
3	5	60082.0	3		
4	5	62057.7	5		
3	4	62130.3	4		
4	4	64137.5	5		
3	3	64201.9	5		
4	3	66173.9	2		
3	2	66322.8	2		
4	2	68290.6	3		
3	1	68454.6	3		
3	0	70640.9	3		
4	0	72600.6	2		

[a] Observed in the disruptive discharges of pure nitrogen and pure nitric oxide.

high population at the level. If we consider the resonance excitation by He^+, (24.580 ev), the population might be rather high in the $v'=4$ level, (24.576 ev), instead of $v'=3$, (24.330 ev). Whenever this system is well developed, the line spectra of atomic nitrogen appear very strongly, and we can also observe an irregularity in the ΔG curve of the upper C state between $v'=2$ and $v'=3$. These observations seem to support the theory of inverse predissociation at the $v'=3$ level.

Takamine and his co-workers[6] have observed a change in the intensity distribution of the band system when neon was used in place of helium in the mixture. They attributed the distribution obtained with neon to a high population in the $v'=0$ and $v'=1$ levels due to three body collisions; $Ne^+ + N_2 + N(^2D) \rightarrow Ne + N_2^+ + N(^4S)$. Their suggestion seems probable but, if the resonance excitation is the major factor, then the (1,6) and (2,7) bands should be stronger than the (0,5) band in the $\Delta V = -5$ sequence. This follows from the fact that the $v'=1,2$ levels are closer to 23.934 ev, which is the sum of the ionization potentials of Ne and the excitation energy of $N(^2D)$.

In conclusion, the author wishes to express his sincere thanks to Professor R. S. Mulliken and Professor J. R. Platt for their cooperation in this work, and to Mr. M. Schagrin for his assistance in the laboratory.

*This work was assisted in part by the U. S. Office of Naval Research under Task Order IX of Contract N6ori-20 with The University of Chicago, and in part by the Office of Ordnance Research under Project TB2-0001(505) of Contract DA-11-022-ORD-1002 with The University of Chicago.

† Present address: Geophysics Research Division, Air Force Cambridge Research Center, 230 Albany Street, Cambridge 39, Massachusetts.

[1] W. W. Watson and P. G. Koontz, Phys. Rev. **46**, 32 (1934).
[2] R. B. Setlow, Phys. Rev. **74**, 153 (1948).
[3] R. Miescher and P. Baer, Nature **169**, 581 (1952).
[4] A. G. Gaydon, *Dissociation Energies and Spectra of Diatomic Molecules* (Dover Publications, New York, 1950).
[5] A. E. Douglas, Can. J. Phys. **30**, 302 (1952).
[6] Takamine, Suga, and Tanaka, Sci. Papers Inst. Phys. Chem. Research Tokyo **36**, 437 (1939).

The Detonation of Pentaerythritol Tetranitrate

M. P. MURGAI
Defence Science Organization, N.P.L. Buildings, Pusa, New Delhi 12, India
(Received May 7, 1953)

KIRKWOOD[1] has extended the Lennard-Jones Devonshire[2] theory for liquids to multicomponent fluid mixtures. Ficket and Wood[3] have envisaged the possibility of the application of these results to the detonation of solid explosives. We report here some calculations on pentaerythritol tetranitrate (PETN). Its detonation products are determined mainly by the water-gas equilibrium. The parameters used, for CO_2, CO, H_2, and N_2, were as found by Hirschfelder *et al.*[4] from viscosity data and, for water, were those of the spherical potential fitted, between 4000° and 5000°K, to the extrapolated data of Corner[5] on the second virial coefficient. v^0 and $\tilde{\epsilon}$ (parameters for the mixture as defined by Kirkwood) remain sensibly constant in this case, in the range of temperature and volume relevant to the problem. With the values of the constituents as chosen above, $v^0=321$ cc and $\tilde{\epsilon}/k=125$°A. This gave the value of the detonation velocity, at loading density $\rho_0=1.25$ g/cc, to be 8100 m/sec, as compared to experimental value of 6700 m/sec. If, however, the mixture be regarded as a single gas of molecular diameter equal to the average diameter of the products (Kirkwood's results apply to cells of equal size), we have $v^0=250$ cc, $\tilde{\epsilon}/k=125$°A, which give the results compiled in Table I.

Comparison of this with the results of Cottrell and Paterson[6] and Paterson[7] reveals that for the same loading density, the temperatures and pressures attained are least and maximum in the former, greatest and least in the latter solution, respectively, while those found in this solution are intermediate between references 6 and 7. This is so because reference 7 proceeds from a state equation of the form $pv=RTf(v)$, which gives rise to no interaction term in the expression for the internal energy, and hence results in a higher temperature. Cottrell and Paterson's solution depends on a smoothed potential cell model in which only repulsive energy is considered. It takes into account the electronic redistribution in molecules at high densities and the consequent decreases in polarizability and hence neglects the attractive energy. A considerable amount of the heat evolved is used up in overcoming the repulsive forces, and therefore the temperature is lower. In the LJD method, on the other hand, both attractive and repulsive energies are comparable. In this case the ionization potential and polarizability, etc., are absorbed into a constant whose change with density is not considered. The dependence of the energies on the intermolecular distance alone is taken into account.

TABLE II.

Temperature T° A	Pressure $P\times10^{-10}$ dyne/cm²	Volume v cc/g mole of PETN	γ
4900	0.836	234	2.60
4700	0.675	254	2.52
4500	0.558	274	2.49
4300	0.453	298	2.44
4100	0.372	326	

The pressures obtained by Paterson[7] are very low, so much so that they mask the effect of higher temperature supposed to be prevailing there. The reason for this may be sought in the compressibility factor, which is a measure of the slope of the curve of $\log \int_0^v e^{-W/kT}dv$ (W being the energy of the molecule in the field of others) against volume. Reference 7 is based on a rigid sphere model, and therefore the curve previously referred to is less steep, while in reference 6, with a small increase in v, there is a considerable change in $\log \int_0^v e^{-W/kT}dv$ as a result of the repulsive forces considered, resulting in a steeper curve and hence large compressibility factor. In the LJD solution the slope lies in between for it takes account of both attractive and repulsive energies.

Jones's[8] inverse approach enables the interaction energy to be obtained without any *a priori* assumption regarding molecular interaction, for the solution is based on a state equation of the form $pv=RT+f(p)$. A formal comparison of these results with reference 8 brings out the fact that the attractive energy is not completely negligible as in 6, nor is it exactly given by the LJD expression.

The exponent of the adiabatic law of the expansion of hot dense products may be determined by finding out the entropy S of the products in the detonation wave front and assuming it to be constant throughout. For $\rho_0=1.0$ g/cc, $S=0.67$ kcal/deg g mole of PETN. If p and v are the values of the pressure at any instant during the process, $\gamma=-d\log v/d\log v$. The results are tabulated in Table II.

TABLE I.

Loading density g/cc	Calculated velocity D m/sec	Experimental velocity D m/sec	Temperature T°K				Pressure P 10^3 atmospheres			
			LJD method	Cottrell and Paterson	Paterson	Jones	LJD method	Cottrell and Paterson	Paterson	Jones
1.00	5671	5550	4900	3650	5150	4400	0.85	0.88	0.74	0.86
1.50	7474	7420	4700	3280	5340	...	1.96	2.25	1.88	...
1.72	8505	8300	4420	1950	...	...	2.56	2.85	...	...

These values agree reasonably with those found by other authors,[9,10] especially with those of Jones and Miller.[11] They found that γ decreases with decrease in pressure. A similar trend is indicated in these results.

The author is grateful to Dr. D. S. Kothari for his interest during the course of this work.

[1] Salsburg, Sevi, and Kirkwood, J. Chem. Phys. **20**, 1538 (1952).
[2] Lennard-Jones and Devonshire, Proc. Roy. Soc. (London) **A165**, 1 (1938).
[3] W. Ficket and W. W. Wood, J. Chem. Phys. **20**, 2624 (1952).
[4] Hirschfelder *et al.*, Chem. Rev. **44**, 205 (1949).
[5] J. Corner, Proc. Phys. Soc. (London) **58**, 737 (1946).
[6] T. L. Cottrell and S. Paterson, Proc. Roy. Soc. (London) **A213**, 214 (1952).
[7] S. Paterson, Research **1**, 221 (1948).
[8] H. Jones, *Third Symposium on Combustion and Flame and Explosion Phenomenon* (Williams and Wilkins Company, Baltimore, 1949), p. 590.
[9] L. D. Landau and K. P. Staninkovich, C.R. Acad. Sci. U.R.S.S. **53**, 33 (1946).
[10] G. I. Pokrovskii and K. P. Staninkovich, C.R. Acad. Sci. U.R.S.S. **53**, 33 (1946).
[11] H. Jones and A. R. Miller, Proc. Roy. Soc. (London) **A194**, 480 (1948).

The Total Energy of Substances at the Critical Point

JOHAN VAN DRANEN
Laboratory for Analytical Chemistry, University of Amsterdam, Amsterdam, Netherlands
(Received May 18, 1953)

SOME time ago the author enunciated the hypothesis[1,2] that the critical state is the result of the fact that at the critical point the average kinetic energy (K_c) is equal to the average (negative) potential energy (U_c). Using the symbols, given in reference 2, we have, accepting this hypothesis, the relation: $K_c+U_c=0$ or $K_c+U_c'+P_cV_c=0$, where U_c' is the van der Waals part of the potential energy or the internal energy of gas imperfection. K_c and P_cV_c can be easily calculated; on the other hand it is difficult to obtain an accurate value for U_c'.

In reference 2 we have attempted to test this hypothesis for argon, nitrogen, and methane. In order to find a value for U_c' we have extrapolated experimental values for U', obtained at temperatures between 0°C and 150°C, to the critical temperature. This procedure gives for nitrogen ($T_c=-147$°C) the value $U_c'=-455$ cal/mole; in a recent publication, however, Michels and co-workers[3] have extended their measurements for nitrogen to −125°C. A small extrapolation (−125°C→−147°C) now gives for $U_c'-453.5$ cal/mole, showing that the fairly crude extrapolation method of reference 2 is reasonably accurate.

TABLE I. The internal energy of gas imperfection at the critical point U_c' (cal/mol).

	water ($T_c=374.2$°C)	carbon dioxyde ($T_c=31.04$°C)
hypothetical value	−2220	−1070
	−2232 (365°C)	−1059 (28.05°C)
	−2167 (370°C)	−1036 (29.93°C)
	−2160 (372°C)	−1033 (30.41°C)
		−1000 (31.01°C)

We shall now use a different way for obtaining Uc' to test the hypothesis for CO_2 and H_2O. Michels, Blaisse, and Michels[4] (for CO_2; $T_c=31.04$°C, $P_c=72.85$ atmos, and $V_c=94.0$ cm³) and Jakob and Fritz[5] (for H_2O; $T_c=374.2$°C, $P_c=218.3$ atmos, and $V_c=55.2$ cm³) have published very accurate values for the densities, vapor pressures, and heats of vaporization for the liquid-vapor equilibrium of these compounds.

The heat of vaporization can be divided into the internal latent heat (L) and the work for the change in volume $P(V_g-V_l)$. This internal latent heat is equal to the difference in the internal energies of gas imperfection for the liquid and its coexisting vapor. It appears that the internal energy is, in good approximation, a linear function of the density (compare reference 6, Fig. 1). This leads to the following formula, which enables us to calculate with some accuracy U_c', namely,

$$U_c'=-Ld_c(d_l-d_g)^{-1}, \quad (1)$$

According to the hypothesis $-U_c'=(\frac{3}{2})RT_c+P_cV_c$. In Table I we have reproduced this "hypothetical" value for U'_c and the values obtained with the aid of the formula (1). As the values for the densities and heats of vaporization in the immediate neighborhood of the critical point are less accurate than the extrapolated ones, we have calculated U_c', using the experimental values for d_l, d_g, and the corresponding L, obtained at different temperatures. These temperatures are given parenthetically in the second and the fourth column of Table I.

We think that the reasonable agreement between the hypothetical and the calculated values yields some support to the hypothesis.

Using the Kirkwood formulation of the statistical mechanical theory of the liquid state, Kirkwood, Lewinson, and Alder[7] have calculated the thermodynamic properties of a fluid composed of molecules interacting according to the Lennard-Jones potential. They determined the theoretical values for the critical constants of such a fluid from their theoretical isotherms, showing liquid-vapor transition (reference 7, Fig. 6). These values are expressed in the well-known reduced units: $V^x=V/Na^3$, $P^x=P(a^3/\epsilon)$, and $T^x=T(k/\epsilon)$, where a is the distance for which the LJ potential is equal to zero and ϵ the depth of this potential curve. The theoretical values are $T_c^x=1.433$, $V_c^x=2.585$, and $P_c^x=0.199$. From Table VI, reference 7, where U' (in units $N\epsilon$) *versus* V^x and T^x is tabulated,[8] we deduce $U_c'=-2.77$. The kinetic energy $K_c=\frac{3}{2}T_c^x=2.15$. The potential energy $U_c=U_c'+P_c^xV_c^x=-2.24$. The total energy $K_c+U_c(=0.09)$, which, according to the hypothesis, should be equal to zero, is very small compared with the separate values for K_c and U_c

The experimental values for the critical constants of the inert gases are $T_c^x=1.26$, $V_c^x=3.16$, and $P_c^x=0.115$. The corresponding value for U_c' is equal to -2.31. In this case we have $K_c=1.89$; $U_c=-1.95$ and for the total energy $K_c+U_c=-0.06$ or three percent of the value for U_c. The good agreement in both cases gives us some confidence to apply the hypothesis on a special problem, namely, the disturbed rotation in the liquid state.

[1] J. van Dranen, J. Chem. Phys. **20**, 1175 (1952).
[2] J. van Dranen, J. Chem. Phys. **21**, 567 (1953).
[3] Michels, Lunbeck, and Wolkers, Physica **17**, 801 (1951).
[4] Michels, Blaisse, and Michels, Proc. Roy. Soc. (London) **A160**, 358 (1937).
[5] M. Jakob and W. Fritz, Phys. Z. **36**, 651 (1935).
[6] Michels, Byl, and Michels, Proc. Roy. Soc. (London) **A160**, 376 (1937).
[7] Kirkwood, Lewinson, and Alder, J. Chem. Phys. **20**, 929 (1952).
[8] The internal energy of gas imperfection can easily be determined; the table gives for this quantity a nearly linear dependency of the density.

The Critical Point and the Disturbed Rotation of Molecules in the Liquid State

JOHAN VAN DRANEN
Laboratory for Analytical Chemistry, University of Amsterdam, Amsterdam, Netherlands
(Received May 18, 1953)

SPECTROSCOPIC data indicate that the rotation of the molecules in the liquid state is not even approximately free. We shall try to obtain a value for this rotational energy for a special case, namely, the disturbed rotation of CO_2 at the critical point, for which substance excellent experimental data are available. Michels, Byl, and Michels[1] have obtained from the experimental PVT data the thermodynamic properties of CO_2. For the excess of the total intermolecular, rotational, and vibrational energy over the energy at NTP they obtained at the critical point −1216 cal/mole. We find for the energy at NTP 1475 cal/mole, using the vibrational frequencies 1351 cm^{-1}, 2396 cm^{-1}, and 672 cm^{-1} ($2x$) (ground state and point group of CO_2: $^1\Sigma_g^+$ and $D_{\infty h}$

respectively). For the total kinetic (K_c), potential (P_c), vibrational, and rotational energy we obtain therefore at the critical point -1216 cal/mole$+1475$ cal/mole$+P_cV_c=425$ cal/mole ($P_c=72.85$ atmos and $V_c=94.0$ cc).

Some time ago the author formulated the hypothesis[2] that the critical point of a substance is the result of the fact that at the critical point the average kinetic energy is equal to the average (negative) potential energy. In two recent Letters to the Editor[3] he has given, in his opinion, some further evidence that this hypothesis might indicate the physical cause of the critical point.

Accepting now the hypothesis, thus putting K_c+U_c equal to zero, one obtains for the sum of the rotational and vibrational energy at the critical point 425 cal/mole. As the vibrations of CO_2 can take place in the liquid state without appreciable alteration,[4] the vibrational energy is equal to 175 cal/mole. Therefore, according to the hypothesis, the rotational energy should be equal to 250 cal/mole. For an undisturbed rotation the energy is equal to $2\times(1/2)\ RT_c$ or 604 cal/mole. The shape of the CO_2 molecule does not lend itself easily to undisturbed rotation in the liquid state. When the pressure of the gas is increased we can therefore expect that the rotational energy decreases from the value 604 cal/mole at low pressures to zero in the highly compressed state. It seems reasonable to assume that at intermediate densities ($P_c=72.85$ atmos) one gets then for this energy a value between 604 cal/mole and zero. Some support for this view are the results of the investigations of Weiler[5] concerning the intensity distribution in the rotational Raman spectrum of CO_2 at 60 atmos.

According to the theoretical formula of Placzek and Teller,[6] the intensity is proportional to

$$(j+1)(j+2)(2j+3)^{-1}\exp -j(j+1)A,$$

where $A=h^2(8\pi^2IkT)^{-1}$ and $j=0, 2, 4, \cdots$. Weiler finds that for the transitions between the quantum numbers, in which the rotational energy is mainly concentrated ($14\leq j\leq 50$), the experimental values for the intensities are about three times smaller than given by this theoretical formula. This entirely different method gives therefore for the rotational energy a value of the same order of magnitude, namely, about 200 cal/mole.

We are fully aware that some points in this treatment need a further investigation, especially the fact that we have treated this disturbed rotation as a quasi-quantized rotation for which the theoretical selection rules and intensity formulas are valid. The intensity distribution in the continuum adjoining the exciting mercury line is, however, similar to that in CO_2 at low pressures. For this reason we believe that this procedure is justified.[7]

Besides the disturbed rotation some other problems concerning the critical state can be treated with the aid of this hypothesis. For example, the zero-point energy of quantum liquids (He, H_2, and D_2) can be calculated as the difference of the potential energy and the kinetic energy. In this letter we shall, however, make some short remarks on the value of the specific heat at the critical point.

In the literature some measurements are reported of the specific heat at constant volume (C_v) of some substances in the neighborhood of the critical point. The remarkable fact is, that C_v seems to attain a maximum around the critical density. With the aid of a new, very improved experimental technique, an adiabatic differential method, which allows the direct measurement of the C_v of compressed gases and liquids, Michels and Stryland[8] determined the C_v of compressed CO_2 with an accuracy of 0.5 percent. The fact that in the neighborhood of the critical density, even for the homogeneous single phases, C_v takes an extremely high value, is the most surprising result of this investigation (e.g., at 31.5°C, 0.46° above the critical temperature, C_v is equal to 29 cal/mole).

In reference 3 we have said that, according to this hypothesis, as long as the kinetic energy is smaller than the (negative) potential energy, a liquid, in equilibrium with its vapor, is bound in its own characteristic volume. With respect to the movement of the molecules itself, we add that as long as the total energy is negative, the molecules are, for the major part of the time, in a certain sense, bound in a small volume, e.g., a cluster of 50 molecules. At the critical point the kinetic energy of a molecule becomes greater than the potential energy, and in the temperature range of a few degrees the system gets the remaining part (or nearly the remaining part) of the communal entropy. For, the somewhat arbitrarily chosen cluster of 50 molecules and free migration through the volume, the entropy difference is equal to 0.115 entropy units or 6 percent of the communal entropy. This value corresponds for CO_2 with an additional increase in energy of 35 cal/mole. Using the values of Michels and Stryland, a crude estimate of this additional energy, gives about 50 cal/mole.

We obtain energy differences of this order of magnitude for a constant volume, if we assume that the mean intermolecular distance becomes greater (a few percent) and the coordination number higher (6, 7, 8, →10, 11, 12).

[1] Michels, Byl, and Michels, Proc. Roy. Soc. (London) **A160**, 376 (1937).
[2] J. van Dranen, J. Chem. Phys. **20**, 1175 (1952).
[3] J. van Dranen, J. Chem. Phys. **21**, 567 (1953) and **21**, 1404 (1953).
[4] G. Herzberg, *Infra-Red and Raman Spectra* (D. Van Nostrand Company, Inc., New York, 1945), p. 535.
[5] J. Weiler, Ann. Physik **23**, 493 (1935) and reference 7, p. 533.
[6] G. Placzek and E. Teller, Z. Physik **81**, 209 (1933).
[7] In this preliminary communication we do not apply the small correction for the internal kinetic energy of compression. Application of this correction would improve the agreement.
[8] A. Michels and J. C. Stryland, Physica **18**, 613 (1952); J. C. Stryland, thesis, University of Amsterdam (1953).

A Modified Isotopic Exchange Rate Expression

ROWLAND E. JOHNSON
Department of Chemistry, Florida State University, Tallahassee, Florida
(Received April 14, 1953)

THE common rate expression for isotopic exchange reactions[1]

$$Rt=-\frac{(A)(B)}{(A)+(B)}\ln(1-F), \tag{1}$$

is derived on the basis that the total amount of activity remains constant or that appropriate corrections for radioactive decay are made. If we assume instead that the total amount of activity of tracer remains constant because the tracer isotope is in secular or transient equilibrium with its parent, we may derive a new rate expression which shows a number of interesting features.

In the simplest case, we may consider the parent and daughter isotopes as ions in aqueous solution, the daughter present in a single, well-defined oxidation state (species B). Carrier daughter of the same oxidation state may or may not be present. We are to measure the rate of exchange between species B and another form of the daughter element (species A), as another oxidation state or as a precipitate, for example. For such a system at chemical equilibrium and assuming that the first-order exchange law holds, the rate of increase, $[d(A')/dt]$, in the concentration of radioactive atoms in the form A is given by

$$\frac{d(A')}{dt}=RS_B(1-S_A)-RS_A(1-S_B)-\lambda(A') \tag{2}$$

$$=\frac{R}{(A)(B)}[(A)(B')-(B)(A')]-\lambda(A') \tag{2'}$$

where λ is the decay constant of the tracer isotope. If we assume chemical identity of daughter isotopes,

$$(B_\infty')=\frac{(B)}{(A)}(A_\infty') \tag{3}$$

and correct, if necessary, for the decay of the *parent* isotope,

$$(A')+(B')=(A_\infty')+(B_\infty') \tag{4}$$

then

$$\frac{d(A')}{dt}=\frac{R[(A)+(B)]}{(A)(B)}[(A_\infty')-(A')]-\lambda(A') \tag{5}$$

follows from Eq. (2').

Substituting y [a constant for a series of runs at constant (A) and (B)] for $R[(A)+(B)]/(A)(B)$, integrating Eq. (5), and evaluating the constant of integration gives

$$(y+\lambda)t=-\ln\left[\frac{y(A_\infty')-(y+\lambda)(A')}{y(A_\infty')-(y+\lambda)(A_0')}\right]. \tag{6}$$

To evaluate this expression, let $(A'_0)=0$, i.e., species A is initially inactive.

$$(y+\lambda)t=-\ln\left\{\frac{[(A_\infty')-(A')]}{(A_\infty')}-\frac{\lambda(A')}{y(A_\infty')}\right\} \tag{7}$$

$$=-\ln\left[1-F\left(1+\frac{\lambda}{y}\right)\right]. \tag{7'}$$

F, in Eq. (7') represents the fraction exchange as experimentally determined by the ratio $(A')/(A_\infty')$. Equation (7') reduces exactly to Eq. (1) when $\lambda=0$; this condition is realized in ordinary tracer experiments by making decay corrections which gave an apparently infinite half-life to the isotopic tracer.[2]

It is obvious from Eq. (7') that at $t=\infty$, $F\neq 1$ unless $\lambda/y=0$. If λ/y has any value other than zero, and less than infinity, F will increase with time, from zero time, to some value less than unity at $t=\infty$. The condition of complete exchange will never be attained due to the loss of activity by decay from the A species, and the final fraction exchange will represent a steady state wherein the rate of exchange into the A species will be balanced by exchange out of the A species plus decay out of the A species.

In Fig. 1 are plotted curves of $\log(1-F)$ *versus* time for various values of the ratio λ/y. Notice that, in some cases, equilibration of activity is complete (within experimental error) in a time comparable to the half-time of the tracer isotope. This makes it possible to measure exchange reactions with isotopes of very short half-lives since decay corrections on the daughter need be made only during the separation and counting procedures, and a steady source of the isotope is incorporated into the experimental system. Determination of a value of R for this system involves a single determination of F at *any* time after equilibration and calculation of R from known values of (A), (B), and λ, correcting for zero-time exchange if necessary.

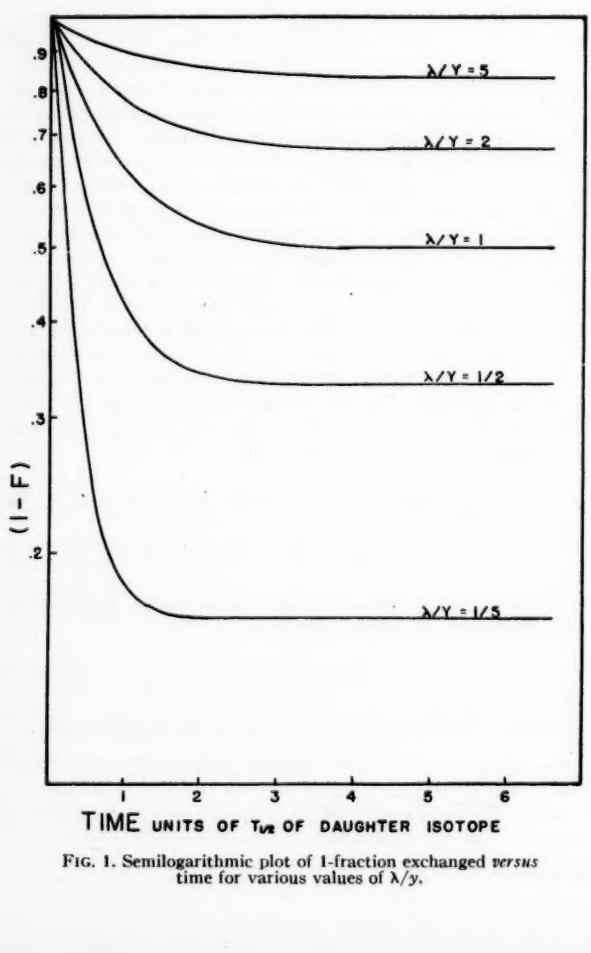

FIG. 1. Semilogarithmic plot of 1-fraction exchanged *versus* time for various values of λ/y.

In actual practice, all of the conditions outlined above may be difficult to satisfy; for instance, the parent isotope may produce the daughter activity in a number of oxidation states with different rates of inter-conversion and exchange. However, a number of parent-daughter pairs might be used, for example Sr^{90}—Y^{90}, A^{42}—K^{42}, or Cs^{137}—Ba^{137}. Furthermore, a neutron source may be considered a "parent"; thus a continuous extraction (into an aqueous phase) of ethyl iodide, continuously irradiated with neutrons might give a steady-state concentration (in the water) of elemental I^{128} whose apparent half-life would be that of the neutron source.

This work was done under the auspices of the U. S. Atomic Energy Commission.

[1] A. C. Wahl and N. A. Bonner, Editors, *Radioactivity Applied to Chemistry* (John Wiley and Sons, Inc., New York, 1951), Chap. I. All symbols used in the following derivation will be the same as those in this reference.
[2] Equation (7') may also be derived by treating the decay and exchange processes as a series of coupled first order reactions; see F. A. Matsen and J. L. Franklin, J. Am. Chem. Soc., **72**, 3337 (1950).

The Accuracy of the Knudsen Effusion Method for Measuring Vapor Pressures

M. G. ROSSMAN
Department of Natural Philosophy, The Royal Technical College, Glasgow, Scotland
AND
J. YARWOOD
Department of Mathematics and Physics, The Polytechnic, Regent Street, London, England
(Received February 10, 1953)

IT is apparent that the difference between Langmuir's method and Knudsen's effusion method of finding small vapor pressures is often not completely understood. In Knudsen's effusion method the vapor in the crucible is assumed to be saturated and the loss of mass is due to the escape of the vapor through a small orifice. In Langmuir's method, on the other hand, the vapor near the evaporating substance is so far from being saturated that practically no molecules return to hit the substance again. In Knudsen's method the number of molecules hitting the substance should equal the number that leave it. This cannot be satisfied completely because some of the molecules are escaping, but their number is a small fraction of the whole. The outstanding advantage of Knudsen's method in practice is that *apparently* the surface area of the evaporating substance does not need to be known but only the area of the small orifice. It can hence be used for liquids which might wet the sides of the crucible (e.g., molten aluminum) or collect up into a sphere (e.g., mercury) whereas Langmuir's method demands a defined evaporating area of the substance. Thus to apply such rigid geometry to a consideration of the effusion method as that used by Whitman[1] becomes meaningless, and his working can be substituted by the rather simpler treatment which we give below.

Let the area of the crucible orifice be a. Let the effective area of the evaporating substance be A. Let w grams of the substance be lost through the orifice in unit time.

The lid of the crucible in which the small orifice is made is assumed to be infinitely thin for the present.

If the pressure of the vapor in the crucible is p, then

$$w/a=p(M/2\pi RT)^{\frac{1}{2}}, \tag{1}$$

where M is the gram molecular weight of the vapor, R is the gas constant, and T is the temperature in degrees Kelvin.

From Langmuir it is also known that $\alpha p(M/2\pi RT)^{\frac{1}{2}}$ g condense on the substance per unit are in unit time, where α is the conden-

sation coefficient. Thus, if η g leave the substance per unit area per unit time, therefore

$$w/A=\eta-\alpha p(M/2\pi RT)^{\frac{1}{2}}, \quad (2)$$

because the mass which leaves the substance in unit time must equal the mass escaping out of the orifice in unit time. But $w=0$ when $p=P$, the saturation vapor pressure, because then the number of molecules hitting equals the number leaving the condensate. Therefore

$$\eta=\alpha P\left(\frac{M}{2\pi RT}\right)^{\frac{1}{2}}$$

from Eq. (2), and

$$\frac{w}{A}=\alpha(P-p)\left(\frac{M}{2\pi RT}\right)^{\frac{1}{2}}. \quad (3)$$

Dividing Eq. (3) by (1), one obtains

$$\frac{a}{A}=\alpha\left(\frac{P}{p}-1\right).$$

For the best results with the effusion method, p is very nearly equal to P; it is, in fact, assumed to be the same as P. Thus let $p=xP$, where x is very nearly equal to one. Therefore

$$x=\frac{1}{1+(a/A\alpha)}, \quad (4)$$

or putting $a/A=f$ (as Whitman does)

$$x=\frac{1}{1+(f/\alpha)}. \quad (5)$$

Consider now the effect which is caused by the lid—in which the orifice is pierced—being of finite thickness, and the area A not being equal to the area of cross section of the crucible, i.e., the surface of the evaporating substance is not plane. Then the orifice will be a short tube instead of a simple aperture. The resultant impedance to the flow of vapor will be equivalent to making the aperture area a smaller. The area of the actual surface of the substance can, however, only be larger than A, the cross-section area of the crucible, because wetting of the sides of the crucible by a liquid, or the use of a solid in the form of powder, or shavings, in the crucible can only result in an effective evaporation area increase. Thus the expression (5) gives the maximum possible error in the vapor-pressure determination, the error being zero when $x=I$. It will be seen that, since x is a function of a, A, and α, so the effective area of the condensate is fundamentally related to the pressure of the effusing gas. This is exactly opposite to the conclusion arrived at by Whitman.

[1] C. I. Whitman, J. Chem. Phys. **20**, 161 (1952).

Comment on "The Accuracy of the Knudsen Effusion Method for Measuring Vapor Pressures"

CHARLES I. WHITMAN
Atomic Energy Division, Sylvania Electric Products, Inc., Bayside, New York

(Received March 4, 1953)

A DERIVATION similar to Rossmann's and Yarwood's[1] has also been given by Speiser and Johnston.[2] The validity of these derivations is dependent on the assumption of a uniform steady-state pressure p throughout the vapor volume. Under the usual experimental conditions the relatively slow "free molecule" flow within the vapor volume may not permit such a steady state to exist except under such conditions that the calculated error is insignificant.

Referring to the experimental arrangement discussed by me earlier,[3] an expression analogous to R and Y's (Eq. (4)) follows readily from my Eq. (7). Thus

$$p/P=K=\frac{1}{1+f/W_A-f} \quad (1\geq W_A>0) \quad (1)$$

for a cell with an infinitely thin orifice. The condensation coefficient $\alpha=1$ and p is determined by the measured effusion rate. It is apparent from Eq. (1) that K will be greater than, equal to, or less than R and Y's x, depending on the depth of the cell (which determines W_A). The effusion rate is, therefore, not only dependent on how much "effective area" of condensate is present but also on *where* it is located relative to the orifice.

This would prove a pertinent consideration for any experimental arrangement and hence, in general, the assumption of a steady-state pressure is not justifiable. R and Y's x would not be, therefore, a particularly reliable estimate of the accuracy of an effusion measurement.

What R and Y call the "effective area" of condensate is essentially the same as what I termed "the surface bordering the vapor volume"[3] and does not necessarily have any relation to the *total* surface area of the condensate. Actually their conclusion is not exactly opposite to mine; it is exactly the same.

[1] M. G. Rossmann and J. Yarwood, J. Chem. Phys. **21**, 1406 (1953), to be referred to in this paper as R and Y.
[2] R. Speiser and H. L. Johnston, Trans. Am. Soc. Metals **42**, 283 (1950).
[3] C. I. Whitman, J. Chem. Phys. **20**, 161 (1952).

Infrared Spectra of Solutions of Iodine

D. L. GLUSKER, H. W. THOMPSON, AND R. S. MULLIKEN*
Physical Chemistry Laboratory, Oxford University, Oxford, England

(Received May 25, 1953)

DURING the past two years infrared measurements have been made in this laboratory designed to give further information about the nature of the interaction of iodine with organic solvents. Preliminary work of Wood and Morcillo has now been repeated and extended using carefully purified and dried solvents. Meanwhile, similar studies with mesitylene have been described by other workers.[1,2] Since our work and results differ in some important aspects from those given by these authors, we summarize them here, although further detailed measurements are in progress.

TABLE I. Acceptor = Iodine, d = donor, s = solvent, c_1 = donor concentration, % vol., c_2 = iodine concentration, ρ = ratio of intensities of new band and "undisplaced" band.

d	s	c_1	c_2	New band (cm^{-1})	Probably connected with band at cm^{-1}	ρ
Mesitylene	d	100	sat.	1297		
	CS_2	15	sat. in CS_2	1297		
Diethyl ether	d	100	sat.	nil		
	CS_2	15	sat. in CS_2	1098	1119 (ν_{COC})	$\frac{1}{4}$
Dioxane	d	100	sat.	830	875 (ν_{COC})	
	CS_2	15	sat. in CS_2	830	875	
				1098	1119 (ν_{COC})	
Tetrahydro-furan	d	100	sat.	842		
				880?		
				1052	1070 (ν_{COC})	
Ethylacetate	CS_2	15	sat. in CS_2	1698	1718 (ν_{CO})	$\frac{1}{4}$
				1231?	1291	
Acetone	d	100	<sat.	~1690	~1710 (ν_{CO})	
	CS_2	15	sat. in CS_2	1698	1718 (ν_{CO})	~1
Methyl ethyl ketone	d	100	<sat.	~1696	~1714 (ν_{CO})	
Methyl n-hexyl ketone	CS_2	15	sat. in CS_2	1700	1717 (ν_{CO})	~1
				1207?	1219	
Acetophenone	CS_2	15	sat. in CS_2	1658	1678 (ν_{CO})	~1
	CCl_4	15	sat. in CCl_4	1658	1678 (ν_{CO})	$\frac{1}{4}$
Benzophenone	CS_2	15	sat. in CS_2	1623	1640 (ν_{CO})	~1
				1244?	1260	
	CCl_4	15	sat. in CCl_4	1623	1640 (ν_{CO})	$\frac{1}{4}$
Dibenzylidene ketone	CS_2	15	sat. in CS_2	1639	1655 (ν_{CO})	~1
	CCl_4	15	sat. in CCl_4	1639	1655 (ν_{CO})	~$\frac{1}{4}$

TABLE II.

d	New band (cm^{-1}) for Sat. I_2 in 100% d	15% d in CS_2 sat. with I_2	15% d in CCl_4 sat. with I_2	Probably connected with band at cm^{-1}	d	New band (cm^{-1}) for Sat. I_2 in 100% d	15% d in CS_2 sat. with I_2	15% d in CCl_4 sat. with I_2	Probably connected with band at cm^{-1}
Pyridine			~1628?	1616	α-Picoline		1379	1378	1374
	1453	1441	~1446	1441			1237		1232
	1241	1239					1150 1155		1146
	1207	1208		1215		1109	1107		1101
		1150		1144			1054?		1045
	1060	1064		1067		1010	1008		999
	1005	1004				986	983		974?
	~755	752		750		801	801		798
		~700		~703			~750		~746
						714	714		724
							3150		3000
β-Picoline	2490?	2490		2450	γ-Picoline	2480?	2470		2440
	1591			1572			1608		1598
		1258		1225?		1243?	1240		1218 1210
	1187	1187		1190			1115 1095		
	1122?			1126		1064	1067		1069
	1099	1098		1104		1025			1039?
	1049 1058	1050		1040		1011	1008		994
	816	814 803 786		~785		870			872
	~700	694		~705		709	710 705		720 715

We have first studied the changes, if any, which occur in the infrared absorption spectra of various organic solvents after addition of iodine. Most of the results can be interpreted by assuming that the solvent molecule behaves as a donor to the iodine molecule, forming complex, small shifts in position of certain bands of the solvent then being observed. The most pronounced effects occur in those cases where the donor action is attributable essentially to a particular atom, and the shifts occur mainly in bands associated with motions of such atoms. The nature of the iodine complexes has been discussed by Mulliken[3] in connection with ultraviolet measurements of Benesi and Hildebrand,[4] and dipole studies of Fairbrother[5] and Kortüm.[6]

We have explored the phenomenon further by use of a mixed dilute solution of iodine with any one of the donor substances which were used as solvents as described above, in an "inert" solvent such as carbon disulfide or carbon tetrachloride. The use of such dilute solutions in longer path length brings out the characteristic spectral features more fully, and it seems likely that in this way quantitative measurements can be made on the equilibrium for the formation of the complex.

In certain cases, as with pyridine and the picolines, the spectral changes are more numerous. In these cases, the donor-acceptor action may proceed further, perhaps to the extent of formation of ionic molecules, $[Py\,I]^+\cdot[I]^-$ or of ions, $[Py\,I]^+$ and $[I]^-$, as suggested for iodine in pure pyridine from measurements on electrical conductivity by Audrieth and Birr.[7] The spectral features observed are unaffected by careful drying of the solvent.

Typical results are given in Tables I and II. No effects have been found using as solvent donor carbon disulfide, carbon tetrachloride, acetonitrile, benzene, toluene, xylenes, or 2.6 dimethyl naphthalene. The rough measures of intensity recorded were based upon peak heights, and more accurate determinations are in progress. Variable results were found with acetone unless it had been carefully dried; if damp, chemical iodination occurs giving rise to new absorption bands different from those listed here. With benzophenone, this slow chemical reaction does not occur, presumably because no methylene group lies contiguous to the carbonyl group. With dibenzylidene ketone and several other compounds there are a few spectral changes not listed here which are being examined further.

With pyridine and the picolines, addition of iodine causes some changes of intensity of certain bands, as distinct from shifts in position, e.g., in the bands near 3000 cm^{-1} when the mixture is studied in carbon disulfide or carbon tetrachloride. Also, in presence of iodine, a strong new band appears near 1000 cm^{-1} with the nitrogen ring compounds.

Details will be published later elsewhere, together with similar measurements in which cyanogen iodide is used as the "acceptor molecule."

* Visiting Fulbright Scholar 1952–1953, permanent address: University of Chicago, Chicago, Illinois.

[1] Pimentel, Jura, and Grotz, J. Chem. Phys. **19**, 513 (1951).
[2] Hain, Rees, and Walsh, Nature **169**, 110 (1952); J. Chem. Phys. **20**, 1336 (1952).
[3] R. S. Mulliken, J. Am. Chem. Soc. **72**, 600 (1950); *ibid.* **74**, 811 (1952); J. Phys. Chem. **56**, 801 (1952).
[4] H. A. Benesi and J. H. Hildebrand, J. Am. Chem. Soc. **70**, 2832 (1948); **71**, 2703 (1949); **72**, 2273 (1950).
[5] F. Fairbrother, J. Chem. Soc. **1948**, 1051.
[6] G. Kortum and G. Friedheim, Naturforsch. **2a**, 20 (1947).
[7] L. F. Audrieth and E. J. Birr, J. Am. Chem. Soc. **55**, 668 (1933).

A Simplified Algebraic Method for Obtaining Thermodynamical Formulas

HENRY A. BENT
Department of Chemistry, University of Connecticut, Storrs, Connecticut
(Received June 11, 1953)

AN algebraic method is presented whereby relations between thermodynamical first derivatives are easily obtained.

Of the several[1-3] proposed methods for obtaining thermodynamical formulas, Bridgman's is extremely quick and certain provided his "Condensed Collection of Thermodynamical Formulas," portions of which appear in standard references,[4-7] is available. Tobolsky's systematic technique takes slightly longer but requires a familiarity with only the very commonest thermodynamical forms.

It is the purpose of this note to show, perhaps more simply than before, how to obtain thermodynamical formulas from fundamental and generally applicable considerations. The method which is essentially algebraic generates Bridgman's Tables of First Derivatives and extends their scope.

For simple one-component closed systems the internal energy E is a function of the entropy S and the volume V, $E=E(S, V)$, so that

$$dE=(\partial E/\partial S)_V dS+(\partial E/\partial V)_S dV, \tag{1a}$$

or

$$dE=TdS-PdV, \tag{1b}$$

where

$$T=(\partial E/\partial S)_V=T(S, V) \tag{2a}$$

and

$$P=-(\partial E/\partial V)_S=P(S, V). \tag{2b}$$

Now Eq. (1b) written as $dE-TdS+PdV=0$ is clearly linear and homogeneous in the variables dE, dS, and dV with coeffi-

cients 1, $-T$, and P, respectively. Such a system (one equation, three unknowns) has two linearly independent solutions which can be systematically set down if first dV is assigned the value 0 and dS the value 1 giving T for dE and then the $dV-dS$ assignments are reversed yielding $-P$ for dE. These results are tabulated below.

	I	II
dE	T	$-P$
dS	1	0
dV	0	1

Any solution to Eq. (1b) such as dE, dS, and dV equal respectively to 0, P, and T may be expressed as a linear combination of solutions I and II, in this case as $(P)\mathrm{I}+(T)\mathrm{II}$.

From the first solution

$$dE_V/dS_V=T/1,$$

the subscript V indicating that this ratio comes from a solution to Eq. (1b) with $dV=0$ (that is, $V=$constant); this is merely to say that the ratio of the change in E to the change in S along an isometric is T. The usual notation for this is $(\partial E/\partial S)_V=T$. Thus also, from II $(\partial E/\partial V)_S=-P$ and from $(P)\mathrm{I}+(T)\mathrm{II}$ $(\partial S/\partial V)_E=+P/T$.

A nontrivial extension of this point of view is afforded by the set of Legendre-type functions relating to E, TS, and PV; namely $H=E+PV$, $A=E-TS$, and $F=E-TS+PV$. Their differentials together with that for dE, Eq. (1b), give a set of four linear homogeneous equations in eight variables. The two remaining constraints are represented by Eqs. (2a) and (2b) which presumably can be solved for S and V in terms of T and P, thereby conveniently introducing the latter as independent variables. Thus

$$dS=(\partial S/\partial T)_P dT+(\partial S/\partial P)_T dP, \tag{3a}$$

or, from Eq. (1b) and dF,

$$dS=(C_P/T)dT-(\partial V/\partial T)_P dP, \tag{3'a}$$

and

$$dV=(\partial V/\partial T)_P dT+(\partial V/\partial P)_T dP. \tag{3b}$$

Altogether then, we have to do with all possible solutions to the following set of equations.

$$\begin{aligned}
dF &\qquad +SdT &-VdP=0, &\quad (4a)\\
dA &+PdV &+SdT &=0, &\quad (4b)\\
dH &-TdS & &-VdP=0, &\quad (4c)\\
dE &-TdS &+PdV &=0, &\quad (4d)\\
dS &\qquad -(C_P/T)dT &+(\partial V/\partial T)_P dP=0, &\quad (4e)\\
dV &\qquad -(\partial V/\partial T)_P dT &-(\partial V/\partial P)_T dP=0. &\quad (4f)
\end{aligned}$$

Again there are only two linearly independent solutions. Setting dP equal to 0 and dT equal to 1, and vice versa, gives very much as before:

	I	II
dF	$-S$	V
dA	$-S-P(\partial V/\partial T)_P$	$-P(\partial V/\partial P)_T$
dH	C_P	$V-T(\partial V/\partial T)_P$
dE	$C_P-P(\partial V/\partial T)_P$	$-T(\partial V/\partial T)_P-P(\partial V/\partial P)_T$
dS	C_P/T	$-(\partial V/\partial T)_P$
dV	$(\partial V/\partial T)_P$	$(\partial V/\partial P)_T$
dT	1	0
dP	0	1

The components of solution I are given by Bridgman as $d(\ )_P$; those of solution II as $-d(\ )_T$. Any linear combination of I and II whose dV component is zero, such as $(\partial T/\partial P)_V\mathrm{I}+\mathrm{II}$, is equivalent to Bridgman's set $d(\ )_V$, and so forth for S, E, H, A, and F.

However, inspection of Eqs. (4a)–(f) shows that in any particular instance it is scarcely necessary to set down a complete solution such as I or II or some linear combination of these. An example will perhaps show this most clearly.

Suppose for some reason it is desired to evaluate $(\partial A/\partial V)_H$. Imposing the condition $dH=0$ upon Eq. (4c) and then choosing for convenience $dS_H=V$ and $dP_H=-T$ gives upon substituting into Eqs. (4e) and (4f)

$$dT_H=(T/C_P)(V-T(\partial V/\partial T)_P) \tag{5a}$$

and

$$dV_H=(\partial V/\partial T)_P dT_H-T(\partial V/\partial P)_T, \tag{5b}$$

where dT_H in Eq. (5b) is given by Eq. (5a). This essentially completes the problem since from Eq. (4b) $dA_H=-PdV_H-SdT_H$ and as already noted $(\partial A/\partial V)_H=dA_H/dV_H$. [Compare with the solution $(V-T(\partial V/\partial T)_P)\mathrm{I}-(C_P)\mathrm{II}$ which has $dH=0$.] The method is general, and only when $E=$constant is it necessary to solve Eqs. (4e) and (4f) simultaneously.

[1] P. W. Bridgman, Phys. Rev. (2) **3**, 273–281 (1914).
[2] A. N. Shaw, Trans. Roy. Soc. (London) **A334**, 299–328 (1935).
[3] A. Tobolsky, J. Chem. Phys. **10**, 644–645 (1942).
[4] G. N. Lewis and M. Randall, *Thermodynamics* (McGraw-Hill Book Company, Inc., New York, 1923), p. 164.
[5] L. E. Steiner, *Introduction to Chemical Thermodynamics* (McGraw-Hill Book Company, Inc., New York, 1948), p. 228.
[6] S. Glasstone, *Thermodynamics for Chemists* (D. Van Nostrand Company, Inc., New York, 1947), p. 212.
[7] F. D. Rossini, *Chemical Thermodynamics* (John Wiley and Sons, Inc., New York, 1950), p. 128.

Surface Photoconductivity in Cadmium Sulfide Crystals

RICHARD H. BUBE
Radio Corporation of America, RCA Laboratories Division, Princeton, New Jersey

(Received June 15, 1953)

THE existence of surface photoconductivity for cadmium sulfide and zinc sulfide crystals has been previously reported.[1] It was shown in a general way that the photosensitivity (microamp photocurrent per lumen of irradiating light) and time constant (time for photocurrent to decrease to one-half of its initial value after cessation of excitation) decreased in the presence of water vapor.

This letter reports the results of a more detailed investigation of the photosensitivity and time constant as a function of excita-

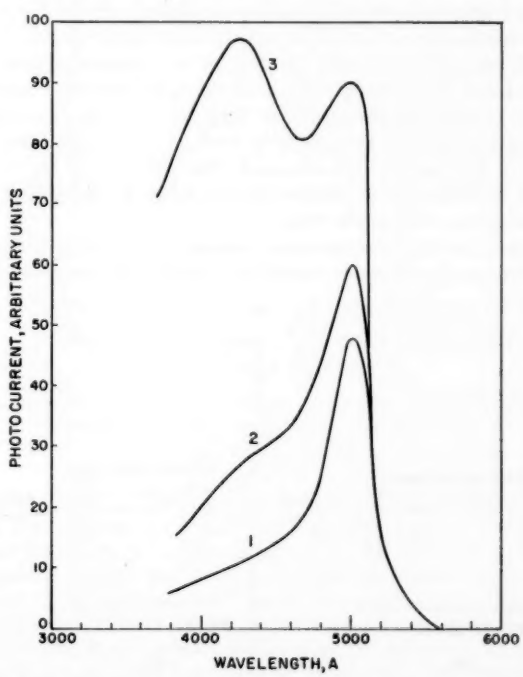

FIG. 1. The relative photocurrent as a function of excitation wavelength for a CdS crystal in an atmosphere of (1) 100 percent humidity at atmospheric pressure, (2) 50 percent humidity at atmospheric pressure, and (3) a vacuum of 10^{-2} mm Hg.

tion wavelength for various concentrations of water vapor in the atmosphere around a CdS crystal. It is found that the presence of water vapor decreases the photosensitivity and time constant for excitation wavelengths shorter than the absorption edge of CdS but does not affect the photosensitivity and time constant for excitation wavelengths longer than the absorption edge. The changes caused by water vapor are reversible. On the assumption that the conductivity of the surface is less than that of the volume in the absence of water vapor, the results may be explained in terms of a model whereby the presence of water vapor increases the conductivity of the surface, thereby increasing the recombination rate for electron-hole pairs generated at the surface.

The CdS crystals were grown[2] by a modified Frerichs technique;[3] the size of the crystal for which data in this letter are given was $3\times2\times0.1$ mm². For excitation by a 100-watt incandescent lamp, the sensitivity in an atmosphere of 100 percent humidity at atmospheric pressure was 9000 μa/lumen, and in a vacuum of 10^{-2} mm Hg, the sensitivity was 31 000 μa/lumen.

The excitation spectra for photoconductivity are given in Fig. 1 for the crystal at atmospheric pressure in 100 percent humidity and 50 percent humidity, and in a vacuum of 10^{-2} mm Hg. The values of the photoconductivity time constants are given in Table I as a function of excitation wavelength. If, for the same wavelengths, the ratio of photocurrents given in curves 3 and 1 of Fig. 1 are compared with the ratio of time constants given in Table I, it is found that the two ratios are approximately the same. These results indicate that the increase in blue sensitivity, obtained by placing the crystal in vacuum, is associated simply with an increase in time constant. The function of the water vapor, therefore, is to provide a mechanism for increasing the recombination rate at the surface.

TABLE I. Photoconductivity time constant as a function of excitation wavelength.[a]

Wavelengths, A	Time constant, milliseconds: Crystal in 100 percent humidity	Crystal in vacuum	Ratio of time constants
3910	0.7	4.5	6.4
4320	1.3	5.4	4.2
4730	2.0	6.2	3.1
5000	3.8	8.6	2.3
5110	23	25	1.1
5350	18	20	1.1

[a] Time constants measured at constant photocurrent for all wavelengths; constant photocurrent maintained by varying excitation intensity.

Such a mechanism is described schematically in Fig. 2. Figure 2(a) represents the energy bands of a crystal with water vapor on the surface, so that the surface conductivity is approximately the same as the volume conductivity. There is little difference between excitations (1) at the surface and (2) in the volume. Because blue light is more heavily absorbed by the CdS than green or yellow light, blue light produces a denser excitation (in surface regions) than does green or yellow llght (in surface plus volume regions). The result is a smaller time constant for the blue excitation than for the green or yellow excitation. The fact that the sensitivity is less for blue than for green cannot be attributed, however, to the difference in density of excitation (for a linear variation of photocurrent with irradiating blue light intensity is found) but must be attributed to an essential difference in the nature of the surface and the volume.

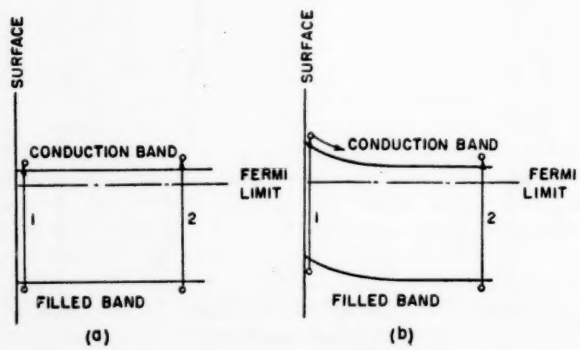

FIG. 2. Energy band diagrams for (a) crystal in an atmosphere of 100 percent humidity at atmospheric pressure, with equal surface and volume conductivity, and (b) "dry" crystal in vacuum with smaller surface than volume conductivity.

Figure 2(b) represents the energy bands of a "dry" crystal, for which the surface conductivity is smaller than the volume conductivity. Excitation in the volume (2) is the same as for Fig. 2(a), but excitation at the surface (1) now produces a hole which is held near the surface and an electron which moves away from the hole toward the volume. The recombination rate at the surface is therefore decreased. The result is an increased photosensitivity and time constant for blue excitation but no change in photosensitivity and time constant for green or yellow excitation.

[1] R. H. Bube, Phys. Rev. **83**, 393 (1951).
[2] Crystals grown by S. M. Thomsen.
[3] R. Frerichs, Phys. Rev. **72**, 594 (1947).

The Rotational Raman Spectrum of Benzene Vapor*

B. STOICHEFF†
Division of Physics, National Research Council, Ottawa, Canada
(Received May 18, 1953)

RECENT advances in experimental methods have made high-resolution Raman spectroscopy feasible. The development of the Toronto-type mercury lamp of high intensity[1] and the introduction of a multiple-traversal mirror system in a Raman tube[2] have stimulated a renewed attempt to photograph rotational structure in the Raman spectra of gases. With further improvements in apparatus in this laboratory, it has been possible to photograph in the second order of a 21-ft grating spectrograph, the Raman spectra of the gases H_2 and N_2 at a pressure of one atmosphere. The initial success of the new Raman techniques in the study of the diatomic molecules was most encouraging. It raised the hope that, with the resolving power available ($\approx$100 000), it might be possible to resolve the rotational structure in the spectrum of benzene and thus to evaluate the moment of inertia of this molecule.

The high-intensity source used in this laboratory consists of a mirror-type Raman tube equipped with mirrors of high reflectance[3] and irradiated along 80 cm by two powerful mercury lamps of new design. The lamps are operated at 25 amperes and are externally water-cooled along their entire one-meter length. This construction facilitates the enclosure of Raman tube and lamps in a diffuse reflector of magnesium oxide[4] with which a five- to tenfold gain in light intensity is realized. In the present investigation the Raman tube was heated to 61°C and filled with benzene vapor at about one-half an atmosphere. A 21-ft concave grating, blazed to give maximum intensity in the second order of 5000A, was used to photograph the Raman spectrum excited by the Hg 4358 line. The slit width was 0.03 mm. Under these conditions, the strong rotational Raman spectrum shown in Fig. 1 was photographed on a Kodak 103a-0 plate in 7 hr.

Past work on the vibrational spectram of benzene[5] gives strong evidence of the highly symmetrical D_{6h} structure for this molecule, i.e., C_6H_6 is planar and has a sixfold axis of symmetry. For this structure, the Raman selection rules for rotational transitions are $\Delta J=0, \pm1, \pm2$; $\Delta K=0$ and therefore the pure rotational Raman spectrum should consist of two branches,

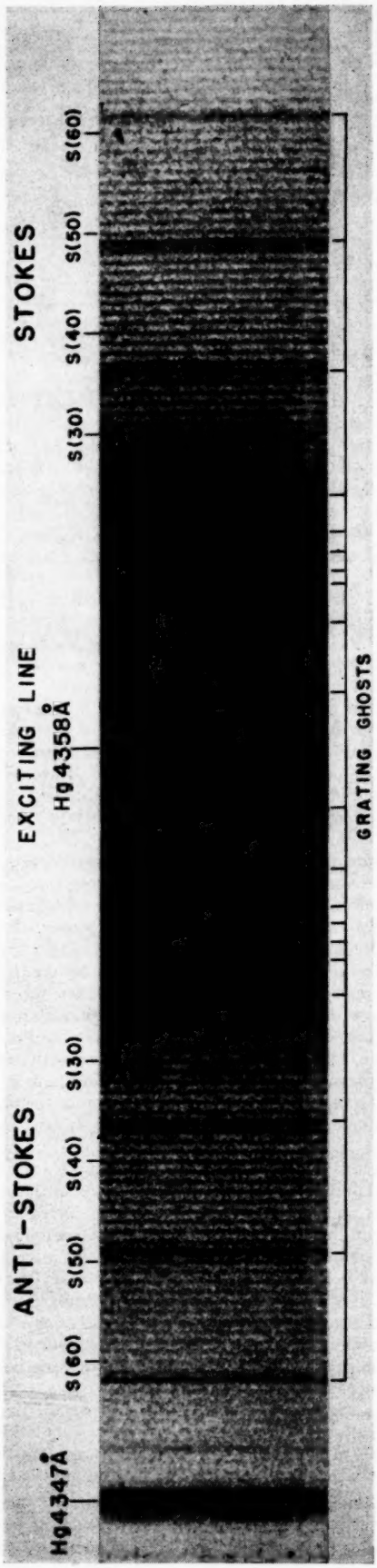

FIG. 1. The pure rotational Raman spectrum of benzene vapor photographed in the second order of a 21-ft grating. The vapor pressure of benzene was ½ atmos. The linear dispersion at λ4358 is 6.75 cm^{-1}/mm, and the resolving power is in excess of 100 000.

$R(\Delta J=+1)$ and $S(\Delta J=+2)$, on either side of an undisplaced line ($\Delta J=0$). The S branches, with spacing $4B$, will have double the spacing of the R branches and hence will extend twice as far from the exciting line.

The main feature of the observed rotational spectrum is a series of sharp lines separated by about 0.75 cm^{-1} and extending from 20 to about 50 cm^{-1} on both sides of the exciting line. Although most of the detail in the neighborhood of the Hg 4358 line is masked by intense grating ghosts, a few lines with half the spacing of the main series can be identified. Thus, in agreement with the predicted spectrum for a symmetric top, there is some evidence of the presence of R branch lines in addition to the main series of lines which constitute the S branches. The Raman displacements for the S branches are given by

$$|\Delta\nu| = (4B_0-6D_J)(J+\tfrac{3}{2})-4D_{JK}K^2(J+\tfrac{3}{2})-8D_J(J+\tfrac{3}{2})^3,$$

where the last two terms are corrections for centrifugal distortion.[6] The second term predicts a splitting of each "line." However, since the observed lines are sharp this term is neglected here. Thirty-five lines in each of the Stokes and anti-Stokes S branches were measured with an accuracy of ± 0.03 cm^{-1}. A graph of $|\Delta\nu|/(J+\frac{3}{2})$ plotted against $(J+\frac{3}{2})^2$ yields the values $B_0 = 0.18955 \pm 0.00005$ cm^{-1} and $D_0 \approx 1.2\times10^{-6}$ cm^{-1}. Hence the effective moment of inertia of C_6H_6 about an axis in the plane of the molecule is $I_0 = (147.64\times0.04)\times10^{-40}$ g cm^2. Although the data on C_6H_6 alone are not sufficient for the determination of bond lengths in benzene, the range of compatible values can be given. A C−H distance in the range 1.06–1.09A seems reasonable, and together with the assumption of a plane hexagonal structure it leads to a value of 1.396–1.401A for the C−C distance in benzene. It is hoped that benzene-d_6 will soon be available for a similar study in order to calculate the C−H and C−C distances independently.

A detailed account of this wor, will be published in the *Canadian Journal of Physics*.

I am indebted to Mr. G. Ensell for help in the design and construction of the lamps, and to Dr. A. F. Turner and Dr. H. H. Schroeder, Jr. for supplying me with mirrors of high reflectance. Also, I wish to thank Dr. G. Herzberg, Dr. A. E. Douglas, and Dr. H. J. Bernstein for several helpful discussions.

* Contribution No. 3037 from the National Research Council of Canada.
† National Research Laboratories Postdoctorate Fellow.
[1] Welsh, Crawford, Thomas, and Love, Can. J. Phys. **30**, 577 (1952).
[2] Welsh, Cumming, and Stansbury, J. Opt. Soc. Am. **41**, 712 (1951).
[3] A. F. Turner and H. H. Schroeder, Jr., of the Bausch and Lomb Optical Company, Rochester, very kindly supplied me with mirrors filmed to give a very high reflectance in the region λλ4000–5500A.
[4] A. C. Menzies and J. Skinner, J. Sci. Instr. **26**, 299 (1949).
[5] See, for example: K. W. F. Kohlrausch, *Der Smekal-Raman-Effekt, Ergänzungsband 1931–1937* (Verlag. Julius Springer, Berlin, 1938); and C. K. Ingold *et al.*, J. Chem. Soc. **1936**, 912–987.
[6] G. Herzberg, *Infra-Red and Raman Spectra* (D. Van Nostrand Company, Inc., New York, 1945), p. 35.

Energy Difference of Rotational Isomers of Some Dihalogenoethanes in the Gaseous and Liquid States

KENJI KURATANI, TATSUO MIYAZAWA, AND SAN-ICHIRO MIZUSHIMA
Chemical Laboratory, Faculty of Science, Tokyo University, Hongo, Tokyo, Japan
(Received June 5, 1953)

IN previous papers[1] we have reported the energy difference ΔE of rotational isomers of 1,2-dihalogenoethanes in the gaseous and liquid states and in solutions. In this short note we shall report some additional data of ΔE obtained from the temperature-dependence of the relative intensity of two absorption bands, one assigned to the *trans*-molecule and the other to the *gauche*-molecule, where the latter molecule differs from the former in an internal rotation about the C−C axis by about 120°. The experimental method and the procedure of calculation of energy difference have been described previously.[2]

In the third column of Table I is shown the excess of energy of the *gauche*-molecule referred to that of the *trans*-molecule in the gaseous and liquid states, and in the fourth and fifth columns the wave numbers of the absorption peaks of the two bands used in the intensity measurement. These data are in general in agreement with, but are more accurate than, those obtained previously by the spectroscopic and electric measurements,[1] and they support

TABLE I. The energy difference ΔE between the rotational isomers in cal/mole.

Compounds	State	$\Delta E = E_g - E_t$	Wave numbers (cm^{-1}) of absorption peaks	
			trans	*gauche*
ClH_2C-CH_2Cl	gas	1140±20	1232	1291
	liquid	{0±50	1451	1430
		{0±50	1230	1284
ClH_2C-CH_2Br	gas	1460±30	1204	1268
	liquid	{420±50	1440	1422
		{410±50	1202	1259
BrH_2C-CH_2Br	gas	1700±40	1187	1251
	liquid	730±50	1437	1420

our view that the decrease of the value of ΔE in the liquid state arises from the molecular interaction, which can be calculated electrostatically.[3] In other words, in the liquid state the *gauche*-molecules with larger moment decrease in their energy much more markedly than the *trans*-molecules, so that the values of ΔE in the liquid state become smaller than those in the gaseous state.

In this connection we should like to add a remark on the predominance of one rotational isomer of $ClH_2C-CHCl_2$ concluded from the dipole measurement of Thomas and Gwinn.[4] This has been confirmed by our infrared measurement, but the less stable isomer exists in an amount still detectable by our spectroscopic measurement, since the disappearance of some absorption peaks takes place on solidification and there is a change of relative intensity of absorption bands between the liquid and nonpolar solution.* For example, the band at 1236 cm^{-1} of the less stable isomer becomes less intense in carbon tetrachloride solution than in the liquid state. From this fact this band can be assigned to the more polar isomer which becomes relatively less stable in a nonpolar solvent.

[1] The summary up to 1949 is given in Mizushima, Morino, and Shimanouchi, J. Phys. Chem. **56**, 324 (1952). See also S. Mizushima, Reilly Lectures, Vol. 5, University of Notre Dame (1952); Morino, Mizushima, Kuratani, and Katayama, J. Chem. Phys. **18**, 754 (1950). The reference to the papers of other authors (including Bernstein, Rank, Kagarise, and Axford) are also given in these papers.

[2] Shimanouchi, Tsuruta, and Mizushima, Sci. Pap. Inst. Phys. Chem. Res. Tokyo **42**, 51 (1944).

[3] Watanabe, Mizushima, and Masiko, Sci. Pap. Inst. Phys. Chem. Res. Tokyo **40**, 425 (1943); S. Mizushima and H. Okazaki, J. Am. Chem. Soc. **71**, 3411 (1949); Morino, Mizushima, Kuratani, and Katayama, J. Chem. Phys. **18**, 754 (1950). In these papers the calculation is made on the assumption of a single dipole located at the center of the molecule. Recently Wada in our laboratory improved the calculation by taking into account individual bond dipoles.

[4] J. R. Thomas and W. D. Gwinn, J. Am. Chem. Soc. **71**, 2785 (1949).

* As to the significance of these spectral changes, see the first two papers of reference 1.

Anomalous Diffusion of Acetone into Cellulose Acetate*

F. A. LONG, E. BAGLEY, AND J. WILKENS
Department of Chemistry, Cornell University, Ithaca, New York
(Received May 18, 1953)

ANOMALOUS or non-Fickian diffusion of small molecules in polymers has been reported for several systems[1–5] and appears to be the normal behavior when the polymer-penetrant mixture is below its second-order transition.[4,5] The anomalies are particularly marked for diffusion into cellulosic polymers.[2,3] For the kinetics of sorption of a vapor by a polymer film the major attention has been focused on the anomalous changes in sorption

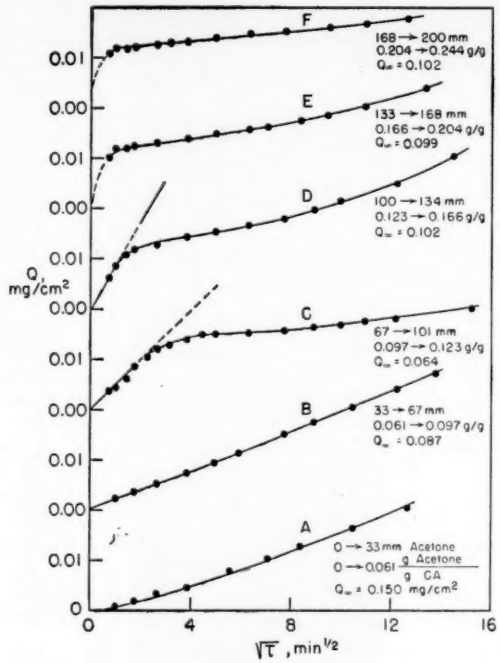

FIG. 1. Interval sorption of acetone into cellulose acetate, 30°C. Plots extend to from 15 to 30 percent of equilibrium takeup. Film thickness is 3.8×10^{-3} cm.

rate which occur at roughly half-time for the total sorption and the tentative explanations so far advanced have dealt essentially with this anomaly.[3,6] We have done some *interval* sorption experiments with acetone and cellulose acetate (37.9 percent acetyl) which put a quite different complexion on the problem since they show that the major anomaly occurs very early in the sorption process.

The procedure and apparatus for interval sorption experiments have been described previously.[4,7] In the present case a dry film of cellulose acetate (cast from acetone on mercury) was suspended from a quartz spiral balance and the sorption kinetics followed for a series of successively higher, narrow pressure ranges of acetone. For each interval the film was equilibrated to the particular pressure of vapor before increasing the pressure for the next interval. The results of one set of interval sorptions are given in Fig. 1 as plots of weight takeup Q in mg/cm² *vs* $\sqrt{t}$. (For Fickian diffusion, Q *vs* $\sqrt{t}$ plots are initially linear.) Along with each curve are given the pressure and concentration range of the interval and the value of Q_e, the equilibrium weight increase for the particular interval. Attainment of final equilibrium generally took from four to seven days.

The curves for the two lowest pressure intervals are similar to those reported previously for anomalous diffusion in that they are initially linear, but at later times the slope *increases* leading ultimately to an inflection in the Q-$\sqrt{t}$ plots. Strikingly different behavior is shown by the curves for all subsequent intervals since for these there is an *initial, rapid* weight increase (the "initial stage") followed by a very much slower weight increase (the "slow stage"). Quite clearly the slopes for the "initial stages" increase considerably with increasing concentration of acetone in the film; in contrast the slopes for the "slow stages" are essentially independent of concentration.

Experiments with films of different thickness show that, for a given concentration interval, the value of $t^{\frac{1}{2}}$ for completion of the initial stage increases directly with film thickness. This indicates that the initial phase is not simple due to a buildup of vapor on the surface; in fact it argues strongly that during the initial stage the vapor penetrates the entire film. Fairly direct evidence that this last is true is shown in Fig. 2, which compares the expansion

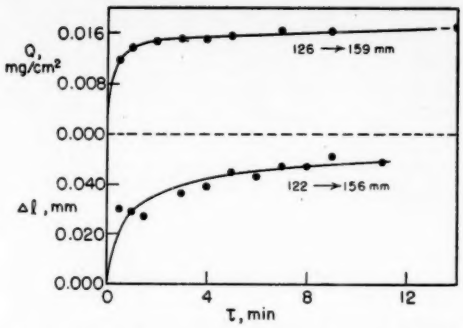

FIG. 2. Comparison of initial change of film length Δl with weight of acetone takeup Q for similar pressure intervals at 30°C. Film thickness is 4.7×10^{-3} cm; length is 3.6 cm.

in length of a film with the acetone takeup for one of the higher concentration intervals. During the rapid initial stage of acetone takeup the film area increases abruptly. The observed length change at the quasi-equilibrium is about half that calculated for isotropic expansion of the polymer, assuming the molar volume of acetone in the film is the same as liquid acetone.

Finally, more detailed sorption and desorption studies suggest that the diffusion in the "initial stage" (but not for the later stages) is Fickian.

A possible explanation for these results is that in the initial stage the diffusion involves an elastic expansion *without* significant destruction of the polymer network and that in the subsequent slow stage the network is being deformed by slow displacement of "cross links." Further studies are in progress with this and related systems.

*Work done under contract with Office of Ordnance Research, U. S. Army.

[1] G. S. Park, Trans. Faraday Soc. **48**, 11 (1952).
[2] L. Mandelkern and F. A. Long, J. Poly. Sci. **4**, 457 (1951).
[3] Drechsel, Hoard, and Long, J. Poly. Sci. **10**, 241 (1953).
[4] Kokes, Long, and Hoard, J. Chem. Phys. **20**, 1711 (1952).
[5] F. A. Long and R. J. Kokes, J. Am. Chem. Soc. (to be published).
[6] J. Crank and G. S. Park, Trans. Faraday Soc. **47**, 1072 (1951).
[7] S. Prager and F. A. Long, J. Am. Chem. Soc. **73**, 4072 (1951).

Free-Electron Network Model for Conjugated Systems. IV*†

CHARLES W. SCHERR
Laboratory of Molecular Structure and Spectra, Department of Physics, University of Chicago, Chicago 37, Illinois
(Received June 3, 1953)

THE object of this note is (1) to investigate the bond length against mobile-electron, bond-population curve obtained empirically in the second paper of the present series,[1] and (2) to make some comments on DE- (delocalization-energy) values. It is possible to derive the empirical equation of the aforementioned curve by starting with the same considerations which Coulson[2] used to derive the theoretical form of a similar curve obtained from LCAO MO calculations. Following Coulson, we say the total energy $\mathfrak{F}$, which allows for the compression of the σ bonds, is

$$\mathfrak{F}=\Sigma_\lambda\tfrac{1}{2}k_s(x_\lambda-s)^2+\Sigma_\lambda E_{\pi\lambda};\quad \partial\mathfrak{F}/\partial x_\lambda)_{\text{equil.}}=0 \text{ for all } x_\lambda, \quad (1)$$

where k_s is the single-bond stretching constant, s the ethane carbon-carbon internuclear distance, x_λ the length of bond λ, and $E_{\pi\lambda}$ the π-electronic energy of bond λ. To write $E_{\pi\lambda}$ explicitly, we assume (1) that the binding energy of the π electrons in bond λ is proportional to $b(\lambda)$, the total mobile-electron population in bond λ, and (gratuitously) (2) that the proportionality factor may be taken as the energy that an ethylene bond would have if the ethylene carbon-carbon internuclear distance were equal to x_λ. Equation 1 is based upon the premise that the orbital energies of the occupied levels are negative; of the unoccupied, positive. Hence, the zero reference level of the free-electron orbital energies must be shifted to the level where $\kappa=\frac{1}{2}\pi$.* We may now rewrite (1) as

$$\left.\begin{aligned}&\mathfrak{F}=\Sigma\tfrac{1}{2}k_s(x_\lambda-s)^2+\Sigma b(\lambda)E_H(a\pi/x_\lambda)^2[(\tfrac{1}{3})-(\tfrac{1}{4})]\\ \text{and}\quad&\partial\mathfrak{F}/\partial x_\lambda=k_s(x_\lambda-s)+b(\lambda)E_H(5/18)x^{-3}a^2\pi^2=0.\end{aligned}\right\}(2)$$

Substituting $E_H=13.596$ev,[3] $a=0.529151$A,[3] $k_s=4.50\times10^5$ dynes/cm,[4] and $s=1.54$A, we obtain for x_λ in angstroms

$$x_\lambda^3(x_\lambda-1.54)+0.372b(\lambda)=0. \quad (3a)$$

The empirical equation, Eq. (7) of II, may be written as

$$x_\lambda=1.52_b-0.1398b(\lambda). \quad (4)$$

Equation (3a) may be approximately compared with Eq. (4) by setting x_λ^3 equal to a mean value, (1.39),[3] leading to

$$x_\lambda=1.54-0.1385b(\lambda), \quad (3b)$$

in a very fine, but perhaps fortuitous, agreement with Eq. (4).

The DE-values for all the molecules treated in II may be computed easily from the tabulated eigenvalues in Table I of that paper. For simplicity, one may use the following:
(for condensed hydrocarbons)

$$\text{DE(kcal)}=\sum_{i=0}^{\frac{1}{2}n}90.90\kappa_i^2-49.84n;$$

(for polyenes)

$$\text{DE(kcal)}=\sum_{i=0}^{\frac{1}{2}n}97.84\kappa_i^2-53.63n,$$

based on D, the free-electron parameter, equal to 1.39 and 1.34A, respectively, and where n is the number of π-electrons. Some of the results are presented in Table I. The results are surprisingly poor, being much too large for small molecules, and occasionally in the wrong order, e.g., styrene and benzene. Nonexistent molecules, however, have satisfactory, relatively small DE-values. This failure, however, is not a serious criticism of the theory, since it is well known that there is almost no justification for the "theoretical calculations" of DE-values, other than that they reproduce experiment remarkably well.[5] In fact, the very simple formula

$$\text{DE(kcal)}=7.2N, \quad (5)$$

where N is the number of bonds in the conjugated system, reproduces the DE-values of the condensed molecules considered in II to within a few kcal (see Table I), so that any theoretical

TABLE I. Calculated delocalization-energy values.

Molecule	Delocalization energy: Free-electron model	Eq. (5)	Experimental[a]
Butadiene	21.4	...	3.5[b]
Hexatriene	45.9	...	6.7[c]
Benzene	99.7	43.2	41
Azulene	103.4	...	46[d]
Naphthalene	122.0	79.2	77
Anthracene	140.6	115.2	116
Phenanthrene	152.9	115.2	130
Pyrene	146.6	129.6	152
Naphthacene	158.5	144	~155[e]
Triphenylene	189.8	151.2	~158[e]
Perylene	177.4	172.8	~180[f]
Styrene	88.2	57.6	51
Diphenyl	158.4	93.8	91
Stilbene	177.9	108.0	101
Nonexistent molecules			
Cyclo-butadiene	−24.9		
Fulvene	36.5		
Pentalene	56.2		
Difulvene	75.8		

[a] Taken from reference 5, p. 81, except as noted.
[b] Heat of hydrogenation data.
[c] Heat of hydrogenation data for cyclo-heptatriene.
[d] E. Heilbronner and K. Wieland, Helv. Chim. Acta **30**, 947 (1943).
[e, f] Estimates made by the present author by a comparison of the heats of combustion reported (e) by A. Magnus and F. Becker, Erdöl u. Kohle **4**, 115–118 (1951), or (f) by J. Syrkin, J. Phys. Chem. URSS **17**, 347 (1943), with reference 5, p. 69.

quantity that happens to increase almost linearly with increasing number of bonds would serve to "predict" the DE-values in such cases.

* This work was assisted in part by the U. S. Office of Naval Research under Task Order IX of Contract N6ori-20 with the University of Chicago.
† This work was assisted in part by the U. S. Office of Naval Research under Task Order IX of Contract N6ori-20 with The University of Chicago.
[1] C. W. Scherr, J. Chem. Phys. (to be published), hereafter referred to as II. See Fig. 4 and Eq. (7).
[2] C. A. Coulson, Proc. Roy. Soc. (London) **A169**, 413 (1939).
[3] This point will be considered in detail by K. Ruedenberg in a forthcoming paper of this series.
[4] J. W. M. DuMond and E. R. Cohen, Am. Scientist **40**, 447 (1952).
[5] G. Herzberg, *Infra-Red and Raman Spectra of Polyatomic Molecules* (D. Van Nostrand Company, Inc., New York, 1945), p. 193.
[6] See, e.g., G. W. Wheland, *The Theory of Resonance* (John Wiley and Sons, Inc., New York, 1944), p. 79.

Raman Spectrum and Cathodo-Luminescence Spectrum of Aluminum Phosphate

B. D. SAKSENA
National Physical Laboratory of India, New Delhi, India
AND
L. M. PANT
University of Allahabad, Allahabad
(Received June 2, 1953)

ALUMINUM phosphate, according to Hittenlocher,[1] has a lattice similar to that of quartz. Strada[2] reports the preparation of cristobalite form of $AlPO_4$ and Gruner,[3] of low quartz, low trydimite, and low cristobalite structures. According to Brill and De Bretteville,[4] quartz type $AlPO_4$ has a hexagonal lattice and has nearly the same a axis as quartz (4.975A against 4.903A for quartz), while the c axis is doubled (10.84A against 5.39A for quartz). Measurements of the intensities of x-ray reflections indicate that the P—O distance is smaller than the Al—O distance, and the authors conclude that a large amount of ionic binding is present. The thermal analysis of quartz type of $AlPO_4$ by Hummel[5] shows that the temperature of inversion is very close to the transition temperature of high and low quartz. The elastic and the piezoelectric constants[6] of both substances are of the same order. The data so far obtained indicate that $AlPO_4$ more closely resembles SiO_2 structurally than any other natural or artificial mineral, and it is therefore of great interest to see whether they also resemble each other in their spectra.

The Raman spectrum, taken with a two prism Hilger spectrograph, is shown in spec. a (Fig. 1). In the 4358A excitation, the

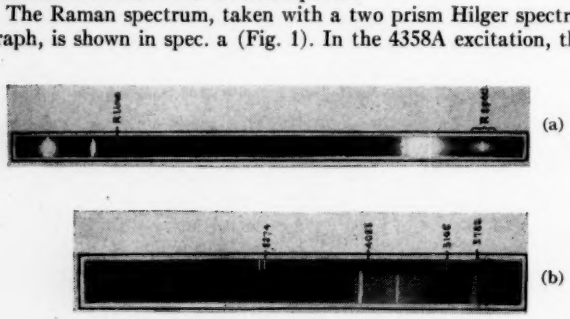

FIG. 1. (a) Raman spectrum of aluminum phosphate. (b) Cathodo-luminescence spectrum of aluminum phosphate.

continuous spectrum extends from 4407A to 4431A, i.e., 112 cm^{-1}. There are two Raman lines, one strong at 320 cm^{-1} and the other weak at 356 cm^{-1}. The stronger Raman line may also be seen in the 4046A excitation.

The cathodo-luminescence spectrum is shown in spec. b (Fig. 1), and its microphotometer curve in Fig. 2. There are two bands, whose band extensions and regions of maximum intensity are shown in Table I.

The crystal first fluoresces very faintly with yellow color, later more strongly with blue color. The crystal became milky and bluish after exposure to cathode rays. The cathode-ray tube was run at nearly 40 000 volts.

TABLE I.

Band extension	Band peak	Intensity
6300–5500A	5750A[a]	v. weak
5000–3700A	4600–4400A	weak

[a] This region of maximum sensitivity occurs in most of the plates and may be due to increased sensitiveness of plates in this region and the presence of two mercury lines.

Both the Raman and cathodo-luminescence spectra of $AlPO_4$ show considerable deviations from the corresponding spectra for α quartz.

In the cathodo-luminescence spectrum of α quartz[7] there is a prominent continuum in the region 6550–5650A, while the continuum between 4900A and 3500A is very faint. In $AlPO_4$ the latter continuum which extends from 5000A to 3700A appears with appreciable intensity, while the former continuum is weak. But it is difficult to say that this difference is due to greater ionic character of $AlPO_4$.

The continuum observed in the Raman spectrum of $AlPO_4$ is interesting as no such continuum has been observed in the Raman

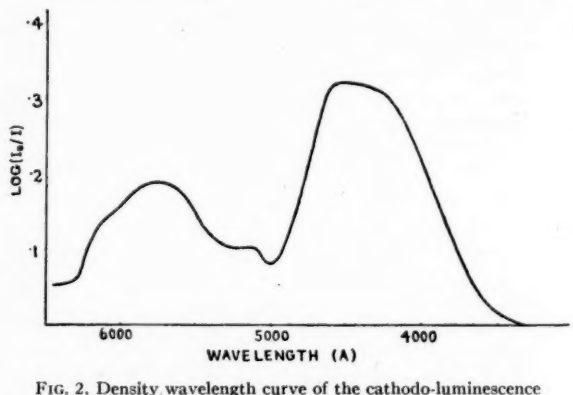

FIG. 2. Density wavelength curve of the cathodo-luminescence spectrum of aluminum phosphate.

spectrum of quartz. Since such continuum is obtained in the secondary Raman spectrum of both diamond and NaCl, it is difficult to say whether it is due to the greater ionic character of $AlPO_4$.

The Raman spectrum of quartz shows a number of frequencies between 128 cm^{-1} to 1200 cm^{-1}, of which the strongest is at 465 cm^{-1}. According to Saksena,[8] this represents the ν_2 vibration of SiO_4 tetrahedron. The strong Raman line at 320 cm^{-1} observed in $AlPO_4$ would represent a frequency of the PO_4 group since the P—O distance is smaller than the Al—O distance and may correspond to the ν_2 vibration of PO_4 group. For the free PO_4 group, this frequency occurs at 363 cm^{-1} (Herzberg).[9] The weaker frequency at 356 cm^{-1} may be an Al—O frequency because the small intensity of this frequency would agree with the greater ionic character of the Al—O bond. The Raman spectrum of alumina (Krishnan)[10] shows two strong and sharp frequencies in this region.

Thanks are due Professor F. Osborne of the Pennsylvania State College for giving us the crystal for study. Thanks are also due the Council of Scientific and Industrial Research for a research grant and a scholarship to one of us (L.M.P.).

[1] H. F. Hittenlocher, Z. Krist. **90**, 508 (1930).
[2] M. Strada, Gazz. Chim. Ital. **64**, 653 (1934).
[3] (a) Gruner, Bull. Geol. Soc. Am. **50**, No. 12, 1163 (1945); (b) Gruner, Am. Miner. Abs. **33**, Nos. 3–4, 197 (1948).
[4] R. Brill and A. De Bretteville, Am. Miner. **33**, Nos. 11–12, 750 (1948).
[5] F. A. Hummel, J. Am. Ceram. Soc. **32**, 320 (1949).
[6] W. P. Mason, *Piezo-electricity of Crystals* (D. Van Nostrand Company, Inc., New York, 1950), pp. 79, 208.
[7] B. D. Saksena and L. M. Pant, J. Chem. Phys. **19**, 134 (1951).
[8] B. D. Saksena, Proc. Indian Acad. Sci. **19**, 357 (1944).
[9] G. Herzberg, *Raman and Infra-Red Spectra of Polyatomic Molecules* (D. Van Nostrand Company, Inc., New York), p. 167.
[10] R. S. Krishnan, Proc. Indian Acad. Sci. **26**, 453 (1947).

The Distortion of Inner Shell Electrons

JOSEPH M. CAHILL AND CHARLES R. MUELLER
Department of Chemistry, Purdue University, Lafayette, Indiana
(Received May 27, 1953)

IN order to study the distortion of inner shell electrons during bonding, hydrides of the first row elements have been taken as a test case. Perturbation theory was applied to calculate the effect of the hydrogen atom at the bonding distance from lithium, carbon, and fluoride. Also, the hydrogen molecule was studied to determine the character of the orbital after molecular formation.

In writing the first-order perturbation potential $H^{(1)}$, the omission of exchange is equivalent to utilizing both the Heitler and London and Mulliken overlap-average approximations.[1] Since the overlap is small, no serious error should result. Thus, the perturbation is expressed as the sum of the potentials existing between the hydrogen atom and the 1*s* orbitals whose distortion is being considered:

$$H^{(1)}=-\frac{1}{r_b}+\int\frac{\psi^2_{1s}}{r_{12}}\,d\tau. \tag{1}$$

To calculate the $H_{mn}{}^{(1)}$ interaction terms, a normalized and orthogonal set of atomic eigenfunctions of the type proposed by Morse, Young, and Haurwitz[2] is used. Transformation to elliptical coordinates facilitates the integration and the terms may be expressed with auxiliary functions. Values computed for the interaction terms are in Table I.

It is seen that the first-order perturbation energy $H_{1s,1s}{}^{(1)}$ is relatively small in all cases. The orbitals lose little of their 1*s* character as may be seen from their eigenfunctions after distortion:

$$\begin{aligned}&\text{Li:}\quad \psi 1s=\psi^\circ 1s+0.00026\,\psi^\circ 2s+0.00067\,\psi^\circ 2p_z,\\ &\text{C:}\quad \psi 1s=\psi^\circ 1s+0.000063\,\psi^\circ 2s+0.00032\,\psi^\circ 2p_z,\\ &\text{F:}\quad \psi 1s=\psi^\circ 1s+0.000025\,\psi^\circ 2s+0.00021\,\psi^\circ 2p_z.\end{aligned}$$

Therefore, neg.ect of the inner shell electrons in molecular calculations becomes a justifiable approximation. It is of interest to note that, although both are small, the 2*p* character is far greater than the 2*s* in the perturbed eigenfunction.

Application of the method to hydrogen varies from the previous and makes the terminology "inner shell" electrons rather weak. However, the results seem somewhat more significant, since the first-order perturbation energy for hydrogen is -0.109 atomic unit. This ascribes to the individual electron in the molecule a twenty percent energy increase over the -0.500 atomic unit it had in the atom.

Characterization of the distorted orbital

$$\psi 1s=\psi^\circ 1s+0.0603\,\psi^\circ 2s+0.0875\,\psi^\circ 2p_z \tag{2}$$

suggests, from the ratio of the coefficients, an sp^2 hybridization. So, upon bonding, the distorted portion of the atomic orbital assumes a form similar to that in a trigonal hybrid.

Coulson and Fischer,[3] employing the variational theorem, describe the atomic orbital in the hydrogen molecule as

$$\psi 1s_a=\psi^\circ 1s_a+0.15\,\psi^\circ 1s_b. \tag{3}$$

Expanding $\psi^\circ 1s_b$ in terms of a normalized set of eigenfunctions on "*a*,"

$$\psi^\circ 1s_b=S1s_b,1s_a\psi^\circ 1s_a+S1s_b,2s_a\psi^\circ 2s_a+S1s_b,2p_a\psi 2p_a. \tag{4}$$

Utilizing the overlap integrals of Mulliken *et al.*,[4] the eigenfunction on "*b*" may then be written as

$$\psi^\circ 1s_b=0.753\,\psi^\circ 1s_a+0.516\,\psi^\circ 2s_a+0.348\,\psi^\circ 2p_a. \tag{5}$$

TABLE I. $H_{mn}{}^{(1)}$ terms[a] for lithium, carbon, and fluorine.

System	Li	C	F
$H_{1s,1s}{}^{(1)}$	-3.87×10^{-3}	-2.22×10^{-2}	-4.93×10^{-2}
$H_{1s,2s}{}^{(1)}$	-5.69×10^{-4}	-6.70×10^{-4}	-6.05×10^{-4}
$H_{1s,2p}{}^{(1)}$	-1.50×10^{-3}	-3.47×10^{-3}	-5.39×10^{-3}

[a] 1 atomic unit = 27.205 ev.

Substituting into Eq. (6) shows

$$\psi 1s=1.11\,\psi^\circ 1s+0.0774\,\psi^\circ 2s+0.0522\,\psi^\circ 2p_z \tag{6}$$

for the orbital after bonding.

Both Eqs. (5) and (9) are left unnormalized, since comparison in such form proves adequate for present purposes. Though the results are of the same order, tbis use of the variational method attributes more 2*s* than 2*p* character to the orbital while the opposite obtains with perturbation theory.

However, the more accurate calculations of Rosen[5] and Weinbaum[6] based on the variational theory tend to corroborate the stress of 2*p* character that results from perturbation considerations.

This rather neglected technique of expanding on one atom for molecular problems should be further investigated to determine its practicality in more complex cases. With a variational treatment, a convergent orbital solution for valence electrons would be obtained, though the suitable extent of expansion remains dubious.

Combined with the appropriate exchange "potential," perturbation theory could be used to study the ways hybridization occurs in the molecule. With both methods, the necessity of making the usual restrictive assumptions, such as orthogonality, would not be present.

[1] C. R. Mueller, J. Chem. Phys. **20**, 1600 (1952).
[2] Morse, Young, and Haurwitz, Phys. Rev. **48**, 948 (1935).
[3] C. A. Coulson and I. Fischer, Phil. Mag. **40**, 393 (1949).
[4] Mulliken, Rieke, Orloff, and Orloff, J. Chem. Phys. **17**, 1248 (1949).
[5] N. Rosen, Phys. Rev. **38**, 2099 (1931).
[6] S. Weinbaum, J. Chem. Phys. **1**, 317 (1933).

Nuclear Quadrupole Resonance of Bromine in Molecular Solids

S. KOJIMA, K. TSUKADA, S. OGAWA, AND A. SHIMAUCHI
Department of Physics, Tokyo University of Education, Otsuka, Tokyo, Japan
(Received June 8, 1953)

ABSORPTION lines due to nuclear electric quadrupole resonance of the bromine isotopes Br^{79} and Br^{81} in some molecular solids have been observed by the method of super regenerative detection. The resonance frequency and the intensity of measured lines are given in Table I. The strong absorbing lines generally were sharp, having a line width of about 10 kc, and the weak lines were broad. From the data on sharp lines the ratio of the resonance frequencies of Br^{79} and Br^{81} isotopes was determined as 1.1970 ± 0.0001.

By summarizing the data on methyl bromide, which was already measured by Dehmelt and Krüger,[1] and on the newly studied three alkyl bromides, it is revealed that the resonance frequency is not a smooth function of the number of carbons in the alkyl radical. To examine this relation further we have measured the resonance of the iodine isotope in alkyl iodides, such as CH_3I,

TABLE I. Quadrupole resonance frequencies (Mc/sec).

Compound	ν [Br^{79}]	ν [Br^{81}]	Temperature	Intensity
C_2H_5Br	248.52 ± 0.03	207.61 ± 0.03	liquid air	strong
$n-C_3H_7Br$	251.49 ± 0.02	210.09 ± 0.01	liquid air	strong
$n-C_4H_9Br$	249.96 ± 0.03	208.86 ± 0.03	liquid air	medium
C_6H_5Br	264.28 ± 0.03	220.89 ± 0.10	dry ice	weak
$CHBr_3$	299.05 ± 0.30	250.26 ± 0.30	liquid air	weak
	299.32 ± 0.30	250.41 ± 0.30	liquid air	weak
	300.95 ± 0.30	251.71 ± 0.30	liquid air	very weak
$SnBr_4$	188.81 ± 0.03	157.72 ± 0.03	16.7°C	medium
	191.78 ± 0.03	160.29 ± 0.05	16.7°C	strong
	191.91 ± 0.03	160.40 ± 0.05	16.7°C	strong
	192.35 ± 0.03	160.63 ± 0.05	16.7°C	strong
PBr_3	218.68 ± 0.03	182.63 ± 0.03	liquid air	weak
	220.93 ± 0.03	184.52 ± 0.03	liquid air	medium

TABLE II. Quadrupole coupling constants of Br^{79} and I^{127} (Mc/sec) in alkyl halide.

Compound	$eQq(Br^{79})$	$eQq(I^{127})$	Ratio
CH_3X	528.9[a]	1753[b]	3.314
C_2H_5X	497.0	1647	3.314
$n-C_3H_7X$	503.0	1672	3.324
$n-C_4H_9X$	499.9	1660	3.321

[a] Reference 1.
[b] H. G. Dehmelt, Z. Physik **130**, 356 (1951).

C_2H_5I, C_3H_7I, and C_4H_9I. From the observed resonance frequency in these iodides the electric quadrupole coupling constant eQq was estimated.[2] The obtained values are listed in Table II with those of Br^{79}. There exists exact parallelism between bromides and iodides and an irregular relation between the coupling constant and the number of carbons. It is interesting that this irregularity is similar to the relation between the melting point and the number of carbons.

For bromoform, $CHBr_3$, the frequency of the absorption lines have not been reported, though its spectrum was known to have a triplet structure.[1] Previously the authors and others[3] measured the microwave spectrum of bromoform and analyzed it by assuming that the electric quadrupole coupling constant of Br^{79} was 577 Mc/sec. The present measurements yield a coupling constant of about 600 Mc/sec from the resonance frequencies at liquid air temperature or of 590 Mc/sec from those at $-23°C$. Since the known values[4] for CH_3Br, CH_3I, and CH_2Cl_2 indicate that the coupling constant in the gaseous state is about 8 percent larger than that in the solid, the value previously assumed seems to be rather small.

In addition to bromoform, stannic bromide and phosphorous tribromide have multiplets in their absorption spectrum. The multiplet of stannic bromide at room and liquid air temperatures was composed of 4 lines, two of which (the line of the lowest frequency and perhaps the line of the highest frequency) disappeared near the temperature of dry ice. Since stannic bromide has two forms of crystalline structure, the change of multiplicity is probably caused by the transformation of the structure. For phosphorous bromide two lines for each isotope were measured. The observation with a good resolution, however, suggested that the line of higher frequency may separate into two lines.

Full details of the experiment and discussion will be published elsewhere.

[1] H. G. Dehmelt and H. Krüger, Z. Physik **129**, 401 (1951).
[2] The resonance absorption of iodine isotope have been measured only for the transition $m_s = \pm\frac{1}{2} \leftrightarrow \pm\frac{3}{2}$. We estimated the electric quadrupole coupling constant from this absorption frequency by multiplying 20/3. The measurements for the transition $m_s = \pm\frac{3}{2} \leftrightarrow \pm\frac{5}{2}$ will be attempted soon.
[3] Kojima, Tsukada, Hagiwara, Mizushima, and Ito, J. Chem. Phys. **20**, 804 (1952).
[4] See, e.g., C. H. Townes and B. P. Dailey, J. Chem. Phys. **20**, 35 (1952).

Raman Spectrum of Gaseous Ethforane*

J. RUD NIELSEN AND C. W. GULLIKSON
Department of Physics, University of Oklahoma, Norman, Oklahoma
(Received May 29, 1953)

THE Raman spectrum of liquid ethforane (hexafluoroethane) at low temperature was studied by Rank and Pace[1] who assigned the six Raman-active fundamentals and made the interesting observation that the over-all intensity of the Raman spectrum of C_2F_6 is about ten times lower than that of the Raman spectrum of ethane. Nielsen, Richards, and McMurry[2] investigated the infrared spectrum of gaseous C_2F_6 and assigned its five infrared-active fundamentals. The lowest e_u fundamental, which was inferred from combination bands, has recently been confirmed by Mann and Plyler[3] with the aid of a CsI prism. Although Mann and Plyler remark that this is the only C_2F_6 fundamental that could be regarded as uncertain, we have felt for some time that there is also some doubt about the assignment of the Raman band at 1420 cm^{-1} as the highest a_{1g} fundamental.

TABLE I. Raman spectrum of ethforane (C_2F_6).

Gas (30°C) Wave number	Gas (30°C) Description	Gas (30°C) Exciting Hg lines	Liquid (−78°C) Wave number	Liquid (−78°C) Description	Interpretation
348	*w,Q*	*e*	349	10 *sh,mp*	a_{1g} fundamental
372	*w,d*	*e*	380	10 *b,dp*	e_g fundamental
619	*w,d*	*e*	620	10 *b,dp*	e_g fundamental
			655	1	
807.4	*vs,Q*	*efki*	809	50 *sh,sp*	a_{1g} fundamental
1250	*vw,d*	*e*	1237	4 *b,dp*	e_g fundamental
1417	*vw,Q*	*e*	1420	5 *b*	a_{1g} fundamental

Rank and Pace were unable to determine the polarization of this band, but reported that it has a broad appearance. This would be expected if it were interpreted as the combination $620(e_g)+809(a_{1g})=1429(E_g)$. Furthermore, the value 1420 cm^{-1} seems to be abnormally high. Not only is it considerably higher than any C−F stretching frequency in partially fluorinated ethanes, but it is 40 to 90 cm^{-1} higher than the highest observed Raman frequency in each of the more than a dozen saturated fluorocarbons studied, with the sole exception of cyclobutforane.[4] For these reasons we have considered it of some importance to obtain the Raman spectrum of ethforane in the gaseous state. The sample was kindly supplied by E. I. du Pont de Nemours and Company.

The irradiation apparatus employed for this purpose has been described elsewhere.[5] Exposure times up to nearly 300 hours were used. The results are listed in Table I together with those of Rank and Pace for liquid C_2F_6. The symbol Q in the second column indicates the presence of a zero branch. This branch, which is very prominent in each of the three bands for which it is observed and entirely absent in the other bands, definitely marks the former bands as associated with totally symmetric vibrations. No Raman band was observed in the region from 1350 to 1400 cm^{-1}. Thus our results verify the assignment of the highest a_{1g} fundamental beyond any reasonable doubt.

* This work has been supported by the U. S. Atomic Energy Commission.
[1] D. H. Rank and E. L. Pace, J. Chem. Phys. **15**, 39 (1947).
[2] Nielsen, Richards, and McMurry, J. Chem. Phys. **16**, 67 (1948).
[3] D. E. Mann and E. K. Plyler, National Bureau of Standards Report No. 2157 (1953).
[4] Smith, Nielsen, Berryman, Claassen, and Hudson, Naval Research Laboratory Report No. 3567 (1949).
[5] H. H. Claassen and J. Rud Nielsen, J. Opt. Soc. Am. **43**, 352 (1953).

Structure of HNCS from Microwave Spectra*

G. C. DOUSMANIS, T. M. SANDERS, JR., C. H. TOWNES, AND H. J. ZEIGER†
Columbia University, New York, New York
(Received June 15, 1953)

THE microwave spectrum and structure of isothiocyanic acid were reported some time ago.[1] More accurate and detailed information on the structure is obtained below from additional measurements of the HNCS spectrum and the quadrupole coupling constant of S^{33} in this molecule is evaluated.

The quadrupole coupling constant of N^{14} in HNCS is so small (+1.2 Mc)[2] that its effect on the spectrum could be neglected within the accuracy of the present measurements. The quadrupole coupling constant of S^{33} obtained from the hyperfine lines listed in Table I is -27.5 ± 0.8 mc. It is not surprising that this is very close to the S^{33} coupling constant in OCS.

The expected frequencies, on a rigid rotator basis, of the observed transitions $1_{11;0}\rightarrow2_{12;-1}$, $1_{01;-1}\rightarrow2_{02;-2}$, and $1_{10;1}\rightarrow2_{11;0}$ are $\nu_1=3C+B$, $\nu_2=2B+2C+\frac{3}{2}(B-C)^2/(2A-B-C)$, and $\nu_3=3B+C$, respectively. The additional term depending on $(B-C)^2$ in the expression for ν_2 is $\sim 1KC$, so that within experimental error ν_2 should be equal to $(\nu_1+\nu_3)/2$. It can be seen from Table I,

TABLE I. Observed frequencies of HNCS in megacycles/sec. The errors in individual lines may be as large as 0.50 Mc.

Rotational transition	$HN^{14}C^{12}S^{34}$	$DN^{14}C^{12}S^{32}$	Rotational transition	$HN^{14}C^{12}S^{32}$ Hyperfine transition	
$1_{11;0} \rightarrow 2_{12;-1}$	22874.59	21841.04		$F=1/2\rightarrow 3/2$	23167.89
				$5/2\rightarrow 5/2$	
$1_{01;-1} \rightarrow 2_{02;-2}$	22906.79	21891.66	$1_{01;-1} \rightarrow 2_{02;-2}$	$1/2\rightarrow 1/2$	
				$3/2\rightarrow 5/2$	23174.56
				$5/2\rightarrow 7/2$	
$1_{10;1} \rightarrow 2_{11;0}$	22946.47	21951.82		$3/2\rightarrow 3/2$	23179.70

however, that $(\nu_1+\nu_3)/2$ is greater than ν_2 by more than 4 Mc; hence $(B+C)/2$ as determined from ν_1 and ν_3 is greater than $(B+C)/2$ as given by ν_2 by about 1 Mc for the various isotopic species (see Table II). Centrifugal distortion of the molecule for

TABLE II. Rotational constants of HNCS in megacycles/sec. Errors in $2(B-C)$ are less than 0.1 Mc, whereas the errors in $\frac{1}{2}(B+C)$ may be larger.

Molecule	$K=1$ $2(B-C)$	$K=1$ $\frac{1}{2}(B+C)$	$K=0$ $\frac{1}{2}(B+C)$
$HN^{14}C^{12}S^{32}$	75.0[a]	5865.5[a]	5864.5[a]
$HN^{14}C^{13}S^{32}$			5793.5[b]
$HN^{14}C^{12}S^{34}$	71.88[b]	5727.6[b,c]	5726.7[b]
$HN^{14}C^{13}S^{32}$		5847.3[a]	
$DN^{14}C^{12}S^{32}$	110.78[b]	5474.1[a,b]	5472.9[b]
$DN^{14}C^{13}S^{32}$		5459.8[a]	

[a] Reference 1.
[b] Present work.
[c] This value is 1.1 mc lower than in reference 1.

the transitions ν_1 and ν_3, as a result of the unit angular momentum ($K=1$) about the axis of smallest moment of inertia (A axis), gives satisfactory account of the observed changes in the rotational constants. The fractional increase in the NH bond length due to an angular momentum of unity around the A axis is of order $(\omega \text{ rot})/(\omega \text{ vib})^2$ and would *decrease* the rotational constants B and C by less than 0.1 Mc, which is of the order of the experimental error. Bending of the NH bond, however, can increase these rotational constants by the observed amount.

There are enough data on the transitions of the various isotopic species of HNCS containing light hydrogen to determine completely the structure when $K=1$. The results are given in Table III. The calculated values of the rotational constants of the

TABLE III. Structural parameters of HNCS.

	($K=1$ state) C–S distance	C–N distance	NH or ND distance	Angle CNH or angle CND
HNCS	1.5609 ±.0020A	1.2158	1.013	130° 15′ ±15′
DNCS	1.5609	1.2158	1.003	132° 16′

deuterated molecules, assuming their structure to be the one determined above from the H[1] data, differ from the experimental values by no less than 8 Mc. This difficulty arises from zero-point vibrations. It can be resolved, as in other cases,[3] by allowing for a change in the effective values of the CNH angle and NH bond length upon substitution of deuterium for hydrogen, assuming that this substitution does not affect the structure of the rest of the molecule.[4] The DNCS frequencies then determine the ND distance to be 10 mA smaller and the NCD angle 2° greater than in HNCS (Table III). The structural parameters listed in Table III fit all the observed constants $\frac{1}{2}(B+C)$ with a rms error of 0.25 Mc. The constants $2(B-C)$ depend strongly on the distance of the hydrogen nucleus from the NCS axis and were fitted to an accuracy better than 0.1 Mc in order to determine accurately the NH distance and NCH angle. The structural parameters are accurate to ±0.002A and ±15′. This structure agrees with those previously given [1,5] to within 0.01A and 5° which are of the order of the stated uncertainties in the previous determinations.

The primary effect of centrifugal distortion is to bend the NH bond, so that the angle in the $K=0$ state (ν_2) is expected to be different from that in $K=1$ (ν_1 and ν_3). Assuming that the internuclear distances in $K=0$ are the same as those given in Table III for $K=1$, the values of the angle for $K=0$ obtained from the ν_2 frequencies are 130° 32′ for HNCS and 132° 27′ for DNCS. Hence an angular momentum of unity around the A axis bends the NH bond by 17′ for H and 11′ for D, and from this bending a force constant equal to $(2.7\pm0.6)\times10^{-12}$ dyne cm/rad can be computed.

The changes in the effective structure upon isotopic substitution depend strongly upon the relative values of the harmonic and anharmonic force constants and upon the zero-point vibrational energy. Using the values of the CNH and CND angles given in Table III and the force constant mentioned above, we derive an approximate shape of the potential well for the bending vibration. This approximate potential function gives an equilibrium angle of 136° and a classical total amplitude for the hydrogen zero-point vibration of 26°(+11° and −15° about the equilibrium angle).

* Work sponsored jointly by the Signal Corps and U. S. Office of Naval Research.
† Carbide and Carbon Chemical Corporation Postdoctoral Fellow, now at Lincoln Project, M.I.T.
[1] C. I. Beard and B. P. Dailey, J. Chem. Phys. **18**, 1437 (1950); **19**, 975 (1951).
[2] Shoolery, Shulman, and Yost, J. Chem. Phys. **19**, 250 (1951).
[3] Miller, Aamodt, Dousmanis, Townes, and Kraitchman, J. Chem. Phys. **20**, 1112 (1952); Bak, Bruhn, and Rastrup-Andersen, J. Chem. Phys. **21**, 752 (1953).
[4] In HCN substitution of D for H does affect the NC bond [Douglas and Sharma, J. Chem. Phys. **21**, 448 (1953)]. Such effects, however, as well as the changes of bond distances due to substitution of C and S isotopes, would change the rotational constants by an amount which is of the order of our experimental error.
[5] C. Reid, J. Chem. Phys. **18**, 1512 (1950). (In particular the angle given in this reference is in good agreement with the present one.)

The Production of Iodine from Solutions of Potassium Iodide Irradiated with Hard X-Rays*

EVERETT R. JOHNSON
Chemistry Department, Brookhaven National Laboratory, Upton, New York
(Received June 1, 1953)

SOLUTIONS of potassium iodide ($3.17M$ to $0.001M$) were irradiated with x-rays from a 2-Mev electrostatic generator made by High Voltage Engineering Corporation, Cambridge, Massachusetts. The iodine formed was determined by measuring the absorption at 350 mμ with a Beckman Model DU Spectrophotometer. The results are plotted as μM/l of I_2 formed *vs* irradiation time in seconds (dose rate = 231.2 μM air-saturated $FeSO_4$ oxid/1000 sec).

Figure 1 shows a plot of rate of I_2 formed as a function of dose for several unbuffered solutions of KI. The initial slope for the 0.027, 0.13, and 0.76 molar solutions is equal, within experimental error, to that found for hydrogen evolution from $10^{-3}-10^{-7}M$ KI solutions[1] (curve A). The same hydrogen yield is obtained from an approximately $0.1M$ KI solution. No iodine was observed in $10^{-3}M$ solutions of KI. The increased yield of I_2 found for the $3.17M$ KI solutions is believed to be due to mass absorption effects. Hydrogen evolution from an approximately $5M$ solution of KI are drawn as curve B. These results, through incomplete, indicate the equivalence of the initial rate of H_2 and I_2 formation from these solutions.

In Fig. 2 are plotted the results obtained by irradiating approximately $0.07M$ solutions of KI in the presence and absence

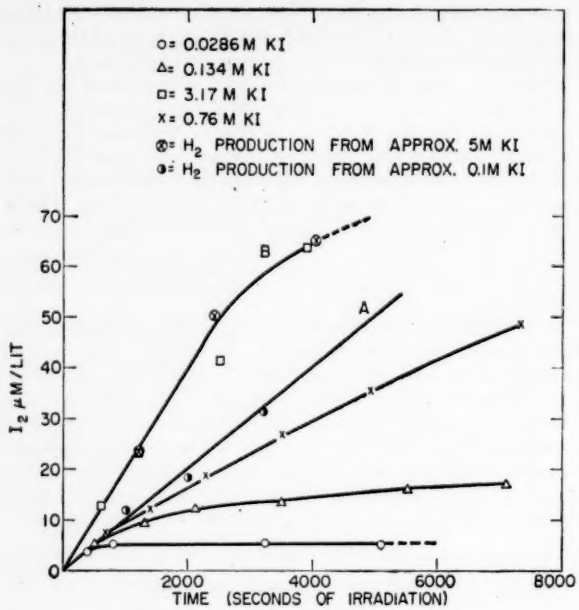

FIG. 1. Iodine formation as a function of dose from unbuffered solutions of KI.

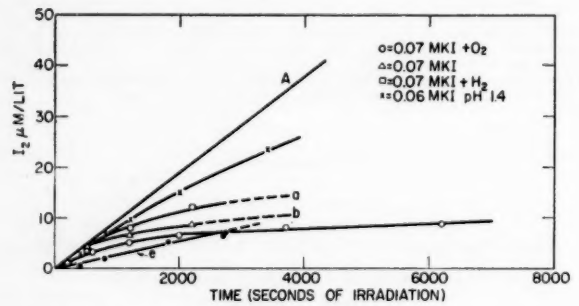

FIG. 2. Iodine formation as a function of dose from 0.07*M* KI solutions in the presence and absence of added gases and acid.

of added gases. The solution used to obtain curves a and b were identical except that the solution used to obtain curve a was saturated with H_2 at about 400-mm pressure, while curve b was obtained from the de-aerated solution. The steady-state concentration of I_2 is increased by the addition of H_2 (this is supported by several other solutions not shown here) and by lowering the *p*H but is decreased by the addition of oxygen. Curve e is the rate of I_2 formation in a 0.024*M* KI solution initially containing 24 μM of I_2. This may be compared with the 0.027*M* KI solution in Fig. 1; it indicates that the initial rate of I_2 formation is inhibited by the presence of I_2. No appreciable amounts (less than 1 μM) of iodate could be detected in the more dilute solutions (0.1*M* to 10^{-3}*M* KI). The presence or absence of iodate was not analyzed for in the more concentrated solutions.

The initial products of irradiation of iodide solutions thus appear to be hydrogen and iodine, with oxygen or hydrogen peroxide appearing only after the iodine concentration has built up to a critical level. The findings are at variance with commonly accepted ideas of this reaction.

* Research carried out under the auspices of the U. S. Atomic Energy Commission.

[1] E. R. Johnson and A. O. Allen, J. Am. Chem. Soc. **74**, 4147 (1952).

Pure Quadrupole Spectra: Alkyl Bromides and Iodides*

HENRY ZELDES AND RALPH LIVINGSTON
Oak Ridge National Laboratory, Carbide and Carbon Chemicals Company, Oak Ridge, Tennessee
(Received May 25, 1953)

PURE quadrupole spectrum measurements on solid alkyl chlorides[1] have been extended to alkyl bromides and iodides. The purpose of this letter is to present preliminary data and to point out the striking similarity in quadrupole coupling trends. The spectrometer was a simple regenerative oscillator with a transmission line tuned circuit, and the absorption lines were viewed on an oscillograph. It was necessary to purify a number of the compounds before resonance lines could be found, and in a few cases slow crystallization of the substance gave satisfactory results where rapid freezing failed. These new data are summarized in Table I where Br^{81} frequencies and the lower iodine frequencies ($\pm\frac{1}{2}\rightarrow\pm\frac{3}{2}$) are given. The values for CH_3Br and CH_3I are consistent with those reported[2,3] at a slightly higher temperature. The computed coupling magnitudes are taken to be twice the observed transition frequency for Br^{81} (spin of $\frac{3}{2}$) and 20/3 times the frequency for I (spin of 5/2). The average frequency is used where multiple lines are found. At a later date, with higher-frequency equipment, we hope to observe the upper-frequency iodine lines and to evaluate the parameter of the field gradient tensor asymmetry.

The coupling trends for the bromides and iodides are very similar to those found for the chlorides. For example, the values for the six one-carbon bromides in Fig. 1 are given, within one percent, by multiplying the corresponding chlorine values (at 20°K) by 6.50. This suggests a similarity in bond type for these Cl and Br compounds and is probably a reflection of the closeness of their electronegativity values. The couplings for the ethyl halides are substantially lower than those for the corresponding methyl halide and in all cases the *n*-propyl halide coupling is slightly higher than the ethyl halide coupling. The value for isopropyl iodide is lower than that for ethyl iodide just as it is for the chlorides. In many of the comparisons made above the corresponding halogen compounds cannot be crystallographically isomorphous since they give different numbers of quadrupole lines cor-

TABLE I. Quadrupole frequencies and couplings for Br^{81} and I in alkyl halides.

Compound	Frequency, Mc 77°K	20°K	$\lvert eqQ\rvert_{Av}$, 77°K
CH_3Br	220.981		441.96
CH_2Br_2	234.805 235.601	235.781 237.093	470.41
$CHBr_3$	250.527 250.666 251.970		502.11
CF_3Br	252.263		504.53
CF_2Br_2	251.624 255.681		507.31
$CFBr_3$	256.592 262.371		518.96
CH_3CH_2Br	207.790	208.968	415.58
$CH_3CH_2CH_2Br$	210.277		420.55
CH_2BrCH_2Br	216.827 218.977	217.275 219.473	435.80
CH_3I	265.102		1767.3
CH_2I_2	286.883		1912.6
CH_3CH_2I	247.374	248.793	1649.2
$CH_3CH_2CH_2I$	250.962		1673.1
$(CH_3)_2CHI$	235.921		1572.8

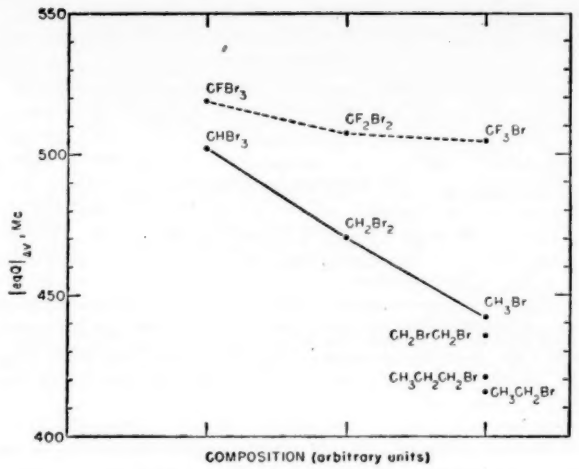

FIG. 1. Quadrupole couplings for Br^{81} at 77°K.

responding to different numbers of nonequivalent halogen lattice positions. For example, $CHCl_3$ gives two lines (for each isotope) while $CHBr_3$ gives three. The 20°K measurements (Table I) indicate that the percentage frequency increase in cooling from 77 to 20°K is roughly the same as that for organic Cl compounds.

We intend to extend these measurements to other related compounds and describe the results more fully at a later date.

* This work was performed for the U. S. Atomic Energy Commission.
[1] R. Livingston, J. Phys. Chem. (to be published).
[2] H. G. Dehmelt and H. Kruger, Z. Physik **129**, 401 (1951).
[3] H. G. Dehmelt, Naturwiss. **37**, 398 (1950).

The Rate Constant of the Reaction between Hydrogen Peroxide and Ferrous Ions

WILLIAM TAYLOR AND JOSEPH WEISS
University of Durham, King's College, Newcastle upon Tyne, England
(Received May 18, 1953)

IT has been shown previously by Haber and Weiss[1,2] that the mechanism of the reaction between hydrogen peroxide and ferrous ions, when the latter are in excess, can be described by the following two consecutive reactions:

$$Fe^{2+}+H_2O_2\rightarrow Fe^{3+}+OH^-+OH(k_1) \quad (1)$$

$$Fe^{2+}+OH\rightarrow Fe^{3+}+OH^-, \quad (2)$$

which correspond to the simple stoichiometry,

$$2Fe^{2+}+H_2O_2\rightarrow 2Fe^{3+}+2OH^-. \quad (3)$$

The simplicity of this mechanism is due to the fact that under these conditions the primarily produced OH radicals react only with the ferrous ions and all other reactions of hydrogen peroxide, e.g., those leading to the evolution of oxygen, can be neglected. As has been shown previously,[2] under these conditions, the rate of the reaction, in the stationary state, is given by the simple differential equation,

$$-\frac{d(Fe^{2+})}{dt}=+\frac{d(Fe^{3+})}{dt}=2k_1[Fe^{2+}][H_2O_2], \quad (4)$$

corresponding to the bimolecular reaction between hydrogen peroxide and ferrous ions according to Eq. (1). It is thus possible to measure the rate constant (k_1) directly. However, this is a fairly rapid reaction and the rate constant was measured, in the first instance, by Haber and Weiss[2] in a flow system. Using a relatively simple apparatus, these authors obtained a value of $k_1(20°C)=23$ moles^{-1} 1 sec^{-1}, and some measurements carried out at 6°C and 45°C corresponded to a value of about 9000 cal for the heat of activation.

Subsequently, the study of this reaction was taken up by Baxendale, Evans, and Park[3] who worked at much lower concentrations of the reactants and followed the reaction by measuring the concentration of the ferrous ions at different times by a colorimetric method with α, α' dipyridyl; this reagent was used at the same time for the "quenching" of the reaction. In this way these authors obtained values for three different temperatures which were within the ranges shown below:

$$k_1(12°)=29.8-30.7;\quad k_1(25°)=59-67;$$
$$k_1(35°)=105-111 \text{ moles}^{-1}\ 1\ \text{sec}^{-1}.$$

More recently, Barb, Baxendale, George, and Hargrave[4] have used again the same colorimetric method but sought to improve the method by adding ammonium fluoride, sodium acetate, and chloride ions to the solution, used for the "quenching" of the reaction These authors, who claimed a relatively high accuracy for their measurements, gave the following values:

$$k_1(0°)=12.6\pm0.15;\quad k_1(14.6°)=31.6\pm0.5,$$
$$k_1(24.6°)=53.0\pm0.7 \text{ mole}^{-1}\ 1\ \text{sec}^{-1},$$

from which they derived a value of 9400 cal for the heat of activation.

We have now redetermined this rate constant by a method which allows one to follow continuously the course of the reaction without the introduction of any foreign substances and without the necessity of any "quenching" process. For this purpose, we have followed the course of the reaction by measuring the light absorption of the ferric salt produced at the wavelength of $\lambda=304$ mμ in a silica absorption cell, which also served as the reaction vessel. This procedure is particularly suitable for this reaction because, at this wavelength, the molar extinction coefficient of the ferric salt is of the order of about 10^3 times greater than that of hydrogen peroxide or of ferrous ions. The actual measurements were carried out in a "Unicam" spectrophotometer (S.P. 500) where the silica absorption cell was placed in a thermostated, specially constructed, cell carriage. In this way the temperature of the reaction mixture (which was prepared by rapid mixing of the prethermostated solutions of the reactants) could be adjusted easily and kept to within ±0.1°C at the lower, and within ±0.2°C at the higher temperatures. All the experiments were carried out in dilute (sulfuric) acid solutions; the rate is independent of the hydrogen ion concentration, as has been shown previously.[2,3] The ferrous and ferric sulfate and sulfuric acid used were of A.R. standard, and the hydrogen peroxide solutions were prepared from triply distilled (concentrated) hydrogen peroxide (free from any stabilizer); triply distilled water was used in all experiments.

The results of these measurements at five different temperatures are given in Table I. These values have been used for the construction of the graph shown in Fig. 1, in which each single point represents the mean of five independent experiments, where the value for each experiment was determined from not less than six points on the usual second order *vs* time plot, which in every case gave a satisfactory straight line.

Within the temperature limits stated these results can be represented by the following equation:

$$k_1=3.9\times10^9\times\exp(-11\,000/RT). \quad (5)$$

It will be seen that these results differ very materially from those published earlier, particularly from those of the last-named

TABLE I. Values of the rate constant (k_1) at different temperatures.

Temperature (°C)	k_1 (moles^{-1} 1 sec^{-1})
15.1 ±0.15	19.3 ±0.5
20.0 ±0.1	26.6 ±0.5
25.1 ±0.1	35.7 ±0.5
35.5 ±0.15	67.2 ±1.0
41.0 ±0.2	96.5 ±1.5

FIG. 1. Showing the linear relationship between logarithm of the rate constant (k_1) and reciprocal of absolute temperature.

authors, although the value obtained at 20°C is not very different from that obtained previously by Haber and Weiss[2] working at higher concentrations and with a flow apparatus.

It is obvious that the method used in this investigation has many advantages over all the methods used previously, as the reaction can be followed continuously over a considerable time interval and no addition of any foreign substances or any quenching of the reaction is necessary. It is therefore very likely that the results given above are more reliable than any of those published previously.

A full account, including some theoretical considerations, will be published elsewhere.

We should like to thank Professor W. F. K. Wynne-Jones for the use of the thermostated "Unicam" spectrophotometer.

[1] F. Haber and J. Weiss, Naturwiss. **20**, 948 (1932).
[2] F. Haber and J. Weiss, Proc. Roy. Soc. (London) **A147**, 332 (1934).
[3] Baxendale, Evans, and Park, Trans. Faraday Soc. **42**, 155 (1946).
[4] Barb, Baxendale, George, and Hargrave, Trans. Faraday Soc. **47**, 462 (1951).

An LCAO MO Self-Consistent Field Calculation of the Ground State of H_2O

FRANK O. ELLISON AND HARRISON SHULL
Department of Chemistry and Institute for Atomic Research, Iowa State College, Ames, Iowa
(Received April 20, 1953)

A THEORETICAL study of the ground state of the water molecule has been carried out utilizing the self-consistent field (SCF) molecular orbital (MO) method in the linear-combination-of-atomic-orbitals (LCAO) approximation.[1] The availability of a systematic approach has encouraged application of this method to a variety of molecular problems. Despite these treatments, it can hardly be said that the limits of applicability of the method have been determined. A complete ten-electron study of H_2O should not only aid in this direction, but also afford a better understanding of the properties of the molecule itself. This letter reports the results for the experimentally observed H—O—H bond angle of 105 degrees and O—H distance of 0.9580A. Further calculations are in progress for other angles, but with the same O—H distance. Results and complete details of these calculations will be published in the near future.

Previous theoretical treatments of the H_2O molecule have been carried out by a number of investigators. Slater[2] and Van Vleck and Cross[3] obtained rather successful results utilizing the semi-empirical and simplified valence-bond (VB) method. On the other hand, Coolidge's[4] nonempirical VB treatment was less encouraging. In the hands of F. Hund[5] and R. S. Mulliken,[6] the simple

TABLE I. LCAO SCF MO's for the ground state of H_2O.[a]

(a) Complete treatment

$1a_1 = -0.0039\ \sigma_1 + 1.0002\ 1s + 0.0163\ 2s + 0.0024\ 2p_z$
$2a_1 = 0.208\ \sigma_1 - 0.029\ 1s + 0.845\ 2s + 0.133\ 2p_z$
$3a_1 = 0.393\ \sigma_1 - 0.026\ 1s - 0.461\ 2s + 0.827\ 2p_z$
$1b_2 = 0.613\ \sigma_s + 0.543\ 2p_y$
$1b_1 = 2p_x$

(b) Approximate treatment

$1a_1 = 1s$
$2a_1 = 0.25\ \sigma_1 + 0.82\ 2s + 0.12\ 2p_z$
$3a_1 = 0.50\ \sigma_1 - 0.55\ 2s + 0.76\ 2p_z$
$1b_2 = 0.59\ \sigma_s + 0.57\ 2p_y$
$1b_1 = 2p_x$

[a] $\sigma_1 = 2^{-\frac{1}{2}}(0.8529)[1s(h_1) + 1s(h_2)]$ and $\sigma_s = 2^{-\frac{1}{2}}(1.2645)$. $[1s(h_1) - 1s(h_2)]$ are the *normalized* hydrogen symmetry orbitals. All other AO's belong to oxygen. The positive z axis bisects the H—O—H angle, the x axis is perpendicular to the molecular plane, and $1s(h_1)$ gives positive overlap with $2p_y$ and $2p_z$.

MO method afforded a rather satisfactory understanding of the general properties of H_2O. It has, however, only been in recent years that sound theoretical bases for describing the water molecule have been sought by more detailed and rigorous treatments.[7–10]

The SCF treatment has been carried out utilizing *orthogonalized* Slater orbitals with the usual effective nuclear charges, *viz.*, $Z(1s)=1$ for hydrogen, and for oxygen $Z(1s)=7.7$, $Z(2s)=Z(2p)=4.55$. The attempt was made in this complete treatment to limit the assumptions to those inherent in the method itself. In addition, a second calculation was performed which contained the conventional approximation of replacing the molecular inner shell ($1a_1$) by an oxygen $1s$ Slater orbital. The MO's in this approximation are not mutually orthogonal as they are in the complete treatment. Table I lists the SCF LCAO MO's resulting from both calculations, and Table II gives the corresponding orbital energies

TABLE II. LCAO SCF energies for the ground state of H_2O.[a]

	Approximate treatment	Complete treatment	Observed
Orbital energies:			
$1a_1$	−559.1	−557.3	
$2a_1$	− 37.4	− 36.2	
$1b_2$	− 19.2	− 18.6	-16.2 ± 0.3[b,c]
$3a_1$	− 14.2	− 13.2	-14.5 ± 0.3[b,d]
$1b_1$	− 12.8	− 11.8	-12.6 ± 0.1[b,e]
Total molecular energy	2063.8	2062.5	2079.9
Total atomic energy	2054.8	2054.8	2070.4[f]
Dissociation energy	9.0	7.7	9.49[g]

[a] All values in electron volts.
[b] Negatives of ionization potentials obtained by electron impact; see reference 13.
[c] Spectroscopic values: 16.0±0.5 ev. Henning, Ann. Physik **13**, 599 (1924).
[d] No spectroscopic value recorded.
[e] Spectroscopic value: 12.56±0.01 ev. W. C. Price, J. Chem. Phys. **4**, 147 (1936).
[f] C. E. Moore, *Atomic Energy Levels*, Nat. Bur. Standards (U. S.) Circ. 467, Vol. I.
[g] G. Herzberg, *Molecular Spectra and Molecular Structure* (D. Van Nostrand Company, Inc., New York, 1950), 2nd ed., Vol. I, p. 481.

as well as the total molecular and dissociation energies. The MO's are denoted by the symbol of the irreducible representation of the group C_{2v} to which they belong, preceded by a running number distinguishing orbitals of identical symmetry.

The importance of observing strict orthogonality among all MO's, a precept stressed by several authors,[11,12] is well verified by the two calculations. The difference between the coefficients of σ_1 in $3a_1$, the most extreme case, is 26 percent, while the average variation of all coefficients is approximately 11 percent. From Table II it is seen that the calculated total molecular energy is depressed by the neglect of *forced hybridization*[12] to a point which nearly gives the correct dissociation energy. The computed dipole moment reflects an even more pronounced difference between the two calculations. The approximate treatment yields the value

1.2D as compared to 1.51D for the complete calculation. The latter is in relatively good agreement with the observed, 1.84D. Both calculated dipoles are directed in the sense $H_2^+O^-$.

An SCF orbital energy should represent a reasonable approximation to the negative of the experimental molecular ionization potential.[1] There is little doubt that the first observed value corresponds to removal of a nonbonding $2px$ electron. There exists some question concerning the assignments of the higher potentials.[13] These calculations favor the designations as listed in Table II. As was also noted in Mulligan's treatment of CO_2,[14] considerably higher ionization potentials are obtained for the nonvalence shells than predicted by Mulliken.[6] The value for $2a_1$ is explained by the fact that Mulliken took his orbital to be nonbonding ($I \sim 32$ ev), whereas the SCF function turns out to be quite bonding. The variance of $-\epsilon(1a_1)$ (and $-\epsilon(1s)$ for CO_2) from the observed K-shell x-ray absorption limit for the oxygen atom (524 ev) is due to the choice of the Slater $1s$ orbital; the *calculated* valence state ionization potential $0(1s^2 2s^2 2p^4) - 0(1s2s^2 2p^4)$, using Slater orbitals, is 557 ev.

In these calculations, all integrals were computed to four-place accuracy with the exception of two small two-center exchange integrals, four of the five three-center bare nuclear field integrals, and the remaining three-center electronic repulsion integrals. Careful study of all approximated terms was carried out in order to assure reliable values.

[1] C. C. J. Roothaan, Revs. Modern Phys. **23**, 69 (1951).
[2] J. C. Slater, Phys. Rev. **38**, 1109 (1931).
[3] J. H. Van Vleck and P. C. Cross, J. Chem. Phys. **1**, 357 (1934).
[4] A. S. Coolidge, Phys. Rev. **42**, 189 (1932).
[5] F. Hund, Z. Physik **74**, 429 (1932).
[6] R. S. Mulliken, Phys. Rev. **40**, 55 (1932); J. Chem. Phys. **3**, 506, 573, 586 (1935).
[7] D. F. Heath and J. W. Linnett, Trans. Faraday Soc. **44**, 556 (1948).
[8] J. A. Pople, Proc. Roy. Soc. (London) **A202**, 323 (1950).
[9] C. A. Coulson, Proc. Roy. Soc. (London) **A207**, 63 (1951).
[10] J. W. Linnett and A. J. Poë, Trans. Faraday Soc. **47**, 1033 (1951).
[11] C. A. Coulson and W. E. Duncanson, Proc. Roy. Soc. (London) **A181**, 378 (1943).
[12] R. S. Mulliken, J. Chem. Phys. **19**, 912 (1951).
[13] W. C. Price and Sugden, Trans. Faraday Soc. **44**, 108 (1948).
[14] J. F. Mulligan, J. Chem. Phys. **19**, 347 (1951).

The Infrared Spectrum of the H_3O^+ Ion in Acid Hydrates

D. E. Bethell and N. Sheppard
Department of Colloid Science, Free School Lane, Cambridge, England

(Received June 17, 1953)

In a recent study of the crystalline monohydrates of nitric acid and perchloric acid by nuclear magnetic resonance techniques, Richards and Smith[1] concluded that the structures were very probably $H_3O^+ \cdot NO_3^-$ and $H_3O^+ \cdot ClO_4^-$. In the present work an attempt has been made to confirm these conclusions from the infrared spectra of the pure acids and their hydrates. They have also been studied in the liquid state, where nuclear magnetic resonance gives no useful information.

There appears to have been no previous spectroscopic study of the structure of H_3O^+; earlier Raman work[2,3] had failed to identify the ion directly, presumably because of its weak Raman spectrum.

Spectra were taken of capillary thicknesses of nitric acid and its monohydrate between flat silver chloride plates. The plates were mounted in a low-temperature cell[4] which was cooled with liquid air when taking spectra of the crystalline acids. On cooling, the spectrum of the monohydrate changed completely, showing that crystallization had occurred. Spectra were taken from 550 cm^{-1} to 4000 cm^{-1}. Both liquid and solid HNO_3 have spectra closely similar to that observed with a gaseous sample.[5] The spectrum of *liquid* $HNO_3 \cdot H_2O$ is substantially the same as that of pure HNO_3 except for additional absorption bands due to water, indicating that the acid hydrate is essentially un-ionized.[6]

Below 2000 cm^{-1}, the spectrum of *crystalline* $HNO_3 \cdot H_2O$ is markedly different from that of the liquid form. New absorption bands at 738, 815, and 1381 cm^{-1} may be identified with those of the NO_3^- ion.[7] We therefore assign the remaining strong absorptions to the H_3O^+ ion, namely those at 1134 (very strong and broad), 1670 (strong), and in the region of 3000 cm^{-1} (very broad).

As H_3O^+ is isoelectronic with NH_3, with very little mass difference, it might be expected that their spectra would be similar. Crystalline ammonia has the following absorption frequencies: ν_2 at 1060 (vs), ν_4 at 1646 (s), ν_1 at 3223 and ν_3 at 3378 cm^{-1} (vs).[8] We therefore assign the absorption bands at 1134 and 1670 in the H_3O^+ spectrum to the vibrations ν_2 and ν_4, because of their great similarity in frequency and intensity to the corresponding bands in the NH_3 spectrum. Indeed the correspondence is so close that it appears very probable that the H_3O^+ ion has analogous pyramidal symmetry. The H_3O^+ fundamentals ν_1 and ν_3 are presumably associated with the very broad absorption from 2650 to 3380 cm^{-1}. Some of this breadth is undoubtedly due to strong hydrogen bonding.

The only strong band of the crystalline hydrate not so far discussed occurs at 670 cm^{-1}. This could be assigned to a torsional oscillation of H_3O^+, which might occur at rather higher frequencies than the analogous NH_3 absorption at 520 cm^{-1} because of stronger hydrogen bonding. Alternatively, it and the band at 735 cm^{-1} might be two components of the usually degenerate NO_3^- frequency near 720 cm^{-1}.

Spectra of perchloric acid and its monohydrate have also been obtained, and are consistent with the hypothesis that the monohydrate exists as $H_3O^+ \cdot ClO_4^-$, although there is some overlapping of the expected H_3O^+ bands with ClO_4^- absorption bands. Further work is being done on the hydrates of other acids. A more detailed account will be published later.

[1] R. E. Richards and J. A. S. Smith, Trans. Faraday Soc. **47**, 1261 (1951).
[2] R. Fonteyne, Nature **138**, 886 (1936).
[3] A. Simon, Z. anorg. u. allgem. Chem. **239**, 329 (1938).
[4] J. K. Brown and N. Sheppard, Disc. Faraday Soc. **9**, 144 (1950).
[5] Cohn, Ingold, and Poole, J. Chem. Soc. **1952**, 4272.
[6] Gillespie, Hughes, and Ingold, J. Chem. Soc. **1950**, 2552.
[7] G. Herzberg, *Infra-Red and Raman Spectra* (D. Van Nostrand Company, Inc., New York, 1945).
[8] F. P. Reding and D. F. Hornig, J. Chem. Phys. **19**, 594 (1951).

The "Chemical Knife"; Preservation of Ozone for Thirty-Six Days

H. O. Albrecht
Bartol Research Foundation of The Franklin Institute, Swarthmore, Pennsylvania

(Received May 18, 1953)

About 1933 I noticed more particularly the action of ozone on rubber. The facts are widely familiar, I assume, but seemingly no emphasis to date has been given to a curious aspect of this reaction and its interpretation.

A tube of thick and new rubber broke off where stretched slightly over a metal nipple, in a matter of minutes after producing ozone in the vicinity. This occurred several times before I realized the cause. The broken ends were traversed by a sharp cracks as though slashed by a razor blade, but the rubber was not visibly deteriorated. I later found that a rubber band stretched in the path of a stream of ozonized oxygen (*ca* 8 percent ozone) parted almost instantly, whereas no effect, even superficial, was seen on an unstretched band in so short a time.

An interesting explanation of these effects is "mechanical activation" of the double bonds in the rubber structure at the point of high stress, namely, the bottom of the forming crack. A more orthodox, perhaps equivalent, view is that the "newly formed surface," unprotected by ordinary oxidation or gas absorption, is responsible for this extreme local rate of penetration of a reaction into a solid. The amount of ozone involved is infinitesimal, compared to the conspicuous effect—accurately likened to

that of a knife. In either case, the result has some practical (and not always realized) significance in connection with the deterioration of rubber connections, when a Tesla leak detector is used.

Another, unconnected, observation made on ozone at the time, was its stability for thirty-six days at fairly high concentration, in a one-liter sealed Pyrex bulb containing $KMnO_4-H_2SO_4$ solution (same 8 percent ozone in oxygen). The bulb lay in full sunlight during summer weather. I have never heard of ozone being preserved for this length of time and ascribe the stability to the absence of nitrogen oxides, as well as organic matter, because of the $KMnO_4$.

On the Relation between Dynamic Viscosity and Rigidity

ALI A. K. IBRAHIM
Physics Department, The University, Alexandria, Egypt
(Received May 29, 1953)

THE object of the present note is to obtain experimentally the relation between the dynamic viscosity η and the dynamic rigidity N, for solids and viscoelastic liquids, when subjected to forced harmonic oscillations of frequency n cps.

Markovitz *et al.*[1] have carried out recently very precise measurements on a 12.8 percent solution of Vistanex B-140 in tetralin (density = 0.96 g/cc) and solid Vistanex compounded with carbon black. It is possible from their original curves $(\eta-n)$ and $(N-n)$

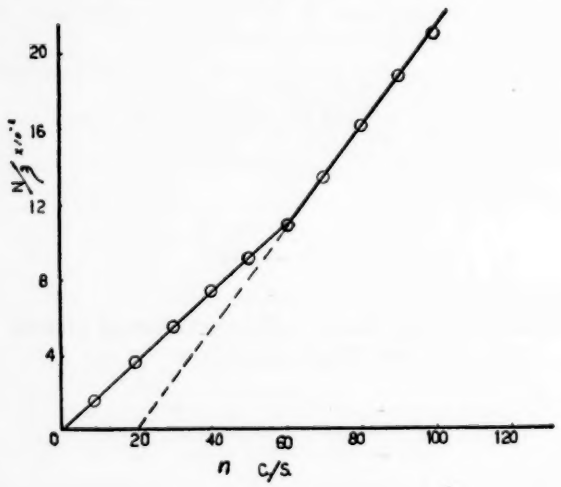

FIG. 1.

to calculate values of N/η for different values of n. New curves can be drawn which show the variation of N/η with n. Figure 1 is for the viscoelastic liquid, and Fig. 2 represents the solid under investigation.

From Fig. 1 (for the viscoelastic liquid) we come to the following three simple and important conclusions.

(1) For a frequency range from 0 to 60 cps it appears that

$$N/\eta \propto n$$

or

$$N/\eta = mn, \tag{1}$$

where m is a constant depending on the nature of the liquid under experiment.

(2) For frequencies higher than 60 cps we have

$$N/\eta = m(n-C), \tag{2}$$

where both m' and C are constants depending also on the nature of the liquid.

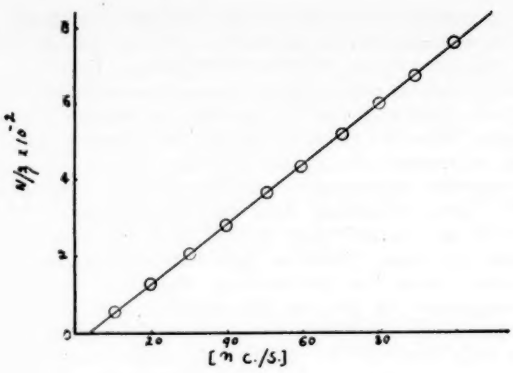

FIG. 2.

(3) m' bears a simple ratio to m where

$$m:m'=2:3.$$

Also from Fig. 2 for the solid it appears that Eq. (2) satisfied the experimental values obtained for all values of n from 10 to 100 cps.

Hence we come to the conclusion that for the liquid under investigation for a frequency range between 0–60 cps it behaves as a viscoelastic liquid governed by Eq. (1) but for frequencies higher than 60 cps it behaves as a solid governed by Eq. (2).

[1] Markovitz, Yavorsky, Harper, Zapas, and Dewitt, Rev. Sci. Instr. **23**, 430 (1952).

The Pair Distribution Function for a One-Dimensional Gas*

ROBERT L. SELLS, C. W. HARRIS, AND EUGENE GUTH
Department of Physics, University of Notre Dame, Notre Dame, Indiana
(Received May 22, 1953)

THE solution of the Born-Green[1] (B-G) or the equivalent Kirkwood[2] equation for the molecular distribution function presupposes some *approximation*, e.g., the superposition principle expressing the distribution function for triplets $n_3(123)$ in terms of that for doublets $n_2(12)$. However, for a one-dimensional gas, and only in this case, the triplet distribution function can be expressed exactly in terms of the doublet distribution functions by an appropriate superposition principle which is thus rigorously valid. The resulting functional equation can be solved for the square-well model. Besides methodical interest, the distribution function may be used to obtain the light scattering for this model.

In the one-dimensional B-G equation

$$\frac{\partial n_2(12)}{\partial x_1}+\frac{n_2(12)}{kT}\frac{\partial \varphi(12)}{\partial x_1}=\frac{1}{kT}\int_{-\infty}^{\infty} n_3(123)\frac{\partial \varphi(13)}{\partial x_3}\,dx_3, \tag{1}$$

[x_i = coordinate of ith molecule, $\varphi(ij)$ = potential energy between ith and jth molecule] the appropriate superposition principle takes on the form:

$$\begin{aligned} \rho n_3(123) &= n_2(r)n_2(s-r): && s\geq r \\ &= n_2(r-s)n_2(s): && 0\leq s\leq r \\ &= n_2(r)n_2(-s): && s\leq 0 \end{aligned} \tag{2}$$

[$r=x_2-x_1$, $s=x_3-x_1$, $\rho=N/L$, L is length of interval, N is number of molecules].

Equation (2) implies nearest-neighbor interaction with a hard core and finite range of attraction, e.g., $\varphi(r)=\infty$ for $r\leq 1$, $\varphi(r)=0$ for $r\geq\lambda$, unit of length = diameter of hard core. With this interaction all multiple distribution functions reduce to products of pair distribution functions.

Putting $n_2(r)=\rho^2 e^{-\beta\varphi(r)}g(r)$ and $\beta=1/kT$, Eqs. (1) and (2) give

$$\frac{kT}{\rho}e^{-\beta\varphi(r)}\frac{dg(r)}{dr}=e^{-\beta\varphi(r)}g(r)\int_0^\infty e^{-\beta\varphi(s)}\frac{d\varphi(s)}{ds}g(s)ds$$
$$-\int_0^r e^{-\beta\varphi(s)}g(s)e^{-\beta\varphi(r-s)}g(r-s)\frac{d\varphi(s)}{ds}ds. \quad (3)$$

The term corresponding to the first line of Eq. (2) vanishes for our nearest-neighbor interaction. Equation (3) together with the boundary condition,

$$g(\infty)=1, \quad (4)$$

determines completely $g(r)$.

Equation (3) with Eq. (4) was solved for the square-well potential with hard core ($R-1$=range of attraction),

$$\begin{aligned}\varphi(r)&=\infty; \quad r\leq 1\\ &=-\epsilon; \quad 1\leq r\leq R\\ &=0; \quad r\geq R.\end{aligned} \quad (5)$$

Equation (3) with (5) reduces to a set of coupled differential-difference equations:

$$\begin{aligned}\frac{dg(r)}{dr}&=A_1g(r)+(1+\Delta)A_2g(r-1); && 1\leq r\leq R+1\\ &=A_1g(r)+A_2g(r-1)-(1+\Delta)A_3g(r-R); && R+1\leq r\leq 2R\\ &=A_1g(r)+A_2g(r-1)-A_3g(r-R); && r\geq 2R,\end{aligned} \quad (6)$$

where $A_1=A_3-A_2$, $A_3=\rho\Delta g(R)$, $A_2=\rho g(1)(1+\Delta)$, $\Delta=e^{\beta\epsilon}-1$. The solution of Eq. (6) is

$$\begin{aligned}g(r)=g(1)\Big[&e^{A_1(r-1)}+a(1+\Delta)e^{A_1(r-2)}\\ &\times\Big\{(r-2)(1+\Delta)-2\Delta(r-R-1)+\frac{\Delta^2(r-2R)}{(1+\Delta)}\Big\}\\ &+\frac{a^2(1+\Delta)^2}{2!}e^{A_1(r-3)}\Big\{(r-3)^2(1+\Delta)-3\Delta(r-R-2)^2\\ &+\frac{3\Delta^2(r-2R-1)^2}{(1+\Delta)}-\frac{\Delta^3(r-3R)^2}{(1+\Delta)^2}\Big\}+\text{etc.}\Big].\end{aligned} \quad (7)$$

For the case of hard spheres, the system (6) reduces to the single differential-difference equation,[3]

$$dg(r)/dr=\rho g(1)[g(r-1)-g(r)]; \quad r\geq 1$$

with the solution

$$g(r)=\frac{1}{1-\rho}\sum_{n=0}^{k}\frac{a^n[r-(n+1)]^n e^{-a[r-(n+1)]}}{n!}, \quad (8)$$

where $k+1\leq r\leq k+2$ and $a=\rho/(1-\rho)$.

This distribution has been obtained from probability considerations by Zernike and Prins,[4] who computed the light scattering for this system. Similarly, the light scattering can also be obtained for the square-well model using the distribution function of Eq. (7).

n_2 is the pair distribution function for any two molecules regardless of the position of the other molecules. At small distances n_2 reduces to the distribution function n_2^* for adjacent molecules. n_2^* can be obtained from Eq. (3) by omitting the second term on the right-hand side. (This term corresponds to putting a third particle between the fixed pair.) n_2^* can then be continued analytically and vanishes at infinity while $n_2(\infty)=\rho^2$. (This condition served to determine n_2 completely.) n_2^*, on the other hand, can be determined completely by the following twofold relation to the equation of state ($\int_0^\infty n_2^* dr=1$):

$$p=-\int_0^\infty n_2^*\varphi'(s)ds \quad (9)$$

and

$$p=\rho kT-\rho\int_0^\infty n_2^* s\varphi'(s)ds. \quad (10)$$

The first relation is a definition for a one-dimensional system; the second relation expresses the virial theorem. From (3) and (9) or (10) one obtains

$$n_2^*=\frac{e^{-\beta[ps+\varphi(r)]}}{\int_0^\infty e^{-\beta[ps+\varphi(s)]}ds}. \quad (11)$$

Then

$$L=\int_0^\infty n_2^* s ds=\frac{\int_0^\infty se^{-\beta[ps+\varphi(s)]}ds}{\int_0^\infty e^{-\beta[ps+\varphi(s)]}ds}. \quad (12)$$

For hard spheres one obtains from (9) and (10), using $n_2^*(r)=Ce^{-\rho g(1)r}$,

$$p=\rho kTg(1) \quad \text{and} \quad p=\rho kT+\rho^2 kTg(1)$$

giving

$$g(1)=\frac{1}{1-\rho} \quad \text{and} \quad p=\frac{kT\rho}{1-\rho}.$$

Similarly, one obtains for the square-well case [$n_2^*(r)=Ce^{A_1 r}$],

$$p=\rho kT[(1+\Delta)g(1)-\Delta g(R)],$$

and

$$p=\rho kT[1+(1+\Delta)g(1)-\Delta\rho Rg(R)]$$

giving

$$g(R)=\frac{1-g(1)[1+\Delta][1-\rho]}{[R\rho-1]\Delta}=g(1)e^{A_1(R-1)}.$$

Here, however, p cannot be obtained explicitly.

It is clear from Eqs. (11) and (12) that the equation of state is determined by n_2^* alone. These equations were derived by Gursey,[5] and earlier by Tonks[6] for the special case of hard rods, using direct integration of the incomplete partition function. For a square-well potential an approximate equation of state was first given by Herzfeld and Goeppert-Mayer,[7] assuming $\epsilon\gg kT$.

A more detailed report of these calculations, including among other things a discussion of the specific heat for a square-well model, the relation to a lattice gas, and a treatment of light scattering is to follow.

Note added in proof.—Actually n_2^* determines n_2 also. A one-dimensional gas with nearest-neighbor interactions with hard core and finite range may be considered as an ideal gas consisting of doublets of adjacent molecules. This point of view leads one to consider the formation of n_2 from n_2^* as a Markoff process in analogy to the well-known random-walk problems, and yields very simply all the results of the recent interesting paper by Salsburg, Zwansig, and Kirkwood [J. Chem. Phys. **21**, 1098 (1953)], as will be shown (with its ramifications) in a later publication.

* Supported in part by the U. S. Office of Naval Research.

[1] M. Born and H. S. Green, Proc. Roy. Soc. (London) **A198**, 10 (1946).
[2] J. G. Kirkwood, J. Chem. Phys. **14**, 180 (1946).
[3] R. Bellman, Ann. Math. **50**, 347 (1949).
[4] F. Zernike and J. A. Prins, Z. Physik **41**, 184 (1927).
[5] F. Gursey, Proc. Cambridge Phil. Soc. **46**, 182 (1950); G. Klein and I. Prigogine, Physica **19**, 74 (1953).
[6] L. Tonks, Phys. Rev. **50**, 955 (1936).
[7] K. F. Herzfeld and M. Goeppert-Mayer, J. Chem. Phys. **2**, 38 (1934).

Rb^{87} and Cs^{133} Magnetic Resonance Shifts in the Solid Halides*

H. S. Gutowsky and B. R. McGarvey†
Noyes Chemical Laboratory, University of Illinois, Urbana, Illinois
(Received May 25, 1953)

CHEMICAL shifts of the Rb^{87} and Cs^{133} magnetic resonances have been found in the solid polycrystalline rubidium and cesium halides. The results are given in Table I in terms of $\Delta\sigma$ which is defined as

$$\Delta\sigma=\frac{(H_s-H_r)}{H_r}\times 10^4.$$

H_s and H_r are the magnetic fields necessary for resonance, at a fixed frequency, for the sample and reference, respectively. The reference was a saturated aqueous solution of the chloride. The sample and reference at room temperature were placed in adjacent coils in two separate rf bridge systems. The narrow resonance of the reference was displayed on an oscilloscope while the broad resonance from the solid halide was detected with a narrow band

amplifier. The experimental procedures and equipment used have been described.[1] The resonances in the two fluorides were broader and weaker than in the other halides, giving less accurate results.

As seen in Table I, the magnetic shielding of the alkali metal nucleus decreases from the fluoride to the iodide, while the ion in solution has the largest shielding of all. Also the cesium shifts are larger than those of rubidium, supporting the observation[1] that the chemical shifts increase with nuclear charge. This dependence of the shift on nuclear charge may explain why we were unable to find resonance shifts in the salts of the lighter alkalies, lithium and sodium.

The chemical shifts reported previously were observed in compounds in which the binding is primarily covalent in character, while the Rb^{87} and Cs^{133} resonance shifts appear to be the first reported for compounds in which the binding is primarily ionic.

TABLE I. Chemical shifts of the Rb^{87} and Cs^{133} magnetic resonances in the solid halides. The reference is the saturated aqueous solution of the corresponding chloride.

Salt	$\Delta\sigma$	Salt	$\Delta\sigma$
RbF	-0.6 ± 0.1	CsF	-0.9 ± 0.2
RbCl	-0.89 ± 0.05	CsCl	-1.63 ± 0.05
RbBr	-1.29 ± 0.05	CsBr	-2.08 ± 0.05
RbI	-1.49 ± 0.05	CsI	-2.52 ± 0.05

Ramsey[2] has shown that chemical shifts result from precessional motions induced by the applied magnetic field in the electrons surrounding the nucleus. This precessional motion produces a small local field at the nucleus in opposition to the applied field, and this local field will vary from molecule to molecule as the result of variations in the electronic structures.

If we assume the alkali halides to be 100 percent ionic in their bonding, Ramsey's theory predicts the shielding to be the same as that in the free ion and, consequently, there would be no chemical shift between the different halides. Some covalent character in the bond, however, would mean that the electrons would be partially restricted to the region between adjacent atoms, with a consequent decrease in the precessional motions of the electrons compared to the free ion. An increase in the covalent character of the bond would increase the restrictions to the free precession of the electrons and should give a decrease in the shielding. The shielding changes observed for cesium and rubidium halides indicate that there is some covalent character in the crystalline bonds and that the amount of this covalent character increases as we go from the fluoride to the iodide. This increase in covalency is quite reasonable, considering the decreasing electronegativity of the anion as we go from the fluoride to the iodide.

* Supported in part by the U. S. Office of Naval Research.
† U. S. Atomic Energy Commission Predoctoral Fellow. Present address: Department of Chemistry and Chemical Engineering, University of California, Berkeley 4, California.
[1] H. S. Gutowsky and C. J. Hoffman, J. Chem. Phys. **19**, 1259 (1951).
[2] N. F. Ramsey, Phys. Rev. **77**, 567 (1950); **78**, 699 (1950); **83**, 540 (1951); **86**, 243 (1952).

Dimerization in NaF*

P. KUSCH
Columbia University, New York, New York
(Received May 25, 1953)

RECENT evidence has indicated[1] that the alkali halides, in the gaseous phase, consist not only of diatomic molecules but also of polymers of diatomic molecules. Previously unpublished observations by the molecular beam magnetic resonance method on the spectrum of NaF at low magnetic fields have indicated the existence of the three lines; by a line is here meant the envelope of an unresolved spectrum. The F^{19} line is symmetrical in shape with a half-width of about 130 kc at fields from 50 gauss to 400 gauss, the range of observation. This width is consistent with a width of 94 kc measured at high magnetic fields where the rf amplitude was adjusted to a value which gives a large probability of transition at the natural half-width. The discrepancy occurs because of the high rf amplitude used in the present experiments to develop other features of the spectrum. The second line has a frequency $2g_I(\mathrm{Na})\mu_0 H/h = 2\nu(\mathrm{Na})$. It has the characteristic shape[2] for resonance in diatomic molecules with a nucleus of spin 3/2 and resulting from a transition between the levels $J+1/2$ and $J-1/2$ at fields so weak that the energy of interaction of the nuclear magnetic moment with the applied field is less than the internal quadrupole interaction energy. The third line has a frequency $g_I(\mathrm{Na})\mu_0 H/h = \nu(\mathrm{Na})$ and can only be attributed to a polymer of the molecule NaF.

Feld and Lamb[3] have discussed the energy levels of a diatomic molecule with large rotational angular momentum and containing a nucleus of spin 3/2 which has both a magnetic dipole and an electrical quadrupole moment. At zero field the levels are characterized by the total angular momenta $J\pm 3/2$ and $J\pm 1/2$. The line $(J+1/2 \leftrightarrow J-1/2)$ has[2,4] a low frequency at zero field while at low fields an unsymmetrical line appears whose maximum has a frequency $2g_I\mu_0 H/h$. At zero field the transitions $(J\pm 3/2 \leftrightarrow J\pm 1/2)$ give rise to an intensity distribution with two maxima, centered about the frequency $eqQ/4h$, where eqQ is the quadrupole interaction energy. In the case of NaF this frequency is 2030 kc.[5] When the parameter x^2 is small $(x = g_I\mu_0 H/[eqQ/4])$ the zero field spectrum symmetrically increases in width with magnetic field at the rate of $4g_I\mu_0 H/h$. In the observations here discussed, the maximum value of $\nu(\mathrm{Na})$ is about 450 kc. The spectrum still has the character described by Feld and Lamb and a line of frequency $\nu(\mathrm{Na})$ cannot appear as a well-defined maximum.

Since the line of frequency $\nu(\mathrm{Na})$ cannot arise in a diatomic molecule under the stated conditions, it seems probable that it arises in a polymer of the diatomic molecule. Figure 8 of reference 1 shows a resonance curve observed for Na in NaF at high magnetic fields. The structure arises from internal interactions of the monomer and polymer of NaF. The details on the edges of the pattern may be accounted for by the known internal interactions in the monomer. The structure of relatively high intensity near the center has been ascribed to the polymer. It appears that the internal interactions within the polymer are considerably smaller than those within the monomer. The relatively small internal interactions within the polymer make possible the appearance of a line of frequency $\nu(\mathrm{Na})$ on the low field spectrum here considered.

The beam under observation was formed by a slit on an iron oven in which the vapor was presumably in equilibrium with the liquid at 950°C. It is possible to obtain a rough estimate of the fraction of molecules which are polymers of NaF from the relative intensities of the lines of frequencies $2\nu(\mathrm{Na})$ and $\nu(\mathrm{Na})$. The maximum intensity in the line of the monomer is about twice that in the line of the polymer. However, the integrated intensity in the line of the polymer is only about 40 percent of that in the monomer under identical experimental conditions. If the other molecular species is primarily the dimer of NaF, two positive ions are produced at the detector per molecule as compared to the single ion produced by the monomer. Only half of the states of the monomer can contribute to the intensity of the spectrum centered about $2\nu(\mathrm{Na})$, while all the states of the dimer, if the internal interactions are sufficiently small, can contribute to the intensity within the line of frequency $\nu(\mathrm{Na})$. Accordingly, a reasonable estimate of the fraction of the total beam which consists of dimers or higher polymers is 10 percent. The data are of insufficient accuracy to warrant a more detailed calculation of the polymeric content of the beam.

The data on which this discussion is based were obtained with the cooperation of Dr. H. A. Taub, now at the College of the City of New York.

* This research assisted in part by the U. S. Office of Naval Research.
[1] Ochs, Coté, and Kusch, J. Chem. Phys. **21**, 459 (1953).
[2] R. E. Coté and P. Kusch, Phys. Rev. **90**, 103 (1953).
[3] B. T. Feld and W. E. Lamb, Phys. Rev. **67**, 15 (1945).
[4] N. F. Ramsey, Phys. Rev. **74**, 286 (1948).
[5] Logan, Coté, and Kusch, Phys. Rev. **86**, 280 (1948).

Microwave Spectrum and Dipole Moment of Ethylenimine

RUSSELL D. JOHNSON, ROLLIE J. MYERS, AND WILLIAM D. GWINN
Department of Chemistry, University of California, Berkeley, California
(Received June 8, 1953)

RECENTLY two letters[1,2] have appeared in this journal on the microwave spectrum of ethylenimine. Similar measurements have been made in our laboratory. In general, our results duplicate and confirm those already published, but we have observed a number of lines in addition to those reported by the previous investigators and have calculated the components of the dipole moment of the molecule from the observed Stark displacements. Table I lists the assigned lines and their agreement with

TABLE I.

Line	Observed frequency	$(a-c)/2$ if $\kappa=0.669876$
$0_{00}-1_{11}$	36 119.4 Mc/sec	...
$2_{02}-2_{11}$	23 634.5	4676.48 Mc/sec
$2_{12}-2_{21}$	28 058.0	4676.33
$3_{12}-3_{21}$	22 262.0	4676.32
$3_{22}-3_{21}$	30 495.8	4676.39
$4_{13}-4_{22}$	40 785.8	4676.33
$4_{22}-4_{31}$	21 360.6	4676.13
$4_{32}-4_{41}$	33 784.2	4675.83
$4_{31}-4_{40}$	18 577.5	4675.52
$5_{32}-5_{41}$	21 474.0	4675.16
$5_{41}-5_{50}$	24 682.8	4675.31
$6_{33}-6_{42}$	36 374.0	4675.87
$6_{42}-6_{51}$	23 025.3	4674.92
$6_{51}-6_{60}$	32 185.8	4675.11
$7_{43}-7_{52}$	34 053.3	4675.57
$7_{52}-7_{61}$	26 314.1	4673.96
$7_{61}-7_{70}$	40 588.6	4673.62
$8_{53}-8_{62}$	32 526.3	4674.72
$9_{63}-9_{72}$	32 406.3	4674.33
$10_{73}-10_{82}$	34 165.1	4676.26

theory. From the 2_{02}–2_{11}, 2_{12}–2_{21}, 3_{12}–3_{21}, 3_{22}–3_{31} lines, the rotational constants $(a-c)/2$ and κ were calculated graphically.[3] These constants are listed in Table II. The discrepancy between our values of the rotational constants and those of the previous investigators lies chiefly in the value given the frequency of the 0_{00}–1_{11} line. The value of $a+c$ was taken direct y as the frequency of the 0_{00}–1_{11} line.

In calculating the dipole moment, we applied the methods of Golden and Wilson[4] to the 0_{00}–1_{11}, the 2_{02}–2_{12}, and the 2_{12}–2_{21} lines. The Stark effect of the 0_{00}–1_{11} line is quadratic in the field strength, but the two $J=2$ lines show definite deviations from this

TABLE II.

$a-c$	9352.36±0.08 Mc/sec
$a+c$	36 119.4±0.2
κ	0.6699±0.0001
a	=22 736.1 Mc/sec
b	=21 192.3
c	=13 383.3

simple dependence. The Stark displacements of the two $J=2$ lines, approximately equal but of opposite sign, are so large that they cannot be explained by any dipole moment of reasonable size lying entirely along the b axis. Both the unusual magnitude of the Stark displacements and their nonquadratic dependence on field strength are consequences of the near degeneracy of the 2_{02} and 2_{12} levels. Because of the presence of the component of the dipole moment in the c-axis direction (the axis nearly perpendicular to the CCN plane), there is a nonvanishing element of the direction cosine matrix connecting these states. This contributes a term $\Phi_{Zc}^2/W_{202}-W_{212}$ in Eq. (14) of Golden and Wilson which is of the order of 100 times as large as the other terms for these levels. In addition, the corrections given by Golden and Wilson for degeneracy must be applied, introducing terms of the form $(k_1+k_2E^2+k_3E^4)^{\frac{1}{2}}$ in the expression for the frequency shift. To secure the best fit to the data, it is also necessary to include the contributions from the degeneracy of the 2_{11} and 2_{21} levels, an effect much smaller than the foregoing, as these levels are farther apart. The values of the dipole moment and its components are given in Table III.

TABLE III.

μ_c	=0.89±0.01 debye
μ_b	=1.67±0.01
μ_{total}	=1.89±0.01 debye
angle between μ_{total} and b axis	=28.0°±0.2

[1] Wilcox, Brannock, DeMore, and Goldstein, J. Chem. Phys. **21**, 563 (1953).
[2] Turner, Fiora, Kendrick, and Hicks, J. Chem. Phys. **21**, 564 (1953).
[3] Cunningham, Boyd, Myers, Gwinn, and LeVan, J. Chem. Phys. **19**, 676 (1951).
[4] S. Golden and E. B. Wilson, Jr., J. Chem. Phys. **16**, 669 (1948).

Rayleigh's Ratio for Benzene and the Problem of Absolute Light Scattering Determinations

M. HALWER, G. C. NUTTING, AND B. A. BRICE
Eastern Regional Research Laboratory, Philadelphia, Pennsylvania*
(Received May 29, 1953)

THE current controversy over the correct value for Rayleigh's ratio for benzene, or, in general, over absolute light scattering measurements, is bound to cause uncertainty in the many laboratories which use the light scattering method for determining molecular weights. Zimm[1] has already emphasized that the light scattering methods[2–4] which lead to the so-called "high" value for benzene have in their favor the fact that they produce correct molecular weight values. It must be assumed that Stamm and Button, who have made the most recent contribution to this controversy,[5] believe that this is due to an accidental compensation of errors. The purpose of the present communication is to point out that such an accidental compensation is most unlikely.

The light scattering literature is not rich in molecular weight determinations, which can be compared directly with reliable values obtained by other methods, on monodisperse molecules of a size suitable for accurate measurement. Perhaps the most extensive series is that of Halwer, Nutting and Brice[6] on the proteins β lactoglobulin, serum albumin, lysozyme, and ovalbumin. Using a light scattering method[3] which leads to a "high" value of 48.4×10^{-6} for Rayleigh's ratio for benzene at 436 mμ, they obtained molecular weights that differ by not more than 5 percent from the averages of modern determinations by other methods, notably, osmotic pressure, sedimentation and diffusion, x-ray diffraction, and amino acid analysis.

From Stamm and Button's Table I, the ratio of scattering by benzene to the excess scattering by the "Styron standard" (solution minus solvent) can be calculated as $27.59/122.1=0.226$ for 436.57 mμ and $10.37/45.42=0.228$ for 546.07 mμ. Our ratios for these quantities are $48.4/209=0.232$ for 436 mμ (3) and $17.6/78.2=0.225$ for 546 mμ. Their *relative* scatterings are therefore in close agreement with ours and with those of Carr and Zimm. However, their *absolute* value for Rayleigh's ratio for benzene is 0.570 times our value, and the excess scattering of the Styron standard 0.584 times our value for 436 mμ. Thus, if in our measurements on the proteins our turbidity values were replaced by theirs, the calculated molecular weights would be about 42 percent *lower* than accepted values determined by independent methods. Clearly, Stamm and Button must believe that one or more of the other measurements that are involved in our determinations must bear a compensatory error of 42 percent.

Our results were obtained using the Debye light scattering equation, $Hc/\tau=1/M+2Bc$, where M is the molecular weight and τ the turbidity. The protein concentration, c, was determined by standard methods, i.e., either the pure, air-dry protein (containing a few percent moisture) was weighed out directly, or an aliquot of solution was dried to constant weight at 100°. It is

not conceivable that c could be in error by the amount required. The constant H involves the wavelength of the incident light, the refractive index of the solvent, and the specific refractive increment, $(n-n_0)/c$, where n and n_0 are the refractive indices of the solution and solvent, respectively. The only one of these quantities about which there can be any doubt is the specific refractive increment. However, our values[6] agree within 2 percent with other independent values.[7–10] As for the slope term, $2Bc$, the slopes of the Hc/τ *vs* c plots are so small that a maximum error of 11 percent would be made by neglecting the slope term entirely. Nor can inadequate clarification of solutions or the presence of fluorescence be invoked, since these would make the results too high, whereas we are seeking a supposed error that makes them too low.[11]

The evidence leads us to conclude that a systematic error exists in the method of Stamm and Button for the determination of absolute light scattering power. If their absolute values are correct, they must show that these values lead to correct molecular weights; that our molecular weight results and those of Carr and Zimm and others are correct only through compensation of errors; that the agreement between turbidities determined by transmittance and by 90° scattering obtained by several investigators[2,4,12] is fortuitous; or that Debye's relationship for determining molecular weights by light scattering is not valid.

* One of the laboratories of the Bureau of Agricultural and Industrial Chemistry, Agricultural Research Administration, United States Department of Agriculture.

[1] B. H. Zimm, J. Polymer Sci. **10**, 351 (1953).
[2] C. I. Carr, Jr., and B. H. Zimm, J. Chem. Phys. **18**, 1616 (1950).
[3] Brice, Halwer, and Speiser, J. Opt. Soc. Am. **40**, 768 (1950).
[4] P. Doty and R. F. Steiner, J. Chem. Phys. **18**, 1211 (1950).
[5] R. F. Stamm and P. A. Button, J. Chem. Phys. **21**, 1304 (1953).
[6] Halwer, Nutting, and Brice, J. Am. Chem. Soc. **73**, 2786 (1951).
[7] G. E. Perlmann and L. G. Longsworth, J. Am. Chem. Soc. **70**, 2719 (1948).
[8] K. O. Pedersen, Biochem. J. (London) **30**, 961 (1936).
[9] H. A. Barker, J. Biol. Chem. **104**, 667 (1934).
[10] Armstrong, Budka, Morrison, and Hasson, J. Am. Chem. Soc. **69**, 1747 (1947).
[11] In support of our values are the recent results of Rhees and Foster, Iowa State Coll. J. Sci. **27**, 1 (1952), who obtained values close to ours for serum albumin, ovalbumin and lysozyme, using an independent light scattering method. Their instrument was calibrated by the transmission method, using Ludox colloidal silica. Mommaerts[12] has shown that this method leads to turbidity values in agreement with our own. Edsall, Edelhoch, Lontie, and Morrison, J. Am. Chem. Soc. **72**, 4641 (1950) obtained a value for serum albumin in good agreement with ours, using our value for the Styron standard to calibrate their instrument.
[12] W. F. H. M. Mommaerts, J. Colloid Sci. **7**, 71 (1952).

Erratum: Possible Explanation of Radioactivity Induced by the Detonation of Shaped Charges

[J. Chem. Phys. **21**, 763 (1953)]

L. GRUNBERG AND K. H. R. WRIGHT
Mechanical Engineering Research Laboratory (D.S.I.R.)
Thorntonhall, Glasgow, Scotland

THE following insertion should be made after "would have been sufficient to record" in paragraph 4, line 4: "an impression. However, many photographic plates require an exposure of at least 24 hours to record."

Erratum: The Infrared Spectra of NF_3 and PF_3

[J. Chem. Phys. **20**, 1716 (1952)]

M. KENT WILSON AND SANTIAGO R. POLO
Mallinckrodt Chemical Laboratory, Harvard University, Cambridge, Massachusetts

THE titles of Fig. 1 and Fig. 2 were interchanged. The title for Fig. 1 should read, "The infrared absorption spectrum of phosphorus trifluoride," and that for Fig. 2 should read, "The infrared absorption spectrum of nitrogen trifluoride."

Erratum: T^2 Dependence of the Low Temperature Specific Heat of Gallium

[J. Chem. Phys. **21**, 168 (1953)]

WARREN DE SORBO
General Electric Research Laboratory, Schenectady, New York

THE following sentence should be added to the Letter as published:

The C_v values for graphite are 0.1 of those shown in Fig. 1.

Normal Coordinate Analysis of CF_3CH_3 Based on a Urey-Bradley Potential Function

CHI YUAN PAN AND J. RUD NIELSEN
Department of Physics, University of Oklahoma, Norman, Oklahoma
(Received May 21, 1953)

ALL of the fundamental vibrational frequencies of CF_3CH_3 have recently been assigned.[1,2] Braun and Meister[3] have made a normal coordinate analysis using a general potential function. In the present note preliminary results will be given of a treatment based on a physically more meaningful, but mathematically cumbersome, Urey-Bradley potential function[4] made up of a simple valence force field plus terms representing repulsive forces between nonbonded atoms.

In the absence of evidence as to whether the CF_3CH_3 molecule is staggered or eclipsed, the latter form was chosen rather arbitrarily. Tetrahedral angles and the following distances CF1.33, CH1.09, and CC1.54A were assumed. The potential energy was first expressed in terms of variations in all internuclear distances and bond angles and then transformed into a form containing only bond lengths and bond angles. The redundancy among the internal coordinates was removed by the method of undetermined multipliers, and all first-degree terms were put equal to zero to satisfy the conditions of equilibrium. The F matrix was then obtained by transforming to symmetry coordinates, the corresponding G matrix was evaluated, and the secular equations for the five normal vibrations of species a_1 and the six vibrations of species e were set up and simplified by splitting off the C−H frequencies.

TABLE I.

Species	Calculated	Observed	Species	Calculated	Observed
a_1	632	604	e	320	365
a_1	831	830	e	601	541
a_1	1158	1280	e	1042	970
a_1	1478	1408	e	1242	1233
			e	1366	1443

Attempts to solve these equations by means of a potentiometric computer failed because of lack of accuracy and constancy of its electric circuit elements. However, an approximate solution reproducing the observed frequencies to within a mean deviation of six percent was found by judicious trial and error. The following force constants were used: F_{FF} 1.3, F_{FF}' −0.3, K_{CF} 4.6, H_{FCF} 0.15, F_{HH} 0.1, F_{HH}' 0.0, K_{CH} 4.5, H_{HCH} 0.4, H_{HCC} 0.15, K_{CC} 2.8, F_{HC} 0.4, F_{HC}' −0.05, F_{FC} 0.23, F_{FC}' −0.04, F_{FH} 0.12, F_{FH}' −0.045 and H_{FCC} 0.15×10^5 dynes/cm. The definition of each of these constants will be clear from the subscripts (in which F, C, and H stand for fluorine, carbon, and hydrogen, respectively) and the statement that primes indicate coefficients to first-order terms in the Urey-Bradley potenital function. In addition, the constants k 0.56 and k' 0.05×10^{-11} dyne cm/rad^2 were used. First introduced as undetermined multipliers, these two constants are associated in a somewhat complicated way with C−F and C−H bendings, respectively. All constants except K_{CF}, F_{FC}, F_{FC}', F_{FH}, F_{FH}', H_{FCC}, and k, were transferred from simpler molecules.[5]

It was first attempted to transfer the constant K_{CF} from CF_4, where it has the value 3.8×10^5 dynes/cm. However, no satisfactory results could be obtained until it was raised to 4.6×10^5. The constant F_{FH}', although small, was found to be quite important in determining the normal frequencies.

The diagonal terms of the f matrix calculated from the Urey-Bradley potential are as follows: Stretching constants C−F 6.37, C−C 4.74, and C−H 4.90×10^5 dynes/cm; angle constants FCF 1.98, FCC 1.04, HCH 0.57, and HCC 0.92×10^{-11} dyne-cm/rad^2.

These force constants agree well with those obtained with the aid of the usual general potential function.[6-9]

The calculated and observed wave numbers are given in Table I.

[1] Nielsen, Claassen, and Smith, J. Chem. Phys. **18**, 1471 (1950).
[2] Cowan, Herzberg, and Simha, J. Chem. Phys. **18**, 1538 (1950).
[3] Reported at the Symposium on Molecular Structure and Spectroscopy held in June, 1951, at Columbus, Ohio.
[4] H. C. Urey and C. H. Bradley, Jr., Phys. Rev. **38**, 1969 (1931).
[5] T. Simanouti, J. Chem. Phys. **17**, 245, 734, 848 (1949); **20**, 726 (1952).
[6] D. M. Dennison, J. Chem. Phys. **7**, 522 (1939).
[7] G. Herzberg, *Infra-Red and Raman Spectra of Polyatomic Molecules* (D. Van Nostrand and Company, Inc., New York, 1945), p. 193.
[8] H. H. Claassen, J. Chem. Phys. **18**, 543 (1950).
[9] L. H. Berryman, Ph.D. thesis, University of Oklahoma, 1950.

C_p-C_v in Silicon and Germanium

M. E. FINE
Bell Telephone Laboratories, Inc., Murray Hill, New Jersey
(Received May 7, 1953)

IN the absence of sufficient data for calculating the differences between the heat capacities at constant pressure and the heat capacities at constant volume, the differences are often estimated by the Nernst-Lindemann[1] relation [Eq. (1)] established empirically. In Eq. (1) T_s

$$C_p-C_v=0.0214C_p^2(T/T_s) \quad (1)$$

is the melting temperature. This was the procedure in several recent investigations of the heat capacity of germanium.[2,3]

Recently sufficient experimental information became available to allow calculation of C_p-C_v from the thermodynamic relation for cubic solids,

$$C_p-C_v=9\alpha^2VT/K_T. \quad (2)$$

In Eq. (2) α is the coefficient of linear expansion, K_T is the isothermal compressibility, and V is the atomic volume. The coefficients of linear expansion for Ge from 77 to 450°K have recently been reported.[4] Figure 1 shows the coefficient of linear expansion of high-purity Si compared with previous measurements.[5,6] The elastic constants of Si[7] and Ge[4,7] have recently been measured over a wide temperature range, and the compressibilities calculated[8] from these are shown in Fig. 2.

C_p-C_v values calculated from (2) are shown in Fig. 3. In Si, C_p-C_v is negative at low temperatures reflecting the negative coefficient of expansion. The values of C_p-C_v estimated for Ge and Si from the Nernst-Lindemann equation, also plotted in Fig. 3, are considerably larger than the true values; actually the error in these metals from equating C_p and C_v is less than that from the Nernst-Lindemann approximation.

[1] W. Nernst and F. Lindemann, Z. Electrochem. **17**, 817 (1911).
[2] R. W. Hill and D. H. Parkinson, Phil. Mag. **43**, 309 (1952).
[3] I. Estermann and J. R. Weertman, J. Chem. Phys. **20**, 972 (1952).
[4] M. E. Fine, J. Appl. Phys. **24**, 338 (1953).
[5] S. Valentiner, Ann. Physik **46**, 859 (1914–1915).
[6] H. D. Erfling, Ann. Physik **41**, 471 (1942).
[7] H. J. McSkimin, J. Appl. Phys. (to be published).
[8] R. F. S. Hearman, Revs. Modern Phys. **18**, 409 (1946).

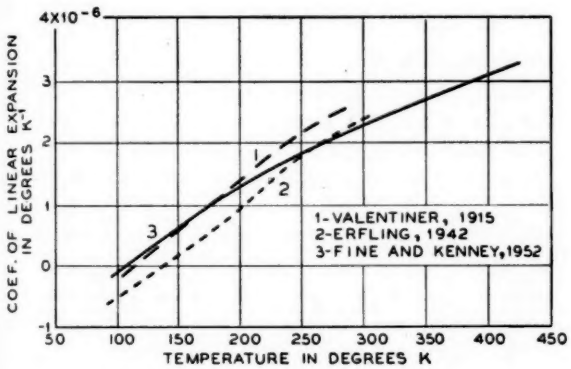

FIG. 1. Coefficient of linear expansion of silicon.

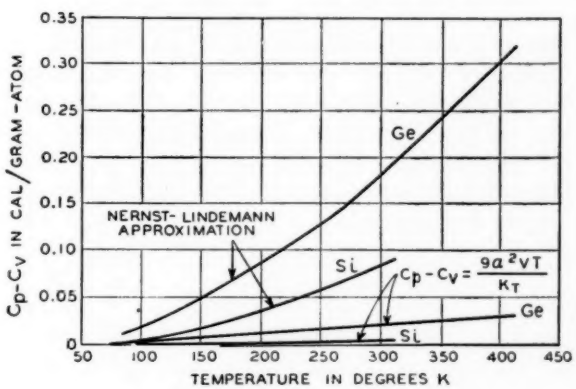

FIG. 3. C_p-C_v in silicon and germanium.

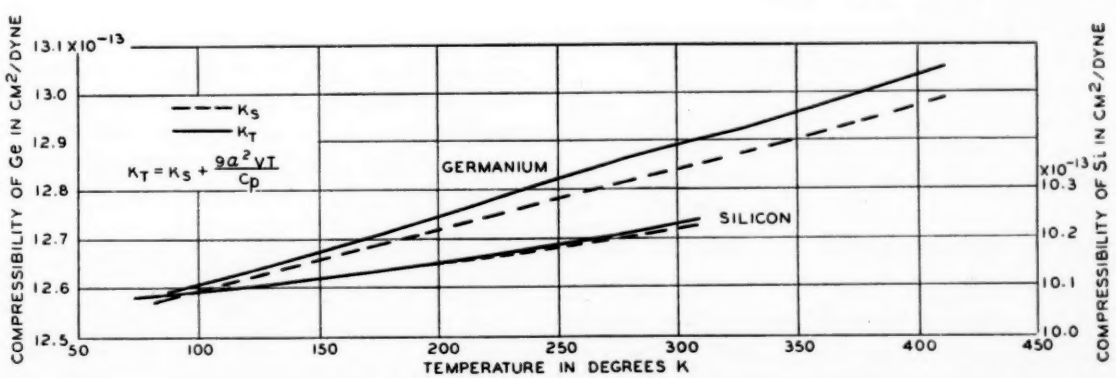

FIG. 2. Compressibilities of silicon and germanium.

Announcement

The following officers, nominated by the Nominating Committee of the Division of Chemical Physics, have accepted the nomination, and in the absence of competing candidates have been elected by the casting of one ballot for each of them by the Secretary:

H. H. Nielsen	Vice-Chairman
A. A. Frost	Executive Committee
K. S. Pitzer	Executive Committee

The incumbent officers of the Division are:

J. O. Hirschfelder	Chairman
Bryce Crawford, Jr.	Secretary
F. G. Brickwedde	Treasurer
D. F. Hornig	Executive Committee
R. S. Mulliken	Executive Committee
J. E. Mayer	Executive Committee

BRYCE CRAWFORD, JR.
Secretary